Advanced Studies in Veterinary Anatomy: Angiogenesis in Caprine Reproductive Organs of Non-Pregnant and Pregnant Normal and Swainsonine-Treated Does

Shireen Abdelgawad Hafez

Dissertation submitted to the faculty of the Virginia Polytechnic Institute and State University in partial fulfillment of the requirements for the degree of

Doctor of Philosophy
in
Veterinary Medical Sciences
(Anatomy)

Thomas Caceci, Chairman
Larry E. Freeman
Bonnie J. Smith
William R. Huckle
Beverly J. Purswell
Robert M. Akers

April 20, 2005
Blacksburg, Virginia

Keywords: Angiogenesis, Goats, Placenta, VEGF, Uterine vessels, Ovarian vessels, Microvascular corrosion casting, Tissue clearing technique.

Advanced Studies in Veterinary Anatomy:
Angiogenesis in Caprine Reproductive Organs of Non-Pregnant and Pregnant Normal and Swainsonine-Treated Does

Shireen Abdelgawad Hafez

ABSTRACT

The female reproductive organs are among the few adult tissues in which periodic angiogenesis normally occurs. Pathological angiogenesis can occur in various conditions, such as solid tumors. Vascular endothelial growth factor (VEGF) signaling often represents a critical rate-limiting step in physiological and pathological angiogenesis. This study utilizes development of utero-ovarian vasculature during pregnancy in goats as a model of physiological angiogenesis. Non-pregnant does and does at 4, 7, 10, 13, 16, and 18 weeks of gestation were used.

Arteries of the reproductive tract were injected *in situ* with Microfil®. The tracts were fixed, dehydrated, and rendered transparent to reveal the paths of arteries. The ovarian artery was tortuous and lay in close apposition to the uterine tributary of the ovarian vein in all specimens studied. In non-pregnant does, this arrangement may serve as a *local* utero-ovarian pathway for the corpus luteum (CL) luteolysis at the end of non-fertile estrous cycle. During pregnancy, this arterio-venous arrangement may transfer luteotropic substances from uterus to ovary, which may serve in maternal recognition of pregnancy and fit the fact that the goat is CL dependent throughout gestation. In some cases of triplets, the size of the uterine branch of the ovarian artery was equal to or even larger than that of its parent artery and/or the ipsilateral uterine artery; and the

vaginal artery contributed a connecting branch to the uterine artery. These physiological adaptations of the ovarian and/or vaginal arteries correlate well with the increasing nutrient demands of the growing multiple fetuses.

In a second experiment, the vasculature of the uterus and ovaries was injected *in situ* with a mixture of Batson's No.17® and methyl methacrylate and then processed for observation by SEM. The microvasculature differed between non-pregnant and pregnant does, and with advancing gestation. We concluded that goats possess a *multivillous* type placenta. Capillary sinusoids and crypts on the fetal surface of the caruncle may compensate for the negative effect of the increased interhemal distance. Intussusceptive angiogenesis should be considered as equally possible and important mechanism as sprouting angiogenesis during placental development. Capillary diameters increased significantly during pregnancy especially after 4 weeks. Capillary density index was 66.8, 68.7, 55.5, 63.5, 70.1, 70.4, 64.5 percent in non-pregnant, 4, 7, 10, 13, 16, and 18 weeks of pregnancy, respectively. In the ovary, coiling of the ovarian branch of the ovarian artery around the ovarian tributary of the ovarian vein was observed. This may represent a local channel required for product transport from ovarian vein to ovarian artery and might have a role in regulating blood pressure to various ovarian structures.

Immunolocalization of VEGF was performed as a third experiment. Immunostaining was observed in cytotrophoblasts, maternal epithelial tissues, and vascular endothelium and smooth muscle, but not in binucleate giant cells or connective tissue. No apparent differences were observed in intensity and

pattern of VEGF staining associated with advancing gestation. Luteal and follicular cells, and endothelium and smooth muscles of the ovarian vasculature positively stained. Patterns and intensity of staining of VEGF suggest that the fetus is directing its own survival by producing growth factors affecting fetal and maternal tissues. VEGF may have a role in growth and differentiation of cytotrophoblasts, as well as, development and maintenance of CL.

In the fourth experiment, the sequential expression of VEGF and its receptors (fms-like tyrosine kinase, Flt-1 and kinase-insert domain-containing receptor, KDR) was measured using real-time quantitative PCR. Targets were detected in all studied tissues; however, levels of expression differed according to the stage of pregnancy. Expression of VEGF and its receptor mRNAs increased with advancing pregnancy, which correlates with the expansion of vasculature during pregnancy. Differences in the time-courses of the expression of Flt-1 and KDR mRNAs during pregnancy suggest that each receptor plays a different role in the angiogenic process.

As an application of our model of angiogenesis, we tested the effect of swainsonine (active compound of locoweed and a potential anti-cancer drug) on the process. Does treated with swainsonine were euthanized at 7 and 18 weeks. No significant differences were found in sinusoidal diameters in treated does at 7 weeks, but a decrease in capillary density index was noted. In the ovary, focal avascular areas were observed in the corpus luteum of swainsonine-treated does at 7 weeks of pregnancy. Swainsonine caused great distortion in the uterine and ovarian vasculature at 18 weeks. A decrease in intensity of the immunoreactivity

to VEGF antibody was observed in tissues from swainsonine-treated does at 7 and 18 weeks. There was no substantial effect of swainsonine on the expression of VEGF and its receptors' mRNAs in any of the studied tissues (except in the left ovary, where it had an inhibitory effect) at 7 weeks of pregnancy, but it had an inhibitory effect at 18 weeks. Demonstration of swainsonine's potential to negatively affect vascular development and suppress genes likely involved in angiogenesis at critical stages of blood vessel proliferation lends credibility to its potential as anti-cancer drug.

Table of Contents

List of Figures

List of Tables

Acknowledgements

I would like to express my deepest gratitude to my advisor, Dr. Thomas Caceci, for his patience, encouragement, and support in the completion of my doctorate degree. Thank you for your endless concern and dedication as a father to me. I would also like to thank my committee members, Dr. Larry Freeman, Dr. Bonnie Smith, Dr. William Huckle, Dr. Beverly Purswell, and Dr. Robert Akers for their guidance and assistance throughout my graduate studies.

I'm grateful to Dr. Kip Panter, ARS Poisonous Plant Research Laboratory, USDA, Logan, UT. for his help and advice in swainsonine part of the study and his kind supply with ground locoweed. My deepest gratitude to the late Dr. Antorio Garcia for his sincere help. Thanks to my colleague Dr. Marcelo Gomez for his truthful help and especially for the initial drawing of Figures 21 and 22.

My deepest gratitude to John Strauss for his excellent technical support. Thanks to the excellent technical support provided by Pam Arnold, Virginia Viers, and Kathy Lowe.

Special thanks to my husband for his continuous support. This dissertation is dedicated to my family: they taught me the meaning of the word "family" and how important it is to know that there is someone there any time you need them. I'm also in eternal debt to whoever taught me that you get what you work for; and that if you do not, that's okay, too, because God wants it that way, and He knows what is best for you anyway.

Thanks to whomever else helped over the years, but whom I've forgotten to mention. Your encouragement is part of the final result, as well.

Introduction and Review of Literature

The Goat as a Research Animal

The goat, *Capra hircus*, is one of the oldest domesticated animals. Goats are raised extensively in many countries, particularly those in Asia, Africa, the Middle East, and Latin America. In these nations, goats are used mainly for meat production; goat meat accounts for 47% of all meat produced in India (Smith and Sherman, 1994). Milk and cheese production is a major source of income in many countries: it is a major industry in Europe. Some goat breeds are very important in fiber production *i.e*. angora goats are a major source of mohair fiber notably in Turkey, South Africa, USA (Texas), and Argentina (Sexton and Mitcham, 1992). Cashmere or pashmina goats are a source of valuable cashmere. They are found mainly in central Asia (Gall, 1996). Goats can also be a good source of hide; some goat breeds are raised to produce high priced leather coats. Even goat horns can be used for ornamental purposes and for musical instruments.

Anatomically and physiologically, it is unwarranted to regard the goat—a valuable animal in its own right—as merely a “miniature cow” or a “wool-less sheep”. The goat is neither. The anatomy of the cattle and sheep has been used as a guide to that of the goat. While this may be adequate from a clinical perspective, when goats are used as a research animal, far more comprehensive and adequate anatomical studies are needed, ones that are specific to the goat. Detailed specific caprine anatomy is of more than purely academic interest, as

goats are often preferred animals for anatomical studies due to their manageable size and lean musculature.

The Caprine Placenta: A Useful Model for Angiogenesis

The placenta is one of the most important transient organs, and has been the subject of extensive research in many species. Probably one of the most important aspects of placental studies is the morphology and development of the vasculature since this directly relates to the principle placental function (gas, nutrient, and waste exchange between the mother and fetus) and of course to the survival of the fetus to term.

According to the classic classification of placentas, the goat placenta is regarded as *chorioallantoic* (Kaufmann and Burton, 1994; Leiser and Kaufmann, 1994). Goats develop a partially *adeciduate* and *villous type* placenta. The areas of villus formation are discrete specialized sites: formation of villi occurs only on areas in apposition to the pre-existing uterine caruncles. The villous processes extend into crypts that develop in proliferating caruncles; as the villi develop a tree-like morphology by secondary and tertiary branching, the adjacent endometrium on the caruncle undergoes hypertrophy and grows around the villi. The result is a more or less complete interdigitation of branched fetal villi with the walls of the maternal crypts. These specialized areas of fetal tissues are termed cotyledons: a cotyledon and its caruncle together form the functional unit of the placenta, the *placentome*.

The interhemal barrier, which separates the maternal and fetal blood streams, is classified as *epitheliochorial* (Kaufmann and Burton, 1994), and

syndesmochorial in older literature. The term *synepitheliochorial* is used in more recent literature (Wooding, 1992; Leiser and Kaufmann, 1994) because of the fusion of the binucleate trophoblasts with the uterine epithelium.

Angiogenesis

Two processes are principally responsible for the formation of new blood vessels. These have been described by Risau (1997): *Vasculogenesis* defines the process of *de novo* blood vessel formation, *i.e.* the events that take place when new vessels are formed by coalescence of blood islands. *Angiogenesis* in contrast refers to formation of new blood vessels from pre-existing ones, either by sprouting (Folkman, 1992) or intussusception (Burri et al., 2004). Of these two processes, angiogenesis is the more important in terms of development of maternal side of the placenta.

Angiogenesis occurs extensively during fetal life, but it happens only under special circumstances in adults. The female reproductive organs, which exhibit dynamic growth and regression accompanied by changes in the levels of growth factors promoting such growth, are among the few adult tissues in which periodic angiogenesis normally occurs (Reynolds et al., 1992; Fraser and Lunn, 2000). Pathological angiogenesis can occur in various conditions, such as atherosclerosis, diabetic retinopathy, psoriasis, rheumatoid arthritis, and solid tumors (Folkman, 1995). One approach to cancer treatment has been to consider the use of drugs which may inhibit the development of new blood vessels, on which some tumors are dependent. Novel anti-cancer drugs are being developed which may interfere with tumor growth by inhibiting angiogenesis (Zogakis and

Libutti, 2001; Folkman, 2002). Animal models of angiogenesis are valuable “test beds” for such possible therapeutic agents.

To learn more about pathological angiogenesis, we can study the normal process as it occurs during pregnancy. Characterization of the structure and development of uterine and ovarian vessel systems is a prerequisite to their functional interpretation; and the caprine placenta can serve as a model of angiogenesis at different levels. Furthermore, quite aside from the potential utility of the caprine model as a general one for angiogenesis, this information is of importance to improving reproductive efficiency in goats themselves.

Tissue clearing and microvascular corrosion casting techniques can provide a good overall picture of angiogenesis of the utero-ovarian vasculature at the macroscopic and microscopic levels, respectively. At the molecular level, examining the expression of a vitally important growth factor, one that promotes vascular proliferation and survival (vascular endothelial growth factor, VEGF) can be correlated with the structural study to give a more complete picture of angiogenesis at a different level. Using immunohistochemistry and real-time quantitative polymerase chain reaction (real-time QPCR) help to complete the picture of angiogenic events at anatomic, cellular, and molecular levels.

Gross Anatomical Studies of Utero-ovarian Vasculature

The importance of understanding the distribution of blood vessels in the female reproductive organs has been recognized for years. By the early 1970s studies of the control of the lifespan of the corpus luteum (CL) by the uterus itself had led to an entirely new concept: that of the internal regulation of physiological

process through *local* venoarterial pathways. This concept was explored by Del Campo and Ginther (1973) and the evidence for it extensively reviewed by Ginther in a 1974 article.

Citing earlier work by Swenson (1970) on the hepatic and hypophyseal portal systems, Ginther opened his review by saying: *"It is well known that venous effluent from an organ can pass directly to an adjacent organ…It is not generally believed that a substance in a major vein of an organ can pass directly into the wall or lumen of an adjacent major artery of the same organ…"*. He then discusses the work of Barrett et al. (1971), who initiated estrus in ewes by infusions of prostaglandin ($PGF_{2\alpha}$), concluding with the statement that: *"Considerable evidence has since evolved which demonstrates that the uterus causes luteolysis through a venoarterial pathway."*

In his 1974 review, Ginther also cited numerous anatomical studies to support the concept of a direct venoarterial transfer of bulk materials. He noted several studies that clearly showed that physical interference with the structural arrangements by which the proposed pathway is believed to work can affect the physiology of normal cycling. For example: *"…it was found that the severance of the vessels at the tubo-uterine junction…delayed the return to estrus and delayed the luteolytic effect of exogenous progesterone"* and cited also the experiments of others in a number of species that demonstrated the same effect.

While the idea that substances passing through one fairly stout vessel can be physically transferred to another equally stout one flowing in the opposite direction may not be intuitively obvious, when the microscopic structure of large

arteries and veins is taken into account, it becomes more easily understood how this may happen. Large blood vessels have walls whose component cells cannot receive nutrient and waste transport directly from the blood flow (as small vessels do). While the endothelium and the sub-endothelial connective tissues may be in close enough proximity to the flowing blood to utilize simple diffusion for their needs, the smooth muscle and connective tissue cells of the thick walls cannot. Therefore, in large vessels there exists an extensive network of *intramural* capillary beds whose principal function is to serve the physiological demands of the large vessels themselves. These "side channels" come directly off the main flow and return to it. They are referred to as the *vasa vasorum*, literally the "vessels of the vessels," and easily demonstrated in large arteries and veins. Since the vasa vasorum by definition reaches the outermost limits of the mural structure, and since they carry substances that are present in the venous outflow from an organ, if two such capillary beds are in close physical proximity, the only barrier to diffusion *from one such bed to the adjacent one* is the intercellular space across which the material must move. The arrangements of the major vessels discussed here are such as lead to the conclusion that Del Campo and Ginther did: they are physically apposed to permit the exchange of physiologically active materials across a minimal intercellular distance. In other words, there is strong morphological evidence that while exchanges of gases and nutrients only occur in capillary beds, exchanges of other, non-nutrient materials of importance can occur in other locations via a paracrine exchange between two blood vessels.

If, then, the uterus has the appropriate mechanical arrangements to affect luteolysis through a venoarterial pathway, it follows that the presence or absence of an embryo in the uterus is the ultimate determinant factor that controls the maintenance or regression of the CL. The uterus therefore is actually terminating the life of the corpus luteum at the end of non-fertile estrous cycle. This may be via a *systemic* pathway in some species, and through a *local* utero-ovarian pathway in others. In this process, $PGF_{2\alpha}$ produced by the endometrium leaves the uterus through the uterine tributary of the ovarian vein, passing directly into the closely adjacent ovarian artery, to cause CL regression. Understanding this mechanism was the key to optimization of the minimal effective dose of prostaglandin that could be given systemically to different species of farm animals, so the knowledge had more or less immediate practical use.

Empirical work has shown that the minimum effective dose of a single systemic injection of $PGF_{2\alpha}$ (as determined by the interval from treatment to estrus) was 6.0 mg in ewes and 1.25 mg in pony mares. The efficacy of the dose of $PGF_{2\alpha}$ can be attributed to several factors, including the bioactivity of the $PGF_{2\alpha}$ of the different species; but it is equally possible that it may be due to the presence of a *local* utero-ovarian pathway in sheep versus a mainly *systemic* pathway in horses (Ginther, 1974).

Descriptive information about the angioarchitecture of the utero-ovarian vasculature in most non-pregnant farm animals has been described (Ginther, 1976). However, to our knowledge, no reports have provided data about the distribution of the utero-ovarian vessels in goats; more surprisingly, none are

available on the state of the vasculature at different stages of pregnancy in any common farm animal. Furthermore, the detailed angioarchitecture of the uterine vessels has been ignored for years, and currently no adequate data are available about their distribution and/or nomenclature. These knowledge gaps add to the difficulty of studies on reproduction and reproductive organs, and introduce variability of interpretation and hence possible misunderstanding of the results of different experiments.

Organization of the Caprine Placental Vascular Systems

Since complete understanding of the utero-ovarian vasculature and how it grows is important, the study of the maternal and fetal vascular systems is valuable. The efficiency of the transplacental nutrient and gas exchange may be influenced by the way fetal and maternal blood vessels are arranged in the placental barrier and this arrangement differs significantly enough from one species to the next (Kaufmann and Burton, 1994), so that no single species can reliably serve as a universal model; but there is a certain amount of information that can be used as a general starting point. In *concurrent* flow, both fetal and maternal blood streams run in the same direction. This arrangement is not seen in placentas of mammals. In the *counter-current* system, represented by the rodent placenta, the fetal and maternal blood streams run in opposite directions. Carnivores (and possibly ruminants, though this is controversial) possess an intermediate form of circulation termed a *cross-current* system. It can be thought of as being intermediate with respect to the efficiency of exchange between an exclusively concurrent or exclusively counter-current arrangement. In higher

primates, there is a combination of these three (counter, cross, and concurrent) systems, termed *multivillous* system.

Study of the maternal and fetal vascular systems in the placentae of sheep and goats has been of particular interest to some investigators, though they are few. Anatomic observations on these systems seem to provide a reasonable interpretation of the placental function. Barcroft and Barron (1946) studied the maternal and fetal vessels in the ovine placenta, and proposed that a *counter-current* arrangement of blood flow exists between the maternal and fetal vessels, where the fetal blood leaving capillaries is adjacent to the maternal blood entering capillaries. Makowski (1968) studied the maternal and fetal vascular systems in the ovine placenta and also in goats. He demonstrated the presence of a *cross-current* arrangement of the maternal and fetal placental circulations. These studies leave open the question of whether the ovine and/or the caprine placenta represent a counter-current or cross-current arrangement. As yet, there is no definitive answer. Prior to the present investigation, microvascular corrosion casting combined with observation in a scanning electron microscope has been used to study the uterine vasculature of the goat only once (Leiser, 1987). Leiser examined the principle of blood flow in the caprine placenta using microvascular corrosion preparations of both maternal and fetal vessels, and concluded that a combination of a counter-current and cross-current arrangement is present.

One reason for the confusion may be that methods used to study the arrangement of the maternal and fetal vascular systems differed among authors.

Certainly, this can partially explain the presence of discrepancy in their results. Barcroft and Barron used reconstructed histological serial sections and corrosion casts observed under a dissecting scope. Makowski used India ink- and latex-injected specimens. While these studies yielded much information, they suffered from inherent limitations, such as lack of three-dimensionality and limited resolution of fine details. The potential for misinterpretation is high. Leiser's microvascular corrosion casts appeared to be the most efficient way of studying these extremely complex systems, but he used cut placentomes, which did not (and cannot) give a complete picture of the vascular system. In the present study both cut and intact caruncles have been examined. This approach provides more information about the three-dimensional arrangement of the maternal vessels system, and can be compared more or less directly to the previous limited work.

Furthermore, even though the placenta has been studied to a certain extent, none of the authors mentioned above examined the uterine vascular system in non-pregnant doe goats and/or in does in early stages of pregnancy. Nor did they provide a picture of its developmental features with advancing gestation. A consideration of the mechanisms of angiogenesis in non-pregnant and different stages of gestation was not addressed and angiogenesis *by sprouting* has been assumed to be the only possible mechanism by which it occurs. To the best of our knowledge, to date no investigator has provided quantitative information about uterine vasculature in non-pregnant and/or pregnant does.

The Ovarian Vascular System

While the placental vasculature is important, the ovary and its vessels have to be regarded as equally significant. The ovary is one of the most dynamic examples of cyclic angiogenesis. Continuous changes in the ovarian structures are accompanied by equally dynamic modifications in ovarian microvasculature (Macchiarelli et al., 1992, 2000). Studies on the microvascular architecture of mammalian ovaries are few (Kardon and Kessel, 1979; Kanzaki et al., 1982; Kitai et al., 1985; Takada et al., 1987; Cavender and Murdoch, 1988; Murakami et al., 1988; Macchiarelli et al., 1991, 1992, 1995, 2000; Forsman and McCormack, 1992; Yamada et al., 1995; Jiang et al., 2002; Jiang et al., 2003) and most of these reports dealt with non-pregnant rodents and lagomorphs, rather than farm animals.

With respect to microvascular changes during pregnancy, only two studies dealing with pregnant lagomorphs have been published (Nottola et al., 1997; Macchiarelli et al., 1998). Details of the proximal ramification of ovarian vessels have been rarely examined. Details of the ovarian vascular pattern are known to vary greatly among different species (Takada et al., 1987), but to our knowledge there have been no publications on the three-dimensional angioarchitecture of the caprine ovary and/or corpus luteum microvasculature of any ruminant species.

Vascular Endothelial Growth Factor (VEGF)

Angiogenesis is a highly complex and coordinated process, requiring many receptor-ligand interactions; but vascular endothelial growth factor (VEGF)

signaling often represents a critical rate-limiting step in physiological, as well as pathological, angiogenesis (Ferrara et al., 2003). Currently, a number of VEGF inhibitors are being tested as potential tumor therapies: recently the Food & Drug Administration approved anti-VEGF antibody (Avastin™, Bevacizumab, Genentech) for metastatic colorectal cancer (Barclay, 2004; Willett et al., 2004).

Vascular endothelial growth factor is a heparin-binding homodimeric glycoprotein. At lease six VEGF isoforms are produced by alternative exon splicing (Ferrara at al., 2003). The biological effects of VEGF are mediated by two receptors; Flt-1 (VEGFR-1, fms-like tyrosine kinase) and KDR (VEGFR-2 or Flk-1, kinase-insert domain-containing receptor). Many investigators have studied the expression of VEGF in the female reproductive organs with the goal of understanding its role in physiological angiogenesis and its potential for application(s) to pathological angiogenesis (Garrido et al., 1993; Sharkey et al., 1993; Cheung et al., 1995; Redmer et al., 1996 and 1998; Reynolds and Redmer, 1998; Reynolds et al., 1998; Berisha et al., 2000 a and b; Reynolds et al., 2000; Bogic et al., 2001; Stouffer et al., 2001; Nayak and Brenner, 2002; Sugino, 2002; Al-zi'abi, 2003). But to our knowledge, none of these reports has provided a sequential study of the expression and/or localization of angiogenic mediators during pregnancy in goats. We know little about the developmental regulation of these factors during pregnancy.

Locoweed and its Effects

Locoweed is a common plant of the American southwest and for many years has been a significant cause of economic loss to livestock producers in the

regions where it grows. Locoweed has a wide geographical distribution; it is not confined to North America, as there are numerous locoweeds in South America, Asia, and Australia. The origin of *loco* is Spanish meaning “crazy”, and the term is appropriate as a casual description of the effects it has on animals. Locoweed poisoning occurs in all classes of grazing livestock. Plants responsible for locoweed poisoning are related to the genera *Oxytropis (Sericea*) and *Astragalus (Lentiginosis, Pubentisimus, Mollissimus)* of the Leguminosae family (James et al., 1967).

Clinical signs of locoweed poisoning are seen in more than one body system. Neurologic and emaciating signs in free grazing sheep include holding the head high, nervousness, stiffness, loss of sense of direction, muscular incoordination, loss of body weight and progressive body weakness, and eventually death (James et al., 1967; Van Kamper and James, 1969). Experimentally poisoned animals exhibit depression, staggering gait, muscular incoordination, development of roughened hair coat, difficulty in eating and drinking, ataxia, proprioceptive deficits, and behavioral abnormalities. Similar neurological symptoms (“knuckling” the rear fetlocks and a hopping gait) as well as histopathologic lesions (principally vacuolation of neurons and visceral epithelial cells and edema) were also reported in goats grazed on locoweed (Stegelmeier, 2001)

Wethers fed 227 g of dried locoweed per day for a period of 60 days showed depression within 20 days after starting feeding. They gained weight in the first 35 days but then suffered rapid weight loss. At 40 days they were

affected with impaired vision, inability to stand for sustained periods, a loss of motor function and proprioception, and emaciation. Weight loss and emaciation were probably due to gastrointestinal dysfunction and metabolic impairment including the production of abnormal digestive enzymes, and altered gastrointestinal reflexes (Van Kamper and James, 1969).

Sheep show neither initial preference nor addiction to locoweed but may acquire preference (habituation). Unavailability of other food sources will cause free grazing animals to feed on locoweed, after which they develop a craving appetite for the plant (James et al., 1967; Ralphs et al., 1990; Ralph and James, 1999). When we tried to feed ground locoweed (*Astragalus Lentiginosis*) mixed with alfalfa hay to a group of goats, they preferred starvation on feeding locoweed, which gives an indication of the relative unpalatability of the plant.

Histologically, locoweed intoxication is characterized by the presence of foamy cytoplasmic vacuolations in the cells of various organs. These represent lysosomes filled with undegraded oligosaccharides. Generalized neurological degeneration and vacuolar degeneration of the central nervous system, liver, kidney, thyroid and parathyroid glands, pancreas, adrenal gland, and reticuloendothelial cells of lymph nodes, are all found in locoweed-intoxicated sheep. Perivascular edema throughout the central nervous and digestive systems has also been reported. Hypertrophy of the thyroid and parathyroid glands has been reported (Van Kampen and James, 1969).

In a study of the sequential development of the lesions in ewes fed 380 g of locoweed per day (Van Kampen, 1972), a group of animals was euthanized

every four days starting at four days after feeding began through the 32 days of the feeding trial. Cytoplasmic vacuoles and perivascular edema were visible in the renal proximal tubular cells as early as 4 days of feeding into the experiment. The lesions were apparent in cells of the central nervous system, in hepatocytes, reticuloendothelial cells, cells in lymph nodes, and in the urinary bladder by day 8. Foamy cytoplasmic vacuolations were first reported in the ovary by day 12. By day 16, the follicular cells of thyroid gland, the acinar cells of the pancreas, and the pineal and adrenal glands were also involved. Depression began by day 16. In the final 16 days, the parathyroid, pituitary gland, glandular epithelium of the abomasums, chorionic epithelial cells of the placenta in pregnant animals, myocardial and skeletal muscles, and reproductive organs, all showed cytoplasmic vacuoles. Generally, in locoweed intoxication not all the tissues are affected at the same time or at the same level, and the severity of the effect differs from one individual to the other.

Studies on the effect of locoweed on the reproductive tract are numerous. Panter et al. (1999) reviewed the effects of locoweed on reproduction. In females, the problems created by these plants include abnormal pituitary and ovarian function in a dose-dependent manner. These changes interfered with estrus behavior and resulted in delayed estrus, a lengthened estrous cycle (after 20 days of feeding), delayed conception (after 30 days of feeding), delayed placentation when fed at early stages of pregnancy (0-30 and/or 20-50 days), abnormal placentome development, hydrops amnii, and abortion (Van Kampen and James, 1971). Abortion caused by locoweed intoxication can occur at any

time during pregnancy in the case of ewes ingesting the plant more than 8 days. Ewes experimentally fed locoweed for as few as 10 days have been known to abort (James et al., 1969). However, abortion generally occurred only after a fairly extended period of feeding in most experiments.

In one study by Panter et al. (1987) abortion occurred about 40 days after the start of feeding locoweed (2.7 kg pellets per day, 15% *Astragalus* and 85% alfalfa hay) for about 40 days beginning at 60 days of pregnancy. Other animals who did not abort became severely intoxicated and were euthanized after 36 days of feeding commencing at 60 days of pregnancy. Abortion occurred after 49 days when locoweed was fed for 51 days; or after 63 days of locoweed feeding for 65 days beginning at day 74 of pregnancy. It occurred after 39 days when fed for 39 days beginning at day 88 of gestation.

In a study by James et al. (1969), three ewes were fed locoweed (525 g per day) between the 35th and 60th days of pregnancy. Two of these ewes died on the 26th day after feeding started, and both these animals had macerated fetuses. The third ewe aborted. Animals fed 454 g per day from 40-50 or 60-70 or 80-90 days of pregnancy had normal offspring. One ewe died from feeding 450 g per day from day 80-100 of pregnancy. The ewe fed 454 g per day between days 100-110 of gestation aborted.

In a sequential study of the effect of locoweed on pregnant ewes (Van Kamper and James, 1971), the subjects were fed 380 g of locoweed per day between days 40-72 of pregnancy. Two ewes were euthanized at four-day intervals, beginning 4 days after feeding. Vacuolation of fetal membranes

(especially chorionic epithelium) was observed. Cells became hypertrophied. Vacuolation of luteal cells occurred on day 16 of feeding and the investigators felt this might have had an effect on progesterone production. They also reported that blood vessels in the intercotyledonary areas of the placenta were reduced in number and in size. Dark hemorrhagic areas were observed throughout the uterine wall. Placentomes became flattened. Atrophy of the vasculature of fetal membranes and fluid accumulation in the placenta were also observed. No gross changes were observed in the uterine wall, cervix, vagina, or ovaries. After 12 or 16 days on locoweed, the fetuses developed severe signs of intoxication characterized by fetal edema. Musculoskeletal malformations were observed on days 28 and 32. As early as day 4 of poisoning, cytoplasmic vacuoles were present in the chorionic epithelium. By day 8, metaplasia of chorionic epithelium to columnar epithelium was manifested. On day 12 there were discrete cytoplasmic vacuoles in addition to metaplasia.

In another study (James, 1972a), ewes were fed 400 g per day dried locoweed for 30 day at different stages of pregnancy (Days 0-30, 30-60, 60-90, 90-120,120-term). Extensive trophoblastic vacuolation was found at all stages of pregnancy. The most extensive vacuolation occurred early in pregnancy. Vacuolations began to resolve soon after cessation of locoweed feeding, taking place gradually within 45 days. In the 0-30 day feeding trial, interruption of vascular development, interference with placental development, and interruption of fetal fluid balance were observed. In the 30-60 day feeding trial, different degrees of hemorrhage over the surface of the fetuses, smaller cotyledons, and

fetal edema were reported. In the 60-90 day feeding period, an enlarged heart, thyroid gland and spleen, ascites, edematous fetuses, and fragile bones were reported. Also ascites, dead and edematous fetuses were observed in the 90-120 day feeding trial. Fetal deformity was observed when locoweed was fed during the 60-90, 90-120, and 90-120 intervals.

In a study by Ellis et al. (1985), pregnant ewes were fed 300 or 400 g of locoweed from the 20 to 50 days of gestation. Serum progesterone significantly decreased in a dose dependent-manner and cotyledonary prostaglandin values were significantly increased. These changes, along with the estrogenic activity of locoweed (James and Foote, 1972) were suggested as the reasons why the toxin induces fetal death and abortion.

Locoweed-induced congenital malformations can occur at any time during gestation, indicating that the time of fetal insult is highly non-specific (James et al., 1969). The principle congenital malformations include brachygnathia, lateral rotation of the fore limbs, contracted tendons, hypermotility of the hock joint, flexure of the carpus, and anterior flexure of the hock and stifle joints. Recovery from flexure of the carpal joint was spontaneous, but there was no recovery from lateral rotation of the forelimbs. Consumption of locoweed especially in late stages of pregnancy is associated with neonatal mortality even of lambs that are apparently normal. Lambs from mothers ingesting locoweed failed to suckle within 2 hours after birth and were slower to stand than controls. Further, locoweed toxin is excreted in milk and can result in further intoxication of nursing offspring (Pfister et al., 1993).

In a study by James (1971), fetal lambs from ewes fed 380-450 g per day at different stages of pregnancy demonstrated thymic hypoplasia. No significant histological findings were found in lambs born to ewes fed between 40-110 days for 20 days; however, one lamb born to a ewe fed from day 100-120 of gestation showed cytoplasmic vacuolation of the proximal renal tubules, hepatocytes, and follicular cells of thyroid and adrenal glands. No neurological symptoms were observed in neonates. The active toxic compound of locoweed had no adverse effect on the development and viability of preimplanation bovine embryos *in vitro* (Wang et al., 1999).

Ultrasonographic examination of ewes at different times of gestation after being fed locoweed (2.7 kg pellets per day, 15% Astragalus and 85% alfalfa hay) at day 60, 74, or 88 of gestation revealed that locoweed decreased fetal heart rate, caused cardiac irregularity, and decreased the strength of fetal heart contractions. Aborted fetuses had cardiac hypertrophy (which is similar to symptoms occurring in cattle grazing locoweed at high elevations), right ventricular dilatation, rounded apex of the heart and generalized edema (Panter et al., 1987). In a similar study by Bunch, et al. (1992), it was suggested that prolonged lack of fetal movement could be the reason for congenital deformities.

Reproductive effects of locoweed ingestion extend beyond maternal and embryologic/fetal manifestations. In rams (James and Van Kamper, 1970), locoweed caused reduction in spermatogenesis. A decreased percentage of normal sperm and reduced sperm motility were also reported. Numerous cytoplasmic vacuolations were found in cells of the testes, epididymis, and vas

deferens and to some extent in those of accessory sex glands. These changes occurred within 40-60 days of feeding. On longer exposure (70 days) rams showed decreased libido and transient degenerative changes of the testis, epididymis, and vas deferens. As seems to be true of most cases of locoweed intoxication, these changes were transient and resolved after cessation of feeding. In a later study by Panter et al. (1989), locoweed feeding in rams caused transient degenerative changes in the seminiferous, epididymal, and vas deferens epithelium.

In a study by James et al. (1986), calves consuming locoweed at high elevations developed clinical signs of congestive heart failure. Further gross and microscopic lesions of congestive heart failure as well as vacuolations associated with locoweed poisoning, were demonstrated in postmortem examination.

Most locoweed lesions progress in a threshold-like fashion (Stegelmeier et al., 1999). After a dose adequate to initiate a lesion in a tissue has been given, the extent and distribution of the lesions do not become more severe with higher doses. Animals may recover in the early stages, but the more severely they become affected, the more slowly they recover (James et al., 1967). Most lesions associated with locoweed resolve within several days of discontinuing locoweed feeding. Neurological effects require several weeks to resolve. Normal estrous cycling resumes after discontinuing locoweed feeding, but conception can be delayed for up to three estrous cycles. Some of the malformed offspring recover spontaneously. Microscopic lesions disappear from both maternal and fetal tissues after locoweed is removed from the diet; however, when the animal that

has consumed locoweed is stressed, it will display abnormal behavior even if the stress occurs years after locoweed was eaten.

Swainsonine (active compound of locoweed)

Observing the similarities between locoweed and swainsona poisoning in Australia (James et al., 1970) was the first step in determining the causative agent of locoweed intoxication. The toxic agent of locoweed (swainsonine) was isolated by Molyneux and James (1982) and confirmed by other researchers (Tulsiani et al., 1984).

Swainsonine, an indolizidine alkaloid, is a potent inhibitor of both lysosomal α-D-mannosidase (involved in cellular degradation of polysaccharides) (Dorling et al., 1980) and Golgi α-mannosidase II (a key enzyme in the processing of *N*-linked glycoproteins) (Kornfeld and Kornfeld, 1985; Elbein, 1991; Jacob, 1995; Moremen, 2002). Inhibition of lysosomal mannosidase leads to accumulation of lysosomal vesicles containing oligomannose structures (a variety of mannose-containing oligosaccharides derived from high-mannose, complex, and hybrid oligosaccharides) (Tulsiani et al., 1988 and 1990) similar to that observed in hereditary lysosomal storage disease (DeGasperi et al., 1991; Jolly and Walkley, 1997). The inhibition is dose-dependent and reversible. Inhibition of Golgi α-mannosidase II leads to accumulation of high mannose or hybrid type oligosaccharide.

Due to swainsonine's ability to inhibit glycoprotein processing, it has been used both diagnostically (in characterizing glucosidases and unraveling of the intricacies of glycoprotein processing) and therapeutically (as experimental anti-

cancer therapy). Swainsonine is the first glycoprotein processing inhibitor to be selected for clinical testing as an anti-cancer agent (Goss et al., 1994 and 1997).

Glycosylation inhibitors such as swainsonine are used to determine the role of specific structures in glycoprotein function by blocking reactions at different steps, causing the cell to produce glycoproteins with altered carbohydrate structures. The function of these glycoproteins can be assessed. Glycoprotein processing inhibitors are used to characterize newly isolated glycosidases, as well as to compare these processing enzymes from different organisms. Stroop et al. (2000) studied the analysis of *N*-linked oligosaccharides on human epidermal growth factor receptors secreted from A431 cells after interference of glycoprotein synthesis with treatment with swainsonine. Kosuge et al. (2000) studied the role of oligosaccharides in triggering of T-cell function using these compounds. Oligosaccharide processing inhibitors were used to investigate the role this processing plays in the function and antigenicity of measles virus glycoproteins (Bolt et al., 1999), and to elucidate the structure of rabies virus glycoprotein (Wojczyk, et al., 1998). They were also used for characterization of biochemical activity of newly discovered enzymes (Porwoll et al., 1999).

Swainsonine is thought to have potential activity in suppressing tumor growth because increased sialylation and branching of asparagine-linked oligosaccharides have been associated with neoplastic transformation and metastatic behavior of murine tumor cell lines (Dennis, 1986; Humphries et al., 1986; Humphries and Olden, 1989; Korczak et al., 1994; Granerus and

Engstrom, 2000). Also, increased branching has been noted in primary tumors of human carcinoma of the breast, colon, and skin and appears to correlate with disease progression (Dennis and Laferte, 1989; Fernandes et al., 1991). It has been shown that up-regulation of the enzymes necessary for the formation of complex-type oligosaccharides is mandatory for expression of a malignant phenotype. Even in normal tissues complex type oligosaccharides are restricted to cells capable of invasion *i.e.* trophoblasts, endothelial cells, interstitial fibroblasts, and activated lymphocytes (Fernandes, 1991; Lemaire et al., 1994). Swainsonine neurotoxicity is dose-limited and may not occur at swainsonine levels capable of preventing metastasis (Bowen et al., 1993).

Several tissue-specific mannosidases have been identified and interestingly, the accumulation of oligomannose structures is *not* observed in murine brain tissues when the animals are fed swainsonine, and the subjects do not develop neurological symptoms. That allowed Dennis (1986) to test swainsonine for its ability to inhibit solid tumor growth and metastasis. This work showed that inhibition of lung colonization by B16F10 melanoma cells can be enhanced by supplementing the hosts' drinking water with swainsonine. He also showed that swainsonine, when administered in combination with the interferon-inducing agent polyinosinic:polycytidylic acid, inhibited solid tumor growth and metastasis *in vivo*. Swainsonine enhanced the antiproliferative effects of interferon *in vitro*. Humphries et al. (1986) showed that swainsonine treatment of B16F10 melanoma cells inhibited experimental metastasis. Dennis et al. (1990)

showed that swainsonine reduced the growth rate of human melanoma cells both *in vitro* and *in vivo*.

Goss et al. (1995) discussed in detail the possible mechanisms of the anti-cancer effect of swainsonine. Their suggestions were that 1) Swainsonine adversely affects tumor cells through interference with tumor cell adhesion to endothelium. This is supported by data showing that swainsonine treatment of tumor cells reduces the number of Galβ1-4GlcNAc antennae in *N*-linked carbohydrate, which contributes to the retention of blood-borne tumor cells in the microvasculature. Swainsonine reduced the attachment of MDAY-D2 tumor cells to endothelial monolayer *in vitro* (Cornil et al., 1990); 2) It inhibits tumor cell invasion through the extracellular matrix *in vitro* (Seftor et al., 1991); 3) It has an effect on the patient immune system. Swainsonine is thought to have a stimulatory effect on different aspects of the immune system. It increases the activity of natural killer cells. Fujieda et al. (1994) studied the effect of swainsonine on the cytotoxicity of lymphokine-activated killer (LAK) cells against autologous thyroid cancer. The cytotoxicity of swainsonine-treated LAK cells against autologous thyroid cancer cells was found to be significantly greater than that of the standard LAK cells incubated with interleukin-2 alone. Also, thyroid cancer cells incubated with swainsonine (as compared to non-treated tumor cells) showed much higher susceptibility to LAK killing. These results suggest that swainsonine has potential immunomodulatory properties in the treatment of thyroid cancer. Humphries et al. (1988, 1990) showed that the growth and metastasis of B16F10 melanoma cells were reduced in the presence of

swainsonine. Pretreating mice with swainsonine had little effect on tumor cells when natural killer cells were eliminated experimentally. Swainsonine increased activity of natural killer cells which participated in elimination of tumor cells. Dennis and Laferte (1985) have shown that the glycosylation mutant of Chinese hamster ovary cells and MDAY-D2 tumor cells were more sensitive than wild cells to natural killer cell lysis. Systemic administration of swainsonine promotes the proliferation of murine bone marrow cells and colony forming activity *in vivo* and *in vitro*, which indicates that swainsonine can be administered in conjunction with chemotherapeutic agents to abrogate myelosuppressive effect of these agents (White, et al., 1991; Oredipe et al., 1991 and 2003; Roberts et al., 1998; Klein et al., 1999). However, Misago et al. (2000) in their *in vitro* study on human bone marrow cells concluded that swainsonine suppressed maturation from myelocytes into mature neutrophils. Also Taylor and Strickland (1998) indicated that swainsonine may have a negative effect on ovine and bovine T-cell function because it suppressed phytohemagglutinin-P-induced proliferation on peripheral lymphocytes. In investigations directed at determining the effect of locoweed on the immune system, locoweed-exposed ewes showed a gradual numerical decrease in total leukocytes, particularly lymphocytes, in peripheral blood (Sharma et al., 1984; Panter et al., 1989). Peripheral leukocytes showed cytoplasmic vacuolation. These authors indicated that locoweed seems to have a selective effect on cell mediated immune responses rather than humoral ones. These findings sound a cautionary note for possible clinical uses of swainsonine as an immunomodulator. A consistent finding in many studies is that shorter,

intermittent treatment periods in mice maintain immunostimulation, which is an important function in cancer therapy, and may be one of the reasons for the clinical efficiency of swainsonine.

In a phase I clinical trial of swainsonine (Goss et al., 1994), patients were given a continuous intravenous infusion over a period of 5 days, repeated at 28-day intervals. Dose levels were escalated in increments of 100 micrograms per kg per day from 50 to 550 micrograms. The maximum tolerated dose and the recommended starting dose were 550 and 450 micrograms per kg per day, respectively. Common side effects included edema and a rise in serum asparatate aminotransferase. One patient with head and neck cancer showed 50% tumor shrinkage. Two patients showed symptomatic improvement.

In a later phase IB clinical trial of swainsonine, Goss et al. (1997) studied the effects of bi-weekly oral swainsonine at escalating dose levels (from 50 to 600 micrograms per kg) in 16 patients with advanced malignancies and 2 HIV-positive patients who were not viable candidates for conventional therapy. The maximum tolerated dose in these trials was defined as 300 micrograms per kg per day, due primarily to serum AST abnormalities and dyspnea. Other adverse events present in more than 20% of patients included increased serum AST (all patients); fatigue (n = 9); anorexia (n = 6); dyspnea (n = 6); and abdominal pain (n = 4). Examination of immunological parameters revealed a transient decrease in $CD25^+$ peripheral blood lymphocytes and, in seven of eight patients, an increase in $CD4^+$:$CD8^+$ ratios at 2 weeks. These investigators concluded that oral swainsonine is tolerated when given as a chronic intermittent administration at

doses up to 150 microgram per kg per day. Adverse effects that were considered to be drug-related were similar to those observed in the infusional study, but additionally, fatigue and neurological effects were encountered. These side effects of swainsonine are somewhat similar to what is seen in animal studies and could be due to its effect on lysosomal α-mannosidase. Such effects might be eliminated by synthesis of swainsonine analogs that have Golgi α-mannosidase II activity, but lacking lysosomal α-mannosidase activity; or by adjusting the dosing schedule to minimize its effect on such enzyme.

Swainsonine Absorption and Clearance

Diagnosis of locoweed poisoning is performed by analyzing serum for α-mannosidase activity (Stegelmeier et al., 1994) and swainsonine concentration (Stegelmeier et al., 1995 a and b). Animals fed locoweed had lower serum α-mannosidase activity, higher levels of alkaline phosphatase (ALP), aspartate aminotransferase (AST) and lactate dehydrogenase. Treated animals also showed a decrease in serum total protein and albumin and thyroid concentrations (Stegelmeier et al., 1994). Serum α-mannosidase activity decreased within 24 hours of feeding locoweed. The levels returned to normal 6 days after treatment was discontinued. There was an increase in serum swainsonine level within 24 hours after treatment with locoweed, and it remained high until it was cleared from the serum. This occurred after treatment was stopped with a 20-hour half life. Swainsonine was cleared from skeletal muscles, brain and heart within 20 hours, but from liver, kidney and pancreas within 60 hours. Swainsonine is rapidly cleared from the serum and serum α-mannosidase

level recovers quickly, but tissue repair and return to normal function occur more slowly (Stegelmeier et al., 1995a and 1998). Mannose-containing oligosaccharides were elevated as early as day 3 of feeding, but maximum levels were not attained until after 6 weeks of feeding.

Swainsonine can be detected in tissues of most organs from animals ingesting locoweed. The concentration in tissues is correlated to the amount of locoweed ingested, but not the length of the exposure. There is individual animal variability in swainsonine absorption, metabolism, and excretion. Animal tissues such as liver and kidney that accumulate high swainsonine concentrations develop lesions more rapidly but at lower rate of locoweed ingestion than other organs. Locoweed intoxication also causes an unusual pattern of urine oligosaccharides, which might be correlated with the onset of the clinical sings (Warren et al., 1983; Daniel et al., 1984).

Swainsonine and Angiogenesis

Some investigators reported an inhibitory effect of swainsonine on the development of placental vasculature (James et al., 1967; Van Kampen and James, 1971; James, 1972a and b), and an anti-angiogenic action has subsequently been assumed to underlie the toxicity of this agent (Balls and James, 1973; James et al., 1992; Bunch et al., 1992; Panter et al., 1999). However, to the best of our knowledge there are no formal quantitative studies of how swainsonine may affect placental angiogenesis, nor of its mechanism of action in mediating such effects. There are no studies of swainsonine's effect on the expression of angiogenic mediators. The work presented here is intended to

provide some important information on the effect of swainsonine on the localization of VEGF protein and expression of VEGF and its receptors' mRNAs. The present study will also provide qualitative and quantitative information on the vascularization of the caprine placenta and ovary during pregnancy and how swainsonine affects the process.

The data on placental development will supplement and expand on what is already known about the goat, an economically important animal; this is one goal. Using the caprine model to correlate anatomical, cellular, and molecular studies of angiogenesis in the presence of a drug now in testing as an anti-tumor agent should also provide a better understanding of the mechanics of the process.

Materials and Methods

Experimental Groups

The experimental protocol and all procedures used in this work were reviewed and approved by the Virginia Tech Animal Care and Use Committee. The procedures described below were applied to three groups of goats: one group of non-pregnant does, and two groups of synchronized pregnant does. Animals were randomly assigned to one of these groups. One group of the pregnant animals was allowed to progress normally; the second was treated with swainsonine. Does were a cross between Boer and Spanish goats and aged between 2.5 and 3 years. All came from the same flock, all had a previous history of successful pregnancies, and all were brought to the college at the same time and housed under the same conditions in identical quarters.

Estrus Synchronization

The entire flock of fifty doe goats was synchronized using a combination of norgestomet ear implants (Synchromate-B®) and $PGF_{2\alpha}$ (Dinoprost) (Lutalyse®) (Hafez et al., in preparation) (Fig. 1). Teaser males were introduced 15 days before the start of the synchronization program and removed on the first day of the synchronization program. Animals were fed 250-500 g of concentrates (Sweet goat feed®, Southern States Cooperative, Inc., Richmond, VA, USA) three weeks before the start of the synchronization program. Synchronization began with a single intramuscular injection of $PGF_{2\alpha}$ (Lutalyse®) followed by an application of norgestomet ear implants (Synchromate-B®) two days later. The does received an intramuscular injection of PG600® (a combination of eCG and

hCG) one day before the implant removal. The implants were removed on Day 11 and were immediately followed by an intramuscular injection of prostaglandin (Lutalyse®). Buck goats of proven fertility from the same farm of origin were introduced to the does late on the same day of implant removal and kept with the does for four days (the ratio of males:females was 1:10). Animals were observed closely for signs of estrus. Pregnancy checks using ultrasonography started at 4 weeks from the last day of bucks' presence and were performed every three weeks. The schedule can be summarized as follows:

Day - 15: Teaser males introduced

Day 0: A single intramuscular injection of 15 mg Dinoprost (Lutalyse®)

Day 2: Insertion of a 6.0 mg norgestomet ear implant (Synchromate-B®). This implant remained in place until Day 11.

Day 10: A single intramuscular injection combining 200 IU eCG + 100 IU hCG (2.5 ml of PG600®).

Day 11: Implant removal and a second injection of 15 mg Dinoprost.

Introduction of males of proven fertility

Day 15: Males removed.

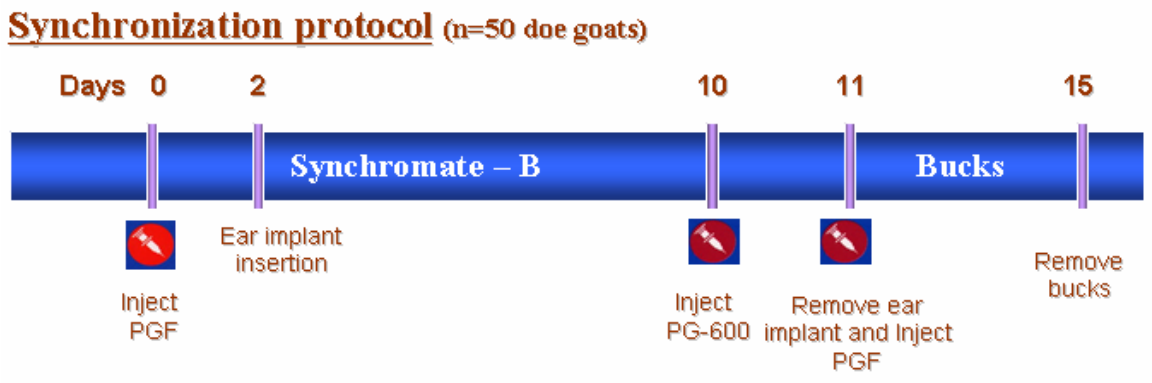

Fig.1. Synchronization protocol

Pregnant untreated does were euthanized at 4, 7, 10, 13, 16, and 18 weeks of pregnancy. Does treated with swainsonine were euthanized at 7 and 18 weeks, after having been given 150 g ground locoweed (*Astragalus Lentiginosus*) containing 0.15% swainsonine (kindly provided by the USDA Poisonous Plant Research Lab Accession # 98-02), which is a relatively high swainsonine content compared to other plants. The locoweed was collected by USDA, ARS personnel in St. Johns, Arizona). Locoweed was administered by gavage twice per day beginning a week before euthanization. Blood samples were collected from swainsonine-treated and control pregnant does at the same stage of pregnancy before the first administration of swainsonine, and then every other day. Serum analysis was performed to obtain an estimate of the amount of swainsonine absorbed (Stegelmeier et al., 1995a and b). Amniotic and allantoic fluid samples were also analyzed for the presence of swainsonine.

Eight reproductive tracts from non-pregnant goats were used to study the normal gross anatomical distribution of vessels to the reproductive organs; three of these were prepared using the tissue clearing technique, three were teaching specimens previously prepared in our laboratory using standard embalming/latex injection, and two were prepared using corrosion casting. At least two cleared specimens were studied at each stage of pregnancy. With the exception of one specimen at the 7-week stage, all specimens had multiple fetuses. Six cleared specimens had triplets and 5 had twins. All specimens (cleared and casted) were used to study the origin of major vessels. Incompletely injected or missing vessels in any particular specimen were excluded from the study and the supply

of the area was reported as missing. We calculated the percentage of specimens showing a particular pattern of vessel distribution by dividing the number of specimens showing that pattern by the number of total specimens used to study the pattern in question. Radiographs were taken from cleared specimens to show the vascular pathways.

Three non-pregnant reproductive tracts were prepared using microvascular corrosion casting and at least two reproductive tracts were studied at each stage of pregnancy. Two reproductive tracts from swainsonine-treated does were studied at 7 and 18 weeks.

Uterine and ovarian tissues were collected from two non-pregnant does, one doe at each stage of pregnancy, and at 7 and 18 weeks of gestation from swainsonine-treated animals to be processed for immunohistochemistry and real-time quantitative polymerase chain reaction (real-time Q-PCR).

Animal Preparation

The following procedures were applied to all animals. The specific procedures for each group of specimens are discussed separately under each technique.

Doe goats received an intramuscular (IM) injection of Xylazine (0.2 mg/kg of body weight) and Atropine (0.04 mg/kg) 10 minutes after administration of an IM injection of Acepromazine (0.05 mg/kg). The does were then anesthetized by intravenous injection of Ketamine (5.0 mg/kg) 10 minutes after sedative injection. They were injected intravenously with 10 ml of Heparin (1000 i.u.) to suppress coagulation. Animals were exsanguinated via a cannula placed in the common

carotid artery, then the cannula was subsequently used as an inflow port for perfusion with heparinized physiologic saline (1.0 ml Heparin per liter). Saline was infused at about 40^{o}C (normal range of body temperature of the goat is 39-40^{o}C). Blood and saline were allowed to flow out of a cannula placed in the external jugular vein. Blood washout was performed using a Portiboy embalming pump, Model PE10 (Portiboy Company, Westport, Connecticut, USA) at a rate of 90 ml/min and a 34.5 kPa pressure. The abdominal wall was opened along a ventral midline incision. The esophagus and rectum were ligated, and the digestive organs were removed to expose the abdominal aorta and reproductive organs.

In animals assigned for preparation of microvascular corrosion casts and cleared specimens, all vessels supplying non-reproductive organs were ligated. The reproductive tract was injected through the abdominal aorta via a high-density polyethylene cannula placed just cranial to the origin of the ovarian arteries. A three-way stopcock was placed in line between the cannula and the syringe to permit change of syringes. The vasculature of the reproductive tract was injected using either Microfil® (Flow Tech Inc., Carver, MA, USA) with subsequent clearing of the surrounding tissues or modified Batson's No. 17® mixture (Polysciences, Inc., Warrington PA, USA) with subsequent corrosion of the tissues.

The following tissue specimens were collected: 1) placentomes from pregnant does; 2) caruncles from non-pregnant does; and 3) right and left ovarian tissues from both pregnant and non-pregnant does. Immediately upon

collection, the specimens were immersed in freshly prepared 4% paraformaldehyde for 4 hours at 4^{o}C to be processed for immunohistochemistry; or immersed in RNA Later® solution (Qiagen Inc, Valencia, California, USA) for storage at 4^{o}C prior to RNA isolation to be processed for real-time QPCR.

Tissue Clearing

The tissue clearing technique consists of the injection of a casting medium into the vascular system, fixation, dehydration, clearing of the surrounding tissues, followed by observation and photography of the resulting cleared specimen. Infusion of the arterial blood vessels of the reproductive tract was performed through the aorta via a cannula placed just cranial to the origin of the ovarian arteries. The tract was infused with physiological saline (40^{o}C) at a rate of 5 ml/min using a Harvard infusion pump, Model 22 (Harvard Apparatus, Inc., Holliston, MA, USA), then with white Microfil® MV series, at the same rate using the same infusion pump. Red Microfil® was used in a few specimens. Microfil compound was mixed with an equal quantity (by weight) of a mixture of MV and HV diluents followed by the addition of 5% of the curing agent. The filling of the vasculature was considered complete when Microfil was visible to the naked eye in the fine vessels of the caruncles. The whole hindquarters were immersed in physiological saline during and after injection to allow free flow of Microfil in the vasculature. The specimen was left in place for 4 hours at room temperature then refrigerated overnight to ensure complete polymerization of Microfil.

The entire reproductive tract with its mesenteries was removed intact, pinned to a dissecting pad, and fixed in AFA (300 cm^3 95% alcohol, 100 cm^3 10%

buffered formalin, 100 cm^3 glacial acetic acid, 500 cm^3 distilled water) for 24-48 hours (Orsini, 1962). At least one tract at each stage was cleared using the alcohol-methyl salicylate clearing sequence and another one using glycerin clearing (Orsini, 1962; Del Campo et al., 1974). When alcohol-methyl salicylate sequence was intended, the tract was dehydrated after fixation in an ascending ethanol series starting at 50% at 10% increment between 50 and 90% then 5% at 95 and 100%, with one change each between 50 and 90%. Two changes were used at each of the 95 and 100%. The time interval between ethanol changes depended on the size of the specimen; it ranged from 24-72 hours to ensure proper dehydration. Hydrogen peroxide was added to each of the 70 and 80% alcohols (one milliliter of 30% hydrogen peroxide per one liter of alcohol) for bleaching. The dehydrated tract was then immersed in methyl salicylate (VWR International, West Chester, PA, USA) where it was stored and studied.

When glycerin clearing was intended, the tract was immersed after fixation in decreasingly dilute glycerin/distilled water baths beginning at 50% at 10% increments. The time interval between glycerin changes depended on the size of the specimen; it ranged from 48-96 hours. These specimens were stored and studied in 100% glycerin (VWR International, West Chester, PA, USA).

Specimens prepared by both of these methods can be stored indefinitely and studied while immersed in the clearing agents. Photographs of the cleared specimens were taken while immersed in the clearing solution using an Olympus digital camera.

Microvascular Corrosion Casting

The microvascular corrosion casting/SEM method consists of the injection of a casting medium into the vascular system, corrosion and thus removal of tissue elements, and observation of the resulting casts under a scanning electron microscope (SEM) (Hodde and Nowell, 1980; Motta et al., 1992). The reproductive tract was injected with saline and a casting medium via a cannula inserted in the abdominal aorta just cranial to the origin of the ovarian arteries. Ovarian veins were opened on both sides to provide outflow ports for saline and the casting medium. The reproductive tract was infused with physiologic saline (40^{o}C) mixed with procaine 0.5% at a rate of 5 ml/min using a Harvard infusion pump, Model 22 (Harvard Apparatus, Inc., Holliston, MA, USA). A second perfusion with cold saline (4^{o}C) was performed to minimize the extravasation of the casting medium and to delay polymerization. Modified Batson's No. 17® mixture, containing 25 ml Batson's No. 17 monomer, 12 ml methyl methacrylate, 7.5 ml catalyst, and 0.5 ml promoter, was infused through the aorta using the same infusion pump at the same flow rate. The casting mixture was modified after the method described by Nopanitaya (1979). Batson's No. 17 monomer was mixed with methyl methacrylate, and this mixture was divided into two equal parts. The catalyst was added to one half and the promoter to the other half. All components of the casting mixture were kept at 4^{o}C even during preparation of the mixture. The intact hindquarters of the goat were kept in cold physiologic saline (4^{o}C) during the injection procedure to prevent premature polymerization of the casting medium and to allow free flow of the medium into the vasculature.

Mixtures containing the catalyst and promoter were combined just before injection. Injection of the utero-ovarian microvascular bed was judged as complete when the casting medium was seen flowing out of the ovarian vein. The aorta and ovarian vein were clamped after injection to prevent efflux of the casting medium and to maintain the injection pressure. Once the injection was completed, the cold saline was substituted with a 25^{o}C saline solution for 30 minutes then at 60^{o}C overnight to ensure complete polymerization of Batson's mixture.

The infused specimen was left floating in distilled water for three days. Subsequently, the reproductive tract was excised from the rest of the hind quarters and immersed in distilled water mixed with papain, 2.0 g/L (Adolph's Tenderizer, available from local food suppliers) for 2-3 days. Chemical corrosion was performed by alternating immersion in 40% KOH (Fisher Scientific International Inc.) and distilled water at 55-60^{o}C. After completion of maceration, the casts were kept for a few days in distilled water with frequent changes to remove KOH residues.

The following areas were excised from each specimen using scissors: at least one caruncle from each uterine horn in the case of multiple pregnancies; and from the pregnant horn in the case of single pregnancy; and the right and left ovaries in all cases. The casts were immersed in 95% ethanol for 15 minutes and air dried overnight in a fume hood. Thereafter they were stored dry under vacuum in a desiccator.

Casts were prepared for SEM examination by mounting on aluminum stubs using double-sided carbon tape and silver conducting paste; and sputter coating with a layer of palladium-gold about 50 nm thick. A thicker coating was necessary in specimens used for the descriptive part of the study in order to reduce the charging caused by the thickness and complexity of the casts. Casts were viewed and photographed on a Zeiss EVO40 XVP scanning electron microscope. Casts were observed for filling defects, presence of blind ends, leakage, and lack of endothelial cell impressions to guarantee good quality casts before taking measurements. Casts were viewed at various levels of magnification to study branching patterns. Most caruncles were studied intact; however, for the descriptive part of the study, manually sectioning of some specimens was necessary.

Image Analysis

Two quantitative measurements could be obtained from the internal (facing the uterine lumen) side of the caruncular casts: capillary diameters from non-pregnant and capillary sinusoidal diameters from pregnant does, and capillary density index coupled with digital imaging analysis (Nelson, 1987). Capillary diameters were measured on the microscope using the *point-to-point marker* tool in the manufacturer's software package. At least 50 capillary diameters in each caruncle could be measured in non-pregnant and 4-week-pregnant does and from 20-50 capillary sinusoidal diameters in specimens at later stages of gestation.

Images for measuring the capillary density index were taken at X1000 magnification in caruncles from non-pregnant and 4-week-pregnant does and at X50 at later stages of pregnancy. We tried to get as many images as we could from each caruncle to represent most of the total surface area of the internal side of the caruncle. Each image was taken in such a way as to begin at the last point covered by the previous one, thus creating a photomontage of the entire caruncular surface. From 1-10 images were obtained from each caruncle according to the size. Micrographs were taken at 10 kv, with final aperture of 100 μm, and a working distance of at least 25 mm.

Computer-assisted image analysis software (IP Lab, Biomedical Imaging Group) was used to measure the capillary density index. The grey level was set to cause the regions covered by capillaries to appear white and other areas to appear black (Fig. 2). The ratio of the number of white pixels to black and white pixels was taken to be the percentage of the surface covered by capillaries. Black-white binary files were made from images and used to calculate the percentage of the surface area of the internal side of the caruncle covered by capillaries. The ratio of white area to the total area was defined as the capillary density index.

Graphic Demonstration and Statistical Analysis

Graphic demonstration of capillary diameters was performed using Microsoft Excel software. For capillary density index measurements, in the cases when more than one image had to be taken to represent most of the total caruncular surface, the mean of the values obtained from image analysis was

calculated. Analysis of the significance of the differences between specimens from non-pregnant and pregnant does, pregnant does at different stages, and normal pregnant and swainsonine-treated at 7 and 18 weeks of gestation were performed using ANOVA and Tukey adjustment for pairwise comparisons. A P value of < 0.05 was considered significant.

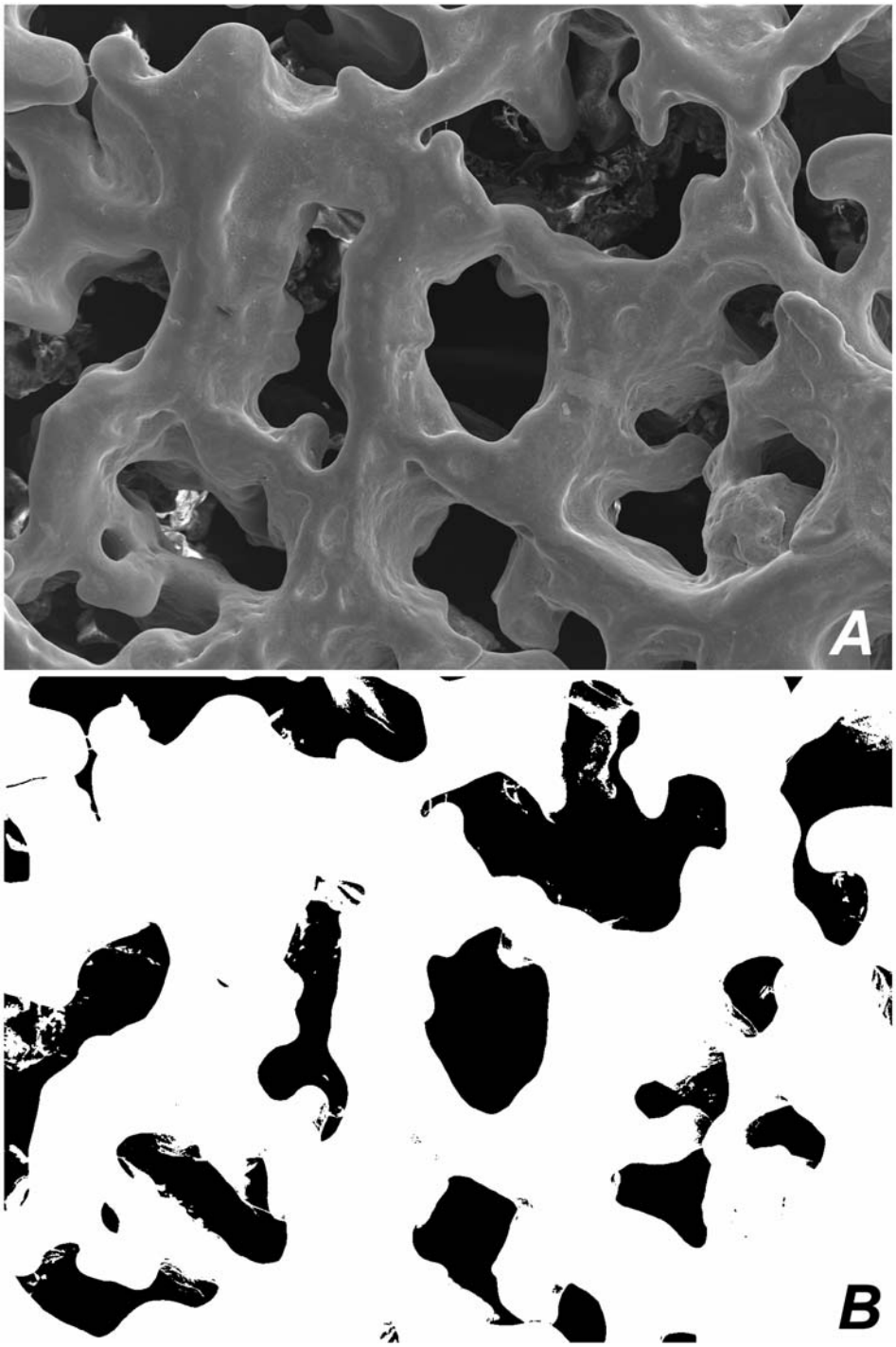

Fig. 2. Scanning electron micrographs of the fetal side of a pregnant caprine caruncle. Using computer-assisted image analysis software, the grey level was set to cause the regions covered by capillaries to appear white and other areas to appear black in ***B***. Black-white binary files were made from images and used to calculate the percentage of the surface area of the fetal side of the caruncle covered by capillaries. The ratio of white area to the total area was defined as the capillary density index (CDI). ***A*** is the image before processing. ***B*** is the image after processing. The CDI of this image is 84.3%.

Immunohistochemistry

Paraffin-embedded sections 6.0 μm thick were prepared and immunolocalization of VEGF was performed using the avidin-biotin-horseradish peroxidase system (R.T.U. Vectastain® universal ABC kit, Vector Laboratories, Burlingame, CA, USA). The embedded sections were deparaffinized in xylene and rehydrated in increasingly dilute ethanol/distilled water baths. For antigen retrieval, slides were heated in a pressure cooker at 103.4 kPa for 5 minutes while immersed in an antigen unmasking solution (Vector Laboratories). Slides were incubated in 1% hydrogen peroxide in methanol for 30 minutes to block endogenous peroxidase, then washed and incubated with 5% bovine serum albumin in phosphate buffer saline (PBS) for 15 min followed by incubation with 2.5% normal horse serum for 20 min to prevent non-specific binding of the primary antibody to tissue components. The sections were then incubated with the primary antibody overnight in a humid chamber at 4^{o}C. Following the incubation they were washed in PBS and incubated with a biotinylated horse anti-mouse/anti-rabbit IgG for 30 minutes at room temperature. A final incubation, after washing, with ABC (avidin:biotinylated horseradish peroxidase complex) reagent lasted 30 minutes under the same conditions.

Immunoreactivity was visualized with 3,3- diaminobenzidine (DAB substrate kit, Vector Laboratories) in a dark place as outlined in the manufacturer's protocol. Slides were counterstained with Mayer's haematoxylin, dehydrated, cleared in xylene, and mounted.

Two primary antibodies from two different manufacturers were used for VEGF immunolocalization: VEGF (AB-2) (Oncogene Research Products, San Diego, CA, USA, dilution 1:1000 in 1.5% normal horse serum in PBS) and sc-507 (Santa Cruz Biotechnology, Santa Cruz, CA, USA, dilution 1:1500 in 1.5% normal horse serum in PBS). VEGF (AB-2) is a rabbit polyclonal IgG that recognizes the 121-, 145-, 165-, 189-, and 206-amino acid splice variants of human VEGF. Sc-507 is a rabbit polyclonal IgG that recognizes the 121-, 165- and 189-splice variants of human, mouse, and rat VEGF. Controls for non-specific immunostaining included incubation in which the primary antibody was replaced with rabbit IgG, normal horse serum, or buffer.

Photographs of histological sections were taken using an Olympus Vanox-T AH-2 light microscope connected to an Olympus DP70 digital camera. Presence or absence and the intensity of immunostaining to VEGF antibody were evaluated blindly and independently by two trained histologists using a scale on which the most intense reaction was assigned a value of 5 and an absence of immunoreactivity was assigned a value of 0, with varying degrees of intensity between these two numbers receiving scores of 1 to 4, based on the observer's perception of the intensity of staining.

Real-time Quantitative Polymerase Chain Reaction

Template Preparation:

Total RNA was isolated from tissues using an RNeasy® extraction kit (Qiagen, Valencia, California, USA). The quantity of total RNA was determined by measuring the absorbance at 260 nm in a spectrophotometer.

Complementary DNA was obtained by reverse transcription of total RNA, using the SuperScript III® first-strand synthesis system (Invitrogen, Carlsbad, California, USA) with random-hexamer priming according to the manufacturer's instructions. Complementary DNA was stored at – 20 ºC to be used for real-time QPCR.

Real-time Quantitative Polymerase Chain Reaction:

The expression of VEGF, Flt-1 (VEGFR-1, fms-like tyrosine kinase) and KDR (VEGFR-2 or Flk-1, kinase-insert domain-containing receptor) mRNAs was measured using the real-time quantitative polymerase chain reaction implementing a TaqMan® probe approach (Applied Biosystems, 2001; Heid et al., 1996; Gibson et al., 1996). This method is based on the 5′ nuclease activity of *Taq* polymerase, which cleaves a specific dual-labeled fluorogenic hybridization probe during the extension phase of PCR, releasing the reporter dye, resulting in an increase in fluorescence emission that is directly proportional to the number of target copies. Fluorescence is detected and quantified in real time. In this study, we used beta actin mRNA as an internal control for the relative quantification of VEGF, Flt-1 and KDR mRNAs.

Primers and Probes

We used Primer Express software® (Applied Biosystems, Foster City, CA, USA) to design primers and probes, based on caprine VEGF, Flt-1, KDR, and beta actin gene sequences obtained from the Genbank database (accession numbers AY114352, AY114355, AY114354, and AF481159, respectively) (Kawate et al., 2003). Primers and probes used for VEGF quantification were

selected to detect all known splice forms of VEGF. To avoid background signals due to amplification of contaminating genomic DNA in the cDNA preparation, probes were chosen to span exon-exon junctions. All primers and probes were checked for the absence of self-complementary sequences using Oligo Calculator software™ (www.basic.nwu.edu/biotools/oligocalc.html). Custom primers were ordered from Qiagen, and the TaqMan fluorogenic probes were prepared by Applied Biosystems (Table 1). A validation experiment (using serial dilutions of control templates) was performed to verify that the amplification efficiencies of targets and reference were equivalent.

Amplification

The amplification mixture of 25 µl contained 1x Universal PCR master mix (Applied Biosystems), 0.3 µ*M* of each primer, 0.2 µ*M* probe and 8 ng (RNA equivalents) of cDNA. In each experiment a master mix of the above components was made for each target cDNA/primers-probe combination and aliquoted into optical reaction tubes in triplicate.

The PCR was conducted under the following cycle parameters: initial holding at 50 ºC for 2 minutes; then 95 ºC for 10 minutes, followed by 40 cycles of melting at 95 ºC for 15 seconds and annealing/extension at 60 ºC for 1 min. Analysis was carried out using the sequence detection software supplied with ABI PRISM® 7700 sequence detection system (Applied Biosystems, 2001). This software calculates the threshold cycle (CT) for each reaction, and this CT is used to quantify the relative abundance of target, normalized to an endogenous reference (beta actin) and relative to a calibrator (we used the amount of

normalized target expressed at four weeks of pregnancy). The CT values for each set of three reactions were averaged for all subsequent calculations. The ratio of expression in test sample:calibrator sample was calculated as $2^{-\Delta\Delta CT}$, where ΔCT is the difference in CT values of the target and endogenous reference. $\Delta\Delta$CT can be calculated by subtracting ΔCT of the calibrator from ΔCT of the test sample (Livak and Schmittgen, 2001). Each assay included tested samples, no-template controls, and non-reverse transcribed RNA controls to verify the cDNA-dependence of signals.

Table (1): Sequences of primers and probes used

VEGF	Forward primer	5′-GCCCACTGAGGAGTCCAACA-3′
	Reverse primer	5′-TCTCCTATGTGCTGGCTTTGGT-3′
	Probe	5′-6FAM-CACCATGCAGATTATGCGGATCAAACC-TAMRA-3′
Flt-1	Forward primer	5′-GTGACCTGCTTCAAGCCAATG-3′
	Reverse primer	5′-AGAAGGCAGGTGTCGAGTACGTA-3′
	Probe	5′-6FAM-ACAACAGGATGGTAAAGACTACATTCCGCTCA-TAMRA-3′
KDR	Forward primer	5′-ATGATACTGGAACCTACAAGTGCTTCT-3′
	Reverse primer	5′-CTTCATGCTGGTCGCTAACAGA-3′
	Probe	5′-6FAM-ACCTGTAATCTTGAACATACACATAAACAGTGGAGGC-TAMRA-3′
β actin	Forward primer	5′-CGGGACCTGACGGACTACCT-3′
	Reverse primer	5′-CGGCCGTGGTGGTGAA-3′
	Probe	5′-6FAM-TGTAGCCACGCTCCGTGAGAATCTTCA-TAMRA-3′

Swainsonine Analysis

The amount of swainsonine present in the serum and uterine fluids was tested using Jack Bean α-mannosidase assay. Details are as follows.

Preparation of Standards and Samples:

Sodium acetate (0.25 M, pH 4.0) was combined with test fluid (serum, uterine fluid, control serum, or control uterine fluid) at ratio of 1:2. The mixture was boiled for 10 minutes, then allowed to cool, which was followed by centrifugation at

14000 rpm for 30 minutes. Test samples were refrigerated. The supernate of the standard samples were placed in the freezer.

Standard Curve Preparation:

Four ml of the standard samples were aliquoted into 4 microcentrifuge tubes and spun for 5 minutes. One hundred fifty µl of standards was placed in the first two wells of a 96 well Corning ELISA plate. Seventy-five µl of the standard sample was placed in the next 11 wells. Swainsonine (2.0 µl at 0.1 µg/µl) was aliquoted and, then mixed in the first two wells. Serial dilution of all wells was performed thereafter. All reactions were done in duplicate.

Samples:

Test samples were re-spun for 10 minutes then 75 µl were aliquoted in wells next to standards. The following steps apply to all wells:

Enzyme Preparation:

For every plate, 1800 ul of 0.25 M sodium acetate and 2.0 ul Jack bean α-mannosidase (Sigma- Aldrich) were mixed in the pipetting trough. Fifteen µl of the mixture was placed into each test well.

Substrate Preparation:

One thousand two hundred ul of 10mM p-nitrophenyl-α-D-mannoside (Sigma-Aldrich) was placed in each well. The samples were then incubated at 37^{o}C for 40 minutes. Using an 8-Channel pipette, 100 ul of glycine (2.5 M, pH 10.3) was allocated in each tested well. Absorbance was determined at 405 nm using a Bio-Rad model 3550 U (Bio-Rad Laboratories, Melville, NY, USA).

Results

Synchronization of Estrous and Breeding:

All does were in estrus within 72 hours after implant removal. Of these 66% (33/50) were in estrus within 24 hours and 22% (12/50) within 48 hours of implant removal. Seventy six percent (38/50) were pregnant when examined at 4 weeks. Of these 38, 2 aborted before 7 weeks, and another one before 10 weeks. Three does had four fetuses; 15 had triplets; and 12 had twins. Five does had single fetuses. Thus, 86 fetuses resulted from 38 pregnancies.

Swainsonine Levels in Treated Does:

Swainsonine level in the serum of treated does averaged 649.1 ng/ml through the week before euthanization, for those killed at 7 weeks of pregnancy; and 632.4 ng/ml at 18 weeks of pregnancy. These levels were higher than those reported in sheep (432 ng/ml) showing no clinical signs by Stegelmeier et al. (1995b); and similar to those reported in sheep (620 ng/ml) showing clinical signs while in a nutrient-restricted state by Taylor et al. (2000). Swainsonine was not detected in the amniotic fluid of does euthanized at 7 weeks of pregnancy, but it was detected in the amniotic fluid in those euthanized at 18 weeks at levels similar to those in serum (646.45 ng/ml). It was detected in allantoic fluid at both the 7- and 18-week time points at levels higher than in serum at 18 weeks (766.5 ng/ml), but not at 7 weeks (304.9 ng/ml).

With the exception of aspartate aminotransferase (AST), serum chemical parameters did not show any significant change in swainsonine-treated does. AST levels increased after swainsonine treatment at both 7 and 18 weeks. AST

increased from 53 and 58 before treatment to 218 and 247 after treatment, respectively in two swainsonine-treated animals at 7 weeks of pregnancy; and from 92 and 118 before treatment to 192 and 221 after treatment, respectively at 18 weeks.

Cleared Specimens

The uterus is supplied by branches of the ovarian arteries (*aa. ovarica*), uterine arteries (*aa. uterina*), and vaginal arteries (*aa. vaginalis*) (Fig. 3). No difference was observed in the origin and distribution of the ovarian, uterine, and vaginal arteries between pregnant and non-pregnant does; however, differences in these aspects existed within specimens from pregnant and/or non-pregnant does.

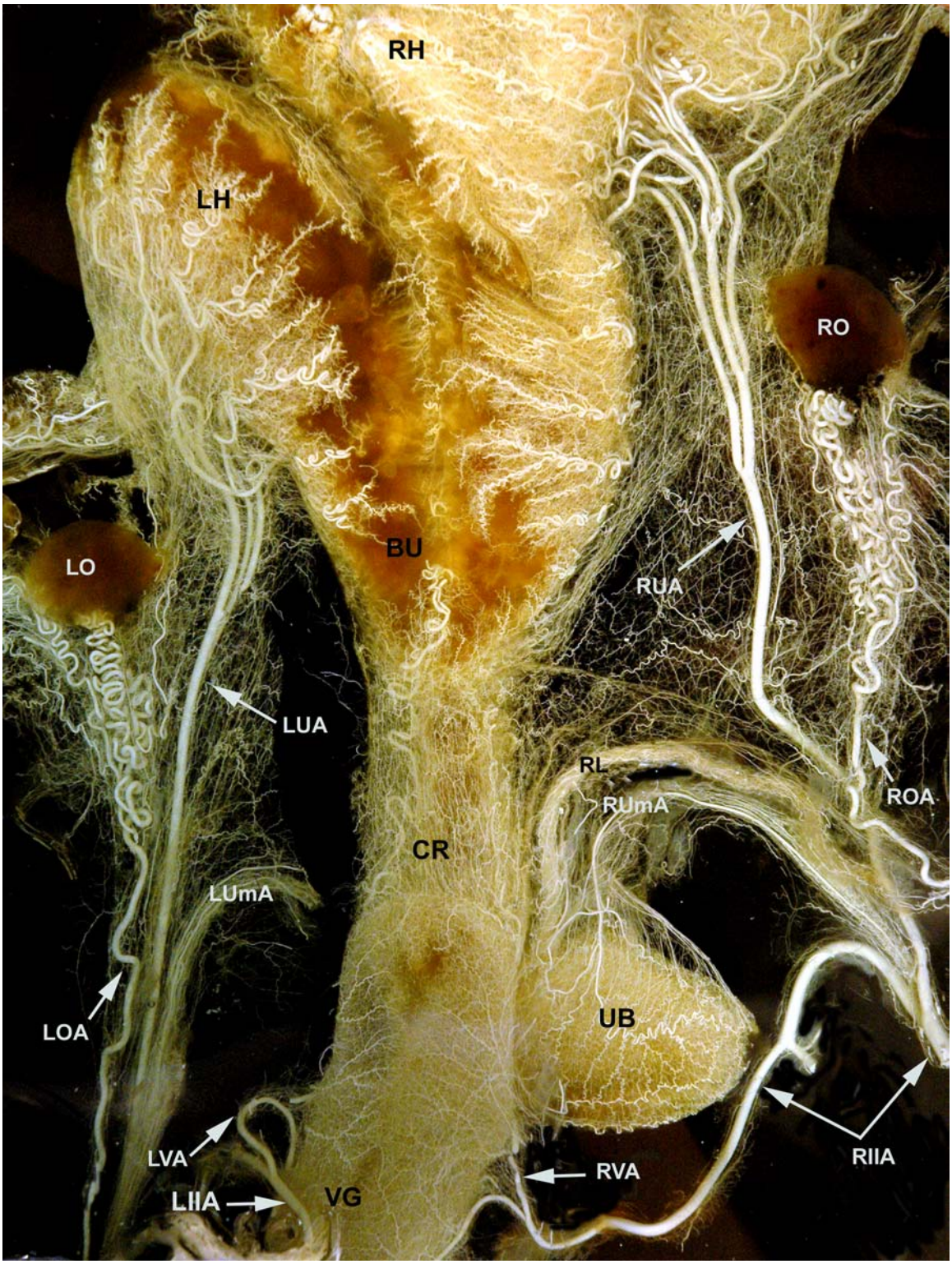

Fig. 3. Legend on the next page (page: 52).

Fig. 3 (figure on previous page). Dorsal view of methyl salicylate cleared uterus from a pregnant doe at 7 weeks. Note the main blood supply to the uterus by branches of the ovarian arteries (right ovarian artery, **ROA** and left ovarian artery, **LOA**), uterine arteries (right uterine artery, **RUA** and left uterine artery, **LUA**), and vaginal arteries (right vaginal artery, **RVA** and left vaginal artery, **LVA**). The ovarian artery arises from the aorta (not shown). The uterine artery arises from the internal iliac artery together with the umbilical artery (shown on the right side). The vaginal artery arises from the internal iliac artery (shown on both sides). **RUma**, right umbilical artery; **LUmA**, left umbilical artery; **RL**, round ligament of the uterus; **RIIA**, right internal iliac artery; **LIIA**, left internal iliac artery; **LH**, left uterine horn; **RH**, right uterine horn; **BU**, body of the uterus; **CR**, cervix; **VG**, vagina; **UB**, urinary bladder; **RO**, right ovary; **LO**, left ovary.

Ovarian Arteries

The ovarian arteries arose from the dorsolateral surface of the abdominal aorta (*aorta abdominalis*). Both arteries originated at the same level in 59.1% of the specimens studied. The right ovarian artery (*a. ovarica dextra*) arose cranial to the left artery in 18.2%. The left ovarian artery (*a. ovarica sinistra*) arose cranial to the right one in 22.7% (Fig. 4).

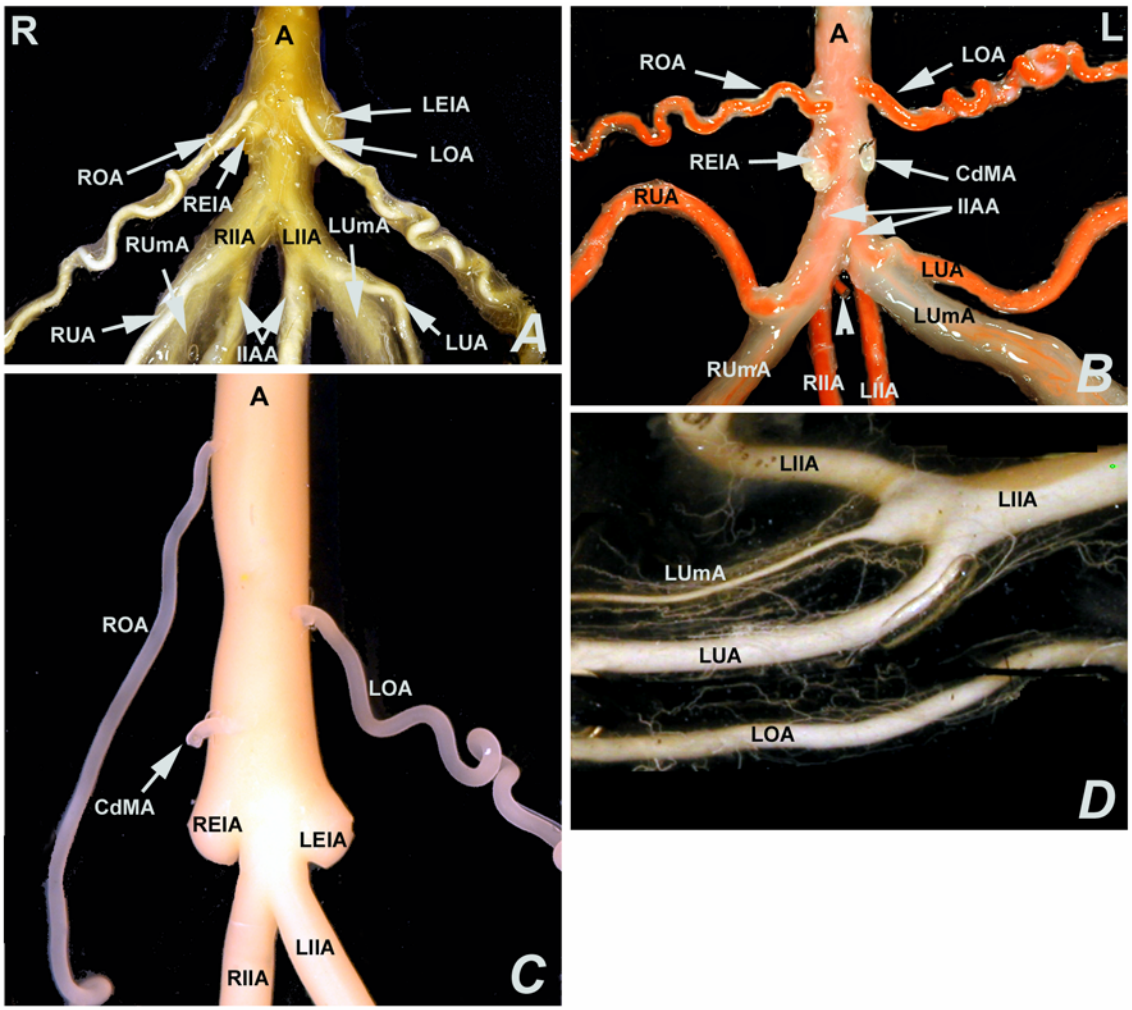

Fig. 4. Anatomical variations in the origin of main vessels supplying the uterus. ***A*** and ***B*** are glycerin cleared specimens. ***C*****:** Methyl methacrylate corrosion-cast specimen. ***D*****:** Methyl salicylate cleared specimen. The ovarian arteries arise from the aorta, showing some variation in the level of origin among specimens, as illustrated. Both right and left ovarian arteries (**ROA**, **LOA**) may arise at the same level (***A***), the right ovarian artery may arise slightly caudal to the left artery (***B***), or the right ovarian artery may arise cranial to the left one (***C***). The uterine artery (**RUA**, right uterine artery; **LUA**, left uterine artery) arises as a common truck with the umbilical artery (**RUmA**, right umbilical artery; **LUmA**, left umbilical artery) from the internal iliac artery (**RIIA**, right internal iliac artery; **LIIA**, left internal iliac artery) in most cases (***A***, ***B***, and ***C***), but the uterine artery arises separately from the internal iliac artery in a few cases (***D***). **IIAA**, right and left internal iliac arteries; **CdMA**, caudal mesenteric artery; **REIA**, right external iliac artery; **LEIA**, left external iliac artery; **R** and **L** are right and left sides, respectively in ***A***, ***B***, and ***C***; arrow head in ***B*** points at the median sacral artery.

Figures 5 through 13 show the course and branching patterns of the right and left ovarian arteries. The ovarian artery was tortuous and lay in close apposition to the ovarian vein in all specimens studied. This arrangement was maintained throughout gestation. The **right ovarian artery** ran caudally in a straight course for a short distance (about 1.5 cm) then coiled around the right ovarian vein (*v. ovarica dextra*). It gave off both a uterine branch (*ramus uterinus*) and uterine tube branch (*ramus tubarius*) then continued to enter the ovary. The uterine branch came off the ovarian artery after the uterine tube branch in 50% of the specimens studied. The uterine tube branch arose from the ovarian artery after the uterine branch in 43%. In 7% of the specimens, both the uterine and uterine tube branches came off the ovarian artery together as a common trunk. The size of branches of the ovarian artery was smaller than the parent artery; however, in some cases (66.7% of triplet pregnancies), the size of the uterine branch was almost equal to that of the continuation of its parent artery.

The *uterine tube branch* ran cranial to the ovary in a serpentine pattern until it reached the abuterine pole of the ovary. It supplied the infundibulum of the uterine tube in all specimens studied and the ampulla in 47% of the specimens. No information about the supply of the ampulla was obtained in 33% of the specimens due to incomplete injection of the area. The uterine tube branch also supplied the isthmus in 13% of the does. The uterine tube branch gave branches to the mesosalpinx and mesovarium. Those branches ran straight and almost parallel to each other in most specimens.

The *uterine branch* ran caudal to the ovary toward the uterus. It gave a branch to the uterine tube, which supplied the isthmus and utero-tubal junction in all specimens. It gave off branches to the ampulla in 20% of the specimens studied. Then it continued and before reaching the uterine horn, divided to supply the dorsal and ventral surfaces of the area close to the tip of the uterine horn in 87% of the specimens. Information about the supply of this area by the uterine branch of the ovarian artery was missing in 13% of the specimens studied due to incomplete injection of the area. In half of triplet pregnancies, the uterine branch of the ovarian artery gave off a branch that joined a branch of the uterine artery, to supply the uterine horn. The uterine branch of the ovarian artery also gave off an additional branch that supplied the dorsal surface of the area adjacent to the tip of the uterine horn in half of triplet pregnancies. There was an anastomosis between branches of the uterine branch of the ovarian artery and branches of the cranial branch (in some cases with the caudal branch) of the uterine artery.

In the case of the **left ovarian artery**, the pattern of branching was similar to that of the right artery. The uterine branch was given off the ovarian artery after the uterine tube branch in 18% of the specimens. The uterine tube branch was given off the ovarian artery after the uterine branch in 73%. Both branches were given off the ovarian artery as a common trunk in 9%. In some cases (16.7% of triplets and 16.7% of all pregnant tracts), the diameter of the uterine branch was larger than that of its parent artery.

The *uterine tube branch* supplied the infundibulum of the uterine tube in all specimens. It supplied the ampulla in 54% and also supplied the isthmus of the

uterine tube in 13%. Information about the supply of the ampulla was lost in 26% of the specimens studied. The uterine tube branch gave branches to the mesosalpinx and mesovarium.

The *uterine branch* gave off branches to the ampulla of the uterine tube in 20% of the specimens studied and to the isthmus and utero-tubal junction in all specimens. Then it continued toward the uterus, and before it reached the uterine horn, it gave branches to the dorsal and ventral surfaces of the area adjacent to the tip of the uterine horn in 87% of the specimens studied. Information about the supply of this area was not available in 13% of the specimens. In some cases (33.3% of triplets and 25% of all pregnant tracts), the uterine branch of the ovarian artery gave off a branch that joined a branch of the uterine artery and supplied the dorsal surface of the area adjacent to the tip of the uterine horn, or supplied the ventral surface of the area adjacent to the tip of the uterine horn in 8.3% of specimens from pregnant does. The uterine branch of the ovarian artery also gave off additional branches to supply the uterine horn in 50% of triplets and 33.3% of specimens from pregnant does. As in the case of the right artery, it anastomosed with branches of the uterine artery. In one doe pregnant with triplets at 18 weeks of pregnancy, the ovarian artery gave rise to an additional branch to supply the uterus; this branch was larger than the ipsilateral uterine artery and supplied the entire dorsal surface of the left uterine horn. It anastomosed with both the uterine branch of the ovarian artery and uterine branch of the vaginal artery.

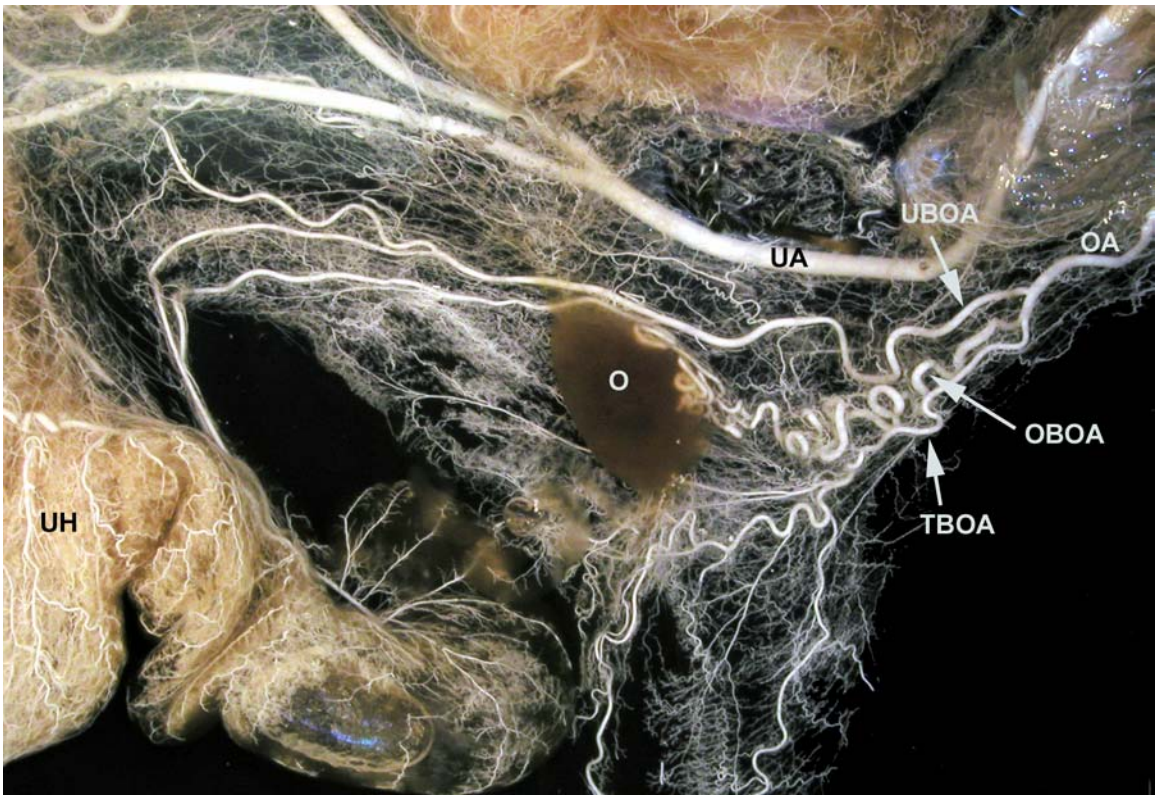

Fig. 5. Methyl salicylate cleared specimen showing branches of the ovarian artery. In this case, the uterine branch of the ovarian artery (**UBOA**) is given off the ovarian artery before it gives the uterine tube branch (**TBOA**). **OA**, ovarian artery; **OBOA**, proper ovarian branch of the ovarian artery; **UA**, uterine artery; **O**, ovary; **UH**, uterine horn.

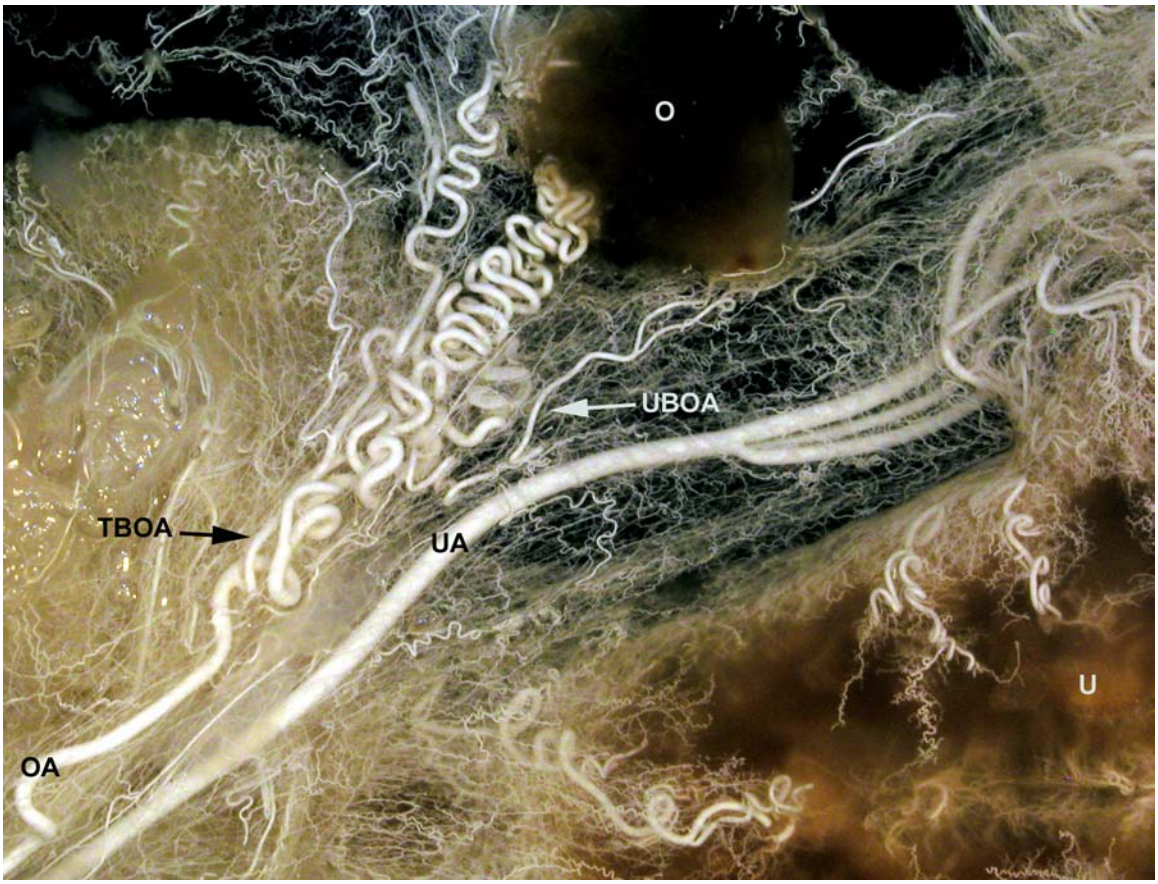

Fig. 6. Methyl salicylate cleared specimen showing branches of the ovarian artery. In this case, the uterine tube branch (**TBOA**) is given off the ovarian artery after it gives rise to the uterine branch (**UBOA**). **OA**, ovarian artery; **UA**, uterine artery; **O**, ovary; **U**, uterus.

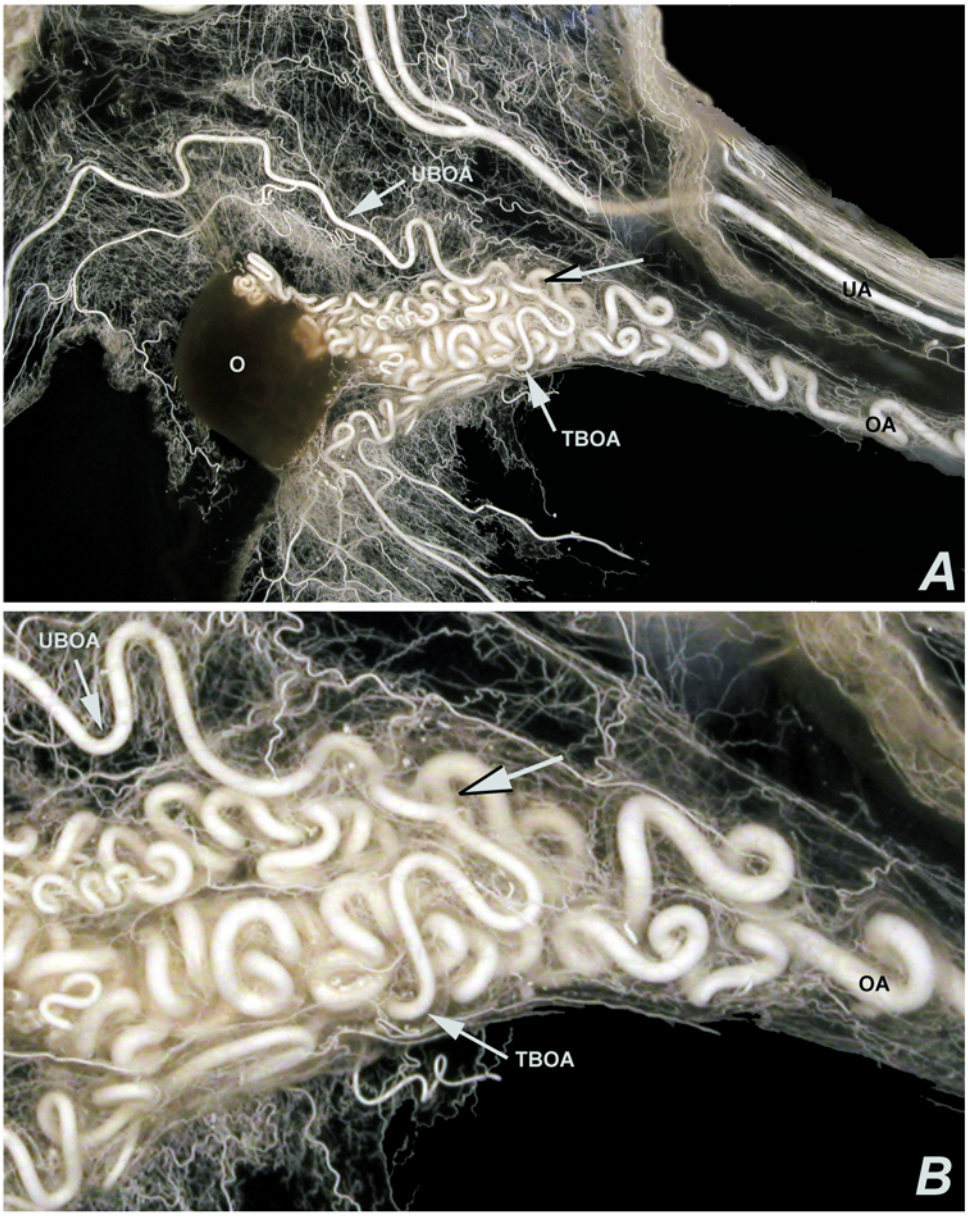

Fig. 7. Methyl salicylate cleared specimen showing branches of the ovarian artery. In this case, both the uterine and uterine tube branches of the ovarian artery originate together as a common trunk (at the tip of the outlined arrow). ***B*****:** High magnification image of ***A***. **UA**, uterine artery; **OV**, ovarian artery; **UBOA**, uterine branch of ovarian artery; **TBOA**, uterine tube branch of ovarian artery; **O**, ovary.

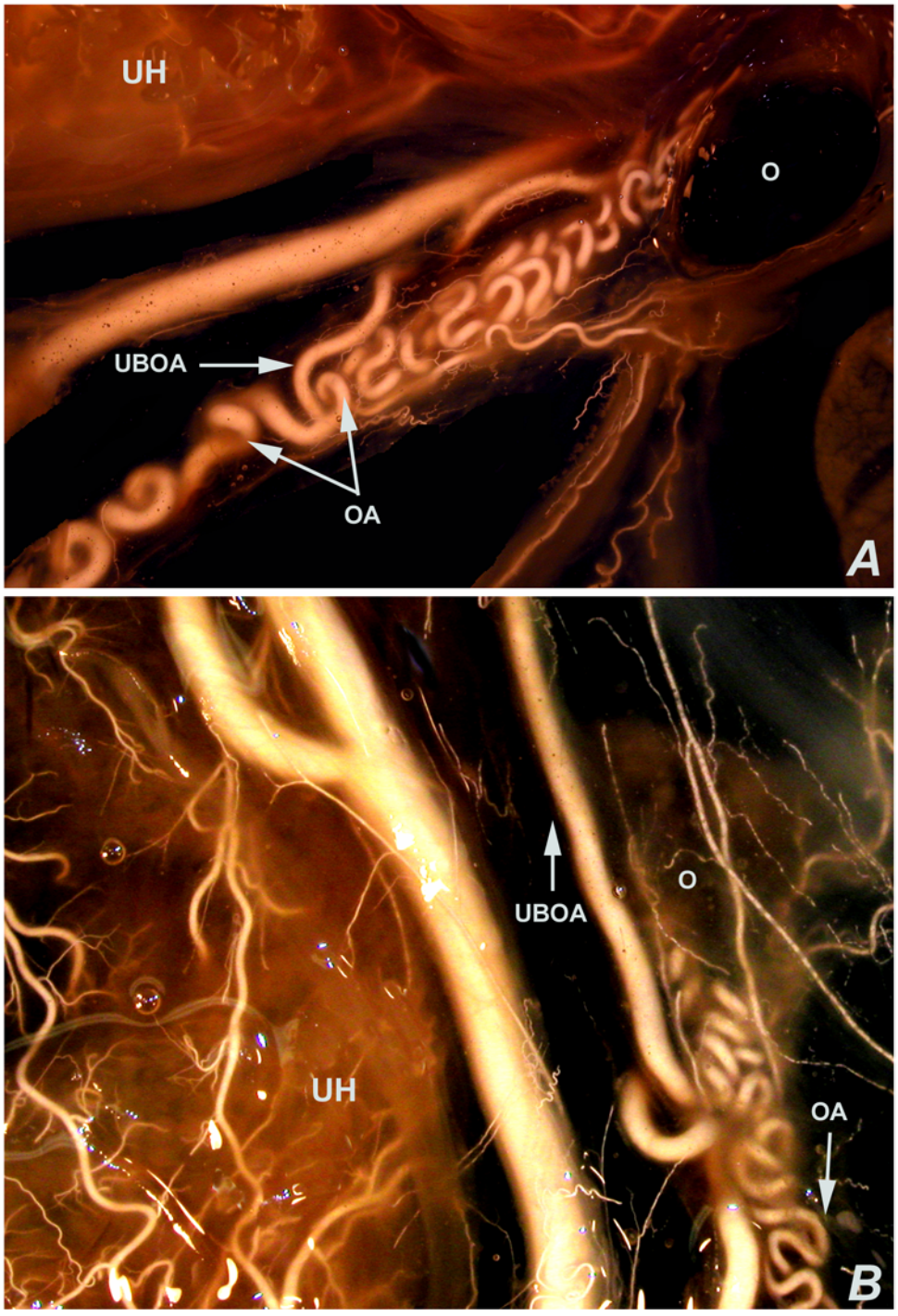

Fig. 8. Glycerin cleared specimens showing examples of adaptation of the ovarian artery to multiple pregnancies. In ***A***, the diameter of the uterine branch of ovarian artery (**UBOA**) is nearly equal to that of the continuation of its parent artery (the ovarian artery, **OA**). In ***B***, the diameter of the uterine branch of the ovarian artery is larger than that of its parent artery. **UH**, uterine horn; **O**, ovary; **OA**, ovarian artery.

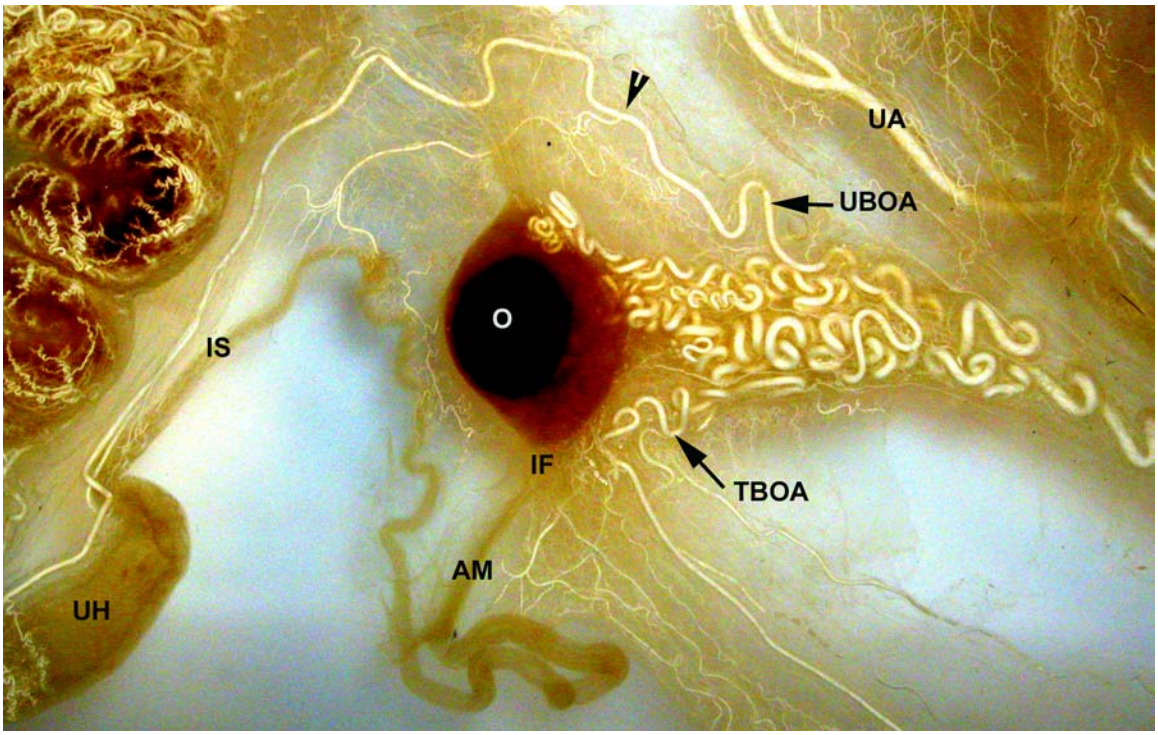

Fig. 9. Methyl salicylate cleared specimens showing the blood supply of the uterine tube via the uterine and uterine tube branches of the ovarian artery. In this case, the uterine branch of the ovarian artery (**UBOA**) gives off a branch at the tip of arrow head, which supplies the isthmus (**IS**) of the uterine tube. The uterine tube branch of the ovarian artery (**TBOA**) supplies the infundibulum (**IF**) and ampulla (**AM**) of the uterine tube. **UA**, uterine artery; **UH**, uterine horn; **O**, ovary.

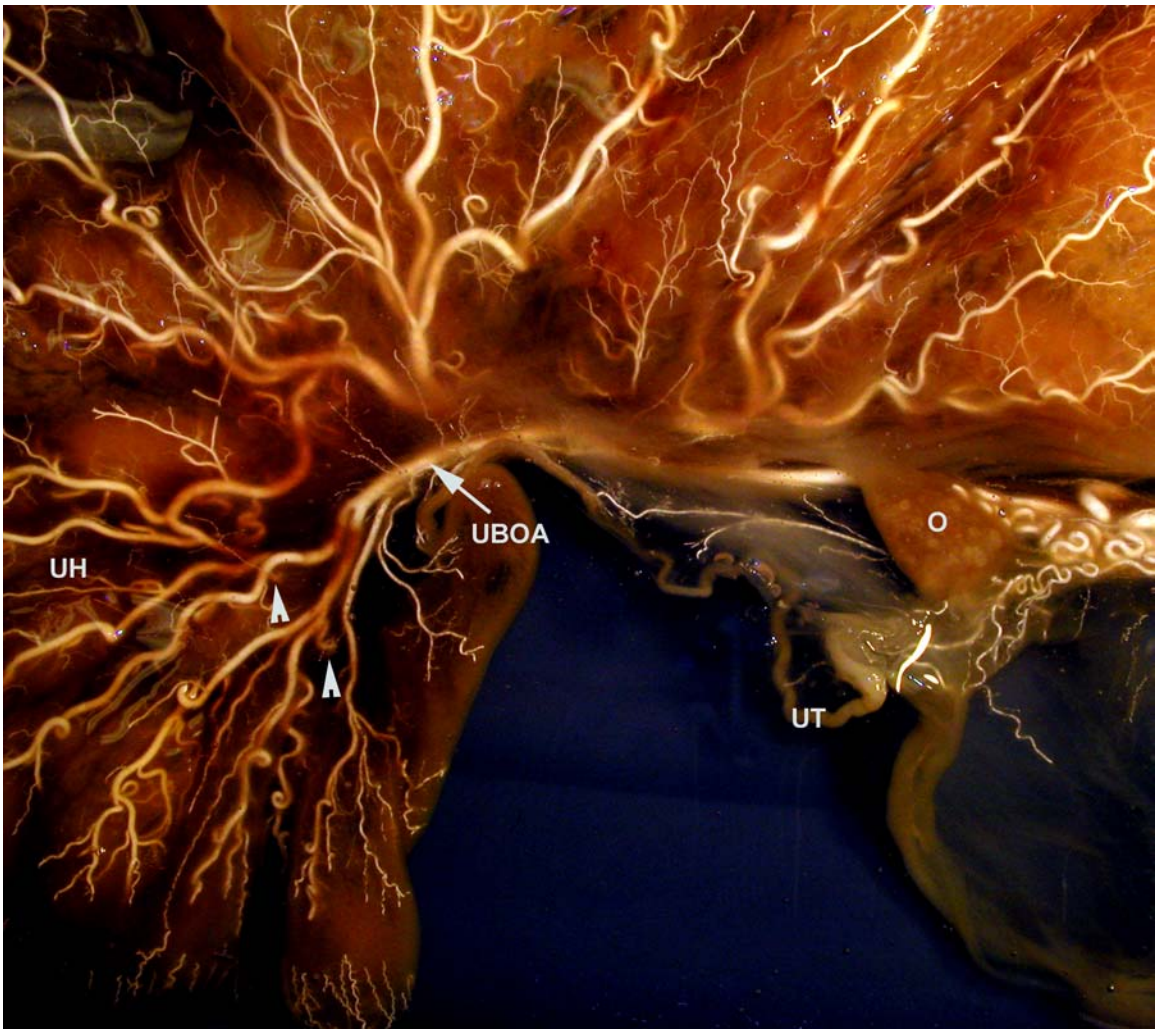

Fig. 10. Dorsal view of a portion of the uterine horn (**UH**) of a glycerin cleared specimen. Note that the uterine branch of the ovarian artery (**UBOA**) supplies the dorsal and ventral (arrow heads) surfaces of the area close to the tip of the uterine horn. **UT**, uterine tube; **O**, ovary.

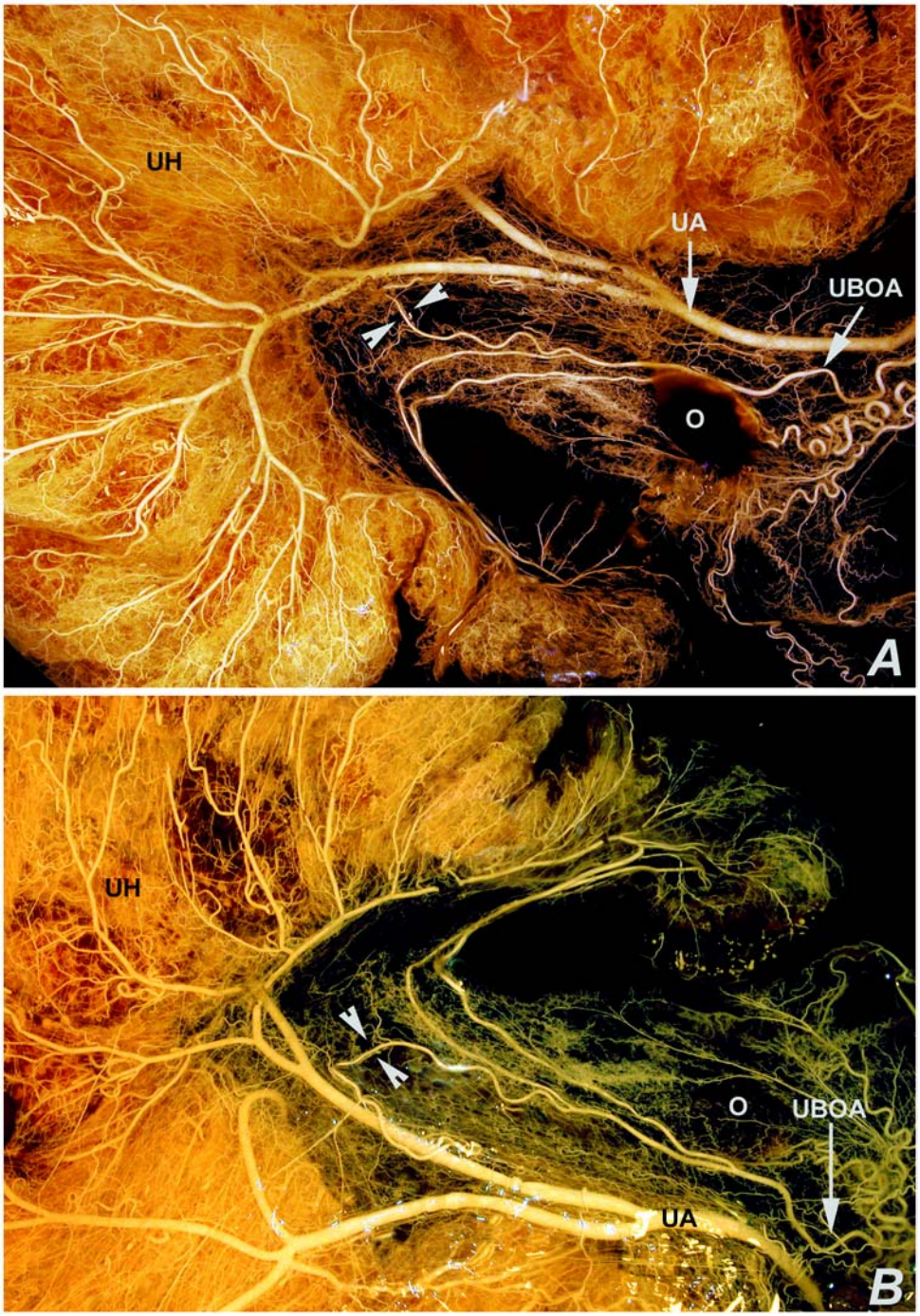

Fig. 11. *A*: Dorsal view of a portion of the uterine horn (**UH**) of a methyl salicylate cleared specimen showing an example of the adaptation of the uterine branch of the ovarian artery to multiple pregnancies. Note that the uterine branch of the ovarian artery (**UBOA**) gives rise to an additional branch (delineated between the two arrow heads) that joins a branch of the uterine artery (**UA**) to supply the uterine horn (**UH**). ***B*:** Ventral view of ***A***. **O**, ovary.

Fig. 12. Dorsal view of a portion of the uterine horn of a methyl salicylate cleared specimen showing the anastomosis (arrow heads) between subdivisions of the uterine branch of the ovarian artery (**UBOA**) and uterine artery (**UA**).

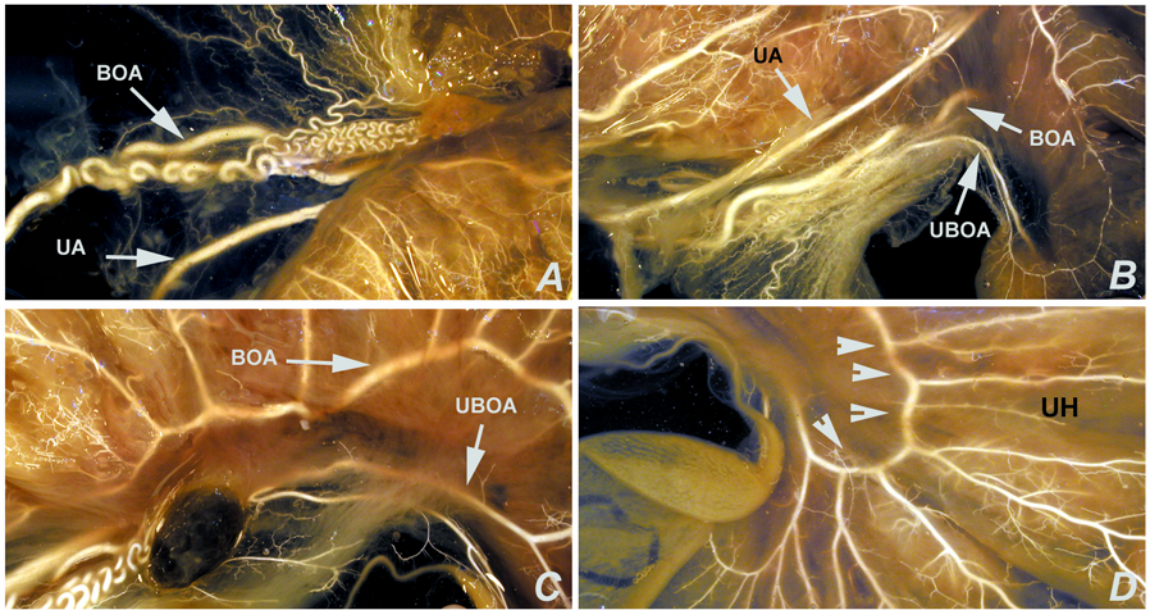

Fig. 13. Glycerin cleared specimen showing an example of the adaptation of the ovarian artery to multiple pregnancies. In this case, the ovarian artery gives an additional branch (**BOA**), which is larger than the ipsilateral uterine artery (**UA**) and supplies the entire dorsal surface of the uterine horn. This branch also anastomoses (arrow heads in ***D***) with subdivisions of the uterine branch of the ovarian artery and uterine branch of the vaginal artery (not shown). ***A*:** Dorsal view showing the origin of the additional branch of the ovarian artery (**BOA**). ***B*:** ventral view showing the course of this branch to the dorsal surface of the uterine horn. ***C*:** dorsal view of an area of the uterine horn showing the supply of the dorsal surface of the uterine horn by the additional branch of the ovarian artery. The arrow heads in ***D*** show the anastomosis of the additional branch of the ovarian artery with the uterine branch of the ovarian artery. **UH**, uterine horn.

Uterine Arteries

Figures 14-16 show the course and branching patterns of the uterine arteries (*aa. uterina*). The **right uterine artery** (*a. uterina dextra*) arose together with the umbilical artery (*a. umbilicalis*) as a common trunk from the internal iliac artery (*a. iliaca interna*) in 96% of the specimens examined; or alone directly from the internal iliac artery in 4% (Fig. 4). The uterine artery ran caudally toward the uterus and divided within the mesometrium into two caudal and cranial branches. This occurred at about the level of the bifurcation of the uterine body into horns in 91% of the specimens, and at a level cranial to the bifurcation in 9%. In some specimens (5.6%), it gave off a branch before dividing into its main cranial and caudal branches. This less-common branch supplied the ventral surface of the uterine horn from the middle portion to the tip. The distribution of the caudal and cranial branches of the uterine artery was consistent in most of the specimens.

The *caudal branch of the right uterine* artery divided into two or more primary branches, which in turn divided into secondary branches. Subdivisions of the caudal branch of the uterine artery supplied the ventral surface of the caudal part of the uterine horn in 100% of the specimens; and the dorsal surface of the same area in 93.3%. The dorsal surface of the uterine body was supplied by these branches in 60% of the specimens. They supplied the ventral surface of the middle portion of the uterine horn in 73.3% and the dorsal surface in 40%. They supplied the dorsal surface of the uterine horn from the middle part to the tip in 13.3% and the ventral surface of the same area in 6.7%. The caudal branches of the uterine artery anastomosed with branches of the uterine branch

of the vaginal artery on the ventral surface of the caudal area of the uterine horn and uterine body in 86.7% of the specimens and on the dorsal surface in 60%.

The *cranial branch of the right uterine* artery divided into two primary branches. Secondary branches arose from these primary ones. Subdivisions of the cranial branch of the uterine artery supplied the dorsal and ventral surfaces of the uterine horn from the middle portion to the tip in 86.7% of the specimens studied. They supplied the dorsal surface of the middle portion of the uterine horn in 60%, and the ventral surface in 26.7%. Subdivisions of the cranial branch of the uterine artery also supplied the dorsal surface of the caudal part of the uterine horn and body in 6.7%. There was an anastomosis between subdivisions of the branches of the right and left uterine arteries in the area between the two uterine horns at the vicinity of the intercornual ligament.

The **left uterine artery** (*a. uterina sinistra*) arose from the same location as in the case of the right artery: together with the umbilical artery in 96% of the specimens or directly from the internal iliac artery in 4% (Fig. 4). It divided within the mesometrium into two branches in a fashion similar to its right counterpart.

The *caudal branch of the left uterine artery* divided into two or more primary branches, which in turn divided into secondary branches, which supplied the ventral surface of the caudal part of the uterine horn in all specimens; and the dorsal surface of the same area in 86.7% of the specimens. Subdivisions of the caudal branch of the left uterine artery also supplied the ventral surface of the middle portion of the uterine horn in 86.7% and the dorsal surface in 53.3%. They supplied the ventral surface of the area from the middle portion of the uterine

horn to the tip in 13.3% of the does. They supplied the dorsal surface of the uterine body in 40%, and the ventral surface in 86.7% of the specimens. Subdivisions of the caudal branch of the uterine artery anastomosed with branches of the vaginal artery on the ventral surface of the caudal part of the uterine horn in 66.7% and on the dorsal surface in 40%.

Subdivisions of the *cranial branch of the left uterine* artery supplied the dorsal surface of the uterine horn from the middle to the tip in 86.7% and the ventral surface of the same area in 93.3%. They supplied the dorsal surface of the middle portion of the uterine horn in 46.7% and the ventral surface of the same area in 13.3%. The dorsal surface of the caudal part of the uterine horn was supplied by these branches in 13.3%. Information about the supply of the dorsal surface of the uterine horn from the middle to tip was not available in 6.7% due to incomplete injection of this area.

Primary and/or secondary branches of the caudal and cranial branches of the uterine arteries gave rise to arcuate arteries, which formed an arch that followed the contour of the lesser curvature of the uterus. Radial arteries arose (or radiated, hence the name) from arcuate arteries. These arteries were longer than the areas of the uterus through which they traveled; therefore, they followed a helical course. As the gestation advanced and the size of the uterus increased, these arteries were drawn out straight (fig. 17). Each radial artery could supply more than one caruncle, and individual caruncles could be supplied by more than one radial artery.

Fig. 14a. Ventral view of a methyl salicylate cleared uterus from a pregnant doe showing the branching pattern of right and left uterine arteries (**RUA**, **LUA**). Closer views are provided in the subsequent two figures (Figs. 14b and 14c). The uterine artery divides into cranial and caudal branches. The cranial and caudal branches of the uterine artery further divide into primary branches, which in turn give off secondary ones. Primary and/or secondary branches of the cranial and caudal branches of the uterine artery give rise to arcuate arteries. Arcuate arteries follow the contour of the lesser curvature of the uterine horn, where they give rise to radial arteries. Each caruncle is supplied by branches of one or more radial arteries.

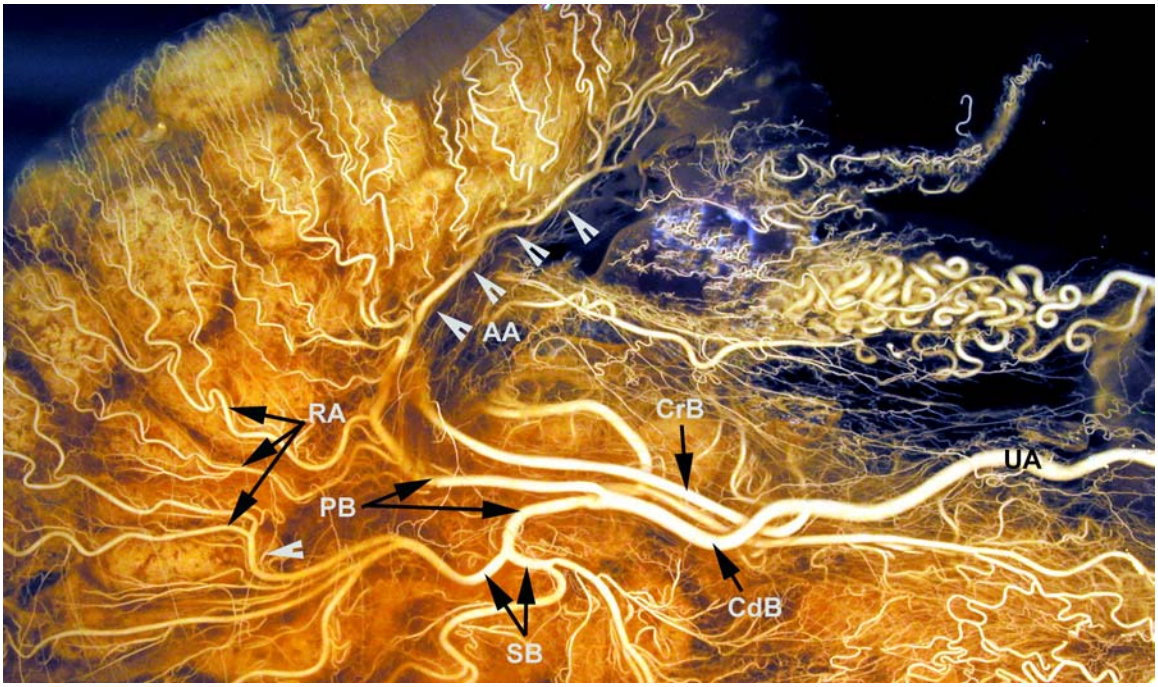

Fig. 14b. A closer view of the specimen in figure 14a providing the nomenclature of the branches of the uterine artery. The uterine artery (**UA**) divides into cranial (**CrB**) and caudal (**CdB**) branches. The cranial and caudal branches of the uterine artery further divide into primary branches (**PB**), which in turn give rise to secondary branches (**SB**). Primary and/or secondary branches of the cranial and caudal branches of the uterine artery give rise to arcuate arteries (**AA**, arrow heads). Arcuate arteries follow the contour of the lesser curvature of the uterine horn, where they give rise to radial arteries (**RA**). Caruncles are supplied by branches of radial arteries.

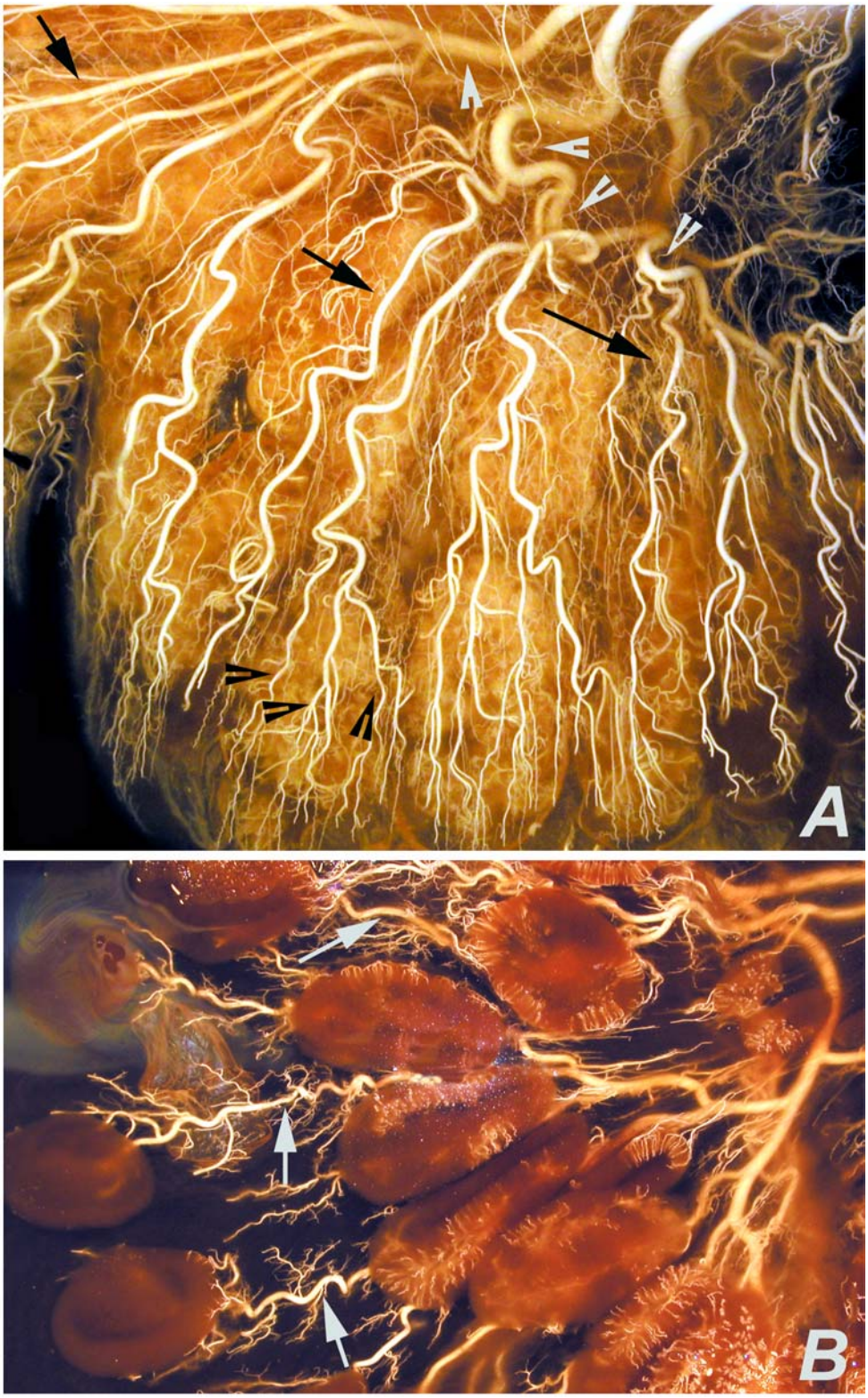

Fig. 14c. Closer views of figure 14a. ***A*:** Dorsal view of a portion of the uterine horn. Radial arteries (black arrows) arise or radiate from arcuate arteries (light arrow heads). Caruncles are supplied by branches (black arrow heads) of radial arteries. ***B*:** Internal view (light arrows are radial arteries).

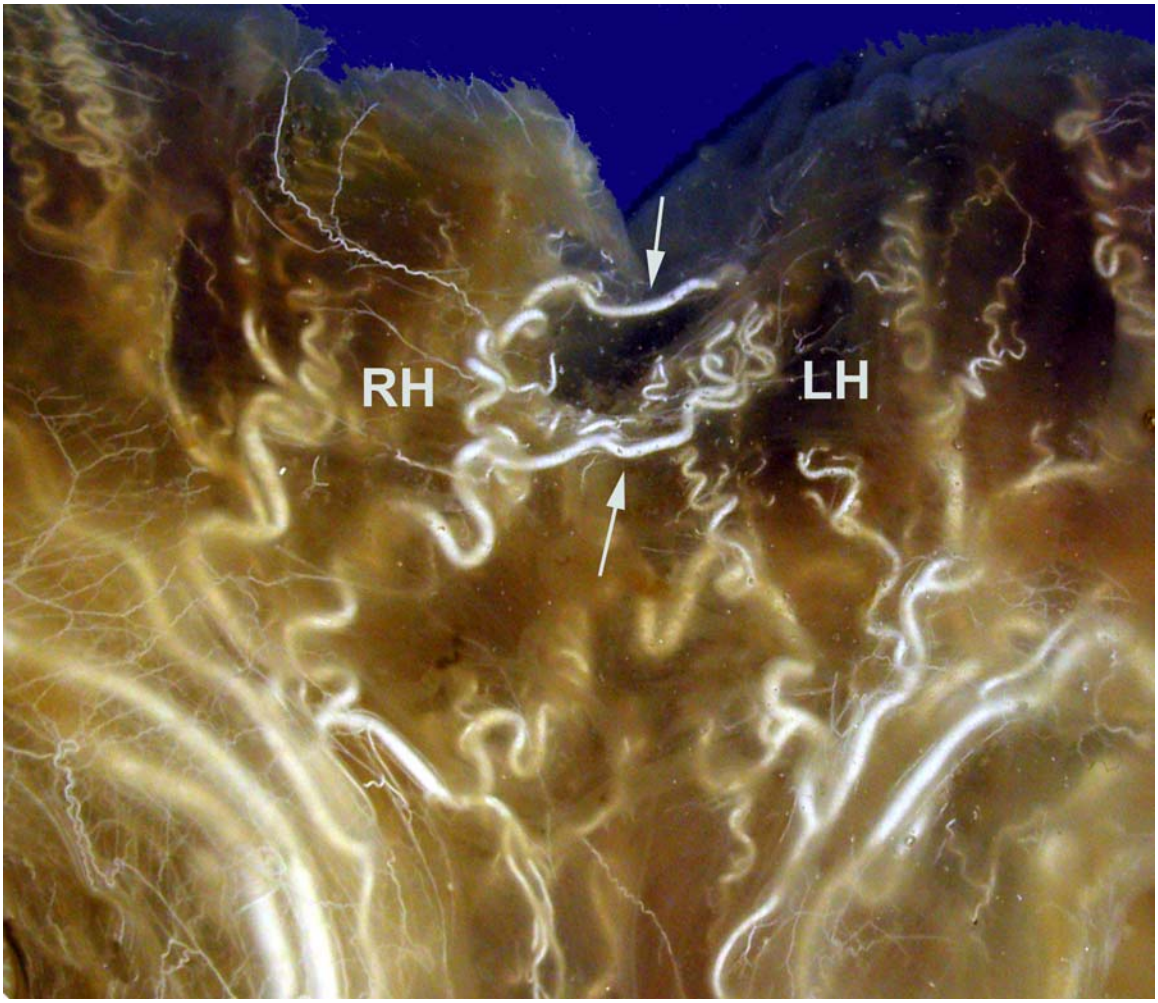

Fig.15. Ventral view of a glycerin cleared uterus showing the anastomosis between branches of the right and left uterine arteries at the area between two uterine horns at the vicinity of intercornual ligament. **RH**, right horn; **LH**, left horn.

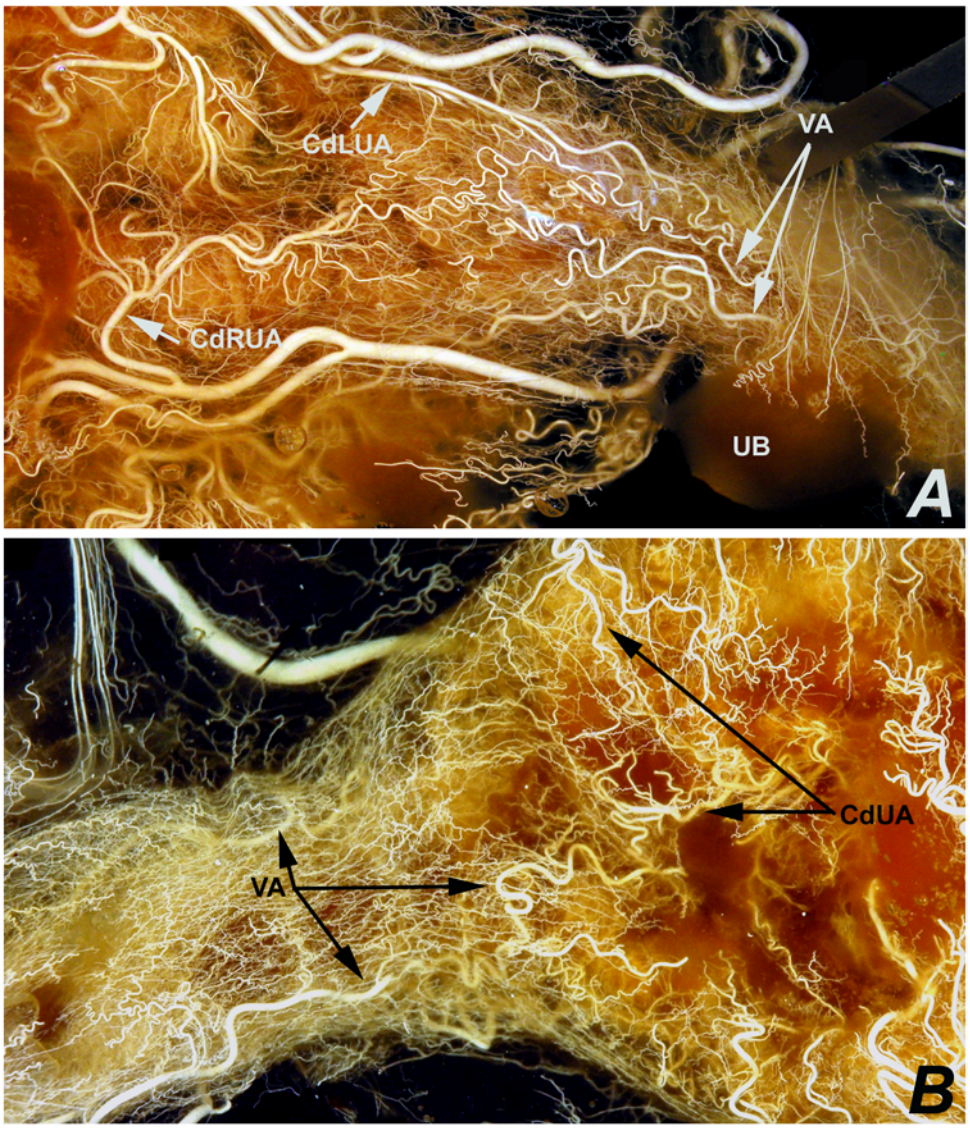

Fig. 16. Methyl salicylate cleared uterus. ***A*:** Ventral view of the uterus showing the anastomosis between subdivisions of the caudal branches of the right and left uterine arteries (**CdRUA**, **CdLUA**, respectively), and branches of the vaginal arteries (**VA**) on the ventral surface of the caudal area of the uterine horns and uterine body. ***B*:** Dorsal view showing the anastomosis between subdivisions of the caudal branches of the uterine arteries (**CdUA**) and of vaginal arteries (**VA**) on the dorsal surface of the caudal part of the uterine horns and uterine body.

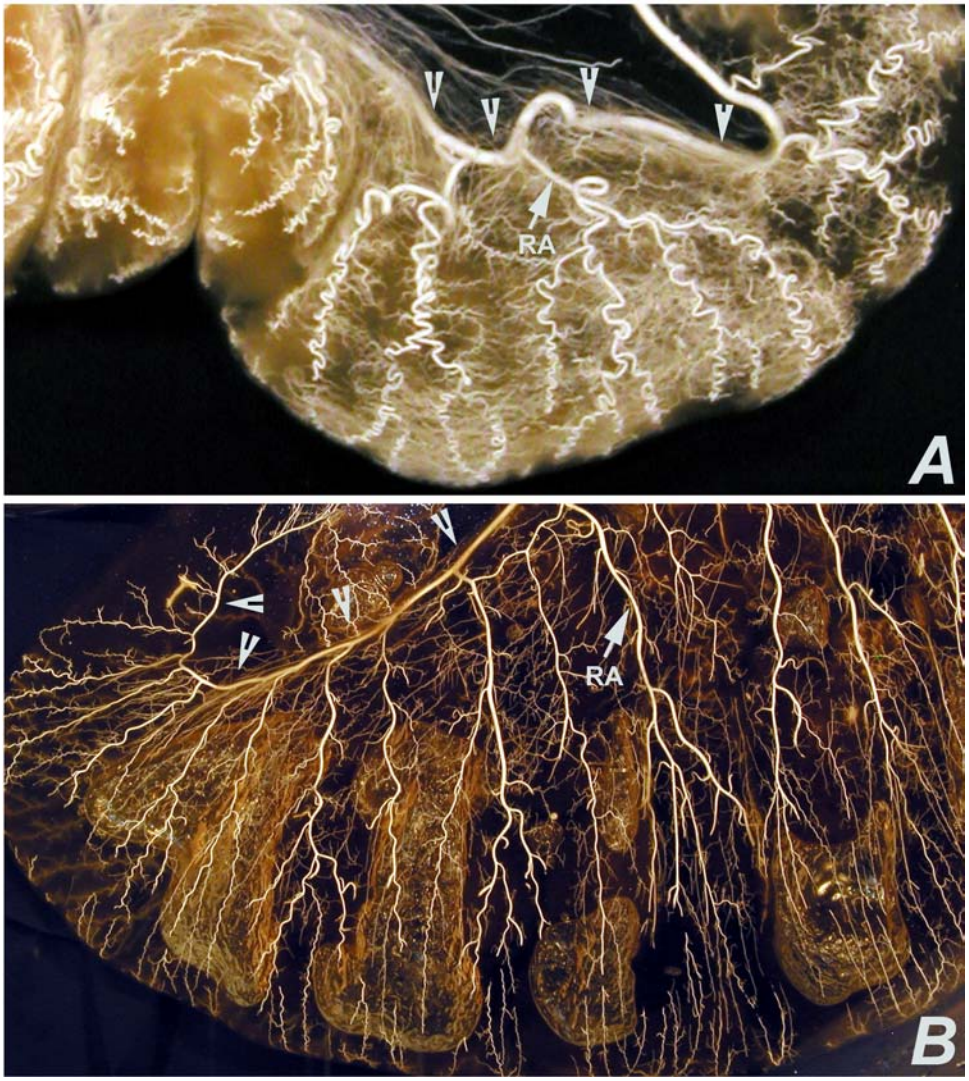

Fig. 17. Methyl salicylate cleared pregnant uteri. ***A*:** Early pregnant (4 weeks). ***B*:** Late pregnant (16 weeks). The radial arteries (**RA**) radiate from arcuate arteries (arrow heads). Radial arteries are longer than the areas of the uterus they travel through, therefore they follow a helical course in early pregnancy (***A***). As the gestation advances and size of the uterus increases, these arteries are drawn out straight (***B***).

Vaginal Arteries

The **right vaginal artery** arose from the internal iliac artery at the level of the vagina. It gave off caudal and cranial branches. The caudal branches of the vaginal artery ran along the lateral border of the vagina to supply the vagina, vestibule, and perineal area. The cranial or uterine branch (*ramus uterinus*) of the vaginal artery ran from the lateral to the ventral surface of the vagina, cervix and uterine body (Fig. 18). During its course to the uterus, it gave off branches to the vagina and the dorsal surface of the cervix at various levels. The *uterine branch* of the vaginal artery supplied the dorsal surface of the uterine body in 73.3% of the specimens studied and the ventral surface in 86.7%. It anastomosed with subdivisions of the caudal branches of the uterine artery on the dorsal surface of the uterine body in 46.7% and on the ventral surface in 80%. There was a connecting branch between the right uterine artery and the right uterine branch of vaginal artery in 16.7% of triplets (Fig. 19).

The **left vaginal artery** also arose from the internal iliac artery, and divided in a similar fashion to that of the right artery. It gave branches to the dorsal surface of the uterine body in 73.3% of the specimens and to the ventral surface in 66.7%. It anastomosed with subdivisions of the caudal branches of the uterine artery on the dorsal surface of the uterine body in 46.7% of the specimens and on the ventral surface in 66.7%. There was a connecting branch between the left uterine artery and the left uterine branch of vaginal artery in 16.7% of triplets (Fig. 20). Figures 21 and 22 show the supply of the dorsal and

ventral surfaces of different parts of the uterus by ovarian arteries, uterine arteries, and vaginal arteries.

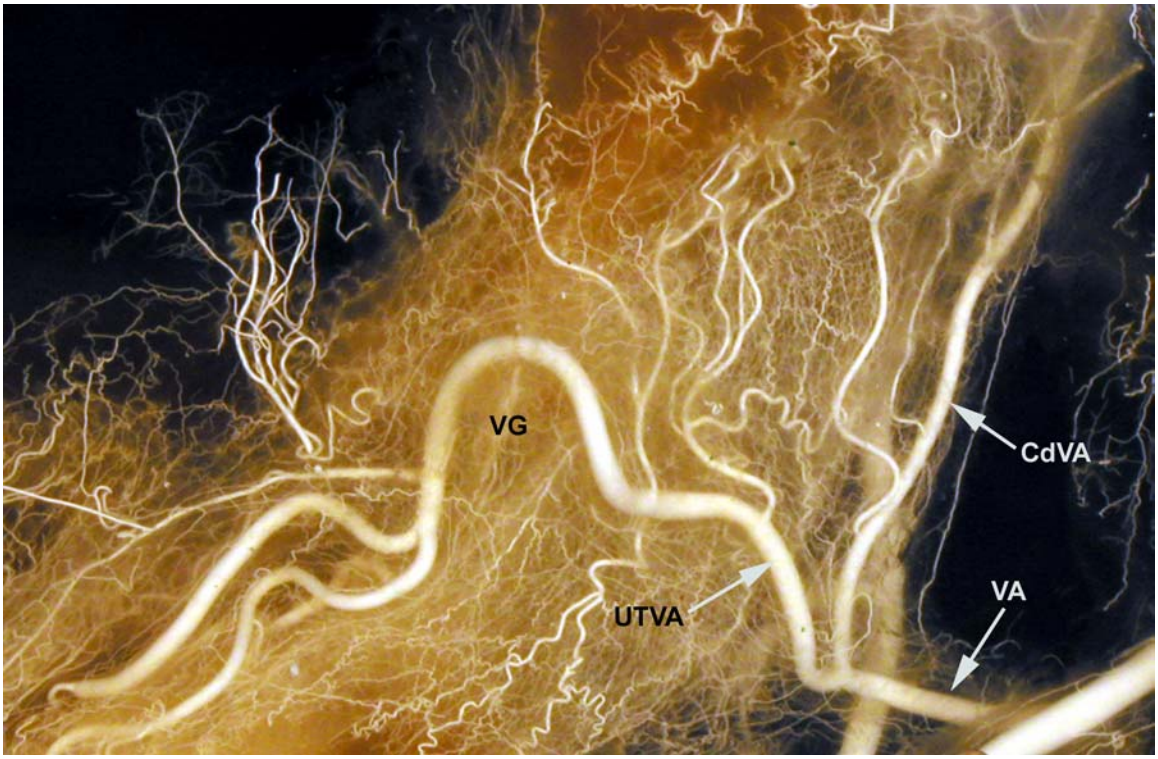

Fig. 18. Ventral view of the vagina (**VG**) of a methyl salicylate cleared pregnant reproductive tract. The vaginal artery (**VA**) gives caudal branches (**CdVA**) to supply the vagina, vestibule, and perineal region, and gives rise to the cranial branch (uterine branch of vaginal artery, **UTVA**) to supply the vagina and uterus. The uterine branch of the vaginal artery runs from the lateral to the ventral surface of the vagina.

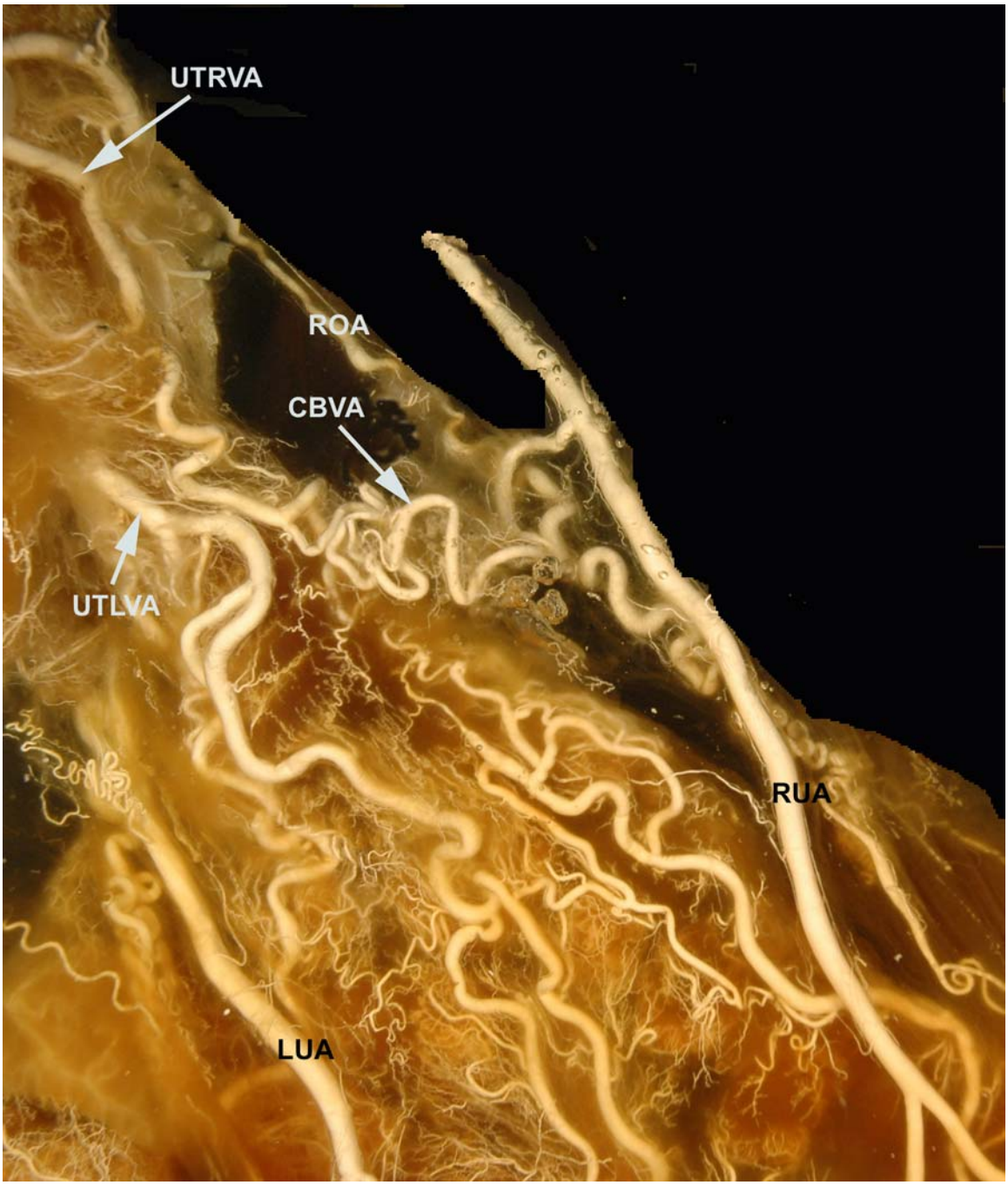

Fig. 19. Ventral view of a methyl salicylate cleared uterus from an 18-week-pregnant doe showing an example of the adaptation of the right vaginal artery to multiple pregnancies. Note the connecting branch (connecting branch of vaginal artery, **CBVA**) between the right uterine artery (**RUA**) and the uterine branch of the right vaginal artery (**UTRVA**). **ROA**, right ovarian artery; **LUA**, left uterine artery; **UTLVA**, uterine branch of the left vaginal artery.

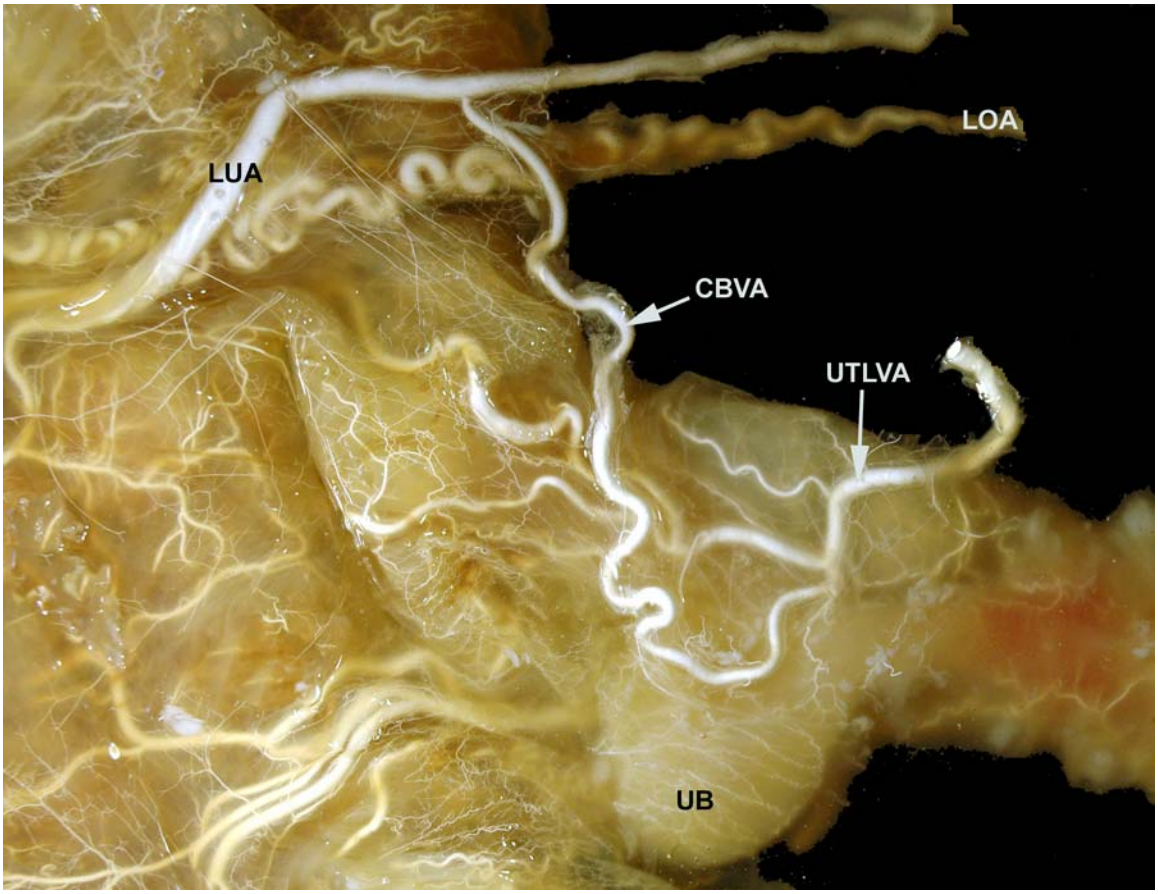

Fig. 20. Ventral view of a methyl salicylate cleared uterus from a 13-week-pregnant doe showing an example of the adaptation of the left ovarian artery to multiple pregnancies. Note the connecting branch (connecting branch of vaginal artery, **CBVA**) between the left uterine artery (**LUA**) and the uterine branch of the left vaginal artery (**UTLVA**). **LOA**, left ovarian artery; **UB**, urinary bladder.

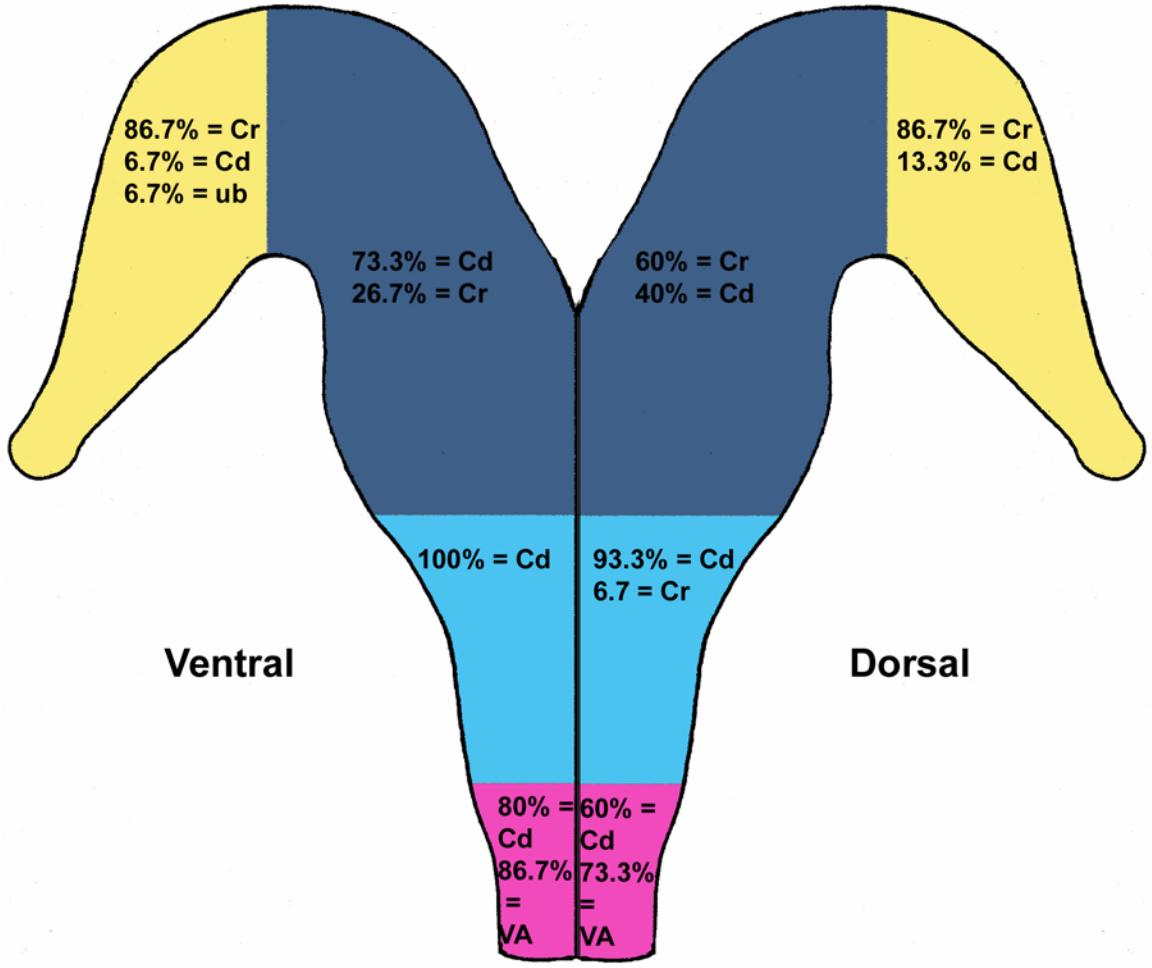

Fig. 21. Schematic diagram of the uterus (horns and body) showing the regional arterial supply of the dorsal and ventral surfaces of different parts of the right side of the uterus. The percentage shown is the percentage of specimens supplied by each artery (*i.e.* the yellow area on the dorsal surface is supplied by the cranial branch of the uterine artery in 86.7% of the specimens studied, and by the caudal branch of the uterine artery in 13.3% of the specimens studied). The dorsal and ventral surfaces of the area close to the tip of the uterine horn are supplied by the uterine branch of the ovarian artery (not shown), which anastomoses with either the cranial branch (in most cases) or caudal branch of the uterine artery. **Cr**, cranial branch of the uterine artery; **Cd**, caudal branch of the uterine artery; **ub**, a branch given by the uterine artery before dividing into its main two branches (the cranial and caudal branches). **VA**, uterine branch of vaginal artery.

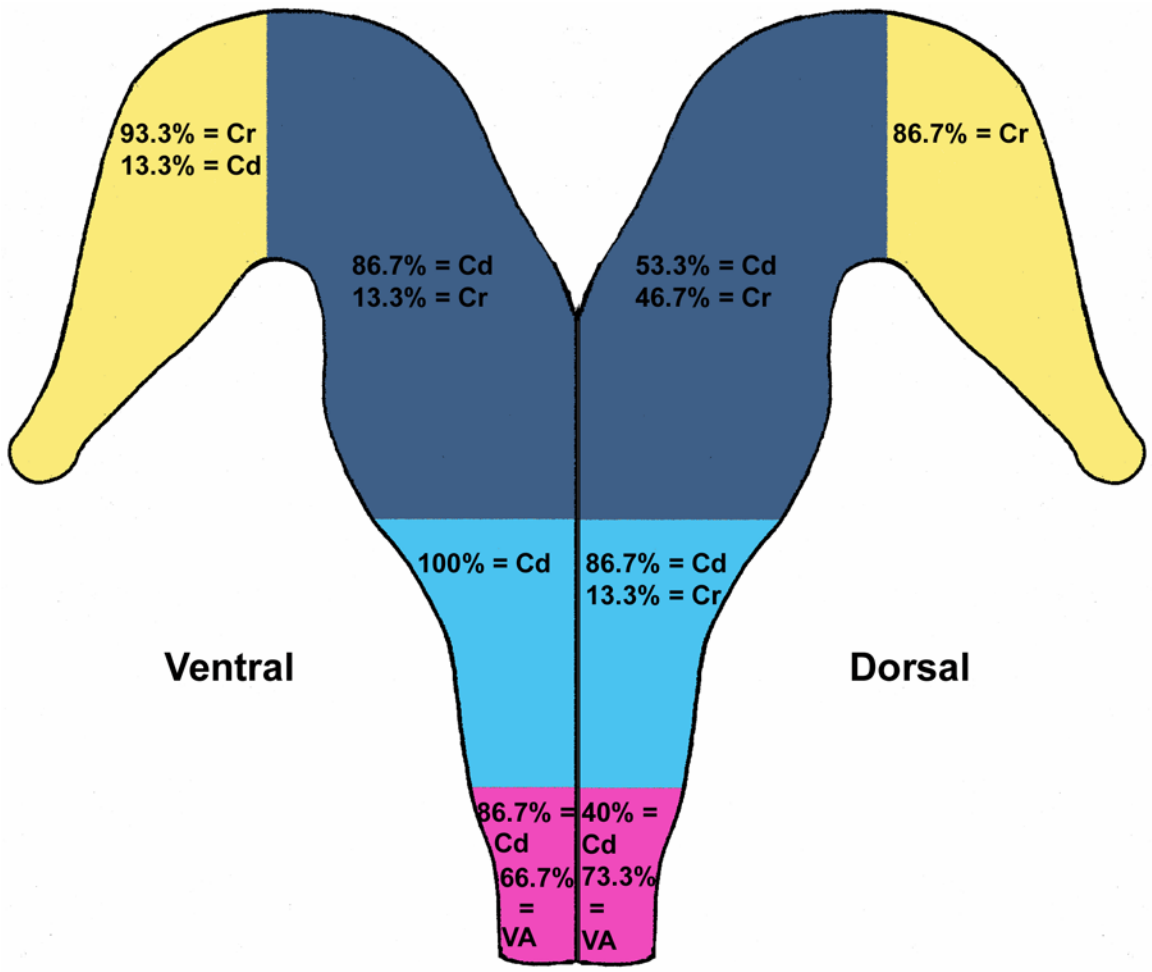

Fig. 22. Schematic diagram of the uterus (horns and body) showing the regional arterial supply of the dorsal and ventral surfaces of different parts of the left side of the uterus. The percentage shown is the percentage of specimens supplied by each artery (*i.e.* the yellow area on the dorsal surface is supplied by the cranial branch of the uterine artery in 86.7% of the specimens studied). The dorsal and ventral surfaces of the area close to the tip of the uterine horn is supplied by the uterine branch of the ovarian artery (not shown), which anastomoses with either the cranial branch (in most cases) or caudal branch of the uterine artery, or the additional branch of the ovarian artery to the uterus in 16.7% of triplets. The ovarian artery gave off an additional branch, which supplied the entire dorsal surface of the uterine horn in 16.7% of triplets (this is not included on the diagram). **Cr**, cranial branch of the uterine artery; **Cd**, caudal branch of the uterine artery; **VA**, uterine branch of vaginal artery.

Radiography

Radiographs showed the path of vessels supplying the reproductive tract (Fig. 23). However, they did not provide any more information than was obtained from the cleared specimens.

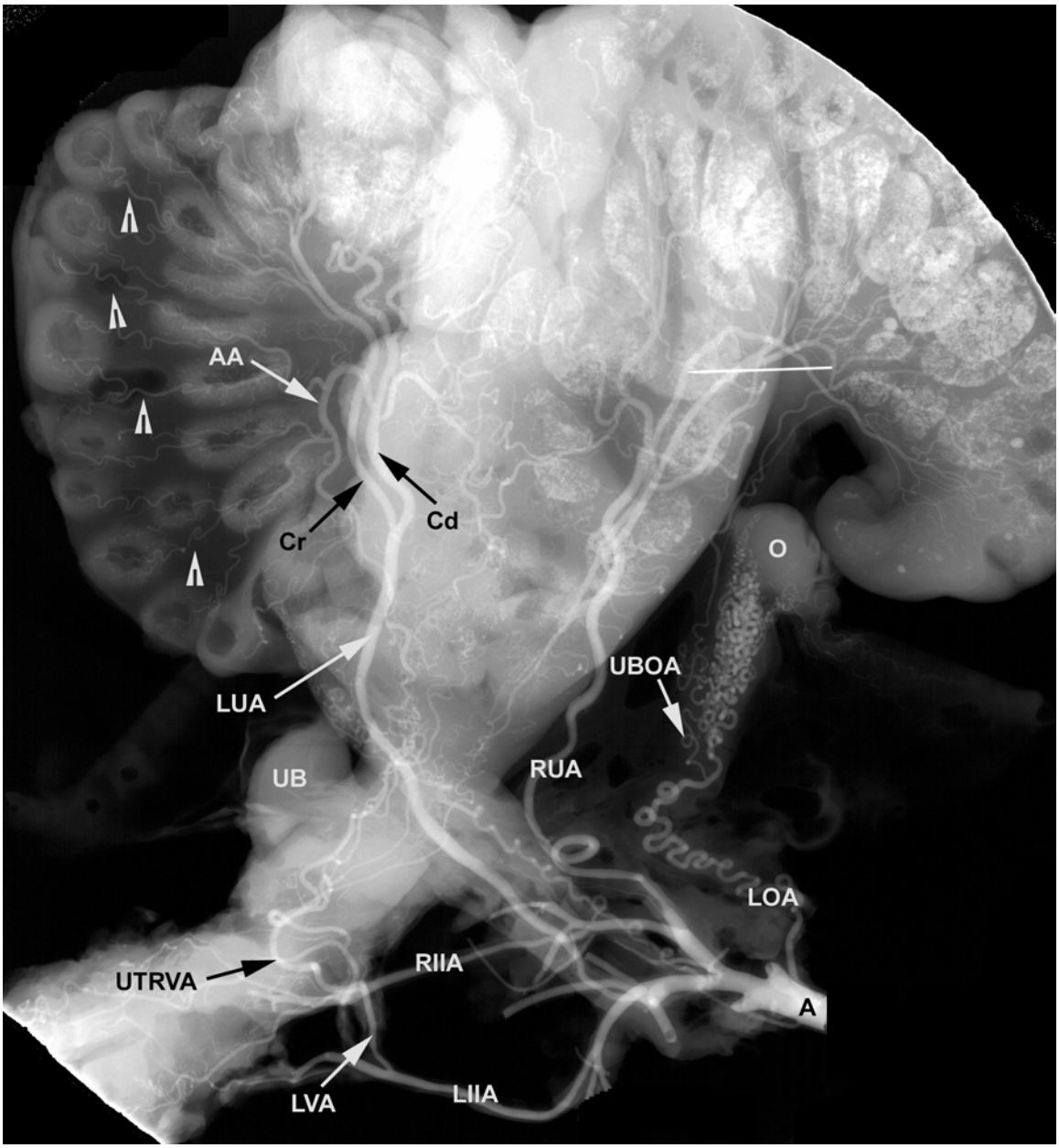

Fig. 23. Legend on next page (page: 83).

Fig. 23. (figure on previous page) A radiograph of a Microfil® injected reproductive tract from pregnant doe showing the vascular pathways of its supplying arteries. **A**, aorta; **LOA**, left ovarian artery; **UBOA**, uterine branch of the ovarian artery; **RUA**, right uterine artery; **LUA**, left uterine artery; **Cd**, caudal branch of the left uterine artery; **Cr**, cranial branch of the left uterine artery; **AA**, arcuate artery; arrow heads, radial arteries, **RIIA**, right internal iliac artery; **LIIA**, left internal iliac artery, **RUTVA**, uterine branch of the right vaginal artery; **LVA**, left vaginal artery; **O**, ovary; **UB**, urinary bladder; the straight dense radio-opaque line is a metal pin used to hold the tract in position.

Microvascular Casting

Arteries and veins were easily distinguished from each other by the different impression patterns made by endothelial cell borders and nuclei (Hodde and Nowell, 1980) (Fig. 24). On arteries, they are deep, slender, and regularly arranged parallel to the longitudinal axis of the vessel. On veins, they are shallow, rounder, and randomly oriented.

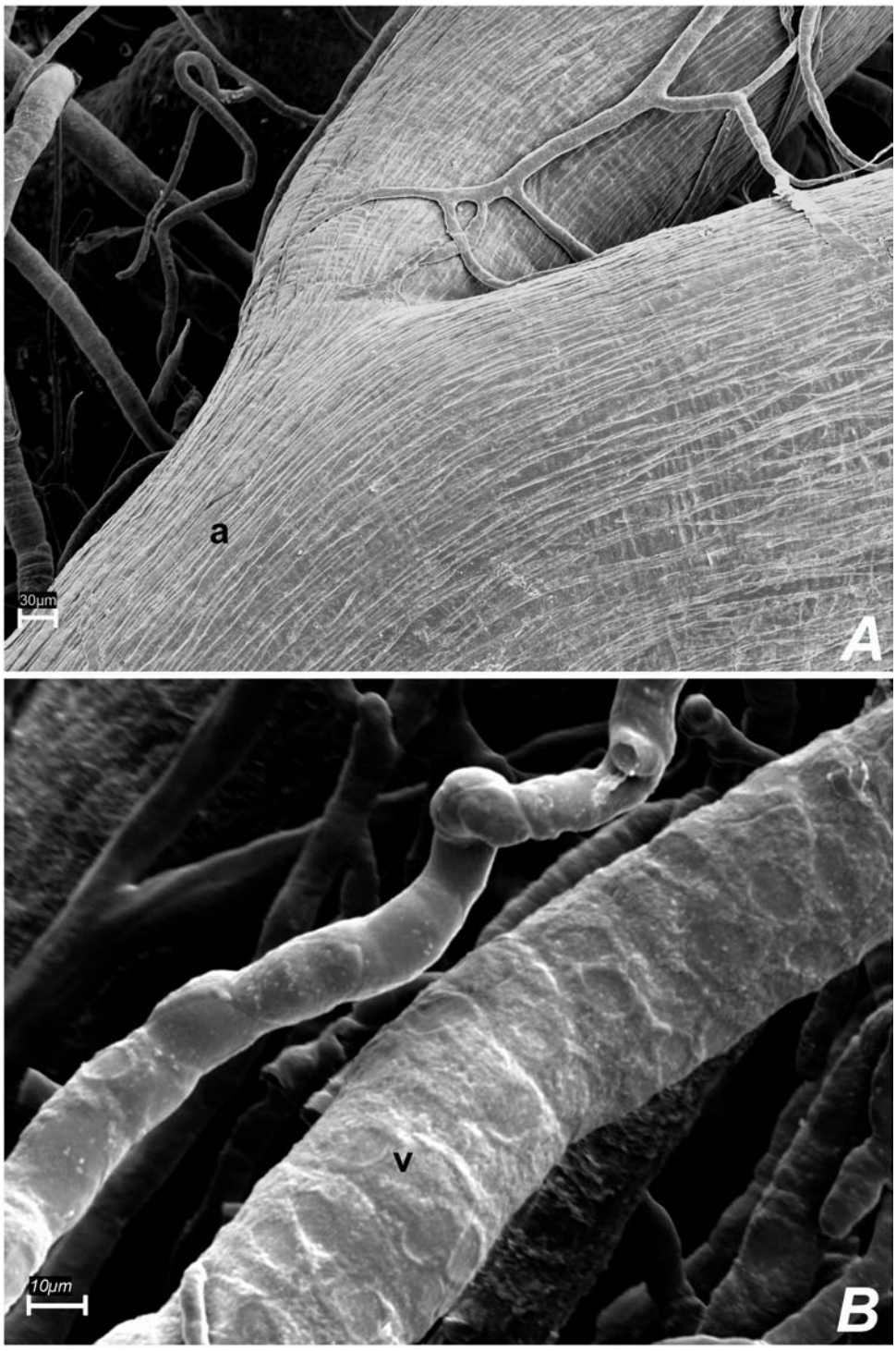

Fig. 24. Scanning electron micrograph of microvascular corrosion casts of an artery (***A***), and vein (***B***). Arteries and veins can be distinguished by the different impression patterns made by endothelial cell borders and nuclei. On an artery (**a**), they are deep, slender and regularly arranged parallel to the longitudinal axis of the vessel. On a vein (**v**), they are shallow, rounder and randomly oriented. Bar = 30 µm in ***A*** and 10 µm in ***B***.

Uterus

Qualitative study

Caruncles were supplied by branches of radial arteries. As mentioned above, any given caruncle could be supplied by one or more radial arteries. Radial arteries gave rise to stem arteries; in non-pregnant does, these stem arteries entered the base of the caruncle, then continued to branch into the substance of the caruncle leading to a mesh of capillaries on the convex (internal, facing the uterine lumen) surface (Fig. 25). Capillaries lead to post capillary venules, in turn small veins and larger veins, which left the caruncle from its base as in the case of arteries. Capillaries covering the internal (convex) surface of the caruncles from non-pregnant does were regular in their diameter and form.

Microvascular corrosion casts of caruncles from non-pregnant does were in the form of ovoid or round elevations with an internal convex surface. This description of the caruncles was maintained at 4 weeks of pregnancy with the exception that at 4 weeks of pregnancy they were larger in size (Figs. 26 and 27). The internal surface of the caruncle in non-pregnant does was covered with capillary meshes with no crypts. At 4 weeks of pregnancy, crypts started to form and the surface of the caruncle showed a pattern of ridges (rugae) separated by troughs (depressions) (Fig. 28). Capillaries on the top of ridges became flattened, irregular, and dilated with signs of the beginning of formation of capillary sinusoids.

Microvascular corrosion casts of caruncles from pregnant does at advanced stages had the characteristic cup shaped appearance with a distinct concave (fetal) and convex (maternal) surfaces. The degree of the convexity of the maternal side of the caruncle showed great variability even within the same area of the same uterus, ranging from a plate to fully convex surface. Maternal vessels entered the caruncle from its convex side. Branches of one or more radial arteries pursued a tortuous course to the base of the caruncle and ramified over the convex surface of the caruncle (Figs. 29 and 30). They give off stem arteries, which penetrated the periphery of the convex surface of the caruncle from all levels. Stem arteries ramified into arterioles through the substance of the caruncle radially toward the fetal (concave) side (Fig. 31). While coursing through the caruncle, they gave off branches at a narrow angle (Fig. 32). These branches connected together and radiated toward the fetal side. Close to the caruncular concave side (fetal side), they broke into an extensive mesh of capillaries, which was arranged to form crypts to receive the cotyledonary fetal villi (Fig. 33). These capillary meshes could lead back to the convex surface of the caruncle (maternal side). Group of capillaries joined their neighbors to form a venule; near the base of the caruncle these united to form small stem veins, which contributed to larger veins (Fig. 34). Stem veins ran in a similar manner to the stem arteries, with regard to their branching as well as their radial course. Veins distributed on the outer surface of the caruncle in a similar fashion to that of arteries, though veins were more numerous.

At the fetal side of the caruncle, capillaries coalesced to form capillary sinusoids (Figs. 35 and 36). Capillary sinusoids covered more or less the entire concave surface of the caruncle. They were irregular in shape and diameter and showed some pericyte nuclear impressions (Fig. 37). In some specimens, capillary sinusoids were formed before the level of the concave surface of the caruncle (Fig. 38).

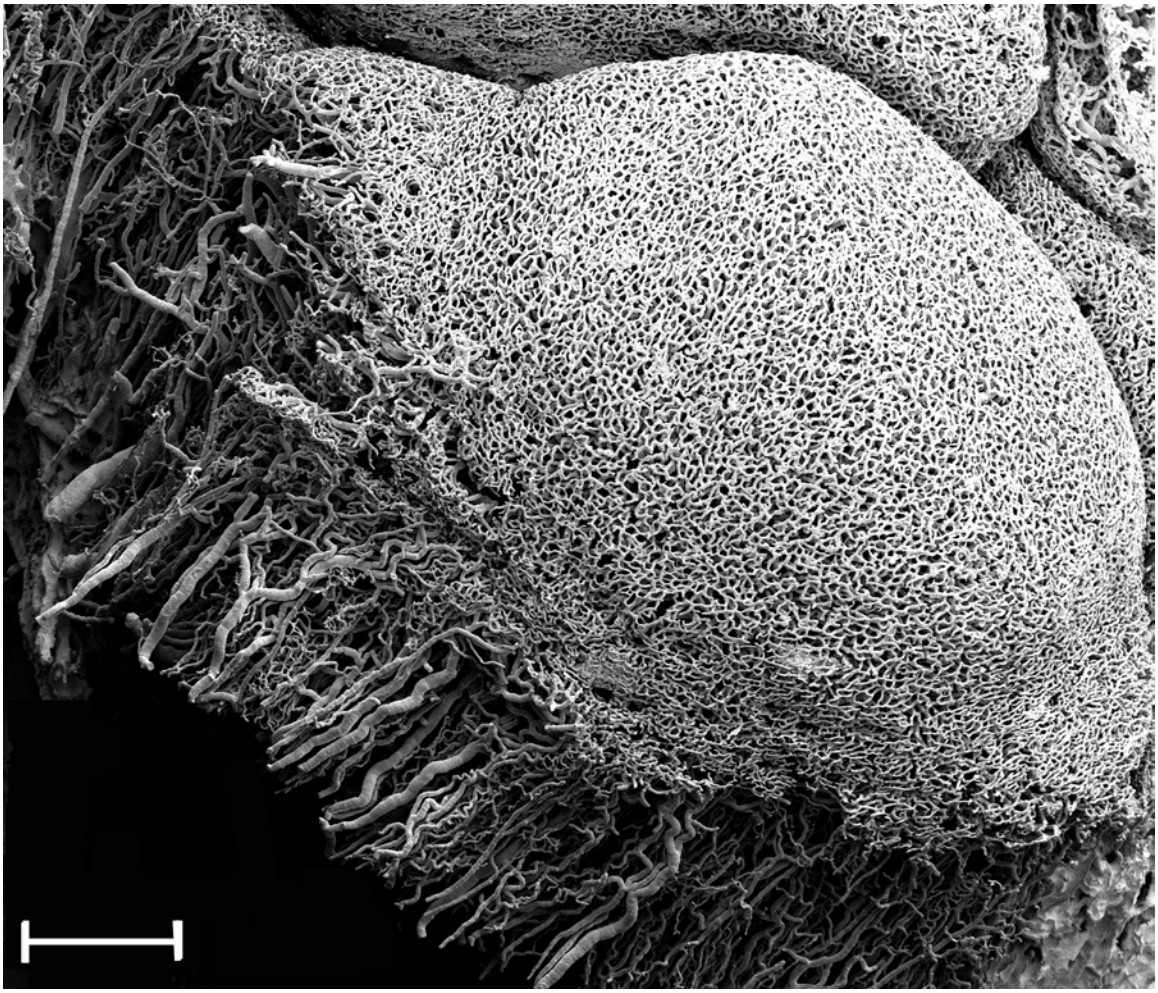

Fig. 25a. Scanning electron micrograph of microvascular corrosions cast of a caruncle from non-pregnant doe. Note that microvascular corrosion casts of caruncles from non-pregnant does are ovoid or round elevations with an internal convex surface. Stem arteries enter the base of the caruncle then continue to branch into the substance of the caruncle leading to a mesh of capillaries on the convex internal surface of the caruncle. Stem veins leave the caruncle from its base as in the case of arteries. Bar = 500 μm.

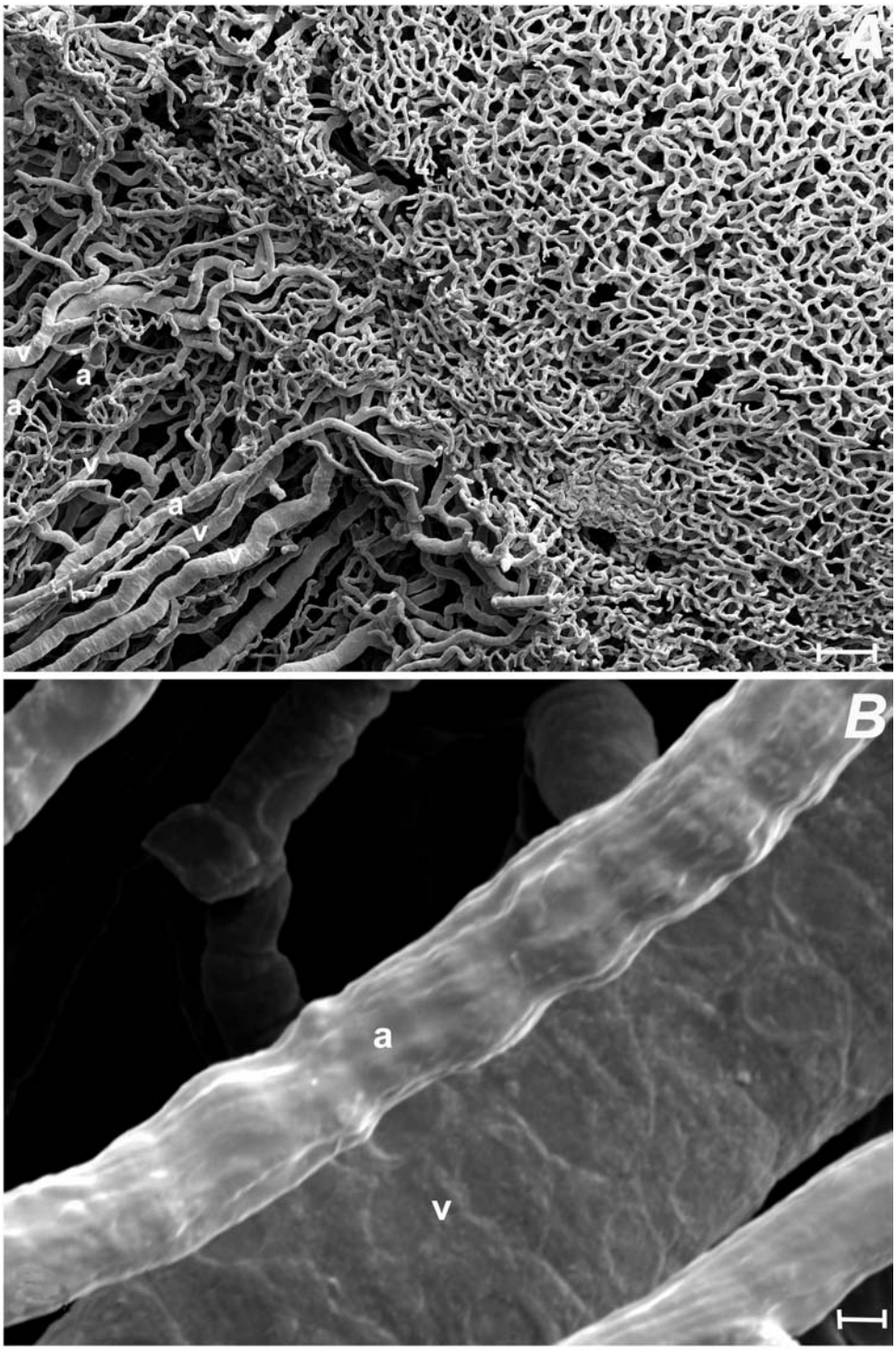

Fig. 25b. Caruncular vasculature. ***A*:** High magnification image of the previous figure (Fig. 25a) showing stem vessels (a, artery; v, vein) entering and leaving the caruncle from its base. ***B*:** High magnification image of ***A***. Arteries and veins can be distinguished as shown in ***B*** by the different impression patterns made by endothelial cell borders and nuclei. On an artery (a), they are deep, slender and regularly arranged parallel to the longitudinal axis of the vessel. On a vein (v), they are shallow, rounder and randomly oriented. Bar = 100 µm in ***A*** and 5 µm in ***B***.

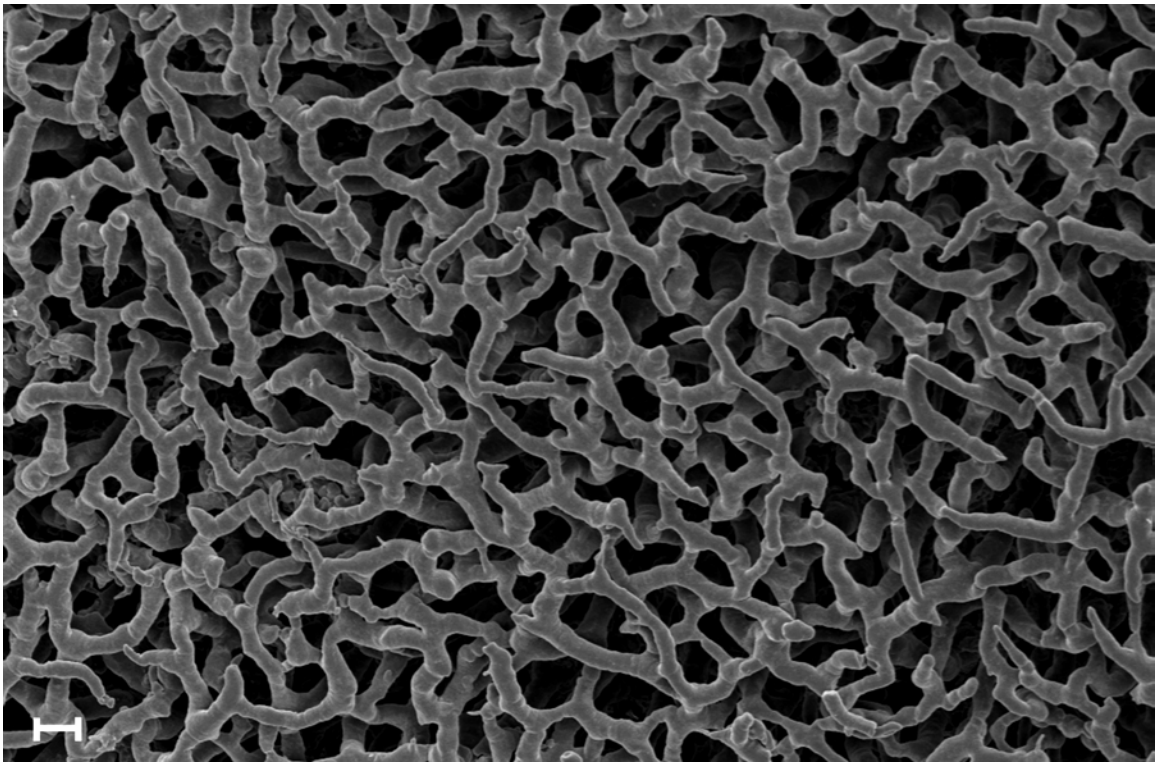

Fig. 25c. High magnification image of the convex surface of the caruncle from non-pregnant doe shown in figure 25a illustrating that the internal convex surface of the caruncle from non-pregnant doe is covered by capillaries of regular form and size. Bar = 20 μm.

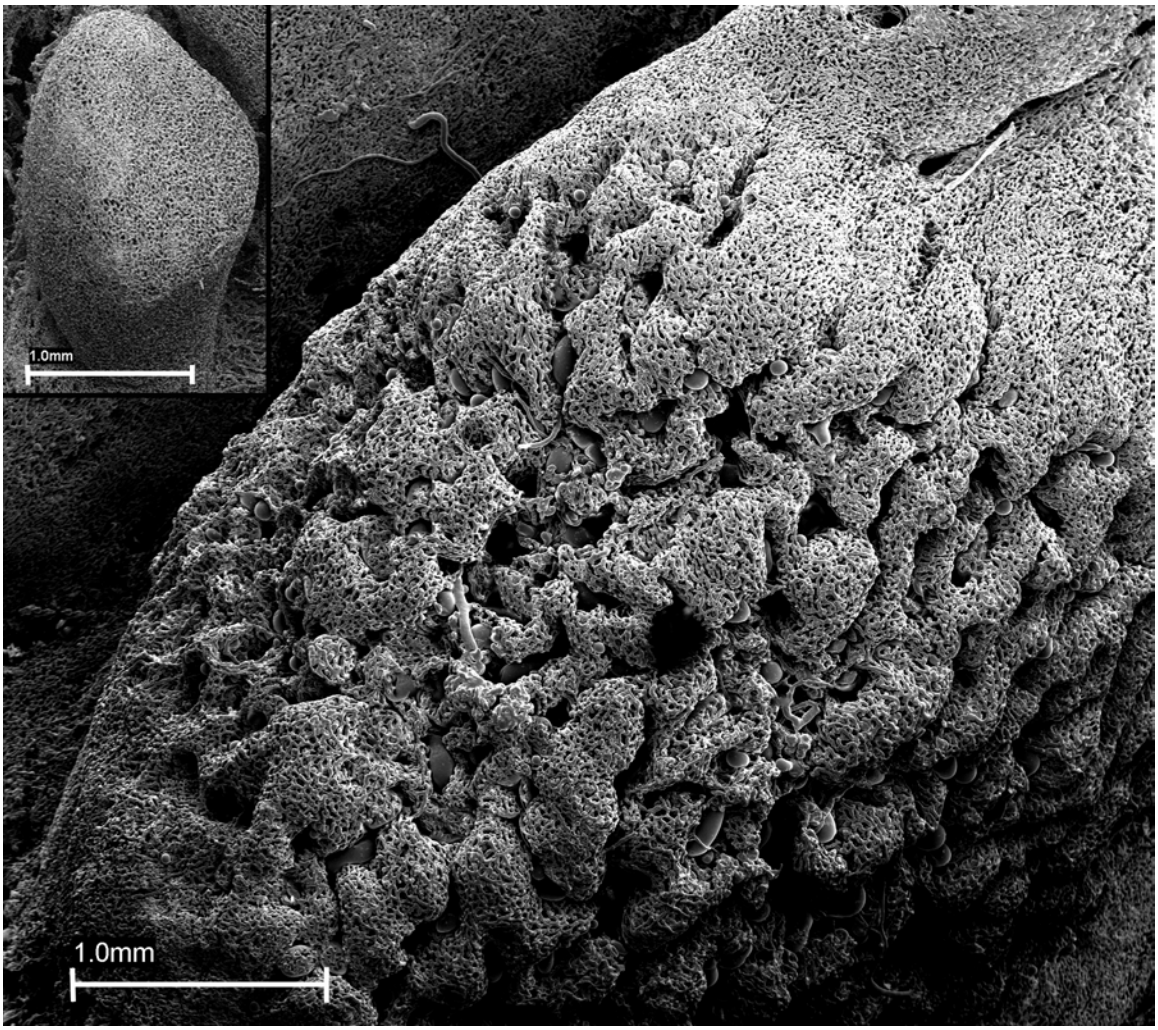

Fig. 26. Scanning electron micrograph of microvascular corrosion cast of a caruncle from a 4-week-pregnant doe viewed from the fetal side showing that the internal (fetal) surface of the caruncle is convex as in the case of non-pregnant does, but the caruncle is larger in size. Compare this to the insert, a scanning electron micrograph of a microvascular corrosion cast of a caruncle from non-pregnant doe. Bar = 1 mm.

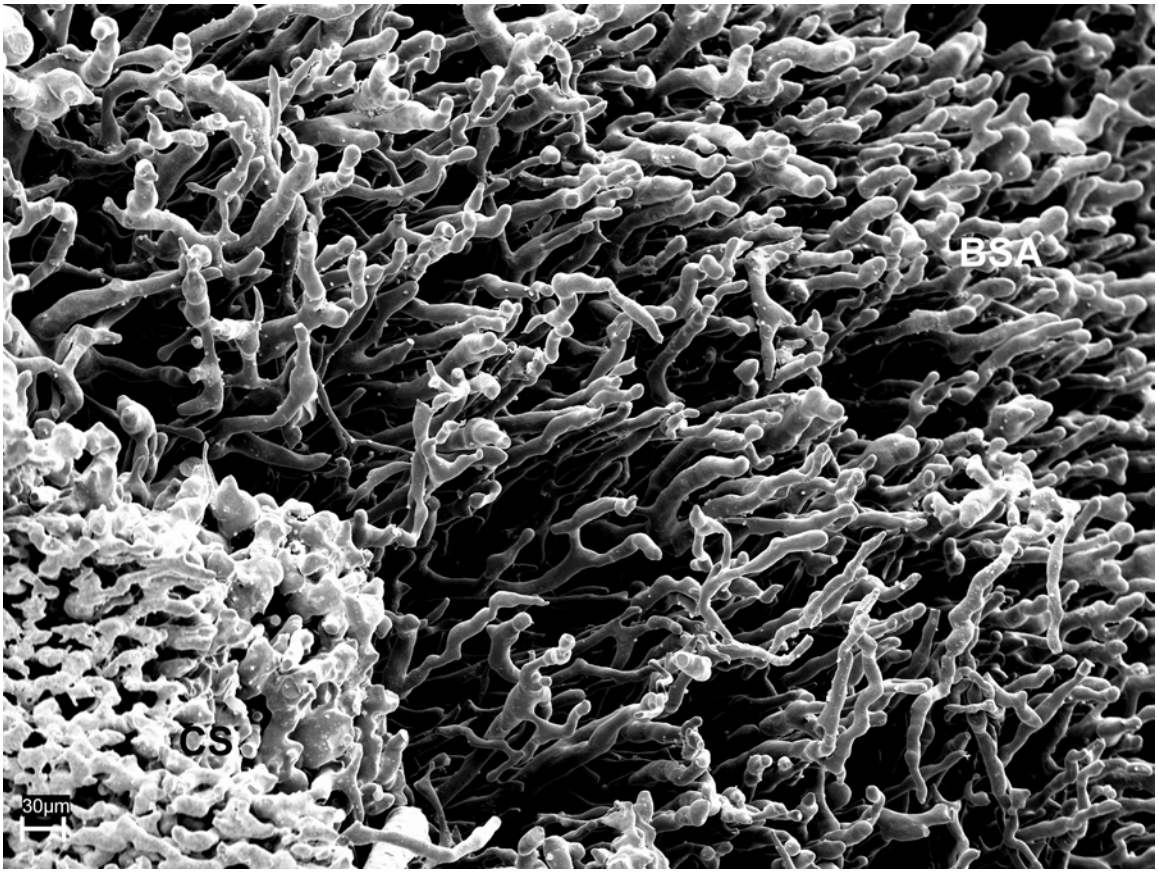

Fig. 27. Scanning electron micrograph of microvascular corrosion cast of an incompletely injected caruncle from a 4-week-pregnant doe viewed from the fetal side. Branches of stem arteries (**BSA**) lead to early forming capillary sinusoids (**CS**) on the fetal surface of the caruncle. Note that the direction of branching of stem arteries is almost parallel to the longitudinal axis of the caruncle and leading to the fetal surface. Bar = 30 µm.

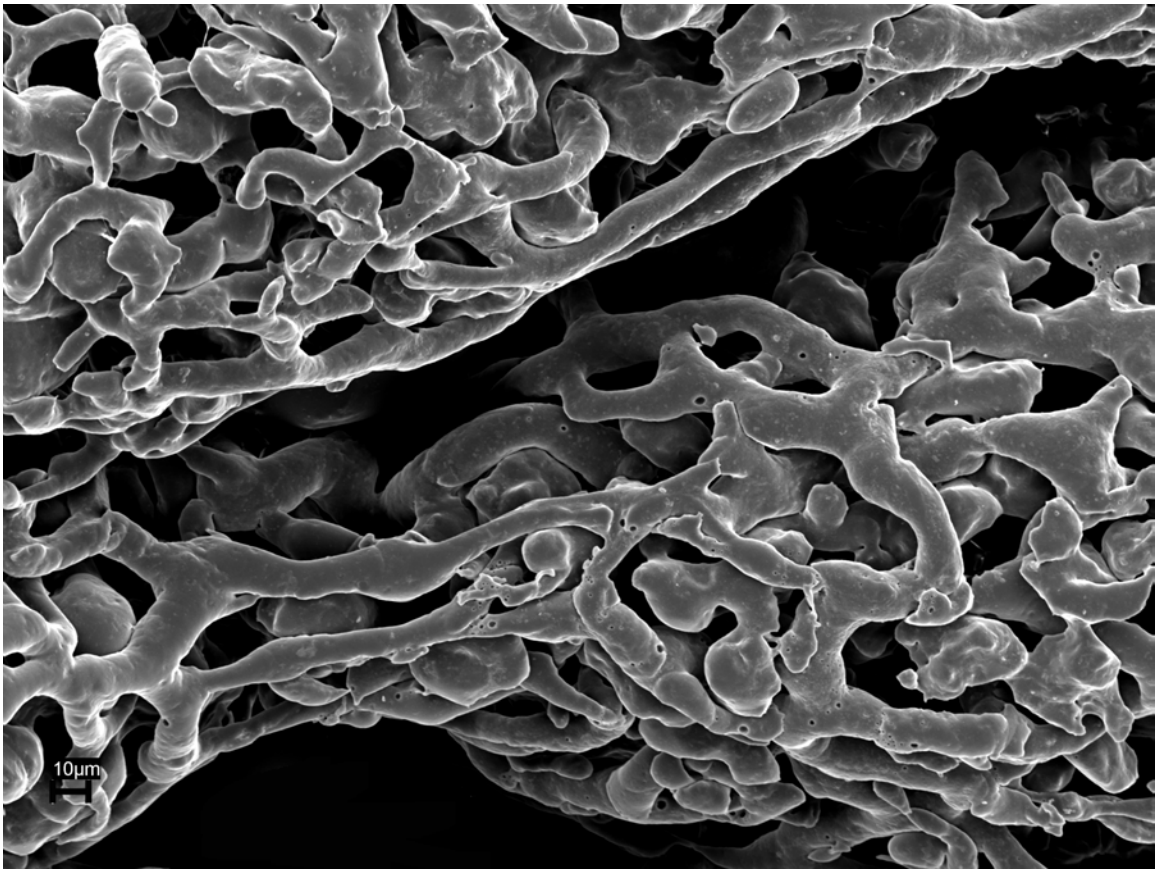

Fig. 28. Scanning electron micrograph of microvascular corrosion cast of a caruncle from a 4-week-pregnant doe taken from the fetal side. At this high magnification, one can observe that the fetal surface of the caruncle shows a pattern of ridges (rugae) separated by troughs (depressions). Capillaries on the top of ridges are flattened, irregular, and show sinusoidal dilations. Bar = 10 µm.

Fig. 29. In this photographic image of a microvascular corrosion cast of 7-week caruncles that have been coated with gold-palladium, branches of the radial artery (**RA**) pursue a tortuous course to the base of the caruncle and ramify over its convex surface giving rise to stem arteries, which penetrate the maternal (convex) surface.

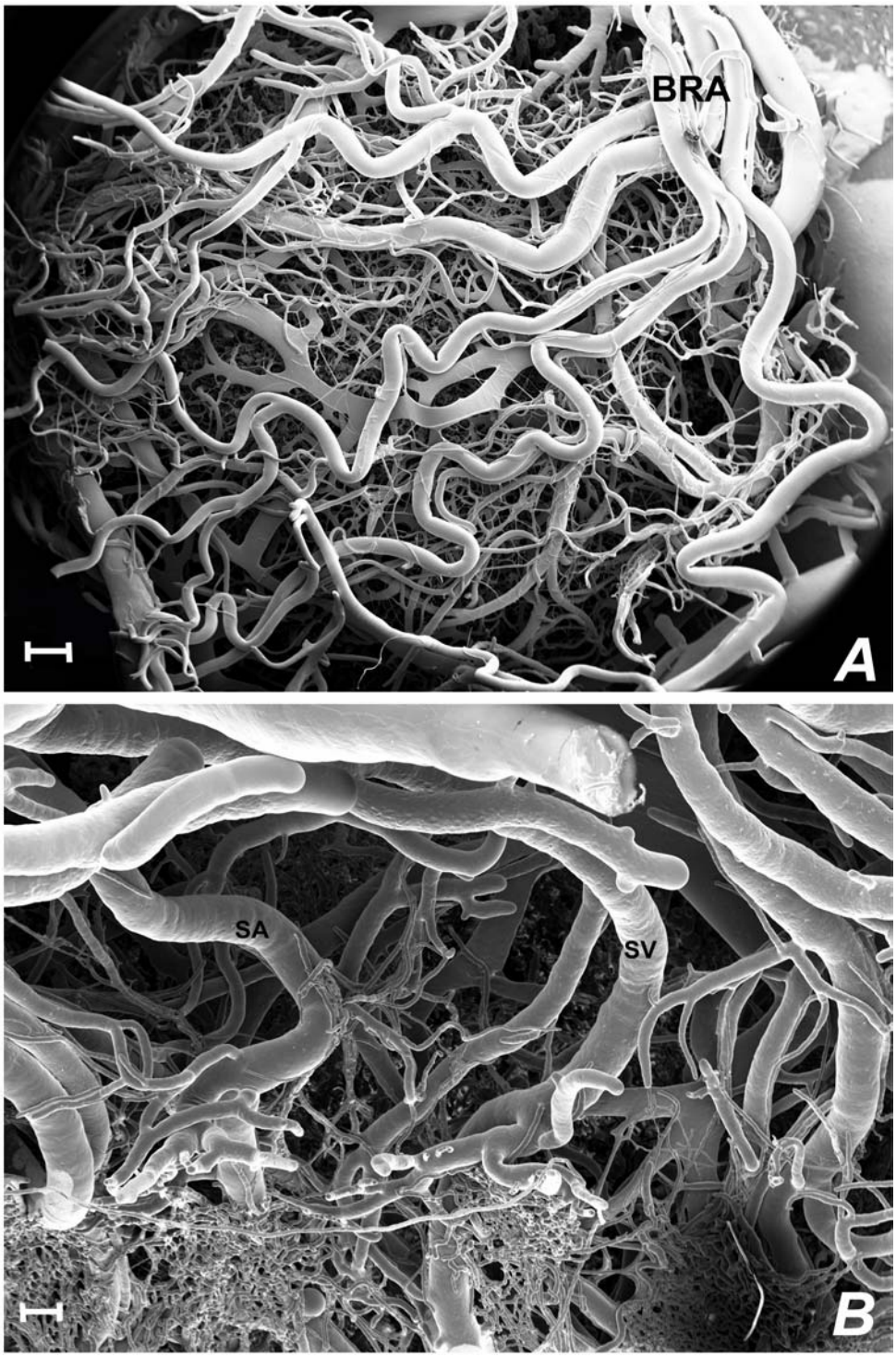

Fig. 30. Scanning electron micrographs of a microvascular corrosion cast from a caruncle from a 7-week-pregnant doe. ***A*:** Convex maternal surface of the caruncle showing branches of the radial arteries (**BRA**) pursuing a tortuous course to the base of the caruncle and ramifying over the convex surface. ***B*:** High magnification image of ***A*** taken from an angle perpendicular to the longitudinal axis of the caruncle. Stem vessels (**SA**, stem artery; **SV**, stem vein) arise from radial vessels and penetrate the entire convex surface of the caruncle. Bar = 500 µm in ***A*** and 150 µm in ***B***.

Fig. 31. Scanning electron micrograph of a microvascular corrosion cast of a sectioned caruncle from a 10-week-pregnant doe showing stem vessels (**SA**, stem artery; **SV**, stem vein) ramifying into arterioles and venules through the substance of the caruncle. They run radially toward and from, respectively, the fetal side of the caruncle (parallel to the longitudinal axis of the caruncle). Bar = 300 µm.

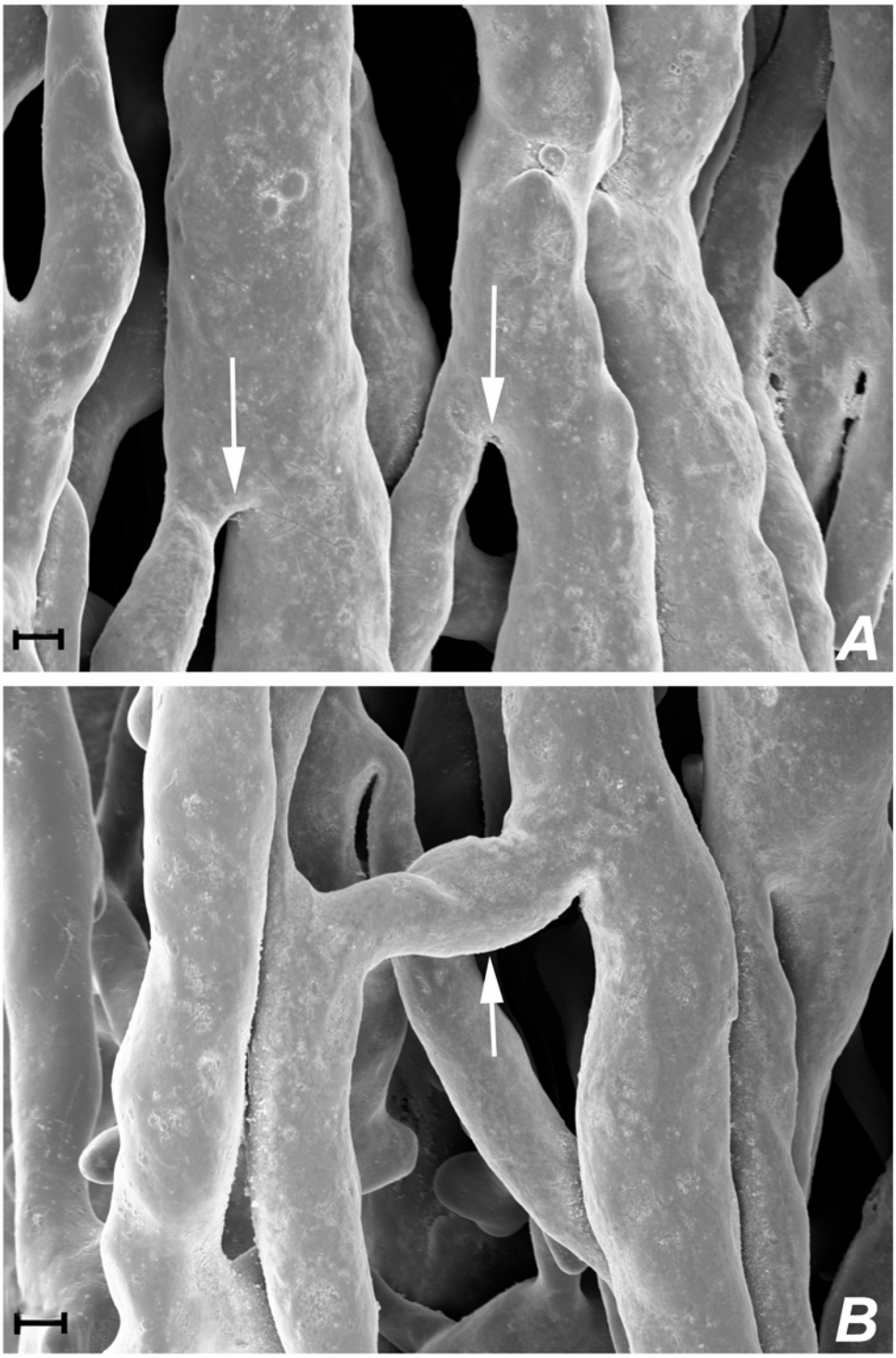

Fig. 32. High magnification scanning electron micrographs of the stem vessels in a 10-week caruncle showing the angle of branching of the stem vessels branches. They diverge at narrow angles (arrows in ***A***), while they course through the caruncle. These branches connect together (arrow in ***B***) and radiate to and from the fetal side of the caruncle. Bar = 10 μm.

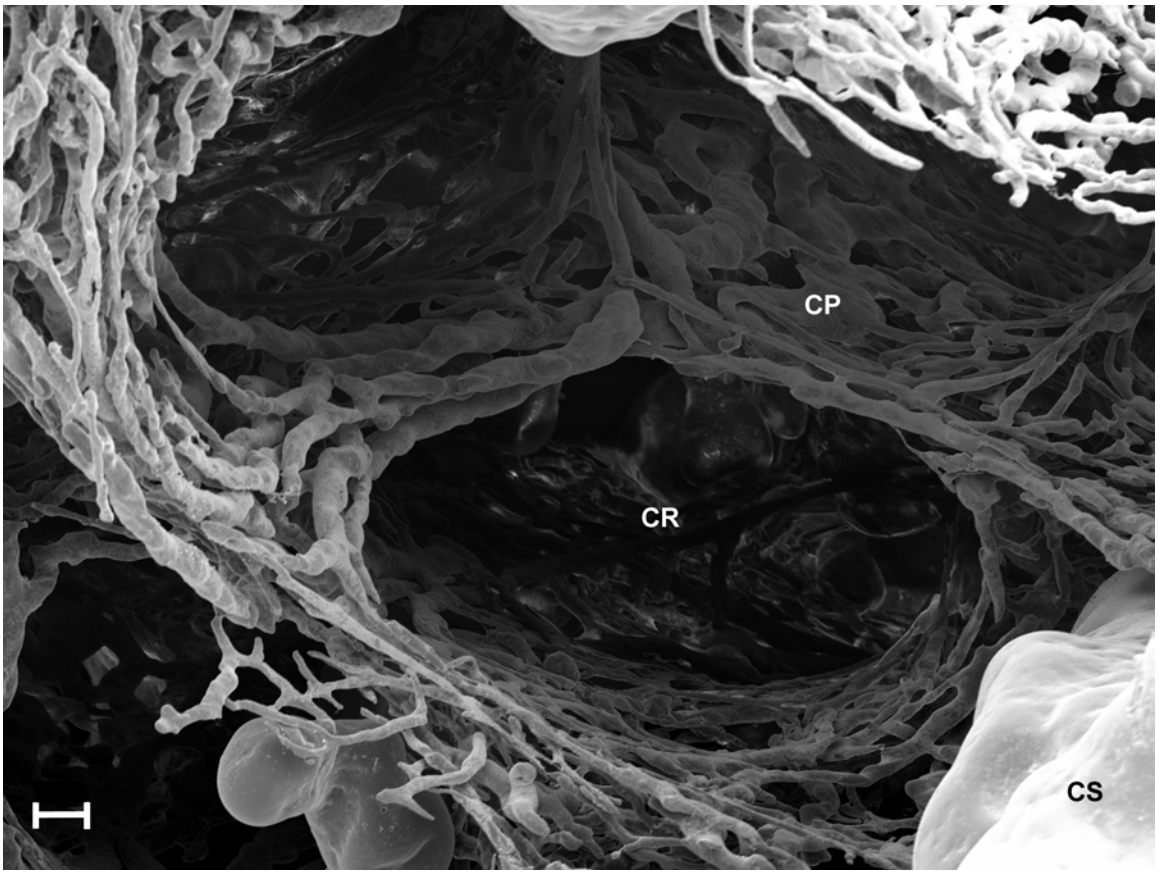

Fig. 33. Scanning electron micrograph of a microvascular corrosion cast of a caruncle from a pregnant doe, viewed from the fetal side displaying the dense capillary network of the maternal crypts. Branches of stem arteries break into an extensive mesh of capillaries (**CP**), which arrange to form crypts (**CR**) that receive the cotyledonary fetal villi. These capillary meshes can lead back to the convex surface of the caruncle (maternal side). **CS**, capillary sinusoid. Bar = 50 µm.

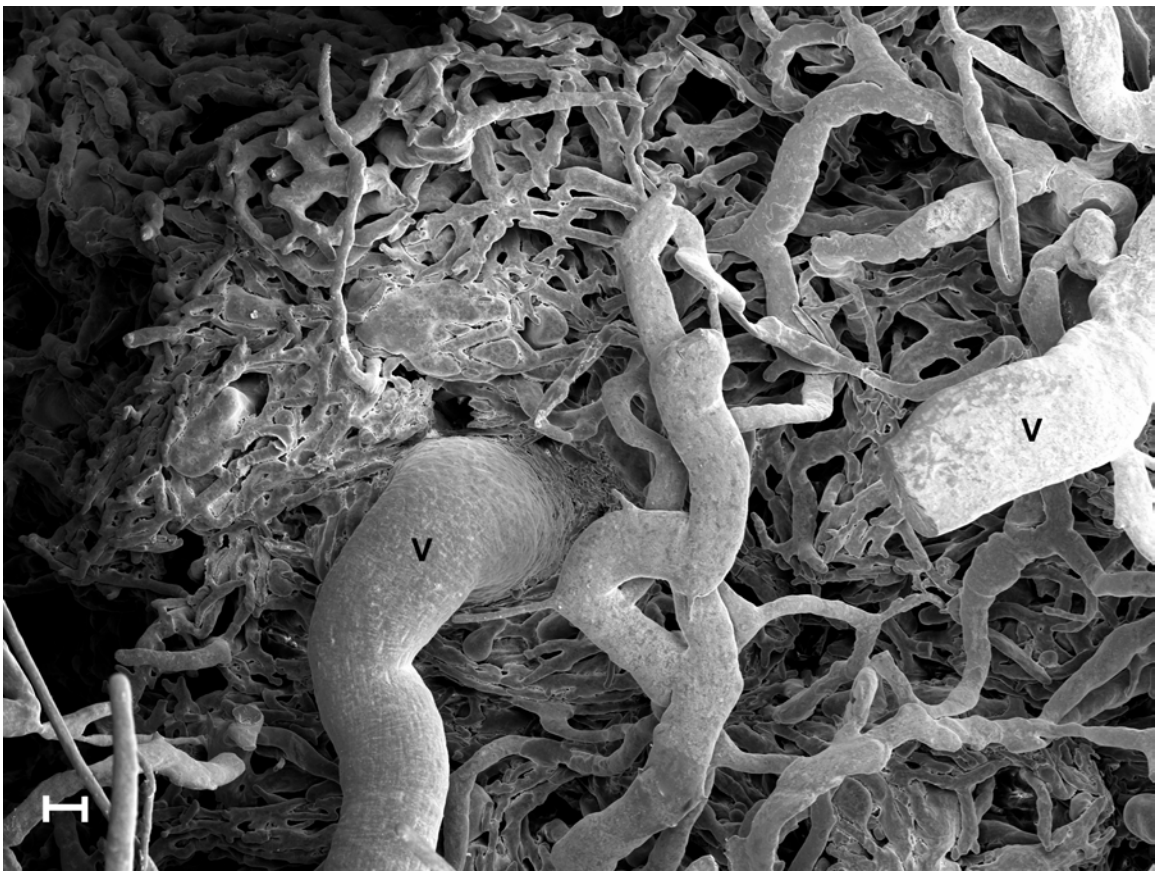

Fig. 34. Scanning electron micrograph of microvascular corrosion cast of a caruncle from pregnant doe showing a group of venules joining their neighbors to form a small vein (**V**), which in turn unites with others to form stem veins contributing to larger veins. Veins distributed on the outer surface of the caruncle in a similar fashion to those of arteries, though veins were more numerous. Bar = 50 µm.

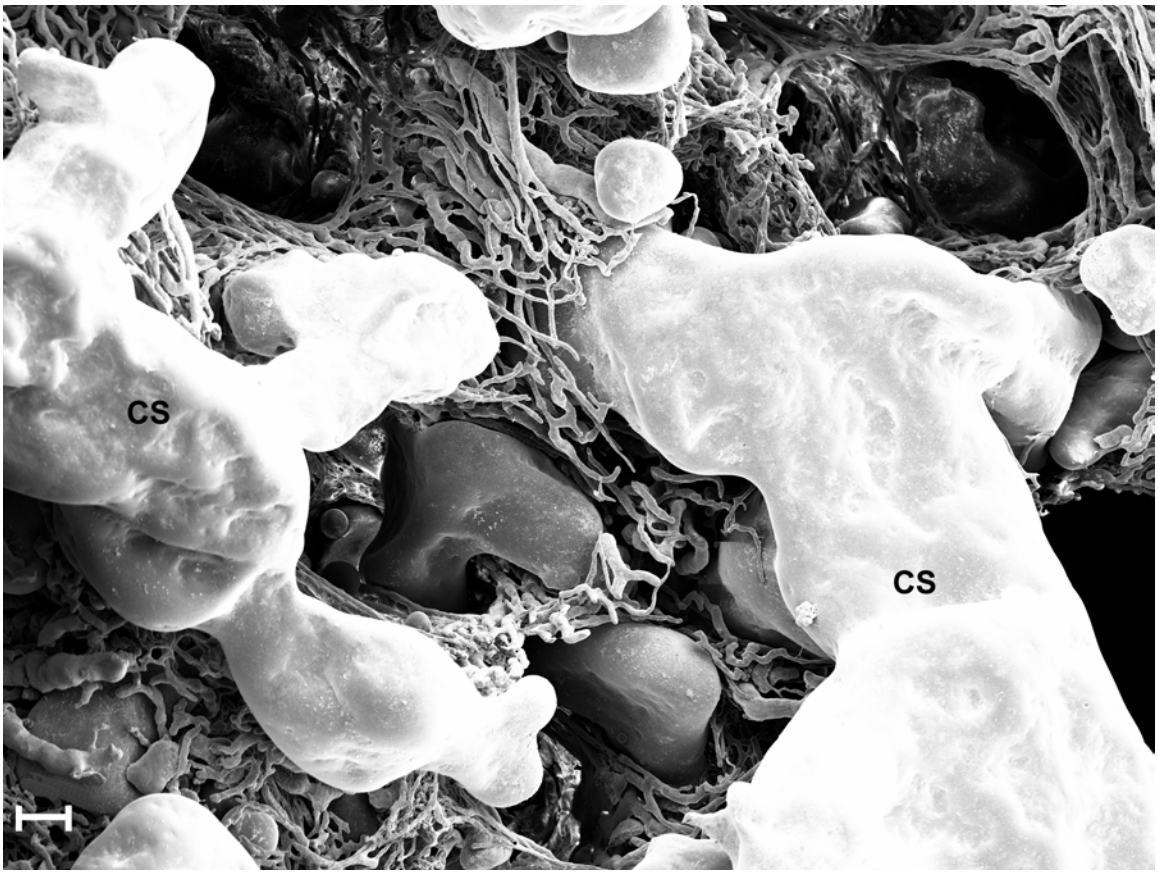

Fig. 35. Scanning electron micrograph of a microvascular corrosion cast of a caruncle from a pregnant doe viewed from the fetal side showing groups of capillaries coalescing to form capillary sinusoids (**CS**). Capillary sinusoids cover more or less the entire concave surface of the caruncle. Bar = 100 µm.

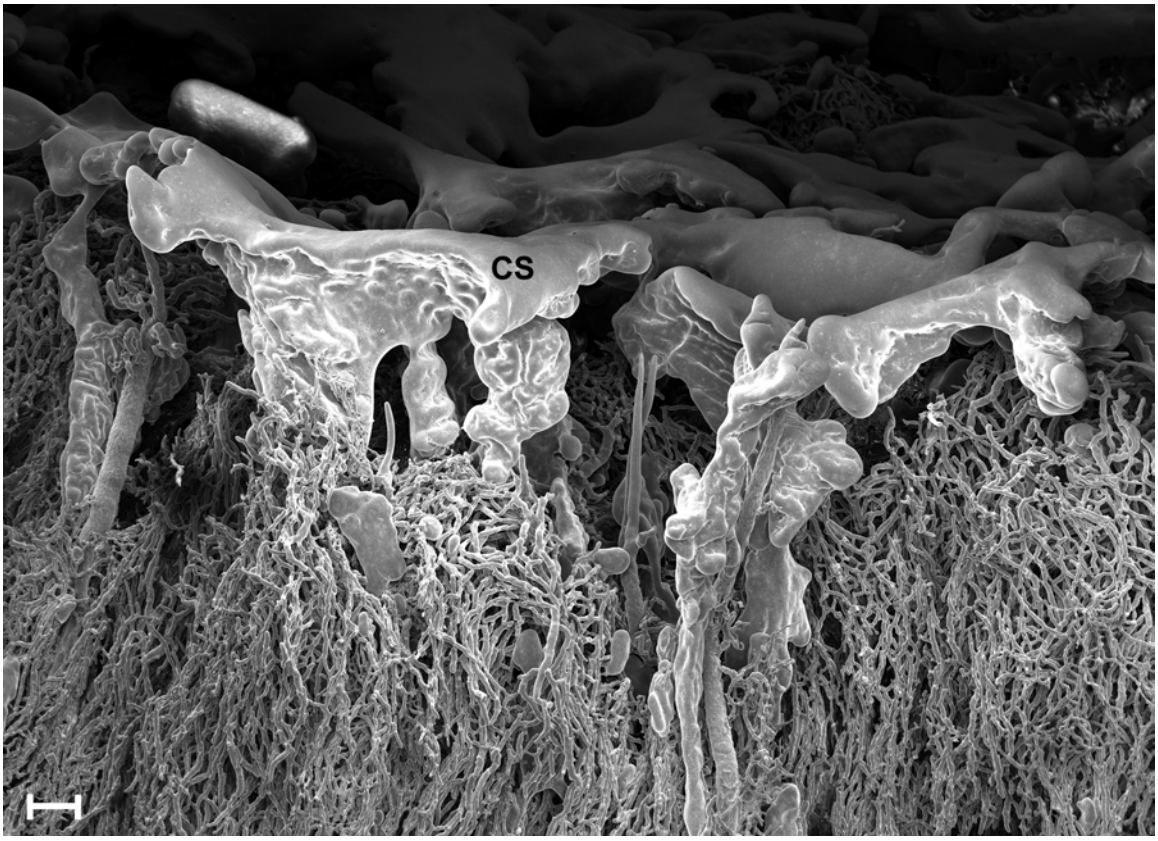

Fig. 36. Scanning electron micrograph of a microvascular corrosion cast of a sectioned caruncle from a pregnant doe taken perpendicular to the longitudinal axis of the caruncle showing the formation of capillary sinusoids (**CS**) on the fetal side of the caruncle. Bar = 300 µm.

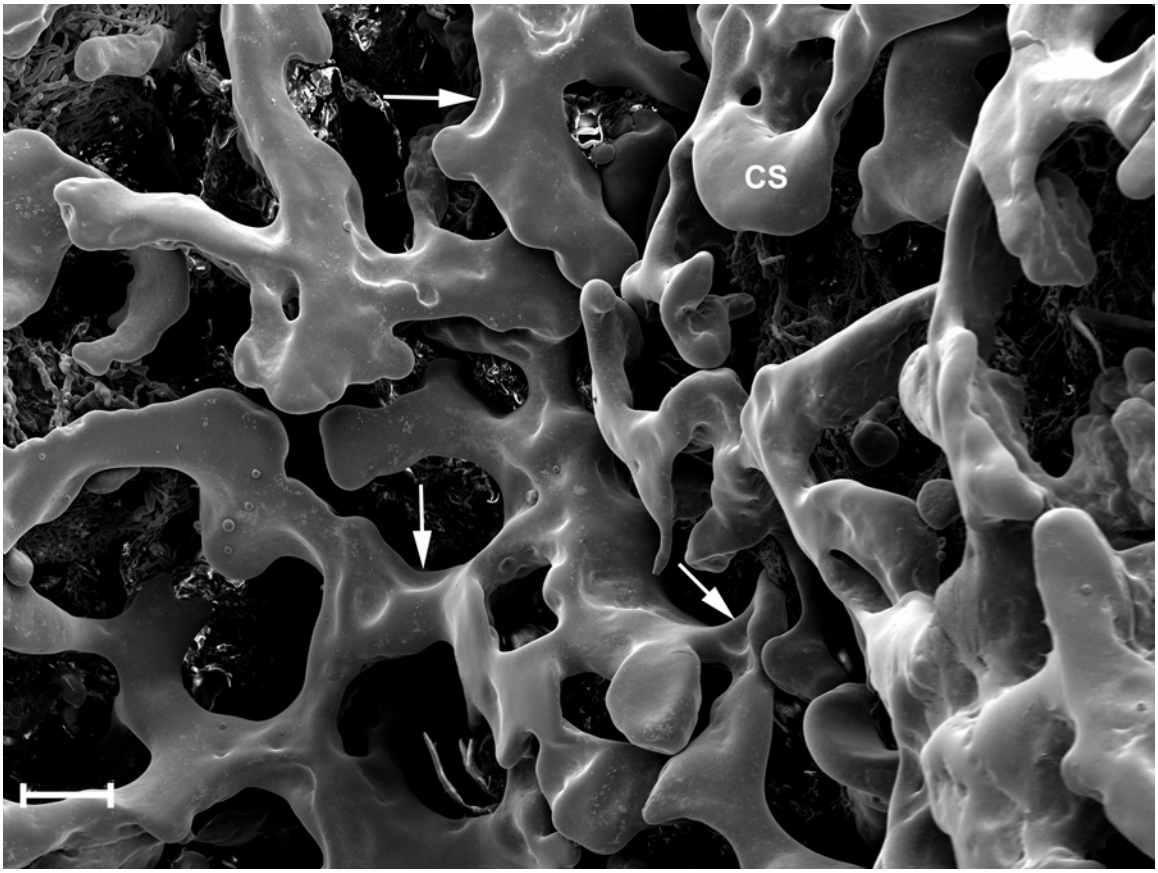

Fig. 37. Scanning electron micrograph of a microvascular corrosion cast of a caruncle from a pregnant doe viewed from the fetal surface showing capillary sinusoids (**CS**). Capillary sinusoids cover more or less the entire concave surface of the caruncle. Note their irregular shape and diameter. Sinusoids show marked impressions from pericyte nuclei (at the tip of arrows). Bar = 500 µm.

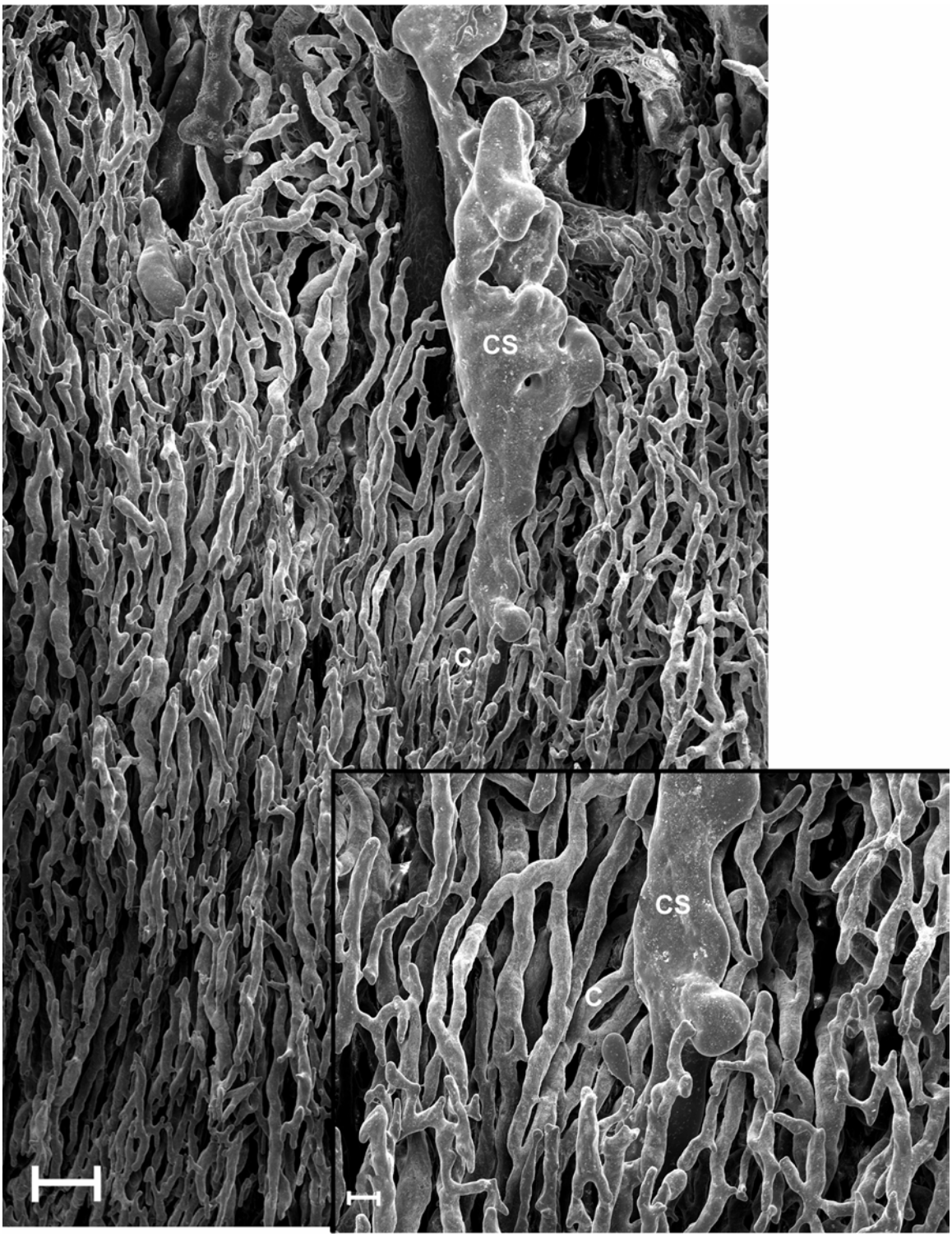

Fig. 38. Scanning electron micrograph of a microvascular corrosion cast of a sectioned caruncle from a pregnant doe taken perpendicular to the longitudinal axis of the caruncle showing a group of capillaries (**C**) coalescing together before the level of the fetal surface of the caruncle to form a capillary sinusoid (**CS**). Insert shows this at a high magnification. Bar = 200 µm and 50 µm in insert.

Signs of angiogenesis were observed in all specimens studied. Evidence of sprouting angiogenesis was marked at all stages. Vascular sprouts were mostly observed in caruncles from non-pregnant does. Short transverse connections and holes corresponding to transcapillary pillar formation, which were regarded as evidence of intussusceptive angiogenesis by other researchers (Burri et al., 2004), were observed at all stages, but mostly at the 4-week stage (Fig. 39).

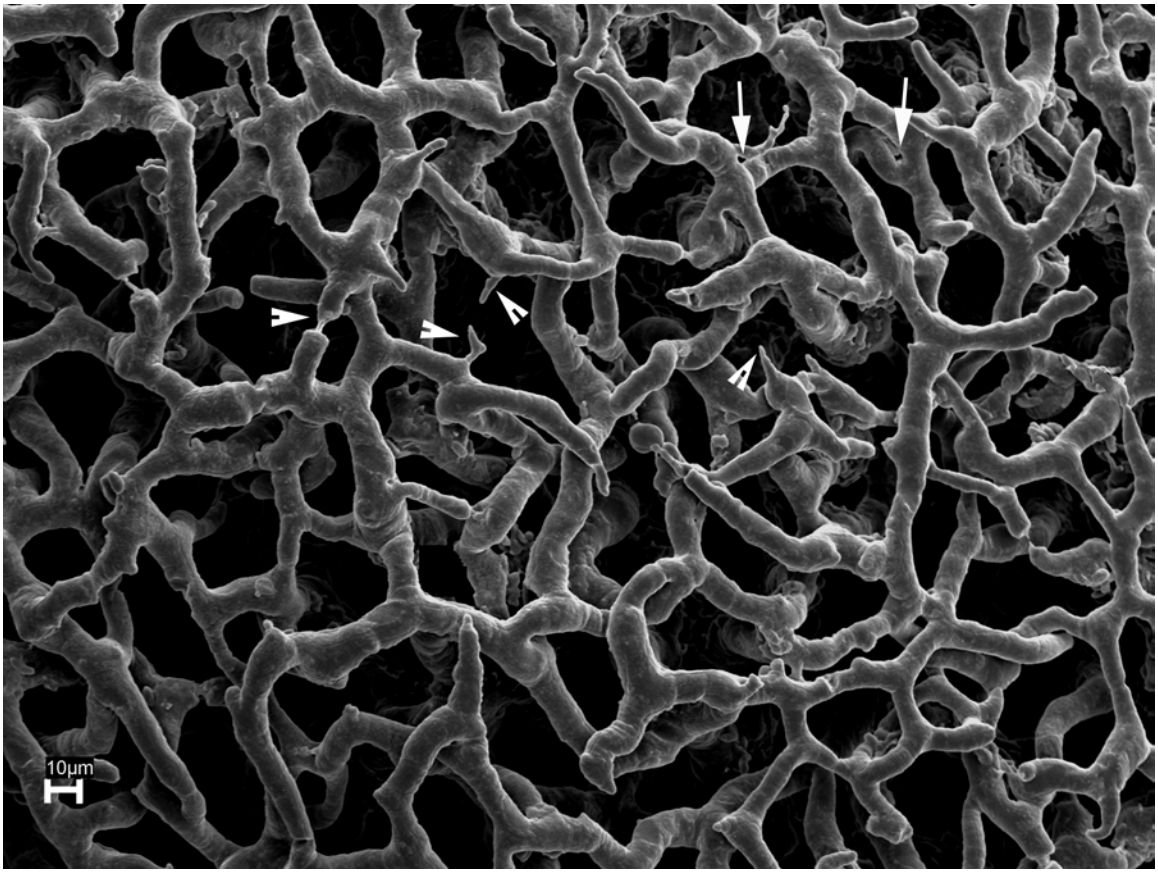

Fig. 39a. Scanning electron micrograph of a microvascular corrosion cast of a caruncle from a non-pregnant doe viewed from the fetal side showing evidence of angiogenesis; vascular sprouts (some are shown at the tip of arrow heads), and holes corresponding to transcapillary pillar formation (at the tip of arrows). Bar = 10 µm.

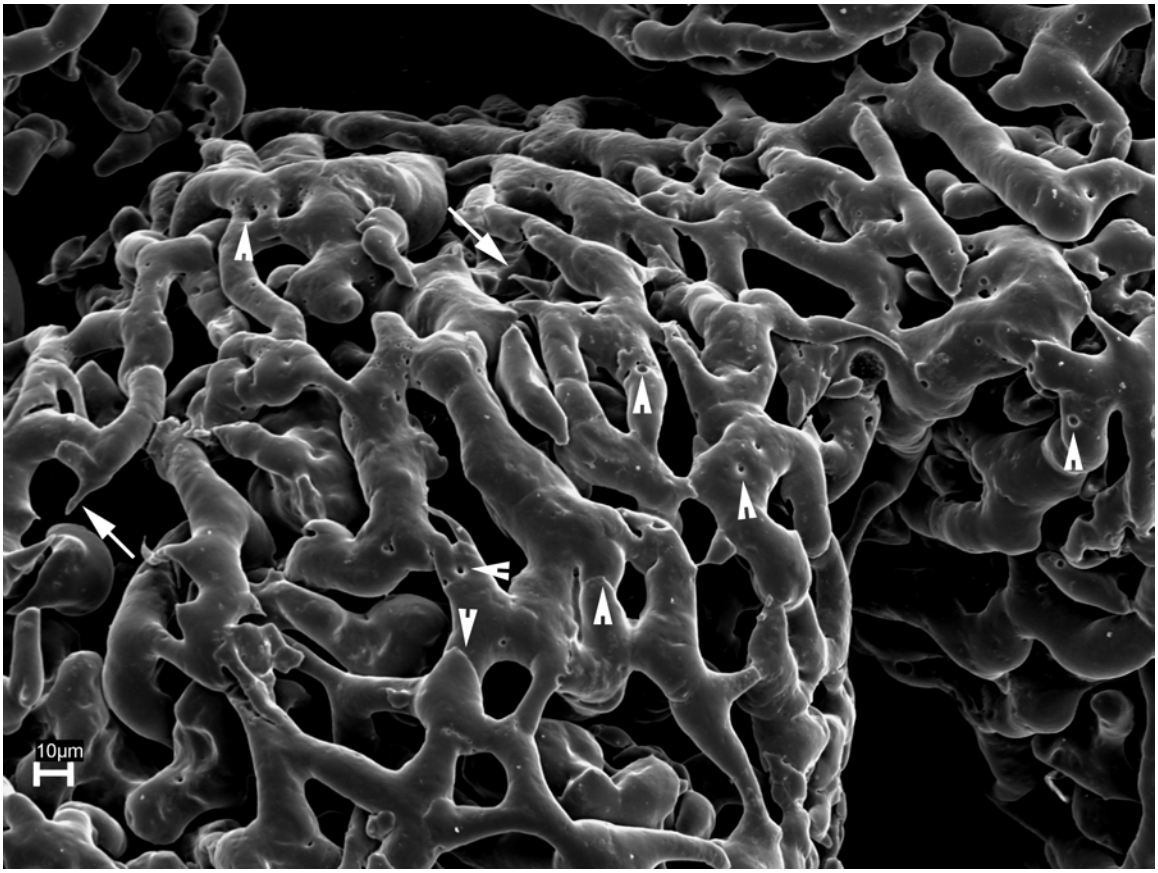

Fig. 39b. Scanning electron micrograph of a microvascular corrosion cast of a caruncle from a 4-week-pregnant doe viewed from the fetal side. Features of what has been regarded as intussusceptive angiogenesis are visible as short transverse connections and holes corresponding to transcapillary pillar formation (some are shown at tip of arrow heads). Vascular sprouts may also be found (at the tip of arrows). Bar = 10 µm.

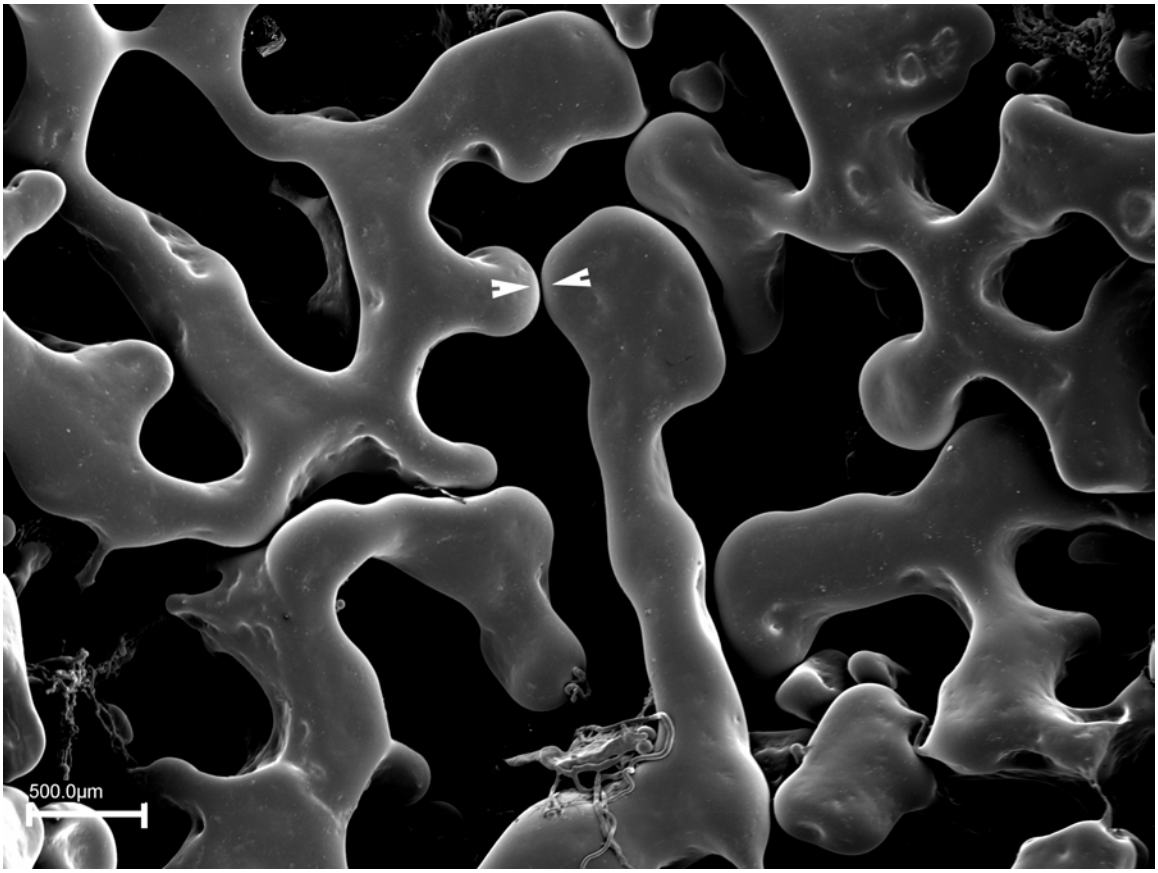

Fig. 39c. Scanning electron micrograph of a microvascular corrosion cast of a caruncle from a 7-week-pregnant doe viewed from the fetal side. Angiogenic features (some are indicated at tip of arrow heads) can be seen. Bar = 500 µm.

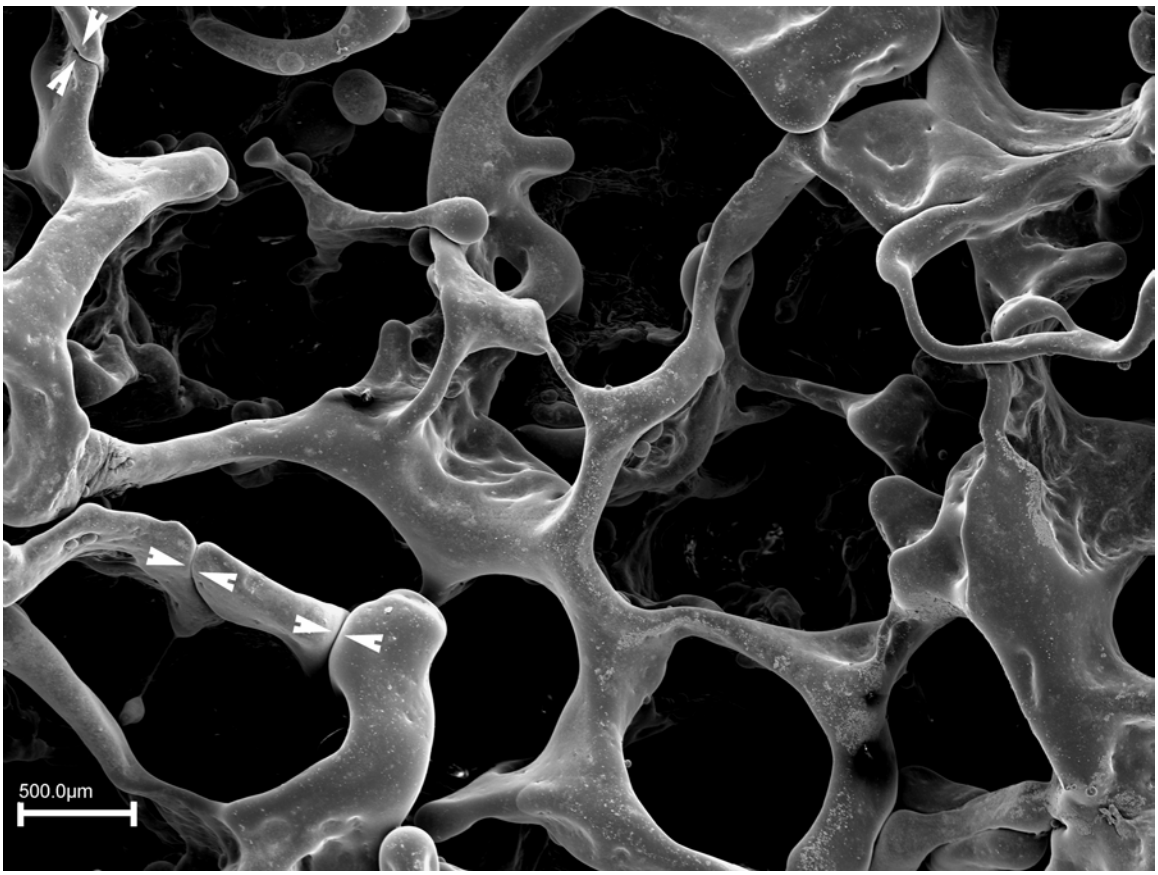

Fig. 39d. Scanning electron micrograph of a microvascular corrosion cast of a caruncle from a 10-week-pregnant doe viewed from the fetal side. Evidence of angiogenesis (some are shown at tip of arrow heads) is visible. Bar = 500 µm.

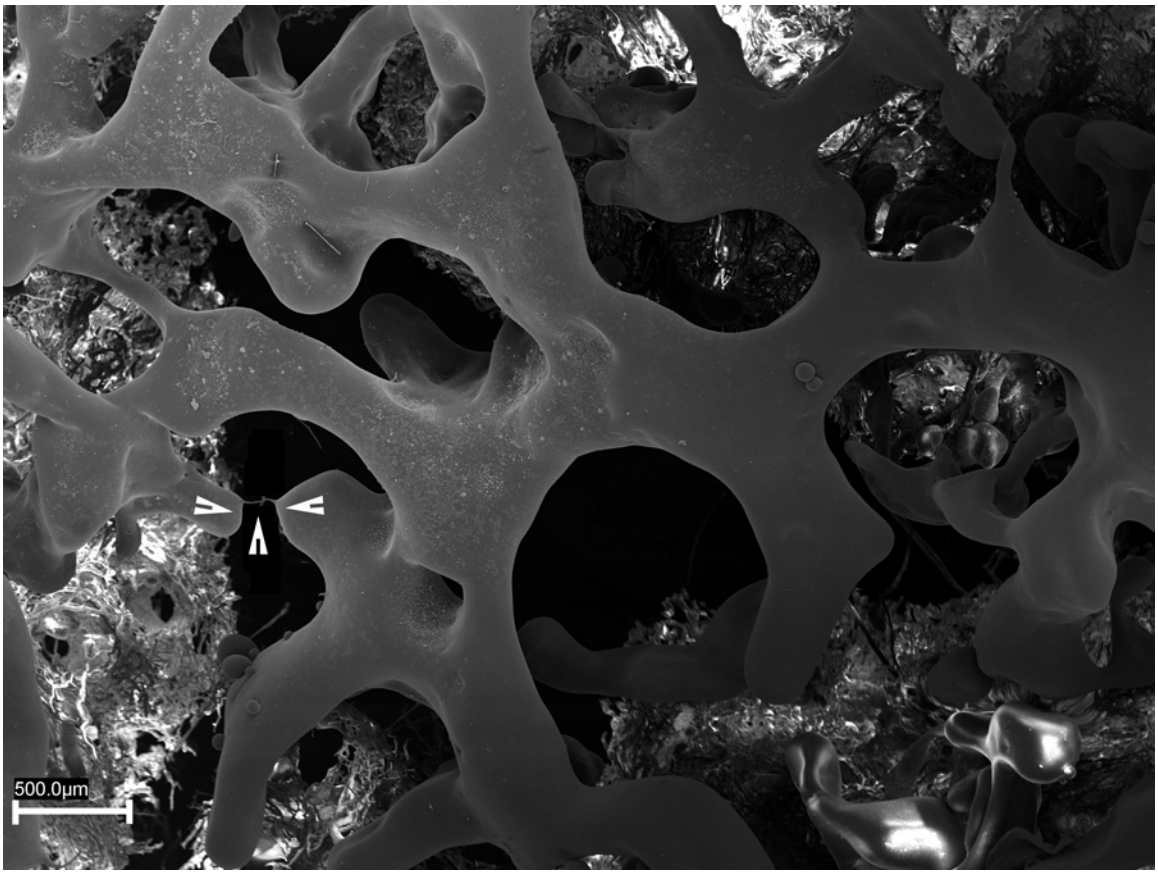

Fig. 39e. Scanning electron micrograph of a microvascular corrosion cast of a caruncle from a 13-week-pregnant doe viewed from the fetal side. Features of angiogenesis (some are shown at arrow heads) can be seen. Bar = 500 µm.

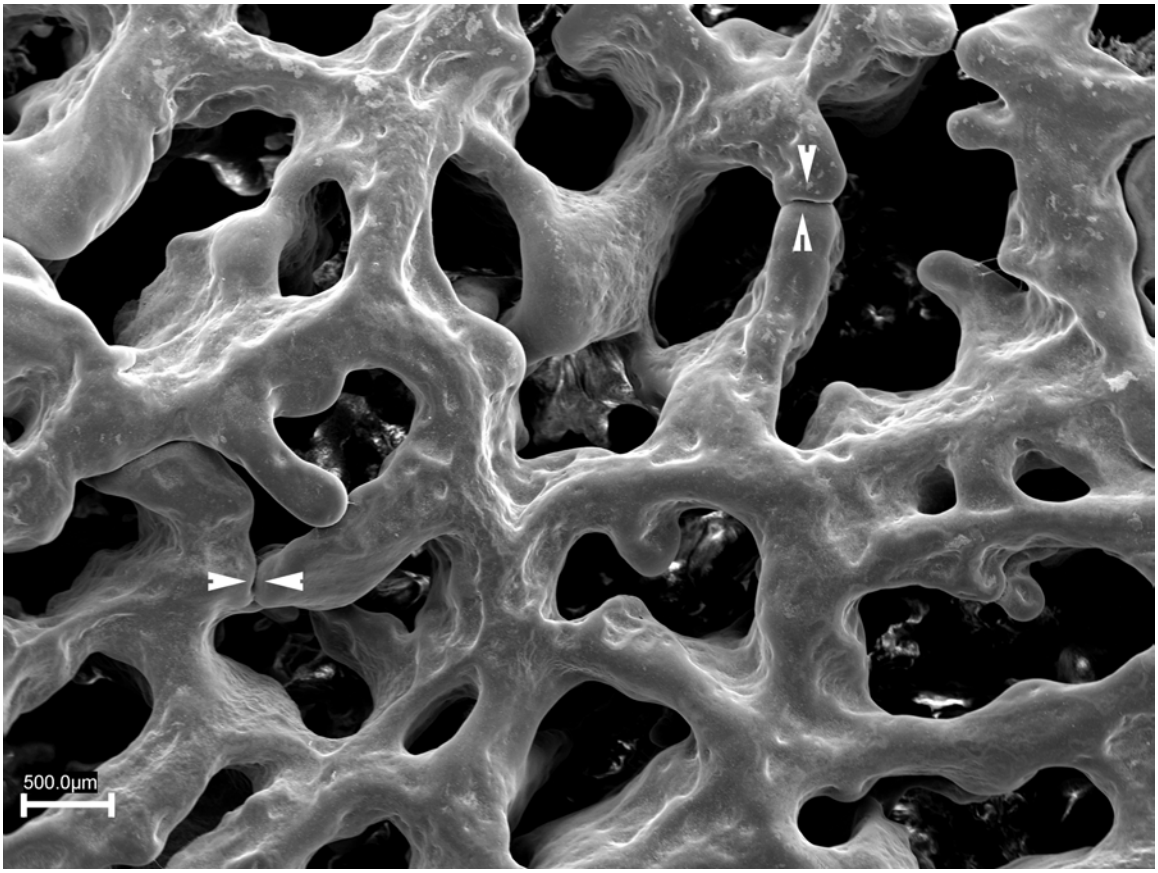

Fig. 39f. Scanning electron micrograph of a microvascular corrosion cast of a caruncle from a 16-week-pregnant doe viewed from the fetal side. Signs of angiogenesis (arrow heads) are seen. Bar = 500 µm.

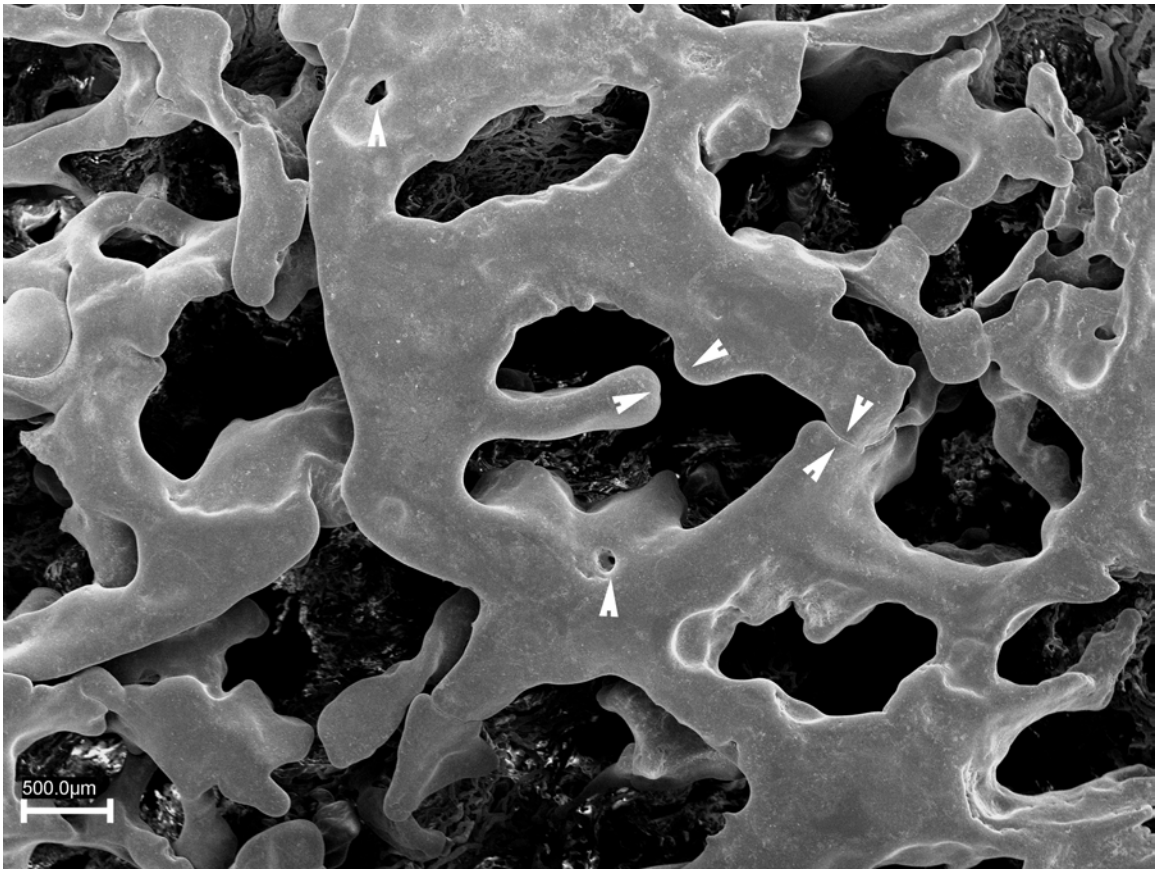

Fig. 39g. Scanning electron micrograph of a microvascular corrosion cast of a caruncle from a pregnant doe at 18 weeks viewed from the fetal side. Angiogenic features (arrow heads) are seen. Bar = 500 µm.

Quantitative study

Measurements of Capillary Diameter

Internal side capillary diameters in non-pregnant does, and capillary sinusoidal diameters in pregnant does are shown in figures 40 and 41. Capillary diameters were significantly greater in caruncles from pregnant does as compared to non-pregnant ones. Also capillary diameters increased significantly after 4 weeks of gestation. No significant differences were found in capillary diameters between stages of pregnancy at and after 7 weeks, except that between 7 and 16 weeks, a significant increase was observed.

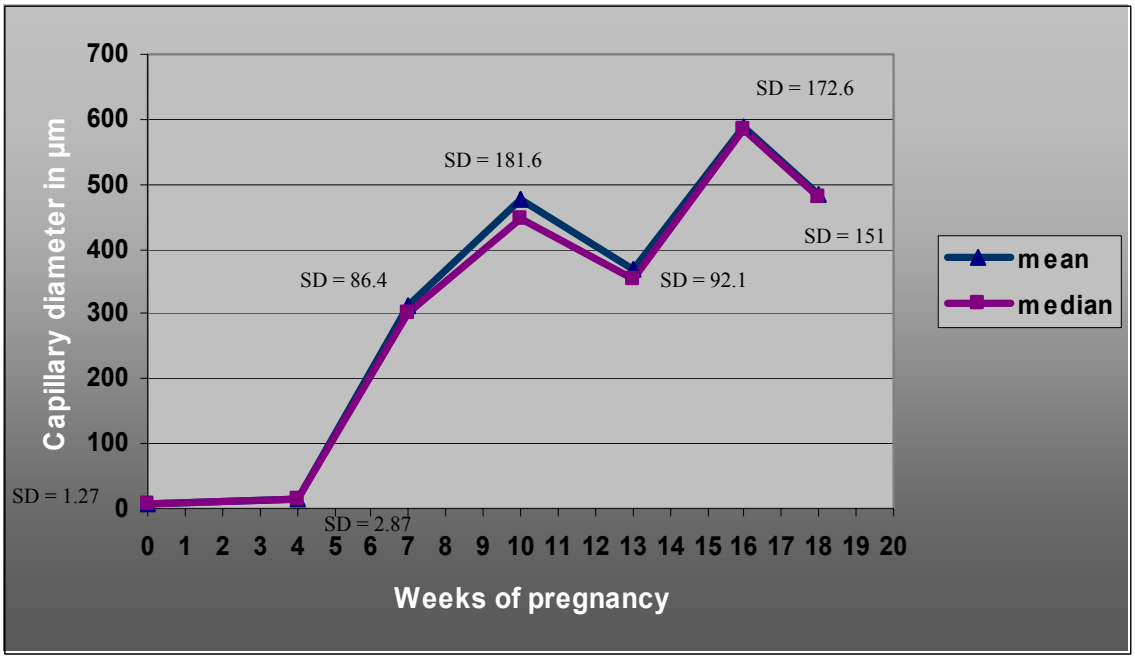

Fig. 40. Mean and median of capillary diameters in non-pregnant (0) and different stages of pregnancy. Capillary diameters increased significantly during pregnancy, especially after the 4-week stage. No significant differences were found in capillary diameters between stages at and after 7 weeks, except between 7 and 16 weeks, where a significant increase was observed. SD = Standard deviation.

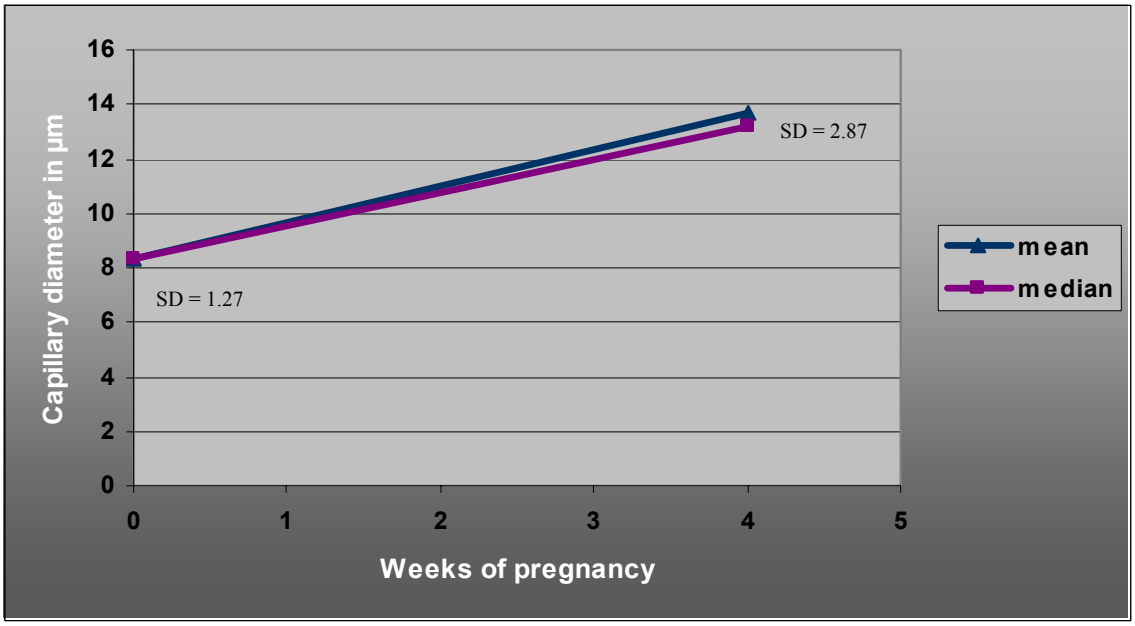

Fig. 41. Mean and median of capillary diameters in non-pregnant (0) and 4-week-pregnant does illustrated on a wider scale figure. Capillary diameters increased significantly at 4 weeks of gestation compared to non-pregnant state. SD = Standard deviation.

Capillary density index

The proportion of surface area covered by capillaries in relation to total area measured was 66.8, 68.7, 55.5, 63.5, 70.1, 70.4, and 64.5 percent in non-pregnant, 4, 7, 10, 13, 16, and 18 weeks of pregnancy, respectively (Fig. 42). No statistically significant differences were found in capillary density index between non-pregnant and pregnant does and/or among stages of pregnancy.

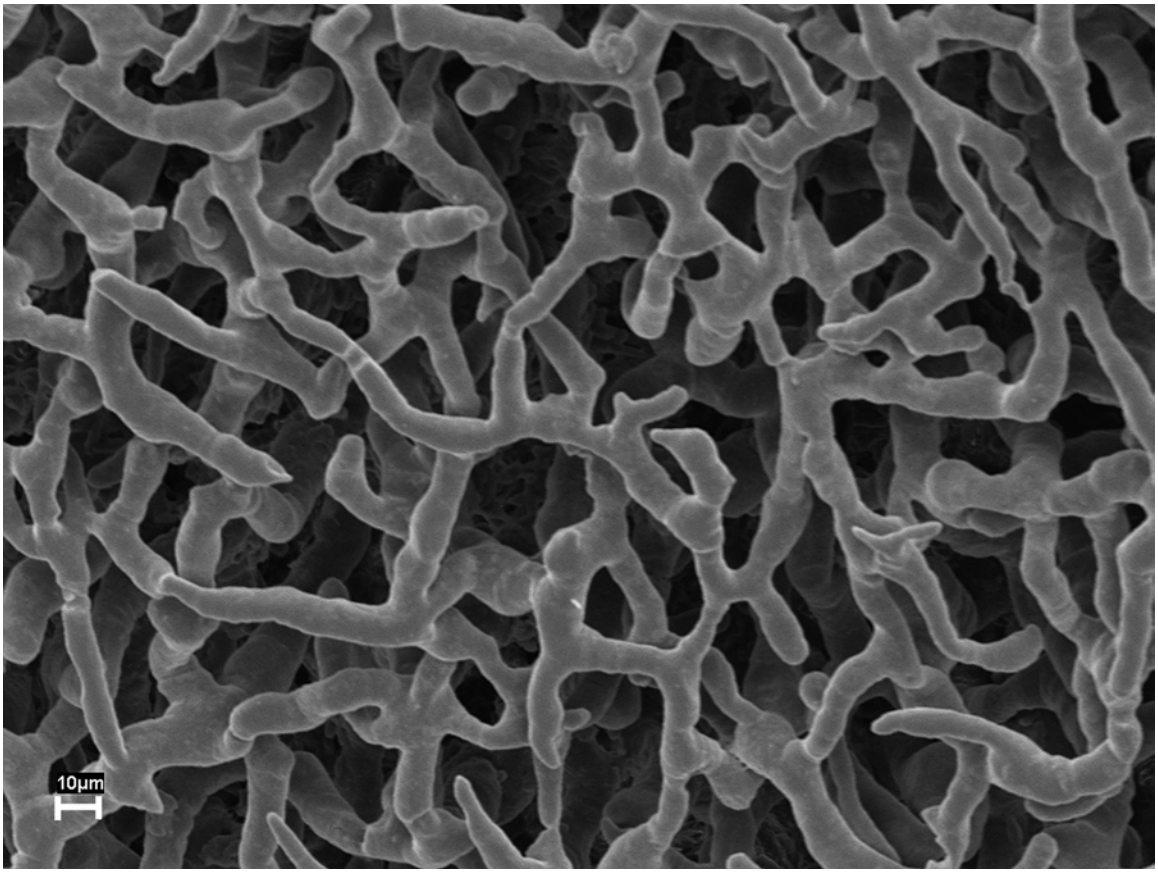

Fig. 42a. Scanning electron micrograph of a microvascular corrosion cast of a caruncle from a non-pregnant doe viewed from the internal side illustrating capillary density. Bar = 10 µm.

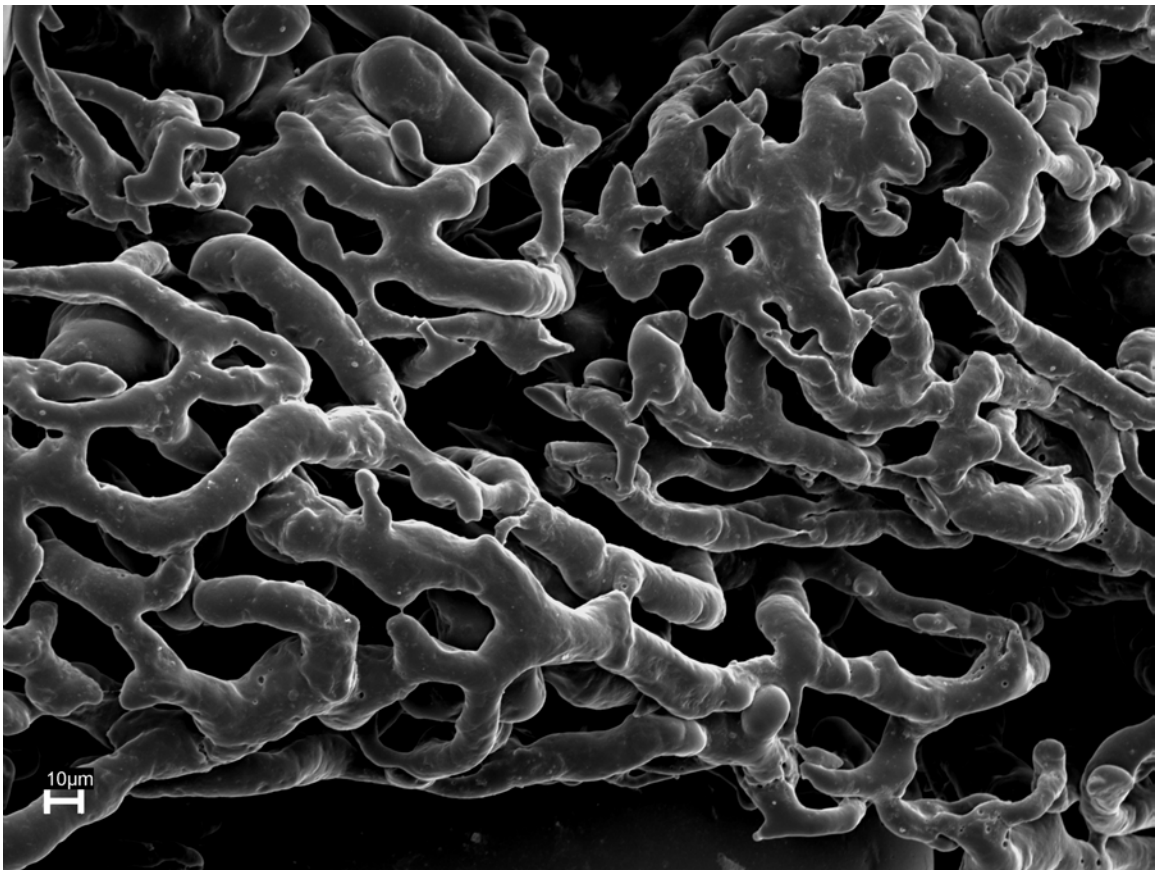

Fig. 42b. Scanning electron micrograph of a microvascular corrosion cast of a caruncle from a 4-week-pregnant doe viewed from the fetal side showing capillary density. Bar = 10 µm.

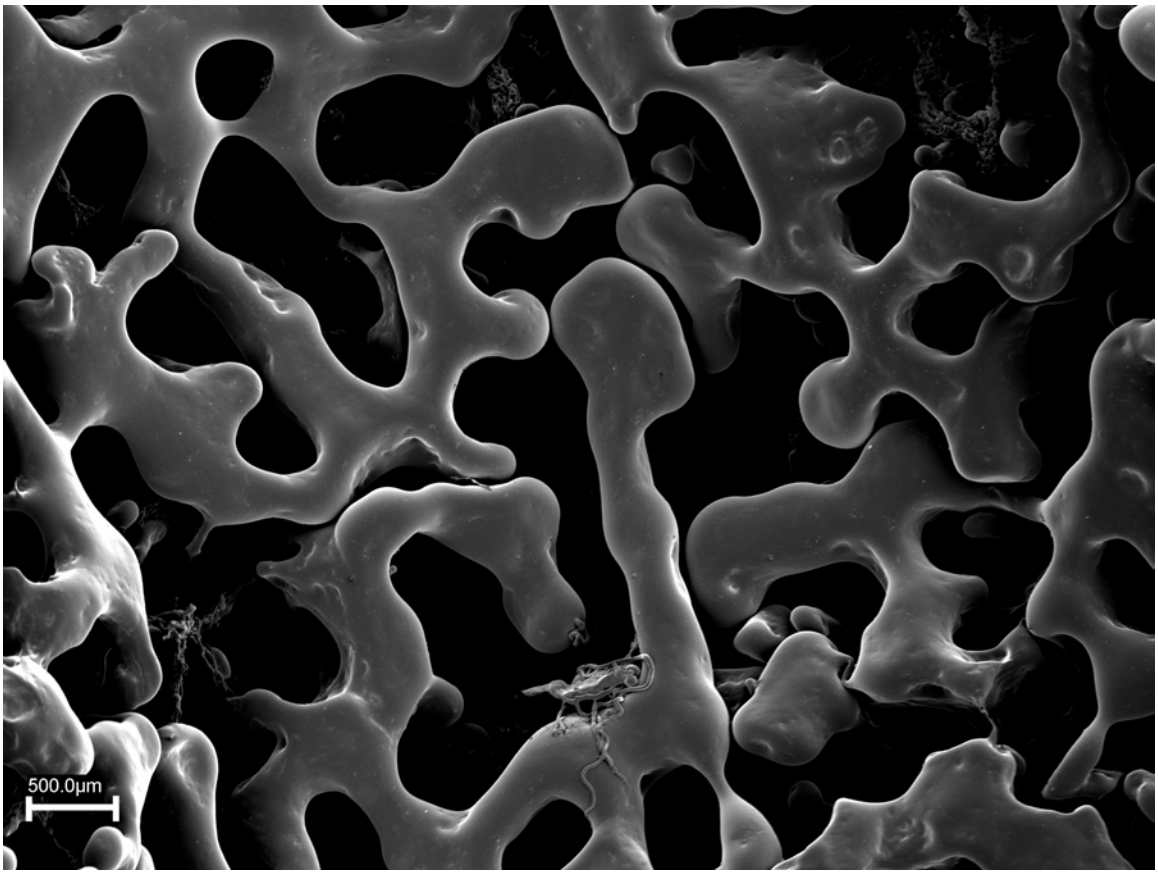

Fig. 42c. Scanning electron micrograph of a microvascular corrosion cast of a caruncle from a 7-week-pregnant doe viewed from the fetal side illustrating capillary density. Bar = 500 µm.

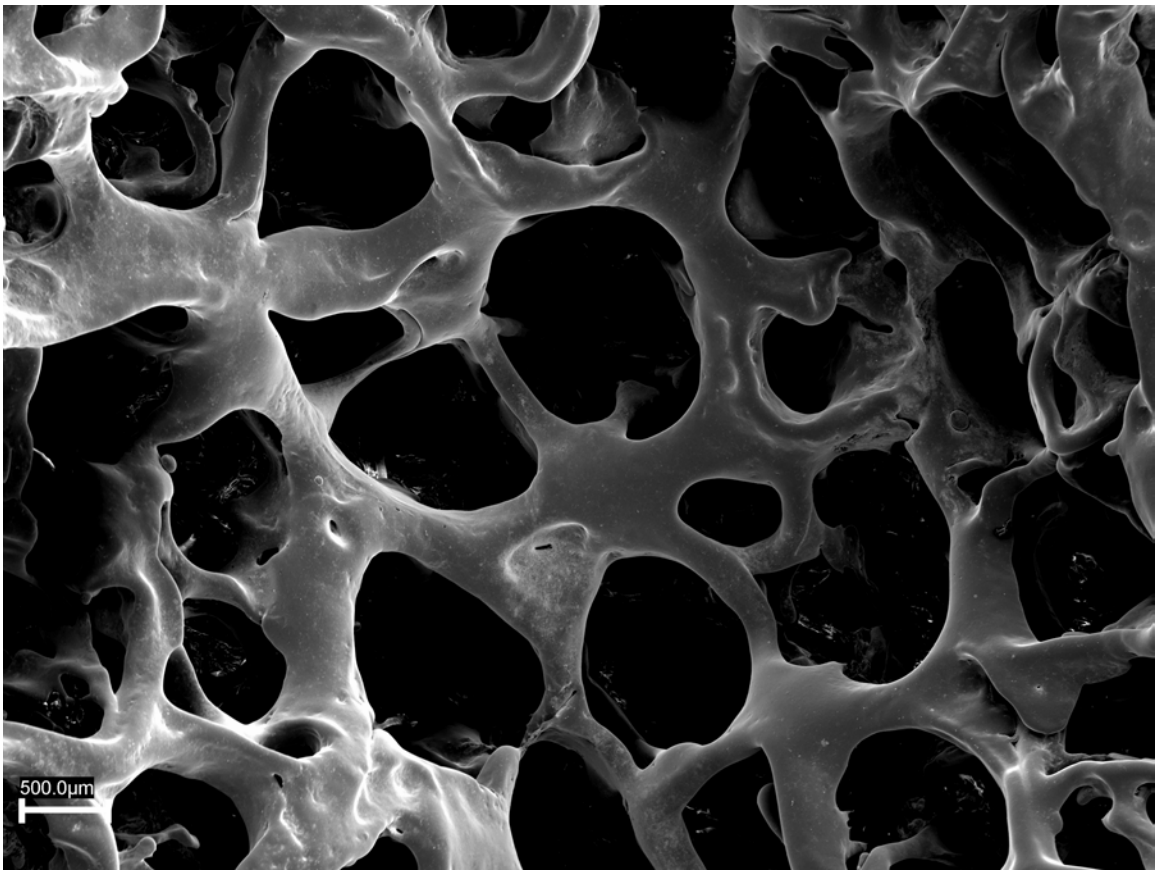

Fig. 42d. Scanning electron micrograph of a microvascular corrosion cast of a caruncle from a 10-week-pregnant doe viewed from the fetal side showing capillary density. Bar = 500 µm.

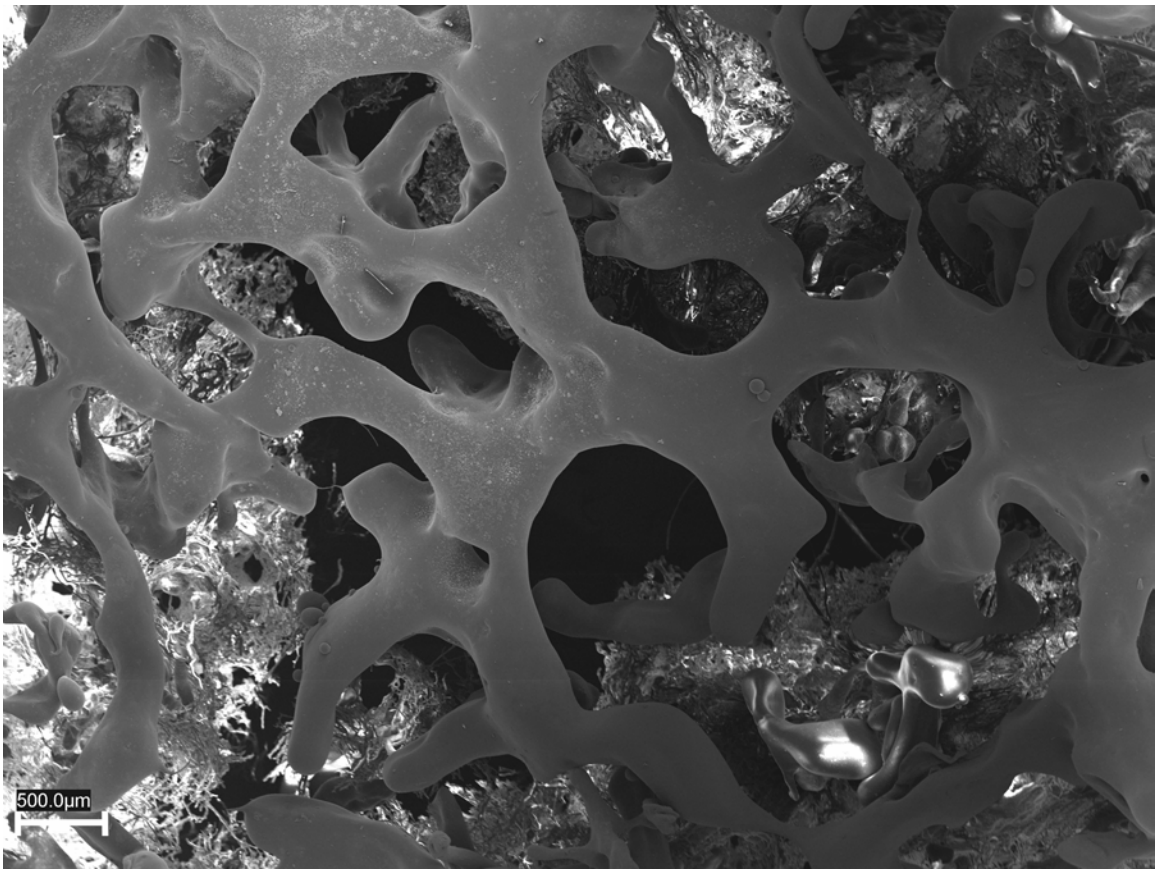

Fig. 42e. Scanning electron micrograph of microvascular corrosion cast of a caruncle from a 13-week-pregnant doe viewed from the fetal side showing capillary density. Bar = 500 µm.

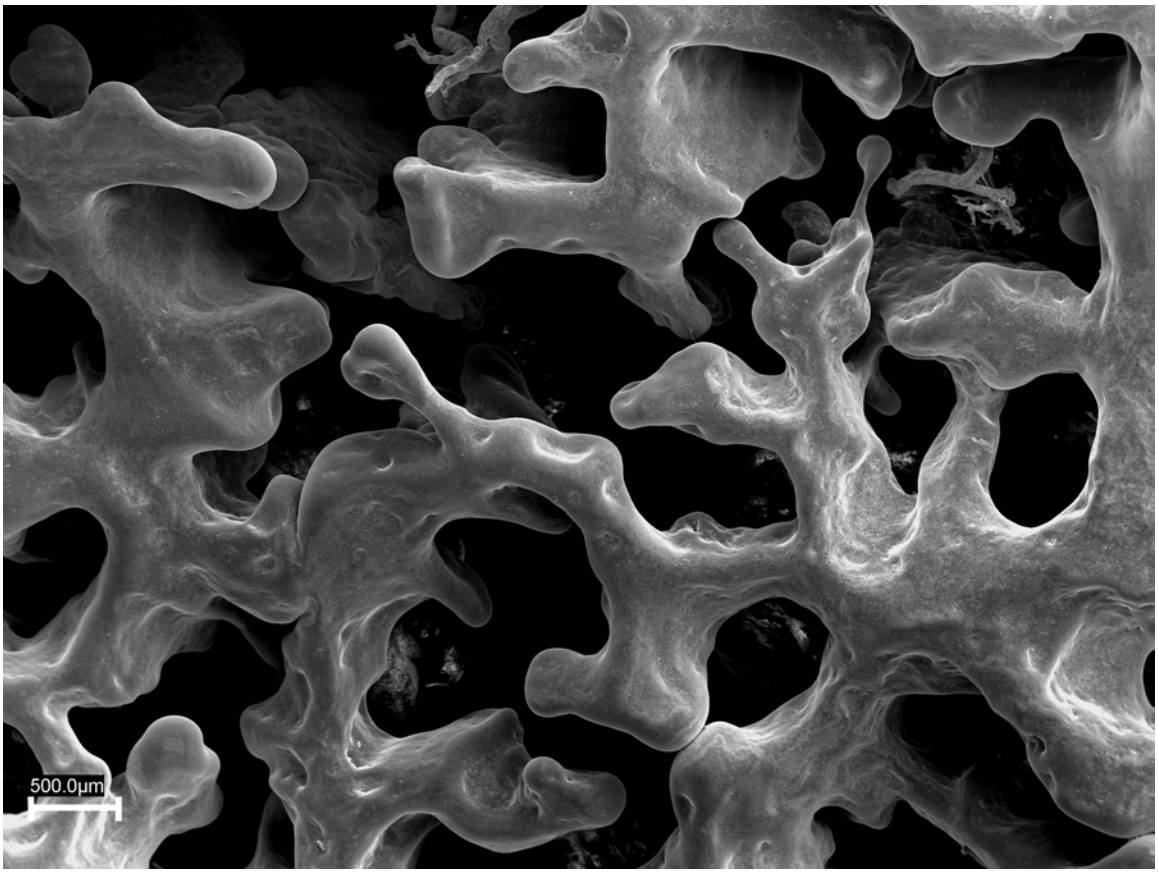

Fig. 42f. Scanning electron micrograph of a microvascular corrosion cast of a caruncle from a 16-week-pregnant doe viewed from the fetal side showing capillary density. Bar = 500 µm.

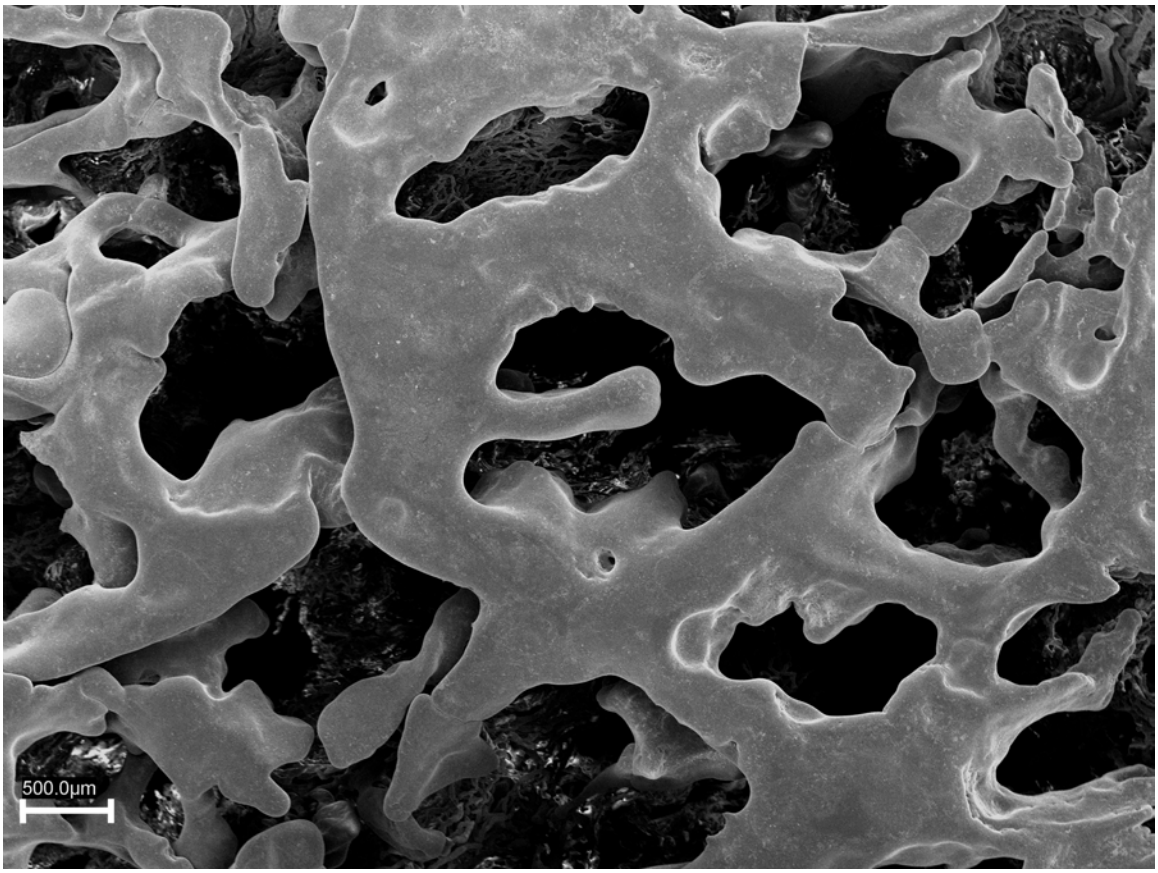

Fig. 42g. Scanning electron micrograph of a microvascular corrosion cast of a caruncle from an 18-week-pregnant doe viewed from the fetal side showing capillary density. Bar = 500 µm.

No significant differences were found in sinusoidal diameters in swainsonine-treated does at 7 weeks, but a decrease in capillary density index was noted. (Figs. 43 and 44). Swainsonine caused great distortion in the vasculature in treated does at 18 weeks of gestation; hence no measurements could be obtained.

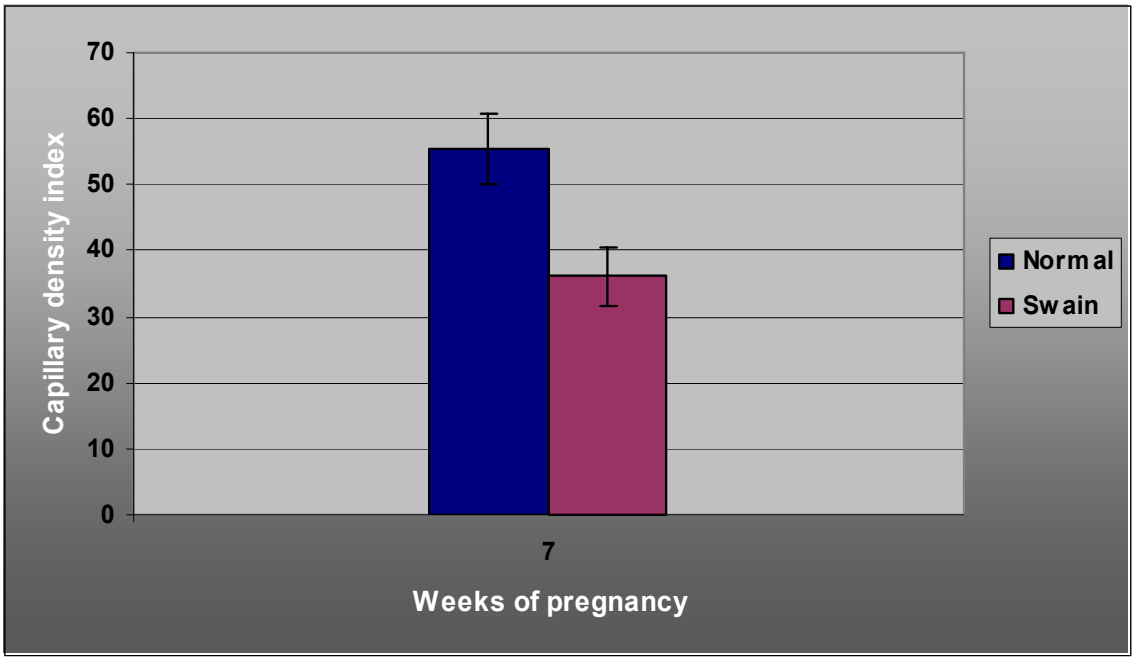

Fig. 43. Capillary density index in normal and swainsonine-treated (Swain) does at 7 weeks of gestation. A significant decease in capillary density index was observed in swainsonine-treated does compared to normal animals.

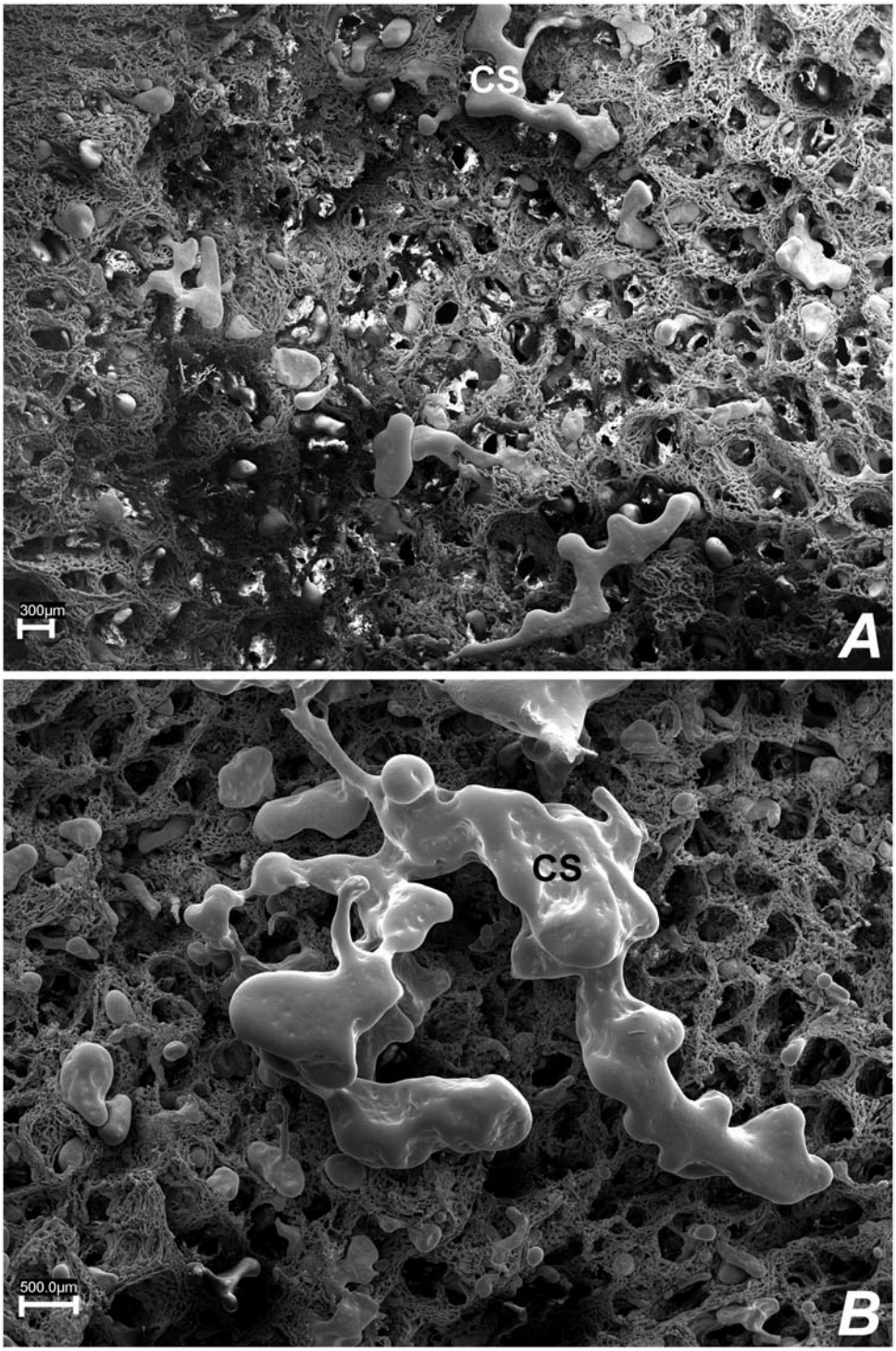

Fig. 44. Scanning electron micrograph of a microvascular corrosion cast of a caruncle from swainsonine-treated doe at 7 weeks of gestation. Note decreased appearance of capillary sinusoids (**CS**) compared to normal does (compare to fig. 42c). ***B*****:** Higher magnification of ***A***. Bar = 300 µm in ***A*** and 500 µm in ***B***.

Ovaries

Morphological changes on the caprine ovarian surface of non-pregnant and pregnant does were examined by scanning electron microscopy. No significant differences were observed on the surface of ovaries from non-pregnant and pregnant does; nor between stages of pregnancy, and/or between the right and left ovaries. The following description applies to all ovaries at all stages. The ovarian artery took a tortuous course around the ovarian vein, then it divided into its three branches, the uterine branch, uterine tube branch, (the later two branches were discussed earlier in the section of cleared specimens), and ovarian branch. The proper ovarian branch of the ovarian artery ran mainly toward the hilus of the ovary, where it penetrated the ovary, and in some cases gave off a smaller branch that entered the ovary from the abuterine pole (or in a few cases it distributed along the caudal surface of the ovary). Subdivisions of the proper ovarian branch of the ovarian artery coiled around the proper ovarian tributary of the ovarian vein from the level of their origin to within the substance of the ovary. Tertiary and secondary subdivisions of the proper ovarian tributary of the ovarian vein originated from the ovary, joined, and formed two primary tributaries. The main primary tributary left the ovary at the uterine pole. The other tributary left the ovary at the hilus. The proper ovarian tributary of the ovarian vein joined the uterine tributary of the ovarian vein (main uterine venous drainage) to form the main ovarian vein (Figs. 45 and 46).

Coiling of the ovarian branch of the ovarian artery around the ovarian tributary of the ovarian vein was more extensive in the branch entering the ovary

at the hilus. A tighter spiral configuration was observed in areas close to the ovary. Coiling of the ovarian branch of the ovarian artery and its ramifications was maintained in all samples, even in parts not surrounding the ovarian vein.

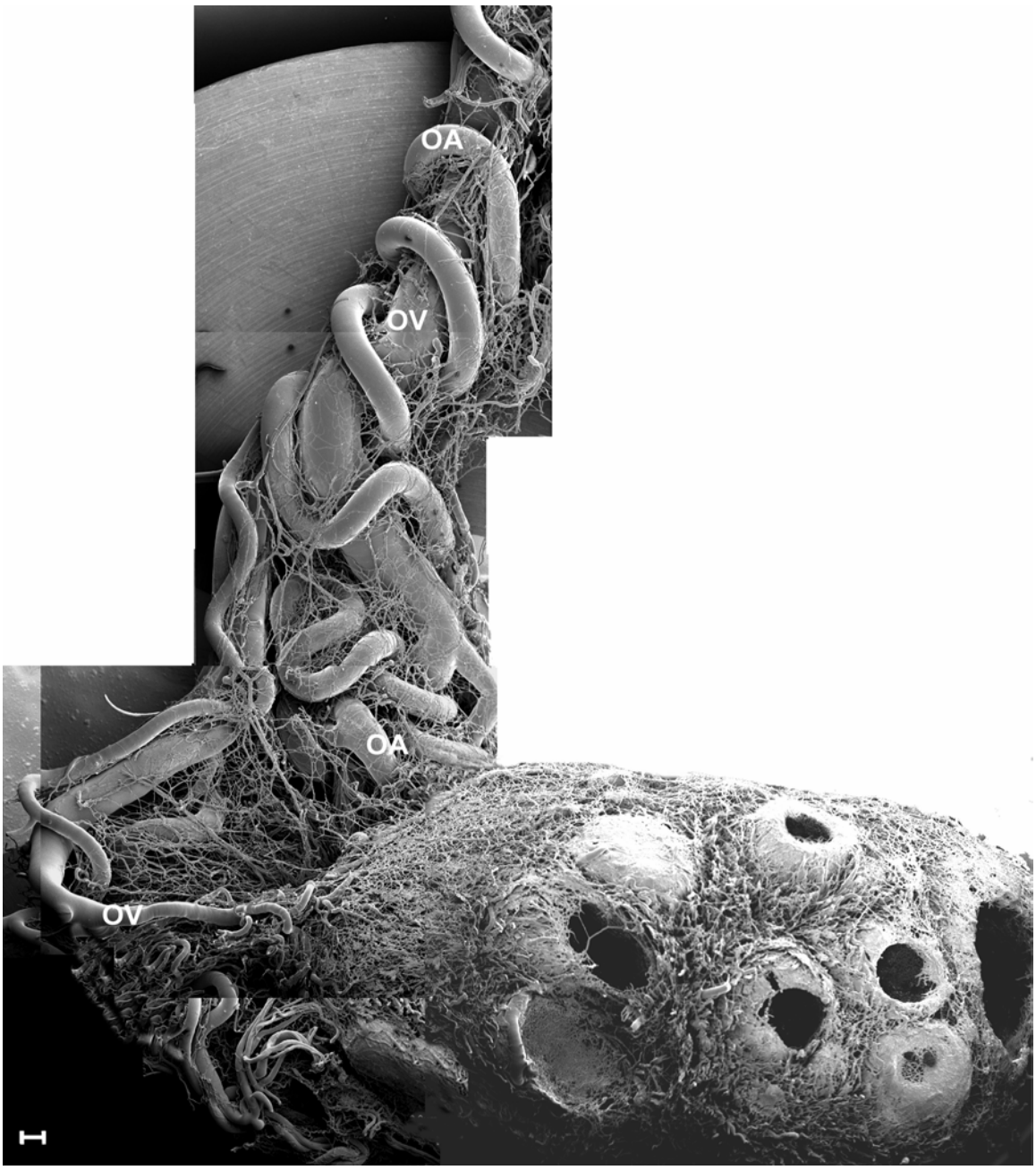

Fig. 45. Scanning electron micrographic composite of a microvascular corrosion cast of a non-pregnant caprine ovary. The proper ovarian branch of the ovarian artery (**OA**) takes a tortuous course around the proper ovarian tributary of the ovarian vein (**OV**). The ovarian branch of the ovarian artery runs mainly toward the hilus, where it penetrates the ovary. Tertiary and secondary subdivisions of the ovarian tributary of the ovarian vein originate from the ovary, join, and form two primary tributaries. The main primary tributary leaves the ovary from the uterine pole of the ovary. The other tributary leaves the ovary from the hilus. Bar = 500 µm.

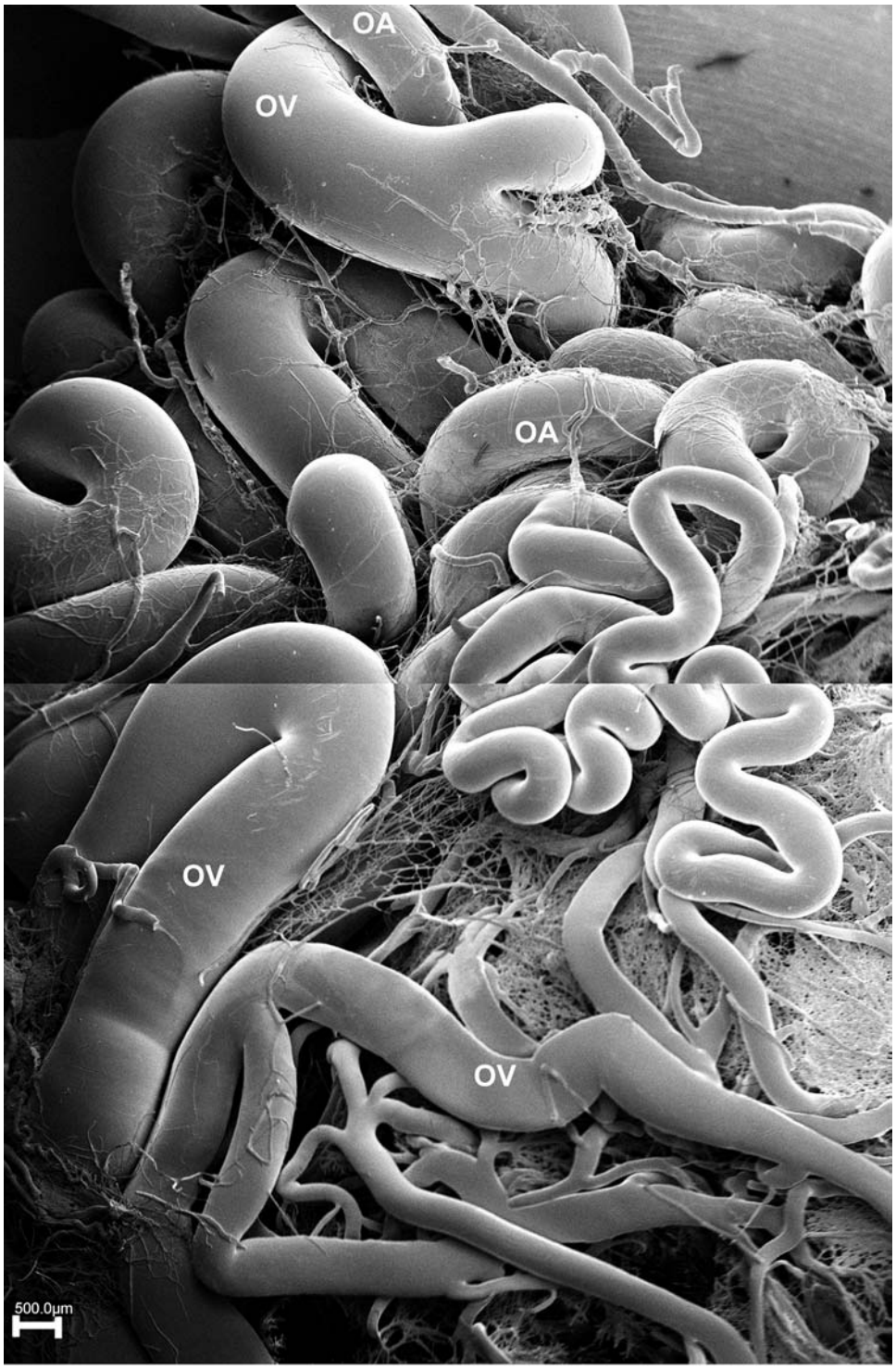

Fig. 46. Scanning electron micrographic composite of a microvascular corrosion cast of an ovary from pregnant doe showing the coiling of the ovarian branch of the ovarian artery (**OA**) and its subdivisions in the area of the hilus. The proper ovarian tributary of the ovarian vein (**OV**) leaves the ovary mainly from the uterine pole. Note flat veins on the surface of the ovary. Bar = 500 µm.

The arterial and venous branches of large vessels penetrating the ovary can be traced to distinct microvascular patterns characteristic of the follicles and corpora lutea. In the ovary, densely vascularized spheres (corresponding to various stages of follicle and corpus luteum development) as well as stromal vasculature could be observed. We used the description provided by Kardon and Kessel (1979) and Kanzaki et al. (1982) as a guide for identification of various vascular spheres.

Primordial follicles do not possess a characteristic vascular pattern that can be used for identification. They are closely associated with interstitial capillaries that form diffuse meshes in between the follicular and luteal vascular spheres. Early preantral follicle appeared as a spherical, basket-like network of capillaries (Fig. 47). At later stages of maturation, follicles possessed a more complex wreath of capillaries, which tend to be arranged into layers (Fig. 48). Late well-developed antral follicles acquired a well defined multilayered basket-like network (Fig. 49), the inner wall of which was characterized by development of capillary sinusoids. Capillary sprouts and evidence of intussusceptive capillary growth due to enhanced angiogenesis were seen in inner wall of the late developed follicles (Fig. 50). The outer wall was formed from larger size vessels. Leakage of the casting medium was observed in advanced stages of follicular development due to increased capillary permeability. Ovulatory follicles were characterized by the presence of avascular apical area (the location of the stigma). Leakage of the casting medium was observed around the border of the stigma due to increased vascular permeability in this region. Positive

identification of atretic follicles was difficult because of the possibility of atresia at any stage of follicular development and possible luteinization (Kessel, 1979; Kanzaki et al., 1982). By its nature the corrosion process destroys the surrounding tissues. Hence assuming the blood supply to an atretic follicle remained intact, it would have a similar structure to the vessels of any other follicle reaching the same stage of growth.

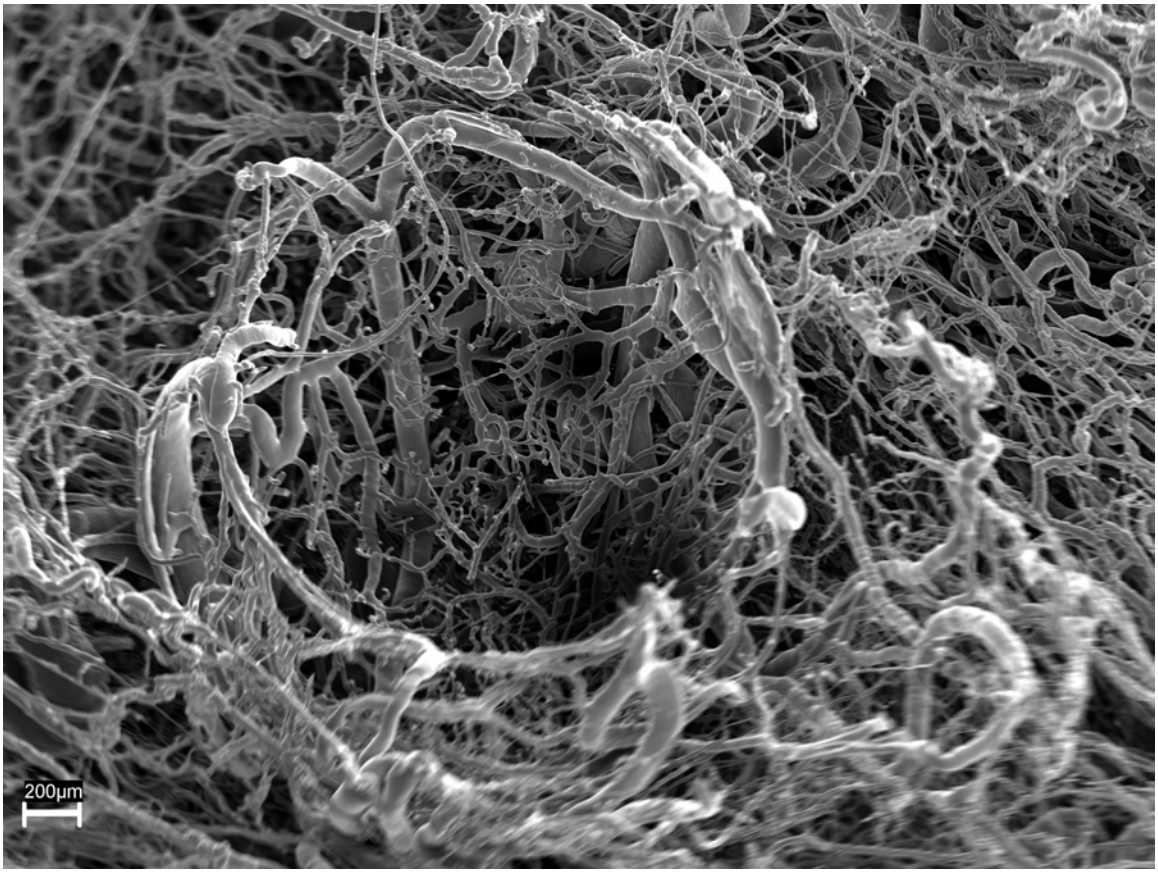

Fig. 47. Scanning electron micrograph of a microvascular corrosion cast of the ovary showing the blood supply of an early preantral follicle. The follicle appears as a spherical, basket-like network of capillaries. Bar = 200 µm.

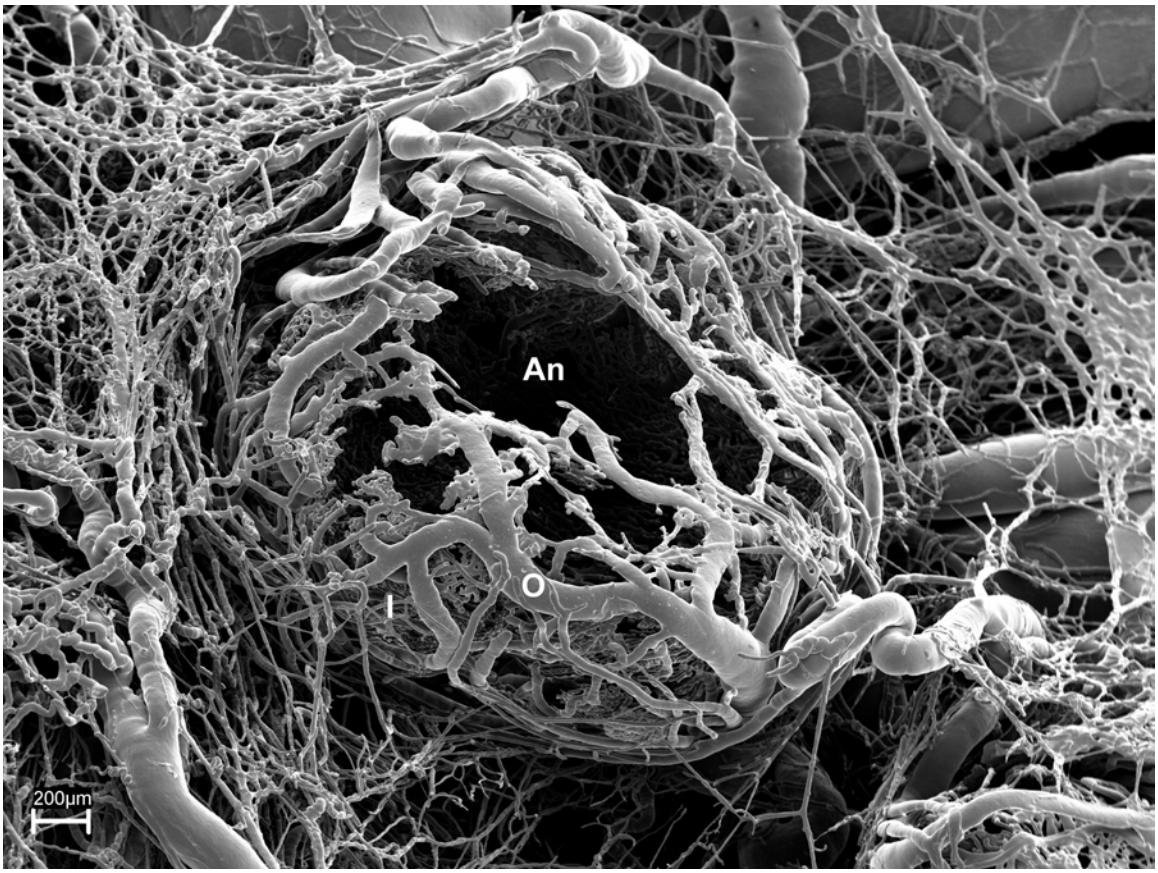

Fig. 48. Scanning electron micrograph of a microvascular corrosion cast of the ovary showing a follicle at later stages of maturation than the one shown in figure 47. The follicle possesses a more complex wreath of capillaries, which tend to be arranged into layers. **I**, inner layer; **O**, outer layer; **An**, antrum. Bar = 200 µm.

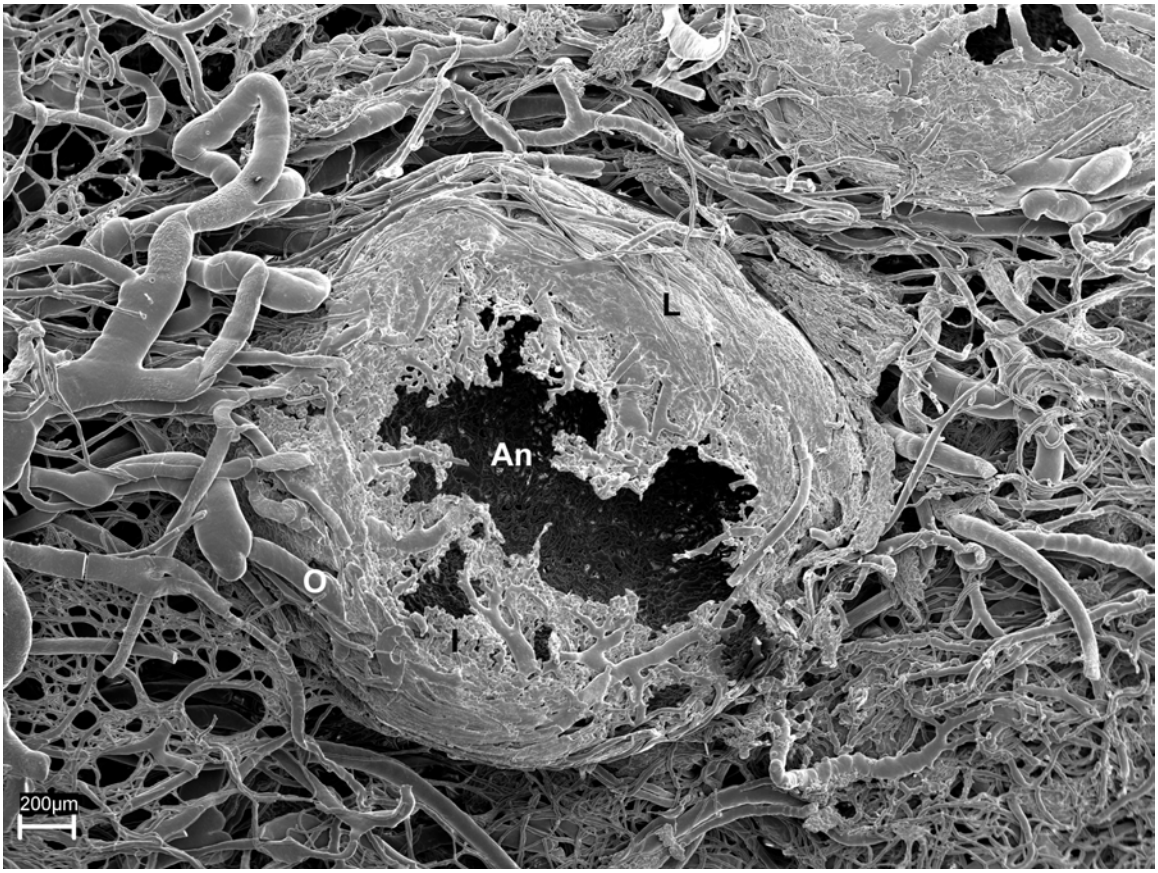

Fig. 49. Scanning electron micrograph of a microvascular corrosion cast of the ovary showing a late developed antral follicle. The follicle has formed a well-defined multilayered basket-like network. **O**, outer layer; **I**, inner layers; **An**, antrum. Leakage (**L**) of the casting medium was observed due to increased capillary permeability.

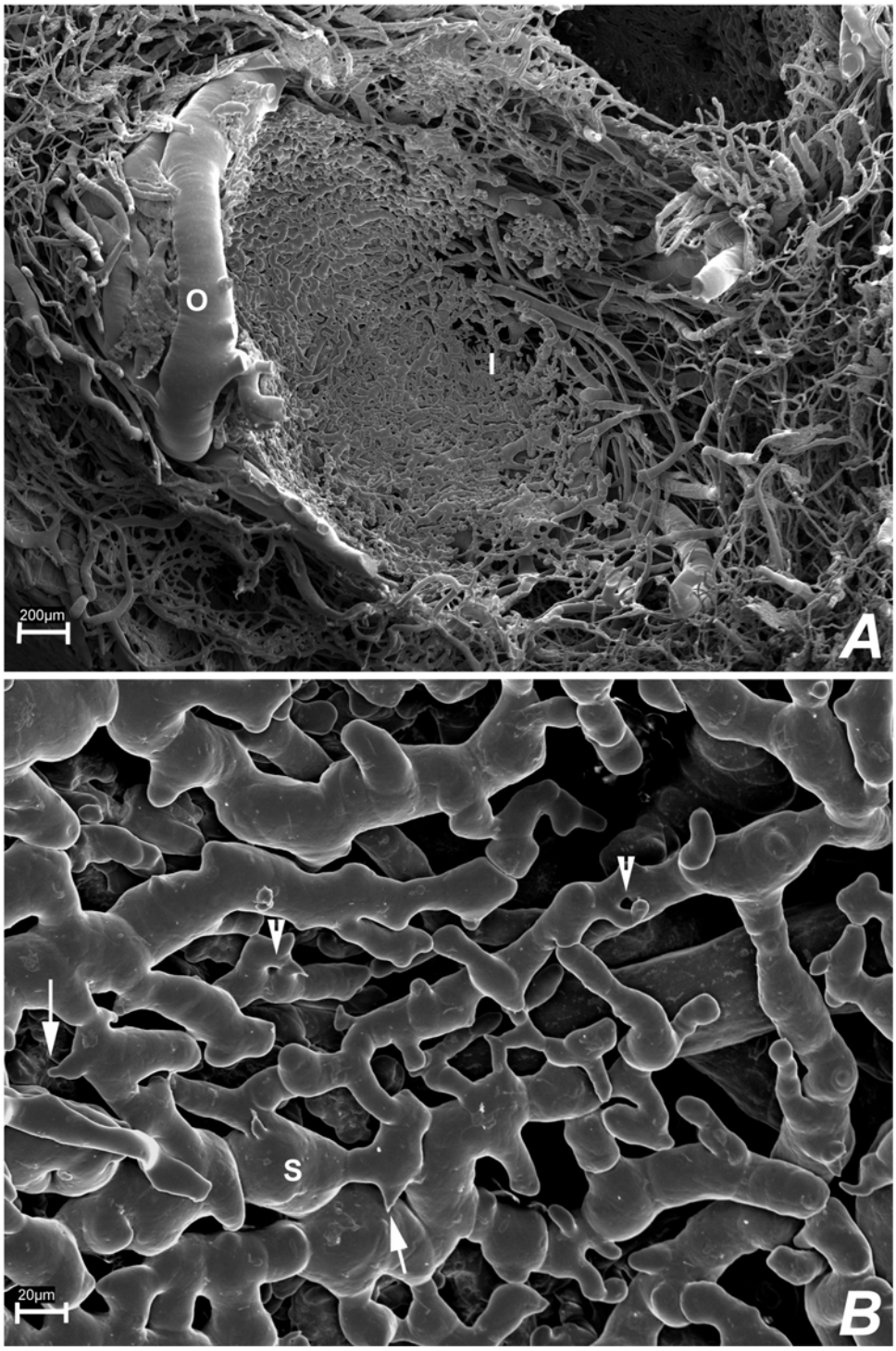

Fig. 50. Scanning electron micrographs of a microvascular corrosion cast of the ovary showing the blood supply of a late developed follicle. In ***A***, note that the outer wall (**O**) is formed from larger size vessels and the inner wall (**I**) is formed from capillaries. In ***B*** (higher magnification image of ***A***), note the presence of capillary sinusoids (**S**). Capillary sprouts (arrow) and evidence of intussusceptive capillary growth (arrow heads), due to enhanced angiogenesis, were seen in the inner wall of late developed follicles. Bar = 200 µm in ***A*** and 20 µm in ***B***.

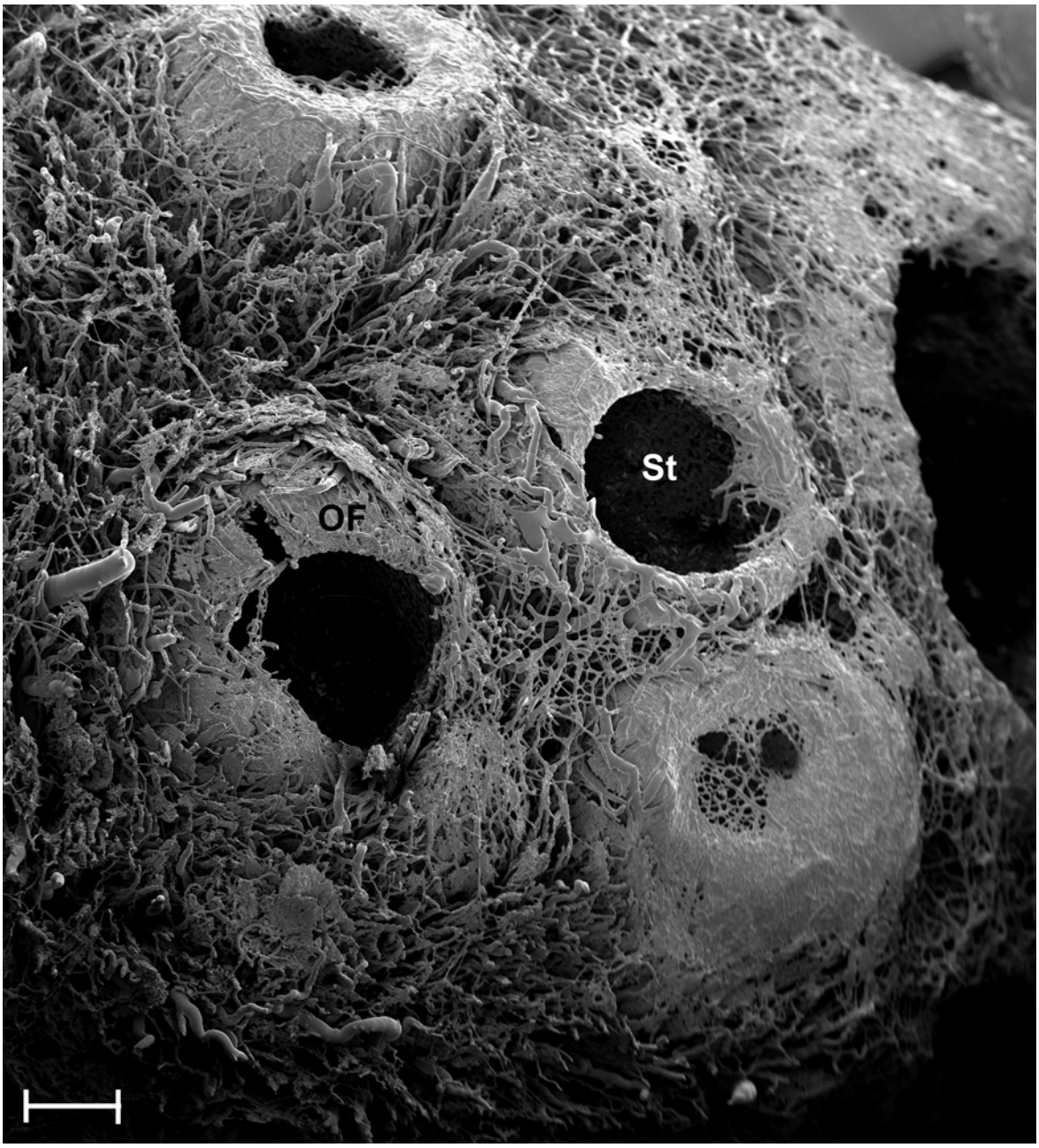

Fig. 51. Scanning electron micrograph of a microvascular corrosion cast of the ovary showing a group of ovulatory follicles (one is marked **OF**) with their characteristic avascular apical area, the location of the stigma (**St**). Leakage of the casting medium was observed around the border of the stigma. Bar = 500 µm.

Early formation of the corpus luteum was characterized by inward growth of vessels from the apical part of the ovulating follicle (Fig. 52). This was followed by intense new formation of capillaries, which filled up the corpus luteum and closed the apical area. Corpora lutea could be recognized by their extensive vasculature. The vascular bed of the corpus luteum consisted of a dense, conglomerated capillary plexus, and large vessels distributed on its outer surface (Figs. 53 and 54). Large flat veins could be observed on the outer surface of the corpus luteum.

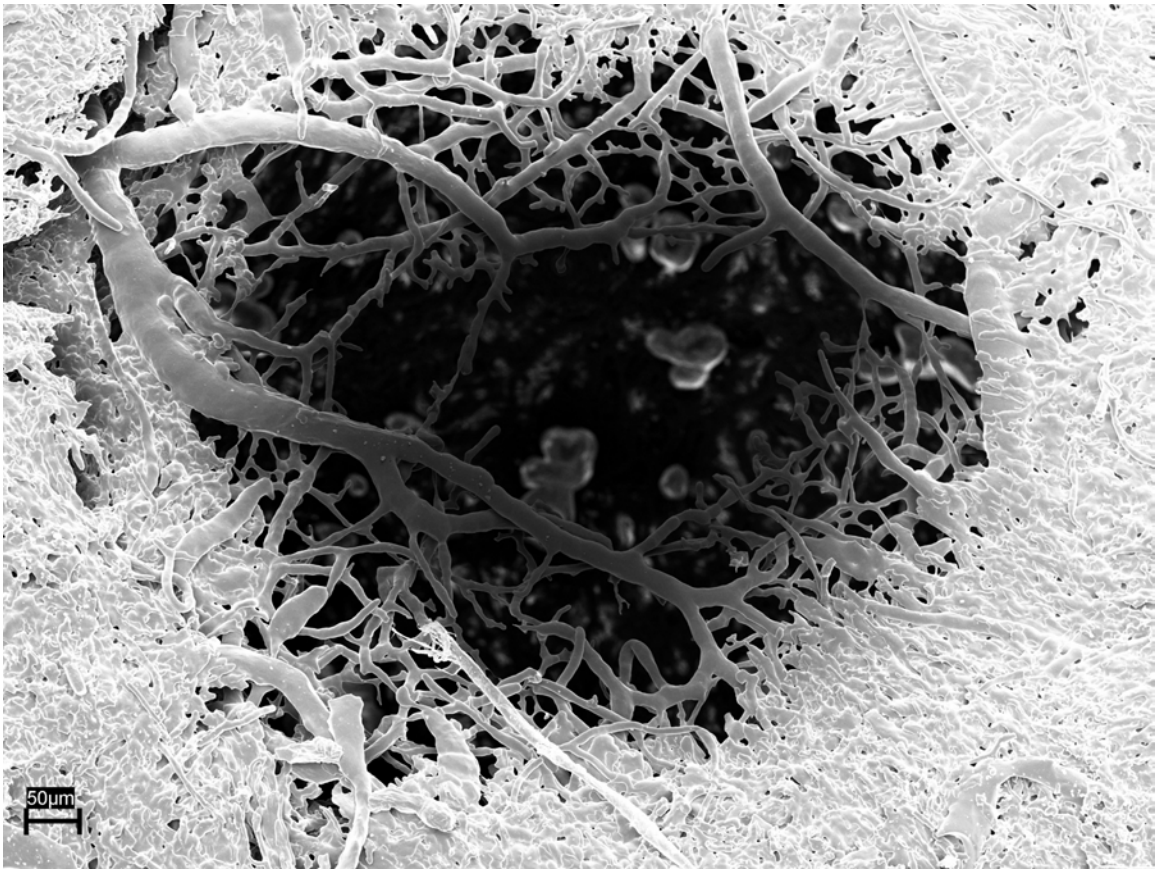

Fig. 52. Scanning electron micrograph of a microvascular corrosion cast of an ovary showing the early formation of the corpus luteum by inward growth of vessels from the apical area of the ovulatory follicle. Bar = 50 µm.

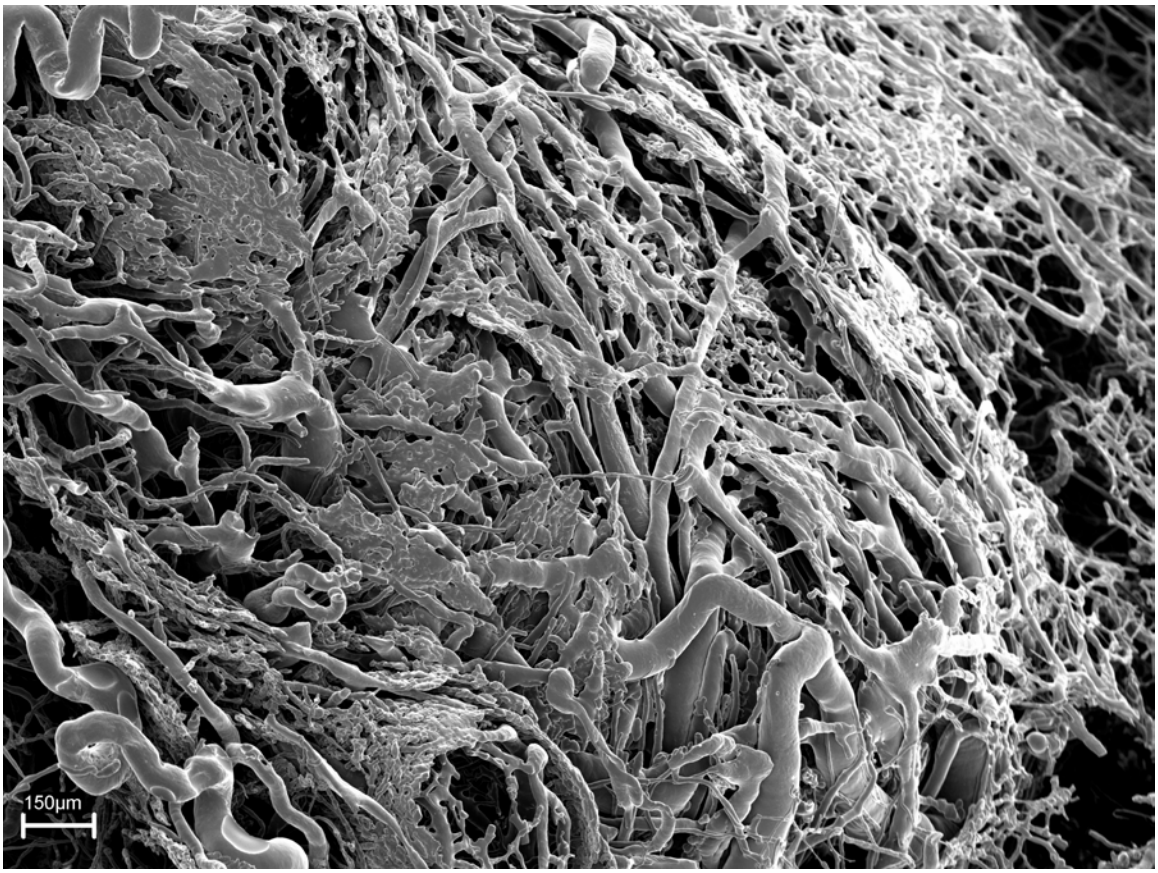

Fig 53. Scanning electron micrograph of a microvascular corrosion cast of an ovary showing a small size corpus luteum. The vascular bed of the corpus luteum consists of a dense, conglomerated capillary plexus and large vessels distributed on its outer surface. Bar = 150 µm.

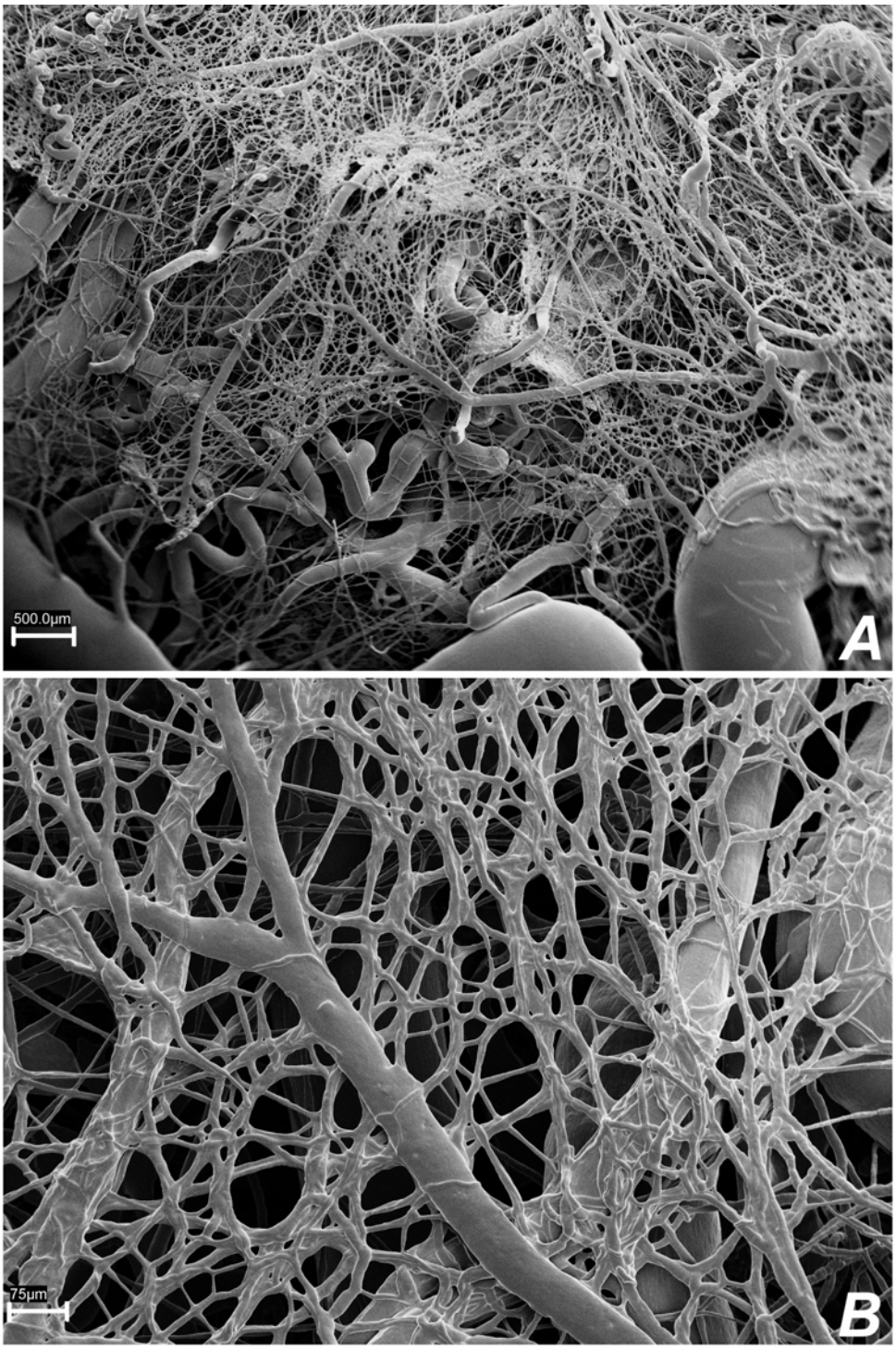

Fig 54. Scanning electron micrographs of a microvascular corrosion cast of the ovary showing a large sized corpus luteum. In ***A***, note that the vascular bed of the corpus luteum consists of a dense, conglomerated capillary plexus and large vessels distributed on its outer surface. ***B*:** Higher magnification image of ***A*** showing the intricate vascular net of the corpus luteum. Bar = 500 µm in ***A*** and 75 µm in ***B***.

In swainsonine-treated does at 7 weeks of gestation, focal avascular areas were observed in the corpus luteum (Fig. 55). These areas corresponded to vascular degeneration and diminished angiogenesis. No information could be obtained from swainsonine-treated does at 18 weeks of gestation due to the great distortion of the vasculature caused by swainsonine.

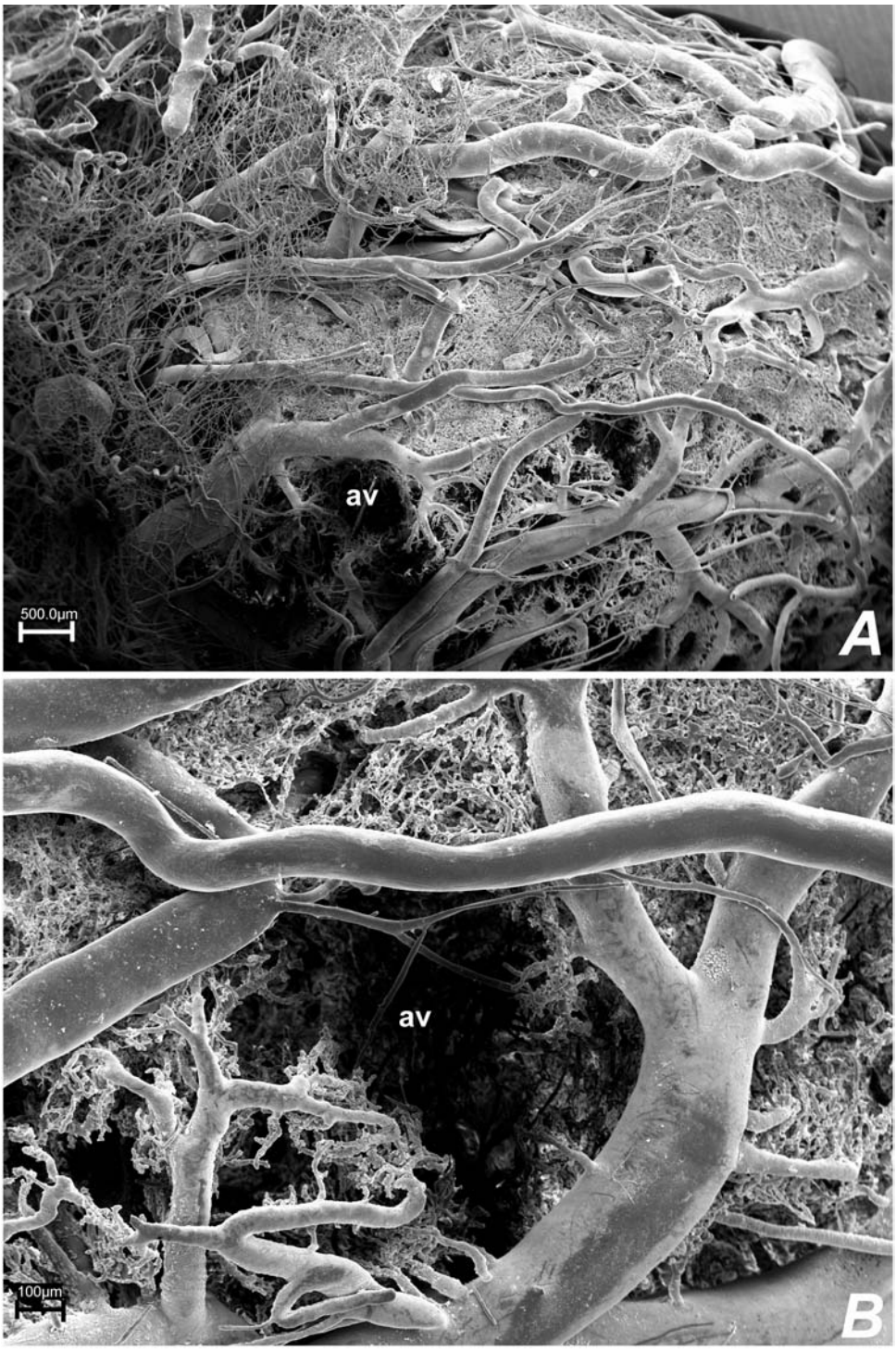

Fig. 55. Scanning electron micrographs of a microvascular corrosion cast of an ovary of swainsonine-treated doe at 7 weeks of gestation, showing focal avascular areas (**av**) in the corpus luteum. ***B*****:** High magnification image of ***A***. Bar = 500 m in ***A*** and 100 m in ***B***.

Immunohistochemical Studies

The results of the evaluation of staining intensity are summarized in Table 2.

Table (2): Immunostaining scores were examined blindly by two independent histologists, who assigned a score of 5 for the most intense reaction and 0 for a negative reaction. VEGF was localized utilizing the avidin-biotin-horseradish peroxidase system in deparaffinized sections treated with rabbit polyclonal antibody against VEGF. DAB was used for visualization of the reactions. Slides were counterstained with Mayer's haematoxylin. This data summarized herein was taken from normal does at 4, 7, 10, 13, 16, 18 weeks of pregnancy; from swainsonine-treated does at 7 and 18 weeks (L7W and L18W); and from non-pregnant does (NP). NA indicates that the selected tissue did not exist in the sample collected and/or should not be found (as, for example the fetal tissues in non-pregnant animals). The intensity of the reaction was given as a range when the two histologists did not agree on it (both scores were cited).

	Stages of pregnancy								
Tissue	4W	7W	10W	13W	16W	18W	L7W	L18W	NP
Fetal epithelium									
Cytotrophoblasts	5	5	5	5	5	5	4	4	NA
Giant cells	---	---	---	---	---	---	---	---	NA
Fetal connective tissue	---	---	---	---	---	---	---	---	NA
Fetal vasculature									
Endothelium	NA	5	5	5	5	5	4	4	NA
Smooth muscles	NA	2	3	3	2	1	2	2	NA
Maternal epithelium	3	2-3	2	2	+/---	NA	2-3	NA	4
Maternal connective tissue	---	---	---	---	---	---	---	---	---
Maternal vasculature									
Endothelium	4	5	5	5	5	5	4	4	4
Smooth muscles	1	2	2	2	1	1	2	2	2
Luteal cells	3	3	2-3	2-3	2	2-3	2	2	2
Follicular cells									
Granulosa cells	3	3	3	3	NA	3	3	3	3
Theca cells	2	2	2	3	NA	2	2	2	2
Ovarian vasculature									
Endothelium	3	3	3	3	3	3	3	3	3
Smooth muscles	2	2	2	2	2	2	2	2	2

In non-pregnant does, immunostaining was seen in the maternal epithelium as well as the endothelium and smooth muscles of blood vessels (Fig. 56).

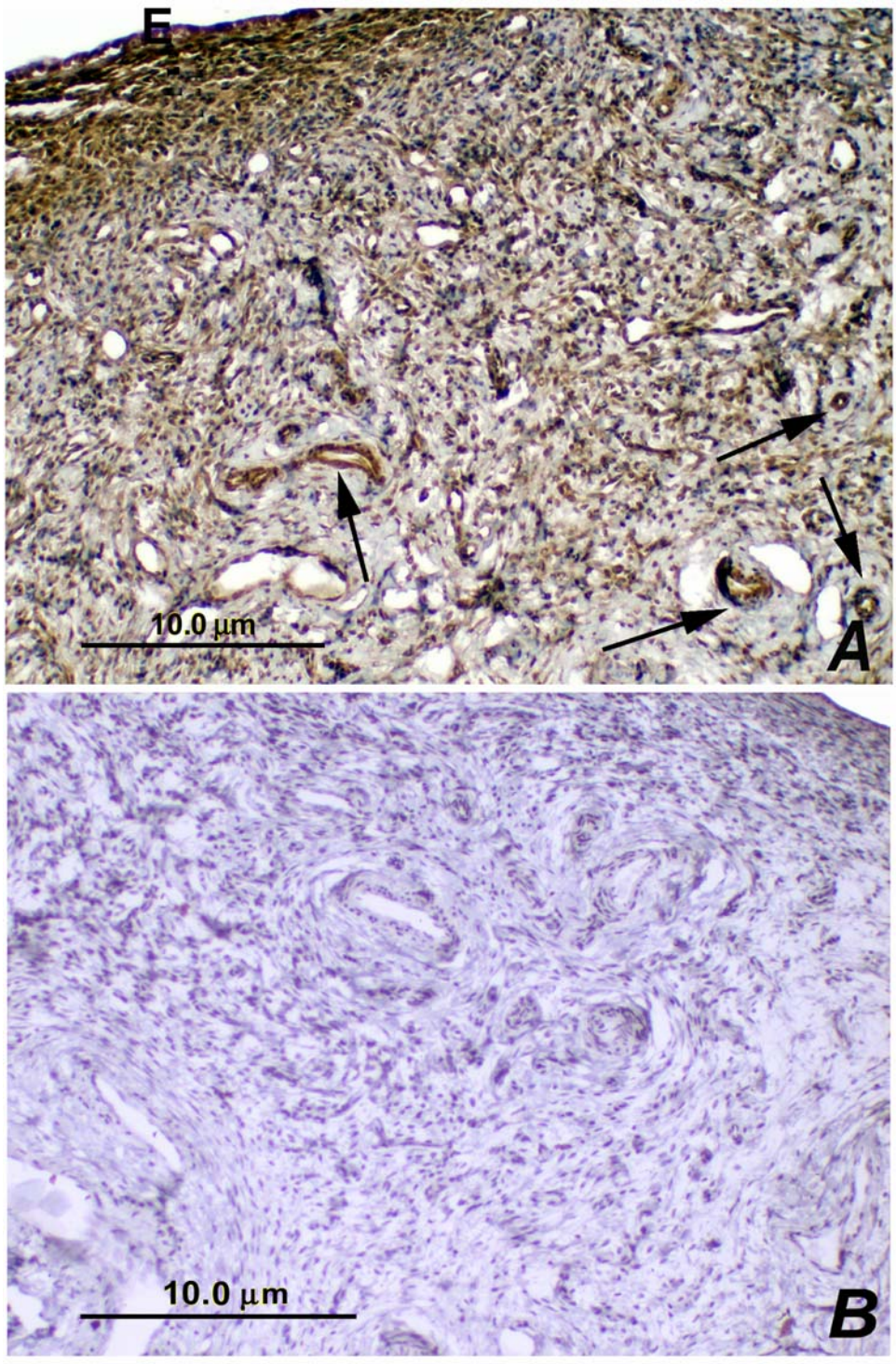

Fig. 56. Light microscopic sections of a caruncle from a non-pregnant doe. ***A*:** VEGF protein was localized in the surface epithelium (**E**) as well as the endothelium and smooth muscles of blood vessels (examples shown at the tip of arrows). Connective tissue shows no immunoreactivity. ***B*:** Negative control shows no immunoreactivity to VEGF antibody. Bar = 10 µm.

In the placentomes of pregnant animals, we assessed the presence or absence and intensity of the immunostaining in the six layers making up the materno-fetal barrier: 1) maternal blood vessels; 2) maternal connective tissue; 3) maternal epithelial tissue; 4) fetal epithelial tissue; 5) fetal connective tissue; and 6) fetal blood vessels. Two distinct populations of cells could be recognized histologically in the fetal epithelial tissues: the cytotrophoblasts (which make up the bulk of the fetal epithelium) and binucleate trophoblasts (giant cells). Differences in immunostaining in endothelium, smooth muscles of the tunica media, and connective tissue of tunica adventitia of blood vessels were determined.

The general features of the arrangement of the materno-fetal barrier were most easily grasped from their appearance at 7 weeks of pregnancy, when the architecture of regions close to the maternal side had not yet been distorted by the invasion of the fetal villi (Fig. 57). However, even at later stages, toward the fetal side it was possible to find fetal villi with the typical organization, in which the two populations of fetal epithelial cells overlaid a core of connective tissue (Wharton's jelly), and were served by fetal blood vessels within the connective tissue (Fig. 58). Intense immunostaining was observed in cytotrophoblasts of the fetal epithelium at all gestational ages. Binucleate trophoblasts showed no immunoreactivity to VEGF antibody (Fig. 59). Maternal epithelial tissue was lost in most areas of the materno-fetal barrier at 16 weeks of pregnancy, and was absent at 18 weeks. When it was present in earlier stages, the maternal epithelial tissues showed only mild immunostaining. Neither chorionic and endometrial

interstitium nor connective tissues (tunica adventitia) of blood vessels demonstrated any immunostaining in either non-pregnant or pregnant does. The endothelium and smooth muscles of blood vessels showed positive immunoreactivity to VEGF antibody, but the endothelium showed a more intense reaction than smooth muscles in all cases (Fig. 60). The pattern and intensity of immunostaining were similar in all stages of pregnancy studied (Figs. 61-66). No apparent differences associated with advancing gestation were observed in the intensity of VEGF protein staining. None of the negative controls (some of which are shown in figures 56 & 57) showed any reaction.

Vascular endothelial growth factor was also localized in placentomal tissues from swainsonine-treated does. The pattern of immunostaining was similar to those from normal animals; though a decrease in intensity was observed at both 7 (Fig. 62) and 18 (Fig. 66) weeks.

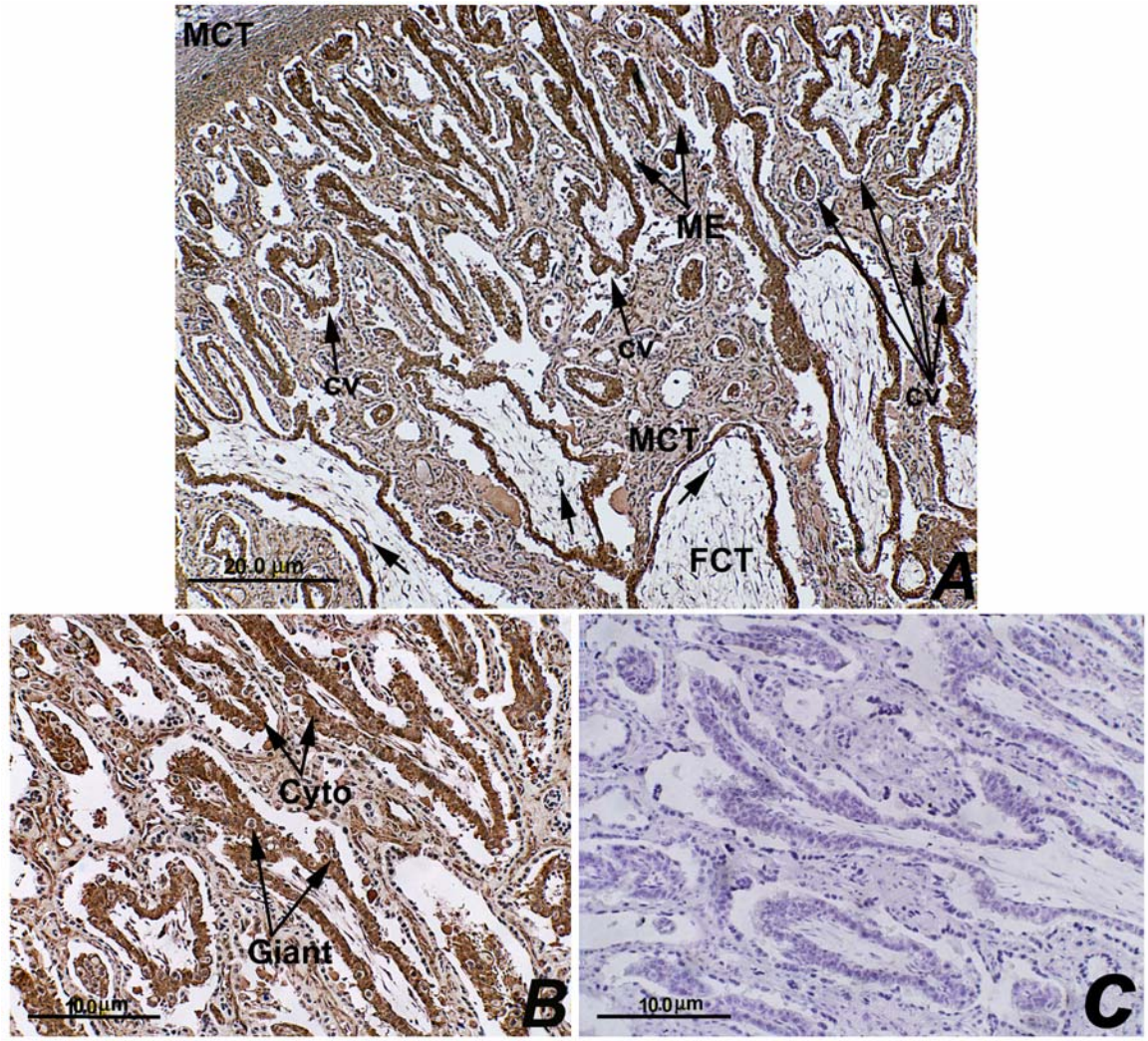

Fig. 57. Light microscopic sections of a placentome at 7 weeks of gestation. ***A*:** Low magnification, showing the general organization of the materno-fetal barrier. The maternal connective tissue (**MCT**) can be seen in the upper left corner and surrounding the chorionic villi (**CV**) of the fetal placenta. Maternal blood vessels could be found within the connective tissue (not shown in this figure, but shown at a higher magnification image in Figure 60. Maternal epithelial tissue (**ME**) can be seen in between the chorionic villi (**CV**). Chorionic villi (some are marked **CV**) are numerous in the image; they are covered with fetal epithelium, which is composed of cytotrophoblasts and binucleate trophoblasts. Fetal connective tissue can be seen within the core of the villi. Fetal blood vessels can be seen within connective tissue of the chorionic villi (arrows). VEGF protein was localized in maternal epithelium (**ME**), but not in maternal (**MCT**) and fetal (**FCT**) connective tissues. The endothelium and smooth muscles of maternal (not shown) or fetal blood vessels (arrows) were positively stained. ***B*:** Higher magnification image of ***A***, cytotrophoblasts (**Cyto**) of fetal epithelium showed intense immunostaining. Binucleate giant cells (**Giant**) were negatively stained. Maternal (**MCT**) and fetal (**FCT**) connective tissues did not show immunoreactivity to VEGF antibody. ***C*:** Negative control. Bar = 20 µm in ***A*** and 10 µm in ***B*** & ***C***.

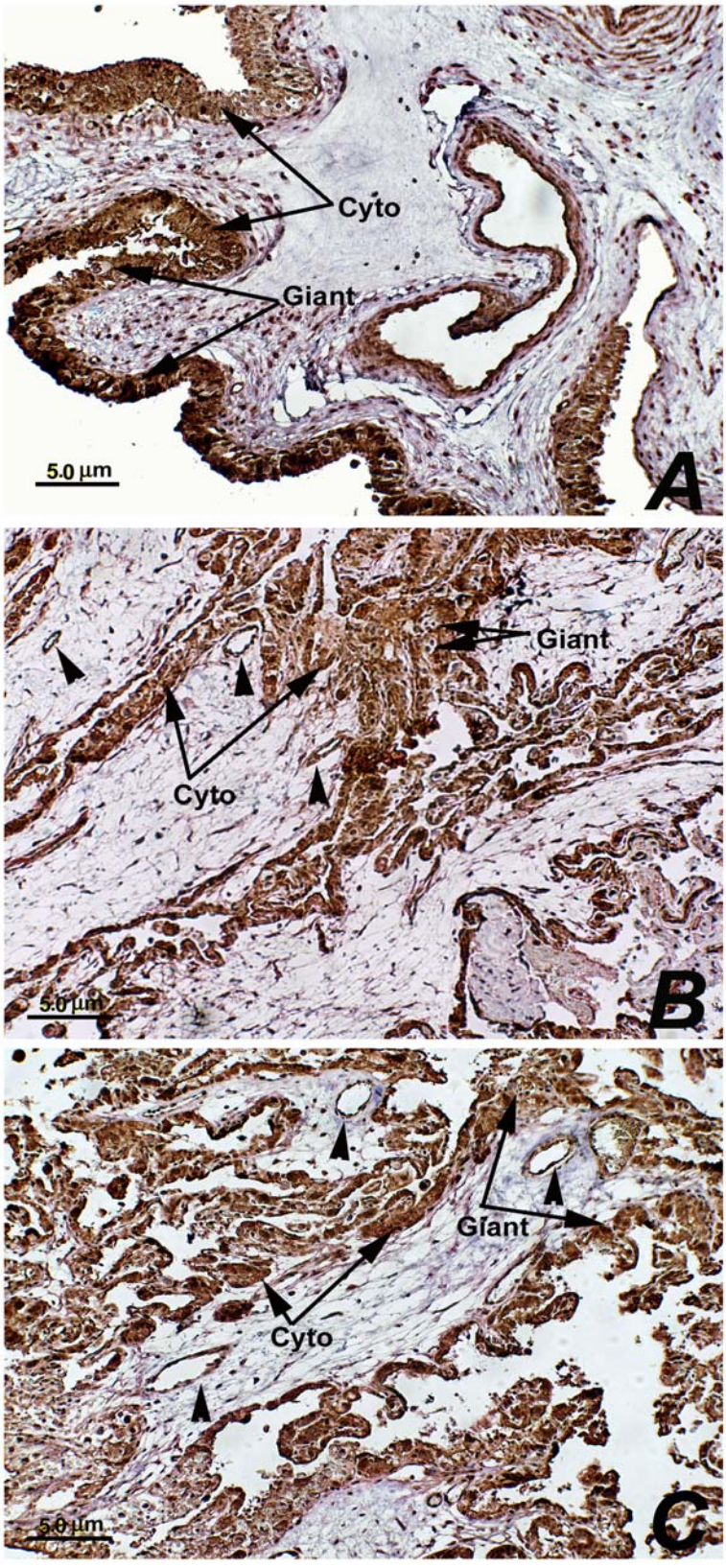

Fig. 58. Legend on the next page (Page: 143).

Fig. 58. (figure on previous page) ***A*:** Light microscopic section of a placentome at 13 weeks of gestation close to the fetal side of the placentome, where the organization of the trophoblasts lining chorionic villi could be easily grasped. VEGF protein was localized in cytotrophoblasts (**Cyto**), but not binucleate giant cells (**Giant**). Some fetal blood vessels can be seen (arrow heads). ***B*** and ***C*** at 16 and 18 weeks, respectively. Bar = 5 μm.

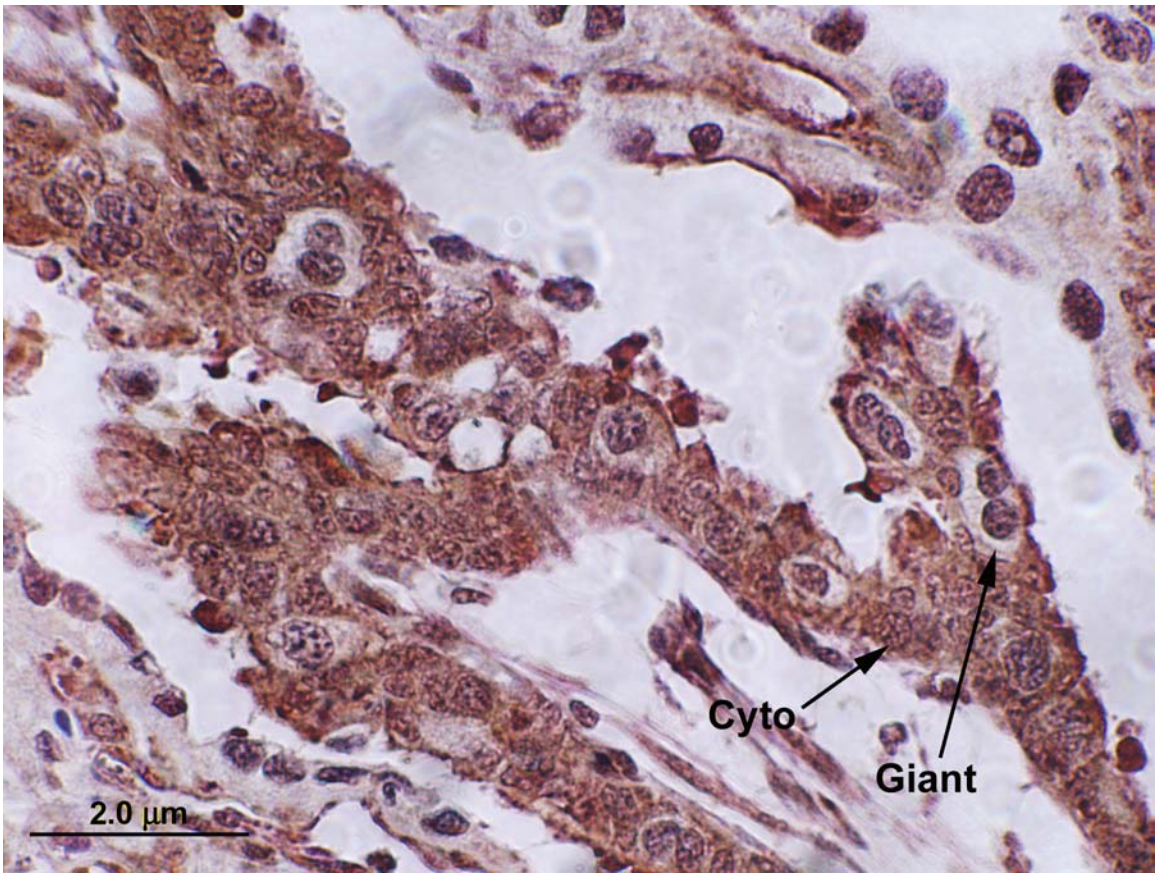

Fig. 59. High magnification image of a chorionic villus. The chorionic villus is covered with fetal epithelium, which is composed of cytotrophoblasts (**Cyto**) and binucleate trophoblasts (**Giant**). Cytotrophoblasts showed intense immunostaining to VEGF antibody. Binucleate trophoblasts stained negative. Bar = 2 µm.

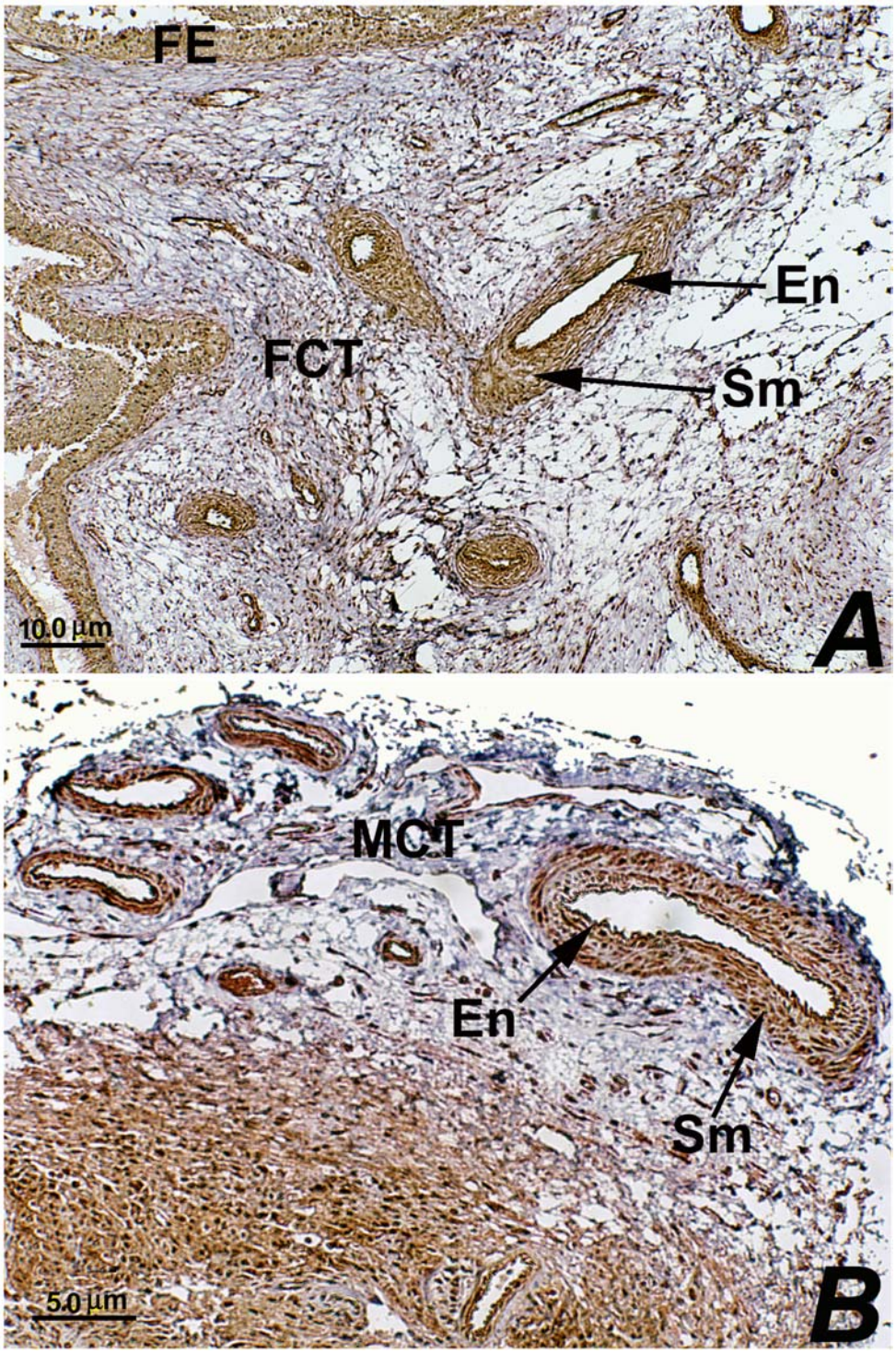

Fig. 60. ***A*****:** Fetal villus close to the fetal side of a placentome. VEGF is localized in fetal epithelium (**FE**) lining chorionic villi and the endothelium (**En**) and smooth muscles (**Sm**) of the fetal vasculature. No immunoreactivity was seen in fetal connective tissue, FCT (Wharton's jelly) within the fetal villi. ***B*****:** Maternal side of a placentome. VEGF was localized in the endothelium (**En**) and smooth muscles (**Sm**) of the maternal vasculature. Maternal connective tissue (**MCT**) showed no immunoreactivity to VEGF antibody. Bar = 10 µm in ***A*** and 5 µm in ***B***.

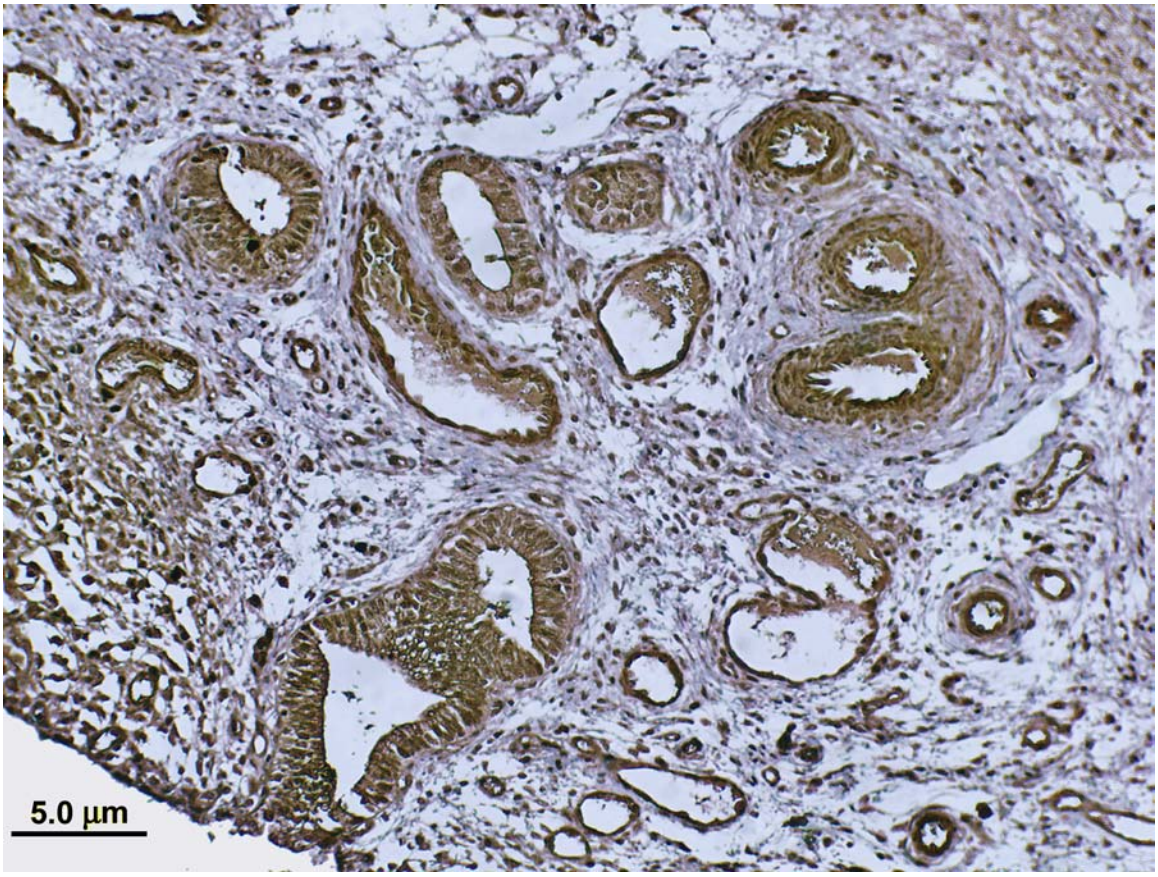

Fig. 61. Light microscopic sections of a placentome at 4 weeks of pregnancy. VEGF protein was localized in both fetal and maternal epithelium. The most intense reaction was seen in cytotrophoblasts. Neither binucleate giant cells nor maternal and fetal connective tissues showed immunostaining. The invasion of fetal villi (chorionic villi) to maternal tissues was the least extensive at that stage. The pattern and intensity of immunostaining were similar in all stages of pregnancy (compare with Figures 62-66) as determined by two independent histologists who examined different fields in the slides at different magnifications. Bar = 5 µm.

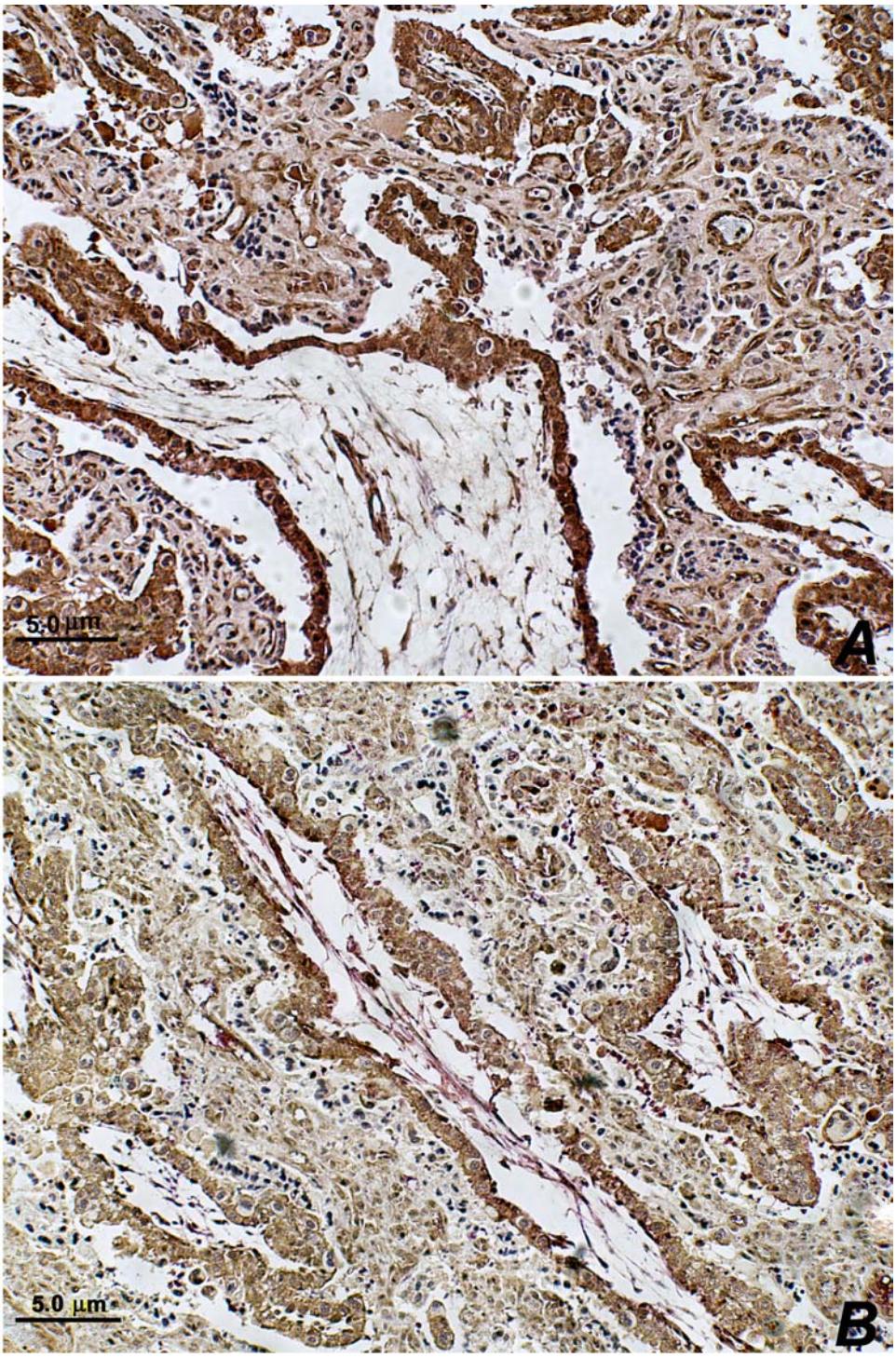

Fig. 62. Light microscopic sections of placentomes of normal (***A***) and swainsonine-treated (***B***) does at 7 weeks of pregnancy. VEGF protein was localized in both fetal and maternal epithelium. The most intense reaction was seen in cytotrophoblasts. Binucleate giant cells and maternal and fetal connective tissues showed no immunostaining. The pattern and intensity of immunostaining were similar in all stages of pregnancy (compare with Figures 61 & 63-66). A less intense reaction was seen in tissues from swainsonine-treated does. Bar = 5 µm.

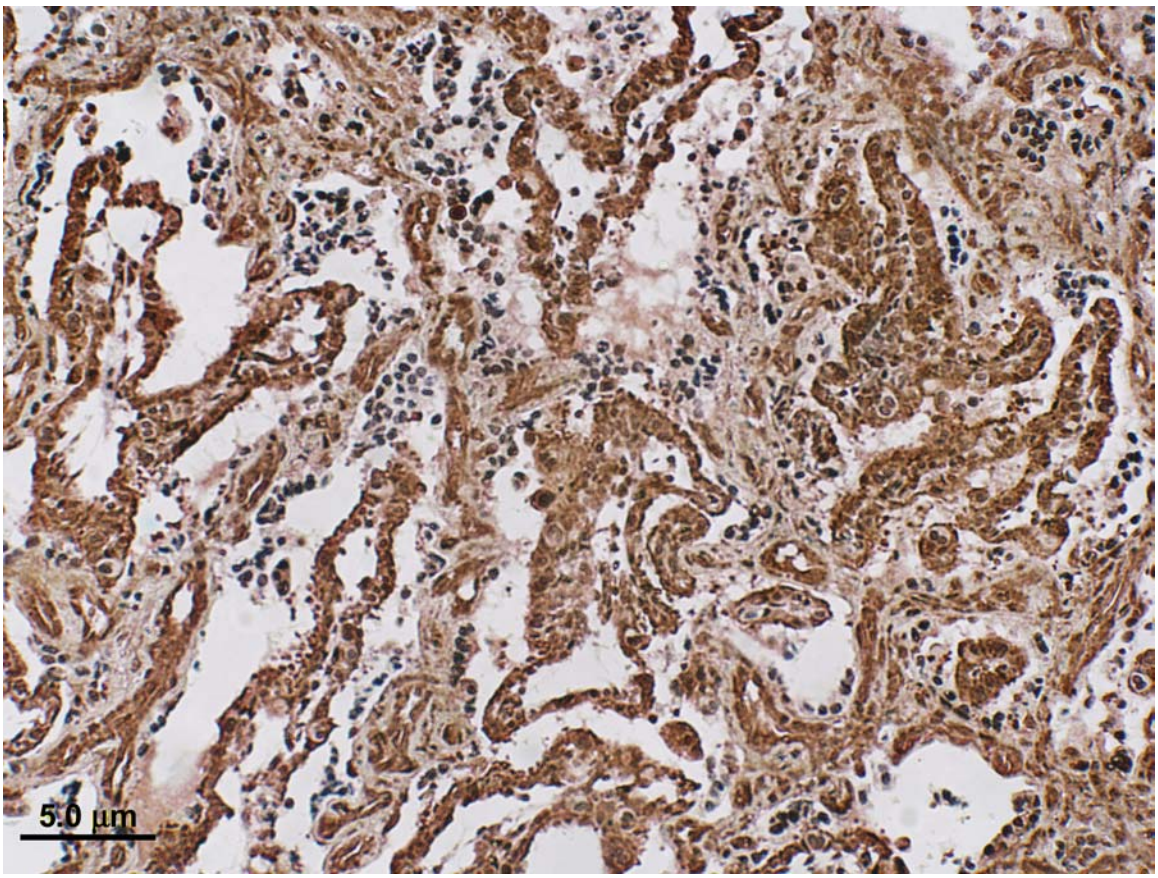

Fig. 63. Light microscopic section of a placentome at 10 weeks of pregnancy. VEGF protein was localized in both fetal and maternal epithelium. The most intense reaction was seen in cytotrophoblasts. Binucleate giant cells and maternal and fetal connective tissues showed no immunostaining. The pattern and intensity of immunostaining were similar in all stages of pregnancy (compare to Figures 61-62 and 64-66). Bar = 5 µm.

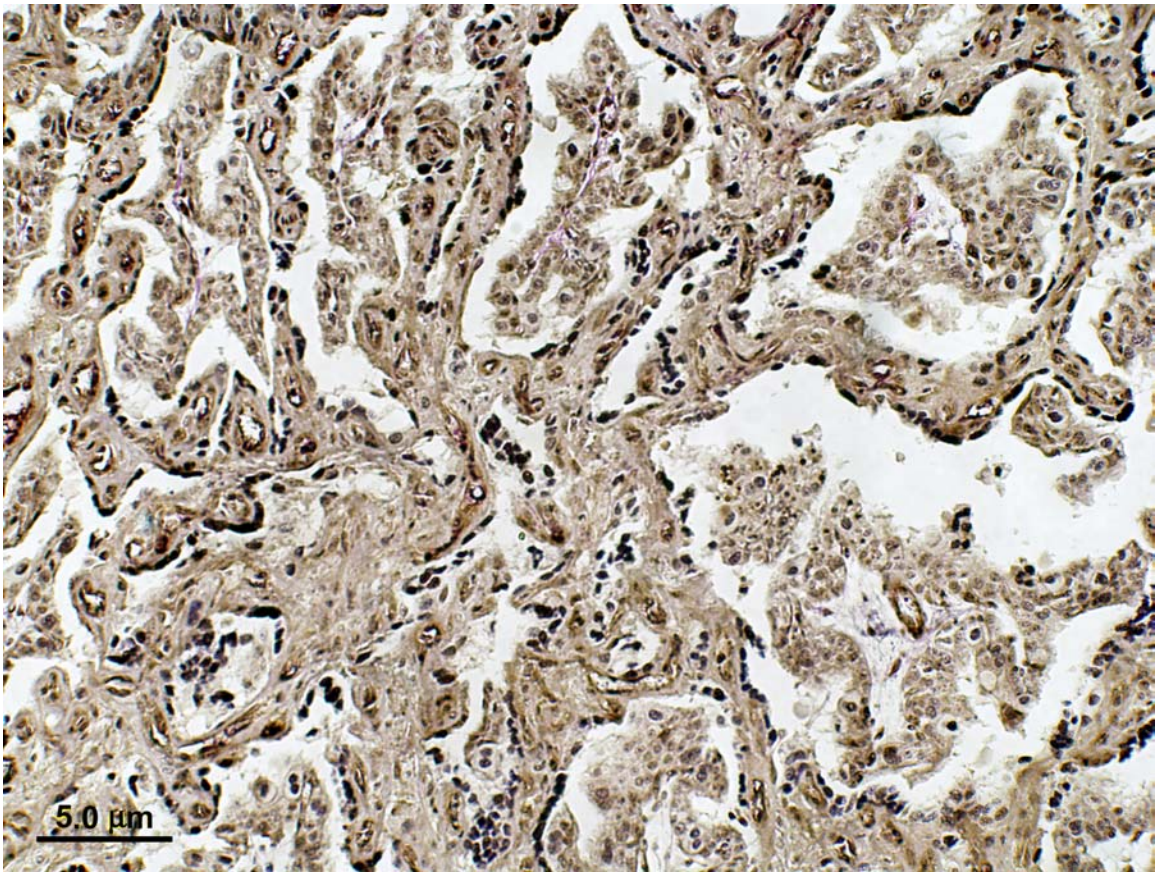

Fig. 64. Light microscopic section of a placentome at 13 weeks of gestation. VEGF protein was localized in both fetal and maternal epithelium. The most intense reaction was seen in cytotrophoblasts. Binucleate giant cells and maternal and fetal connective tissues showed no immunostaining. Invasion of fetal villi to maternal tissues was intensive after 10 weeks of pregnancy to the extent that it was difficult to make out the organization of the materno-fetal barrier; this created the spurious appearance of a less intense immunoreactivity to VEGF antibody (seen in this Figure and in Figures 65 and 66). The pattern and intensity of immunostaining were similar in all stages of gestation (compare to Figures 61-63 and 65-66). Bar = 5 µm.

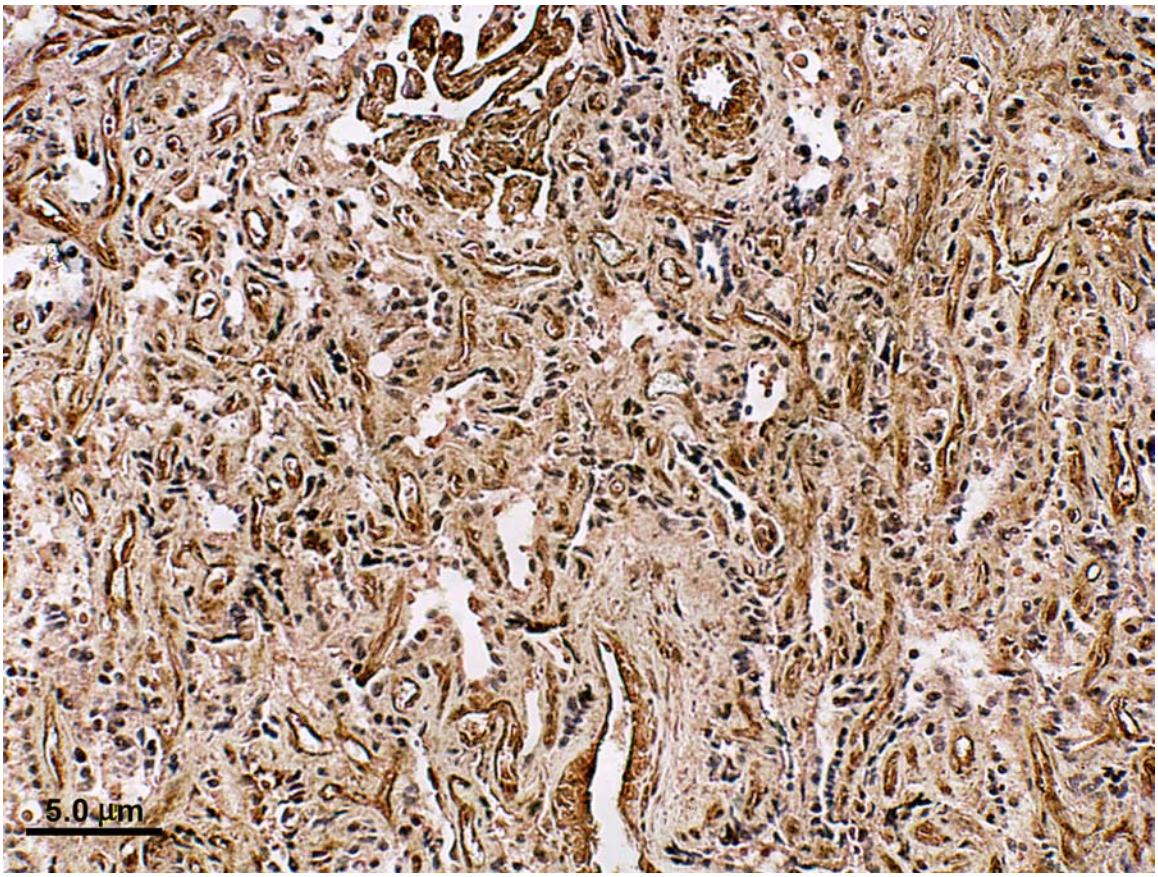

Fig. 65. Light microscopic section of a placentome at 16 weeks of pregnancy. VEGF protein was localized in both fetal and maternal epithelium. The most intense reaction was seen in cytotrophoblasts. Binucleate giant cells and maternal and fetal connective tissues showed no immunostaining. Maternal epithelium was lost at later stages of pregnancy (seen in this Figure and in Figure 66). Bar = 5 µm.

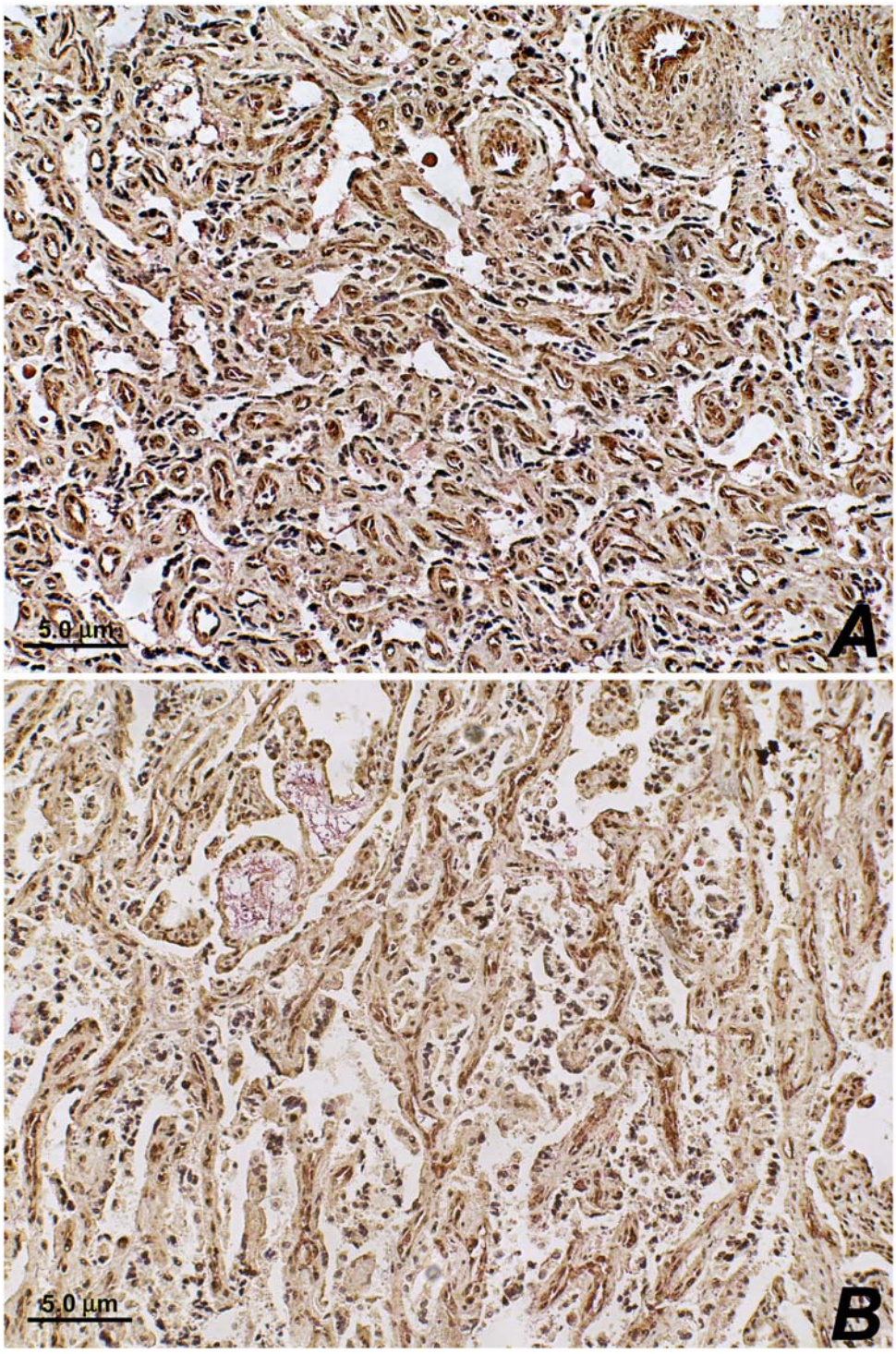

Fig. 66. Light microscopic sections of placentomes at 18 weeks of pregnancy in normal (***A***), and swainsonine-treated (***B***) does. VEGF protein was localized in both fetal and maternal epithelium. The most intense reaction was seen in cytotrophoblasts. Binucleate giant cells and maternal and fetal connective tissues showed no immunostaining. The pattern and intensity of immunostaining were similar in all stages of gestation (compare with Figures 61-65). A less intense reaction was seen in tissues from swainsonine-treated does. Bar = 5 µm.

No differences in intensity of the immunostaining were observed between the right and left ovarian tissues, among different stages of pregnancy, or in pregnant *versus* non-pregnant does. The pattern of immunostaining was similar in all ovaries (Figs. 67-69). The following description applies to all ovaries at all stages. Luteal cells were positively stained. Some luteal cells showed a more intense staining than others, which was not apparently related to whether they were large or small luteal cells. Follicular cells showed positive immunoreactivity. The staining was more intense in the granulosa cells than in theca cells. The endothelium and smooth muscles of the ovarian vasculature showed positive immunoreactivity.

Vascular endothelial growth factor was also localized in ovarian tissues from swainsonine-treated does. The pattern of immunostaining was similar to those from normal animals; however, a decrease in intensity was observed at both 7 (Fig. 70) and 18 weeks (Fig. 71) in the ovarian tissues from swainsonine-treated does.

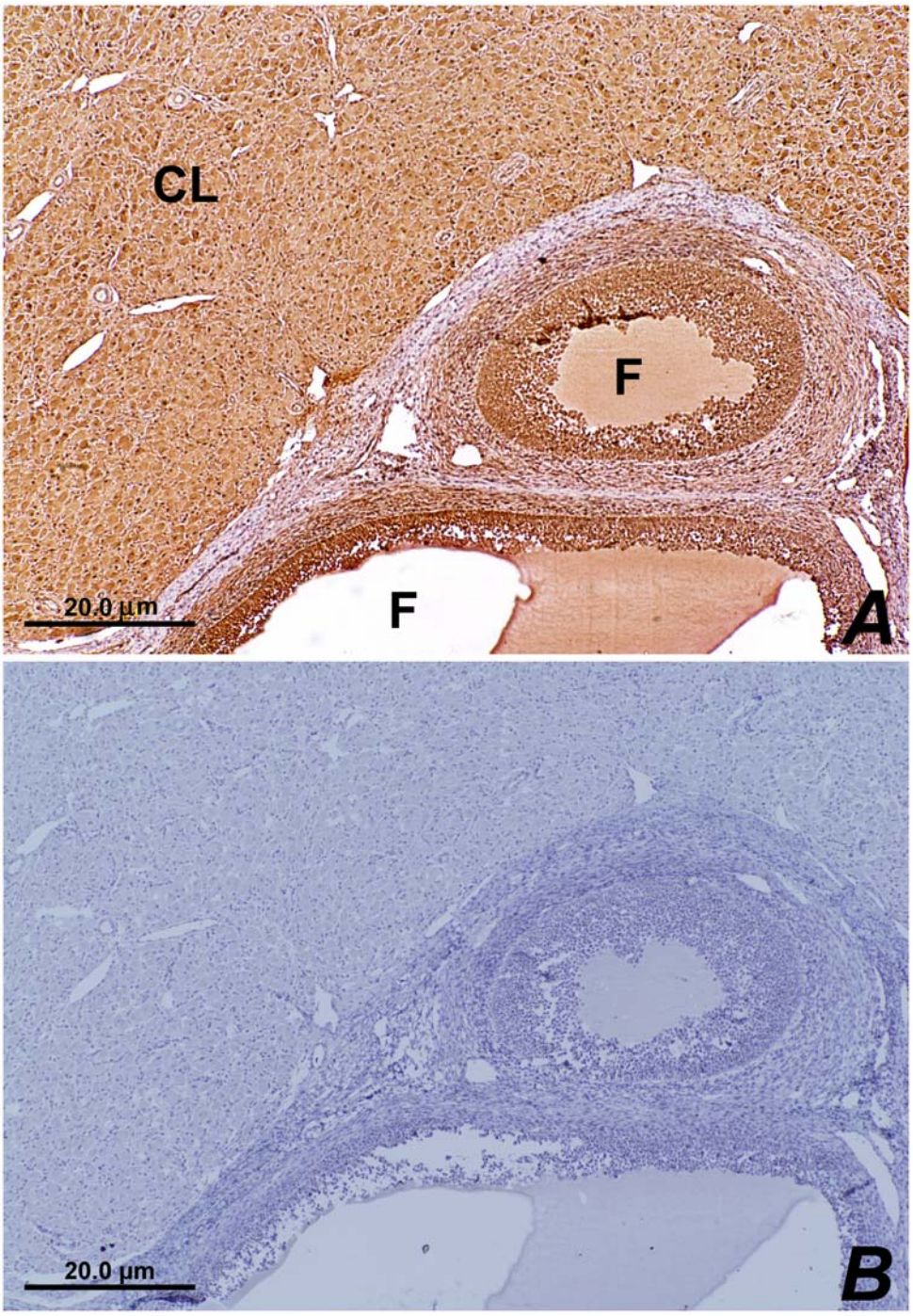

Fig. 67. Light microscopic sections of ovarian tissues at 7 weeks of gestation at low magnification. VEGF was localized in luteal cells (**CL**) as well as granulosa and theca cells of follicles (**F**). ***B*****:** Negative control. Bar = 20 µm.

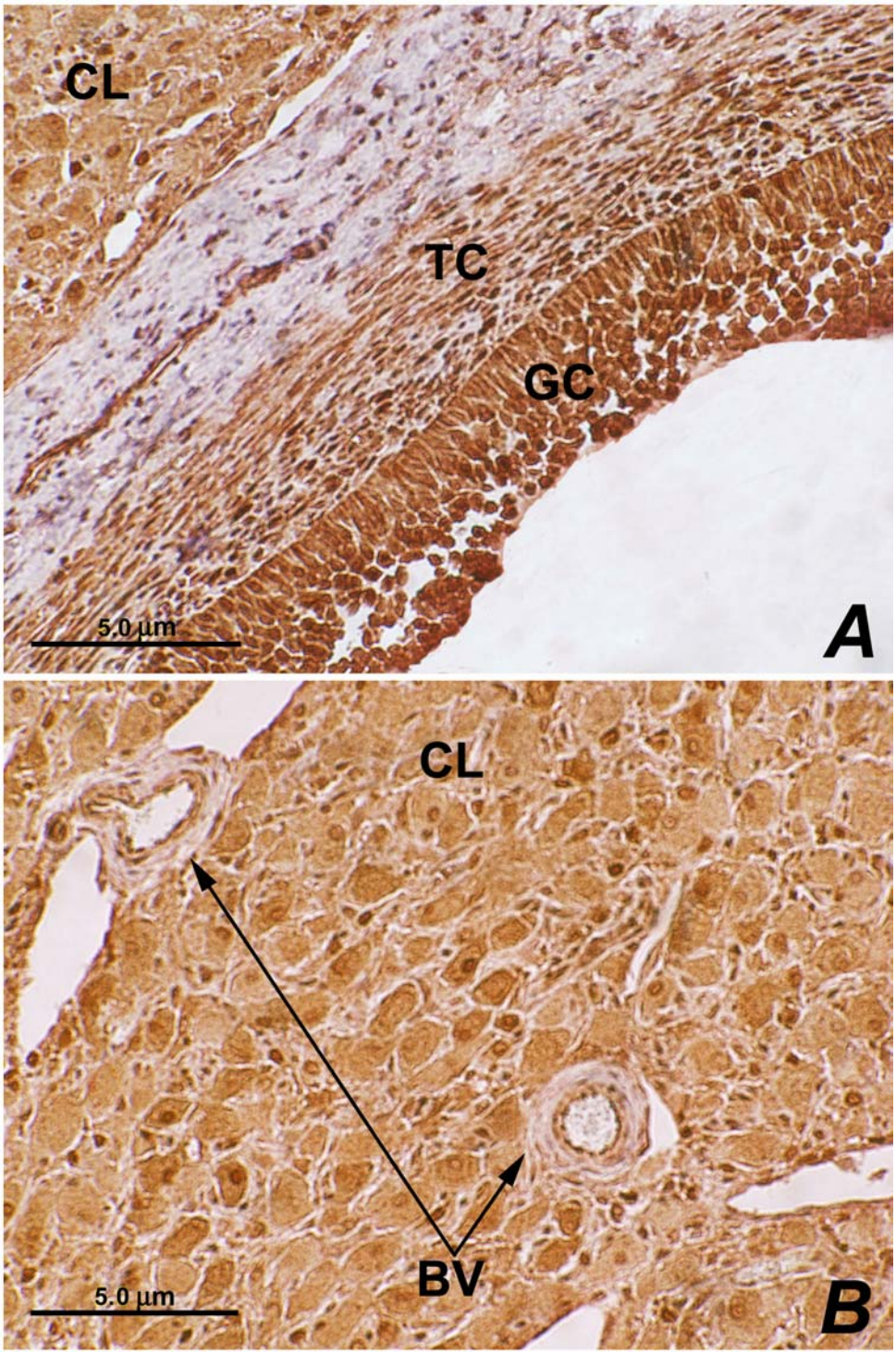

Fig. 68. ***A*** and ***B*** are higher magnification images of figure 67. VEGF was localized in luteal cells (**CL**) and granulosa and theca cells of follicles. Immunoreactivity to VEGF antibody was more intense in granulosa cells (**GC**) than theca cells (**TC**). The endothelium and smooth muscles of ovarian vasculature (**BV**) showed positive immunoreactivity. Bar = 5 µm.

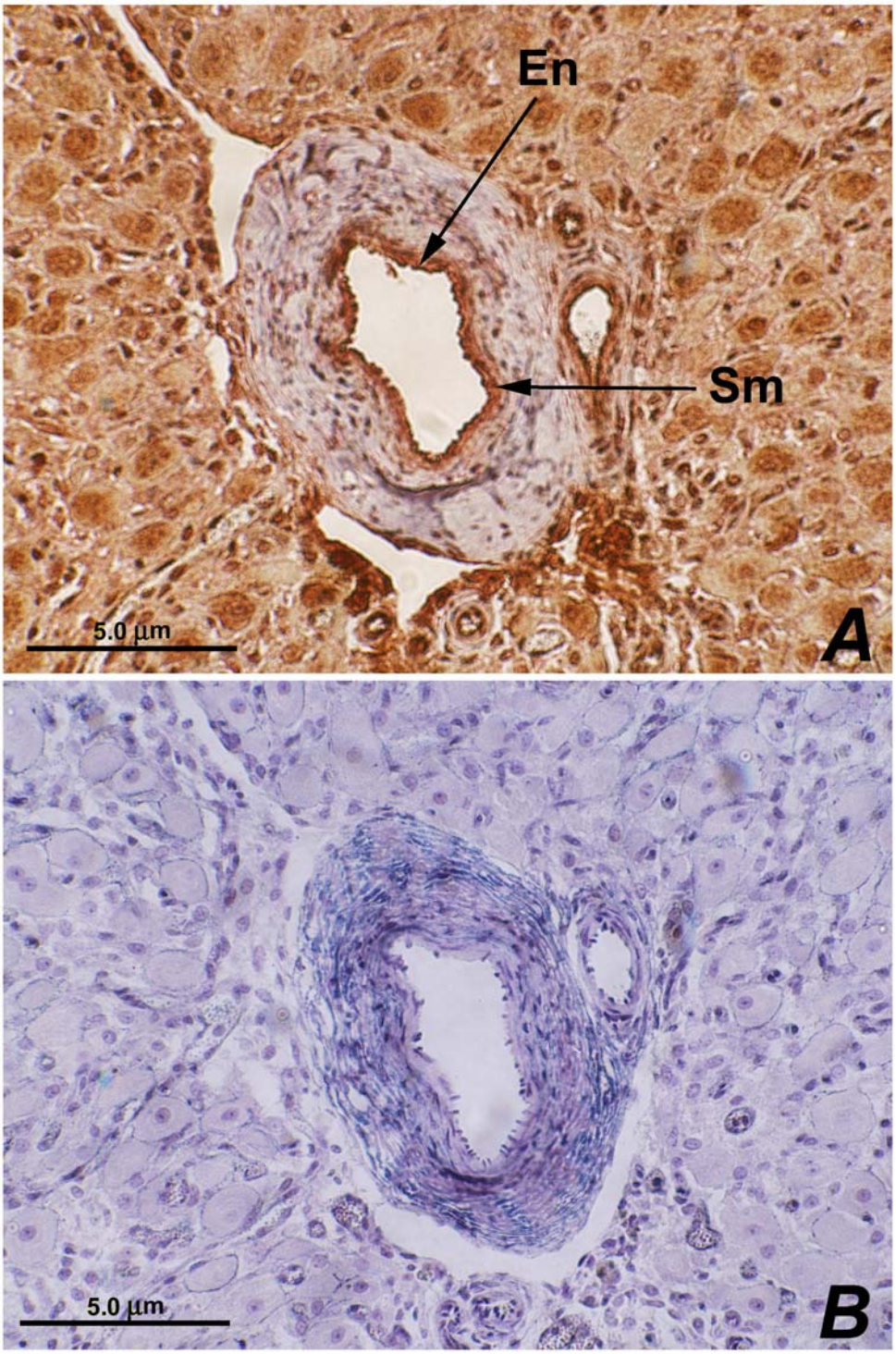

Fig. 69. High magnification images of luteal vasculature. VEGF was localized in endothelium (**En**) and smooth muscles (**Sm**). ***B*:** Negative control. Bar = 5 µm.

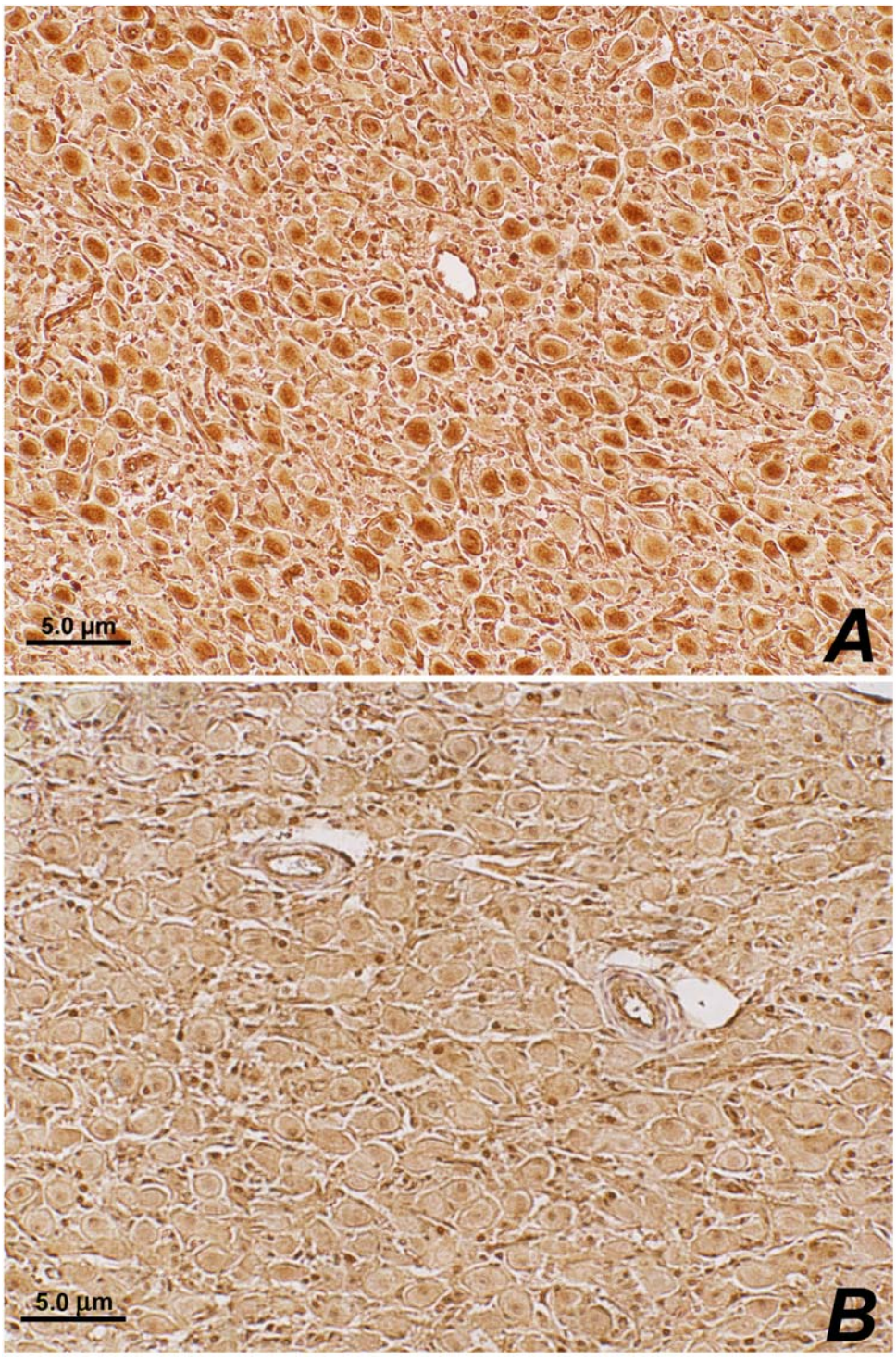

Fig. 70. Light microscopic sections of ovarian tissues in normal (***A***) and swainsonine-treated does (***B***) at 7 weeks of gestation. The pattern of immunostaining of VEGF in swainsonine-treated does was similar to that in normal does, but intensity of the immunoreactivity was lower. Bar = 5 µm.

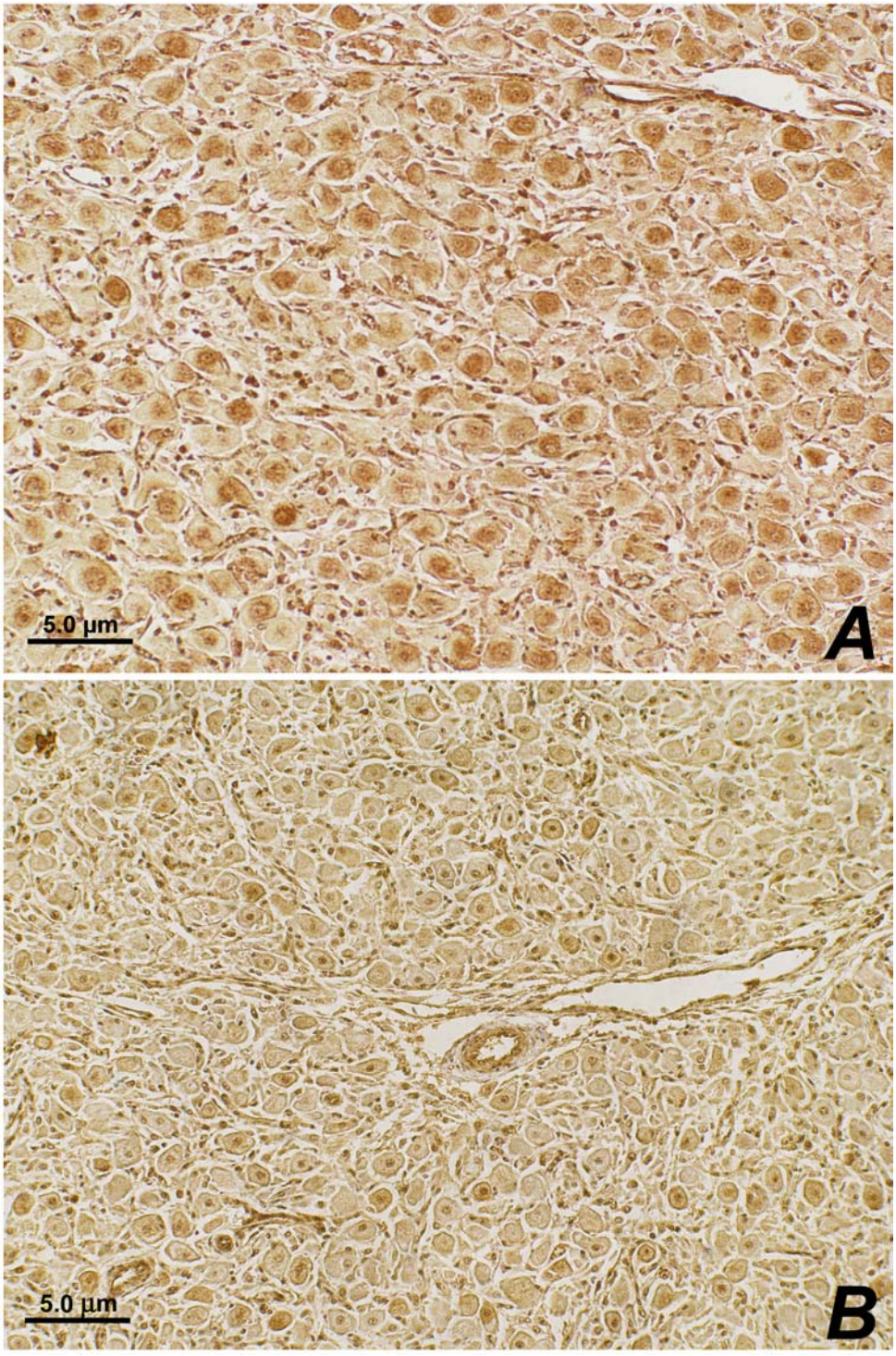

Fig. 71. Light microscopic sections of ovarian tissues in normal (***A***) and swainsonine-treated does (***B***) at 18 weeks of gestation. The pattern of immunostaining of VEGF in swainsonine-treated does was similar to that in normal does, but intensity of the immunoreactivity was lower. Bar = 5 µm.

Real-time QPCR

All tissues studied expressed VEGF, Flt-1 and KDR mRNAs; however, the levels of expression differed at different stages of pregnancy and from that of the non-pregnant state.

Placentomes (Figures 72a & b): Levels of expression of VEGF mRNA appeared to be similar throughout early stages of pregnancy up to 10 weeks; then levels slightly increased. In the later stages (at and after the 13-week-stage), no major differences were observed among stages. Levels were lower than those in the non-pregnant group at the first three stages.

Expression of Flt-1 mRNA was similar to that of VEGF at the first three stages of pregnancy. Subsequently, as in case of VEGF, it increased slightly at and after 13 weeks with a maximum increase observed at 18 weeks. Levels were slightly higher than those of the non-pregnant group, especially at and after 13 weeks.

In the case of KDR, levels of mRNA expression appeared to increase at and after 7 weeks with no substantial changes between stages, except at 18 weeks, when it increased substantially. However, levels were lower in all stages of pregnancy than those of the non-pregnant animals.

No substantial differences were observed in the expression of VEGF, Flt-1 and KDR mRNAs between tissues obtained from swainsonine-treated animals and those from normal animals at 7 weeks. However, at 18 weeks swainsonine had an inhibitory effect on the expression of all targets.

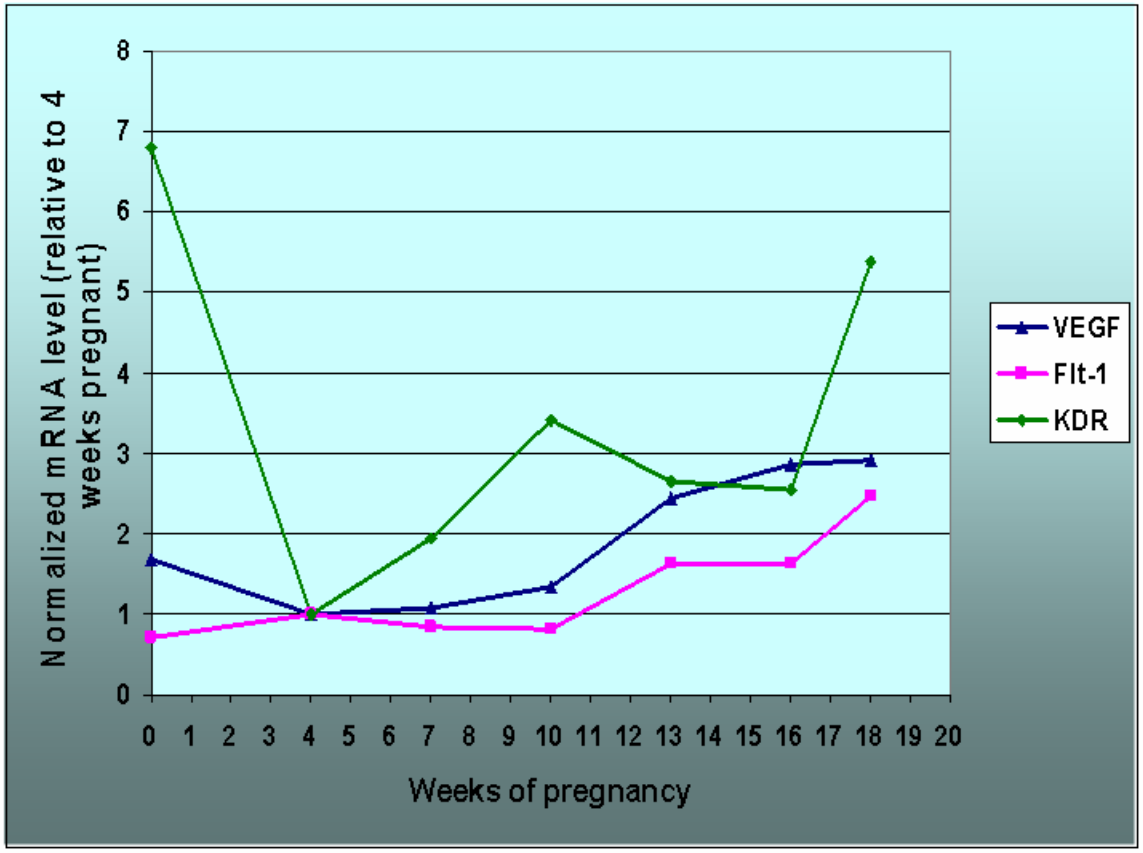

Fig. 72a. Expression of VEGF, Flt-1, and KDR mRNAs in non-pregnant (0) animals and at different stages of pregnancy, as measured in the placentomes.

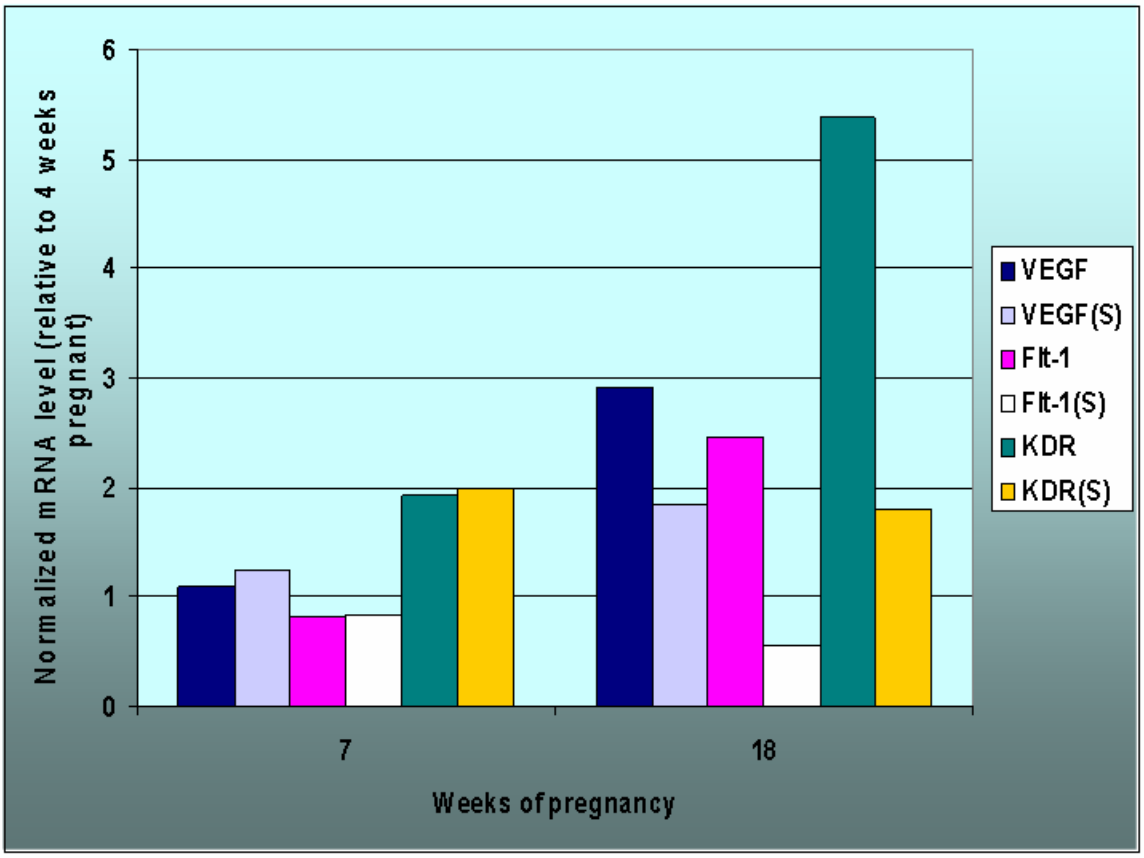

Fig. 72b. Expression of VEGF, Flt-1, and KDR mRNAs in the placentomes of normal and swainsonine-treated (**S**) pregnant does at 7 and 18 weeks of pregnancy.

Right ovary (Figures 73a & b): No substantial variation in the expression of VEGF mRNA was observed in the right ovarian tissues across all stages of pregnancy. Levels of expression of Flt-1 mRNA doubled at 10 weeks with a further increase at and after 13 weeks. The maximum increase was observed at 18 weeks. Expression of KDR mRNA increased during pregnancy up to 10 weeks, with no further increase at 13 weeks and 16 weeks, but at 18 weeks expression increased again.

Levels of expression of all three targets in pregnant does were substantially higher than those in the non-pregnant group. Expression of all targets was lower in the tissues obtained from swainsonine-treated animals at 18 weeks compared to those in untreated pregnant animals at that stage. Data from normal animals at 7 weeks of pregnancy were missing; therefore comparison to 7-week does treated with swainsonine was not possible.

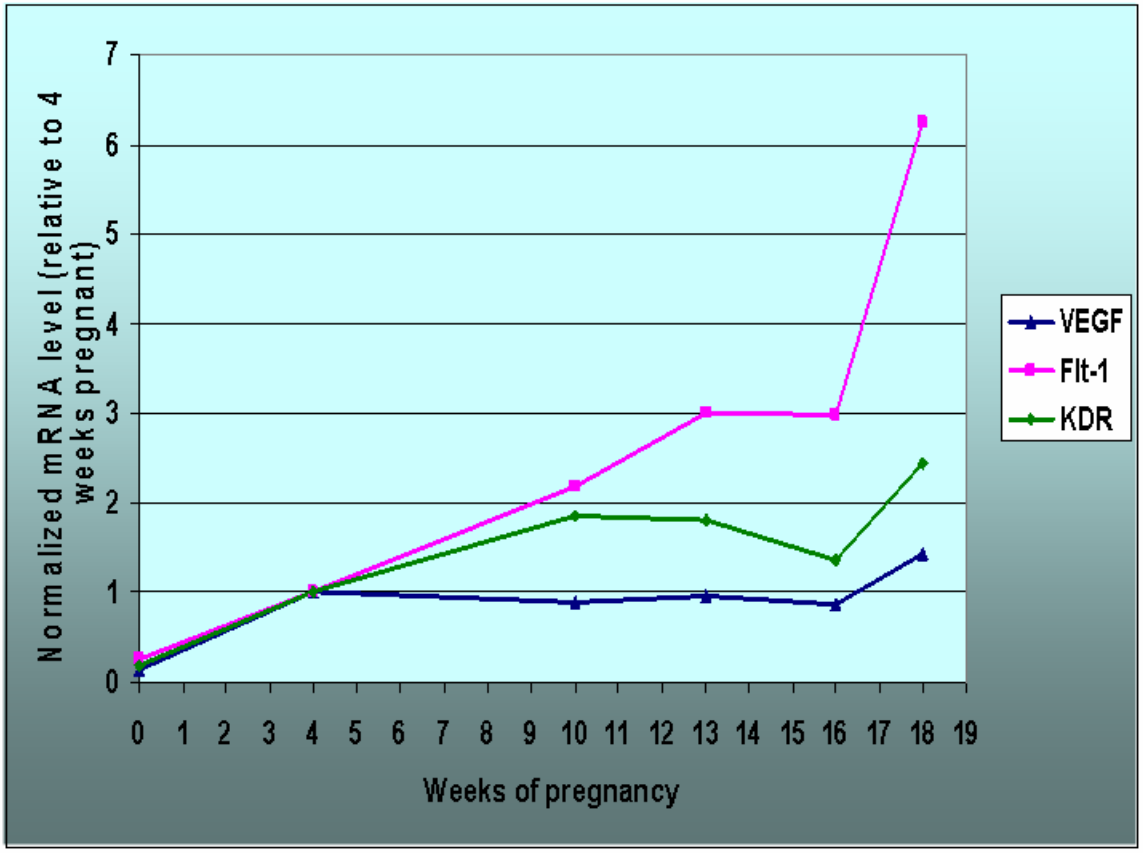

Fig. 73a. Expression of VEGF, Flt-1, and KDR mRNAs in the right ovary of non-pregnant (0) does and at different stages of pregnancy.

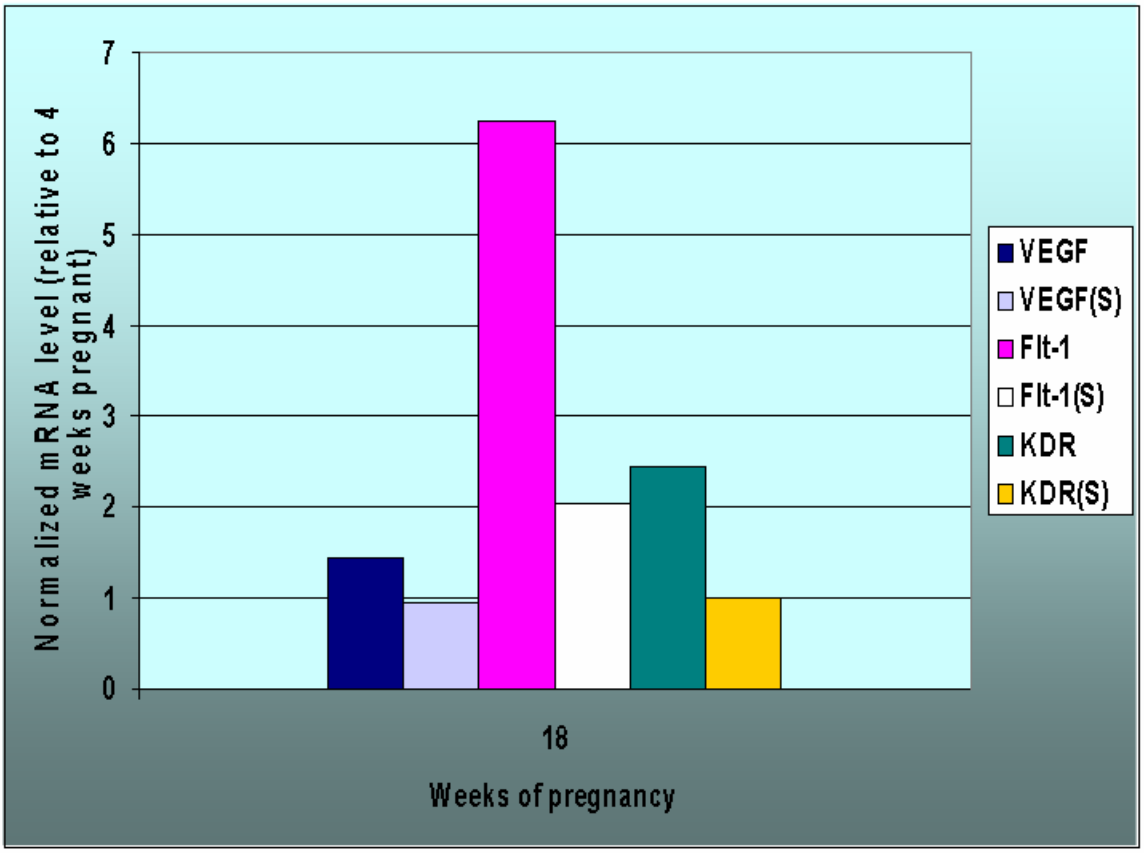

Fig. 73b. Expression of VEGF, Flt-1, and KDR mRNAs in the right ovary of normal and swainsonine-treated (**S**) pregnant does at 18 weeks.

Left ovary (figures 74a & b): Levels of VEGF mRNA expression increased at and after 7 weeks of pregnancy with no major differences among stages. Expression of Flt-1 mRNA substantially increased during pregnancy, especially starting at 7 weeks of pregnancy, followed by a slight decline at 10 weeks, and a return to higher levels at 13 and 16 weeks, followed by marked increase at 18 weeks. Expression of KDR mRNA increased substantially during pregnancy starting at 7 weeks, decreased at 10 and 13 weeks, then increased at 16 and 18 weeks.

Levels of Flt-1 and KDR mRNAs increased substantially during pregnancy, especially at and after 7 weeks, compared to the non-pregnant state. Expression of all three targets mRNAs decreased in the tissues obtained from swainsonine-treated animals at 7 and 18 weeks.

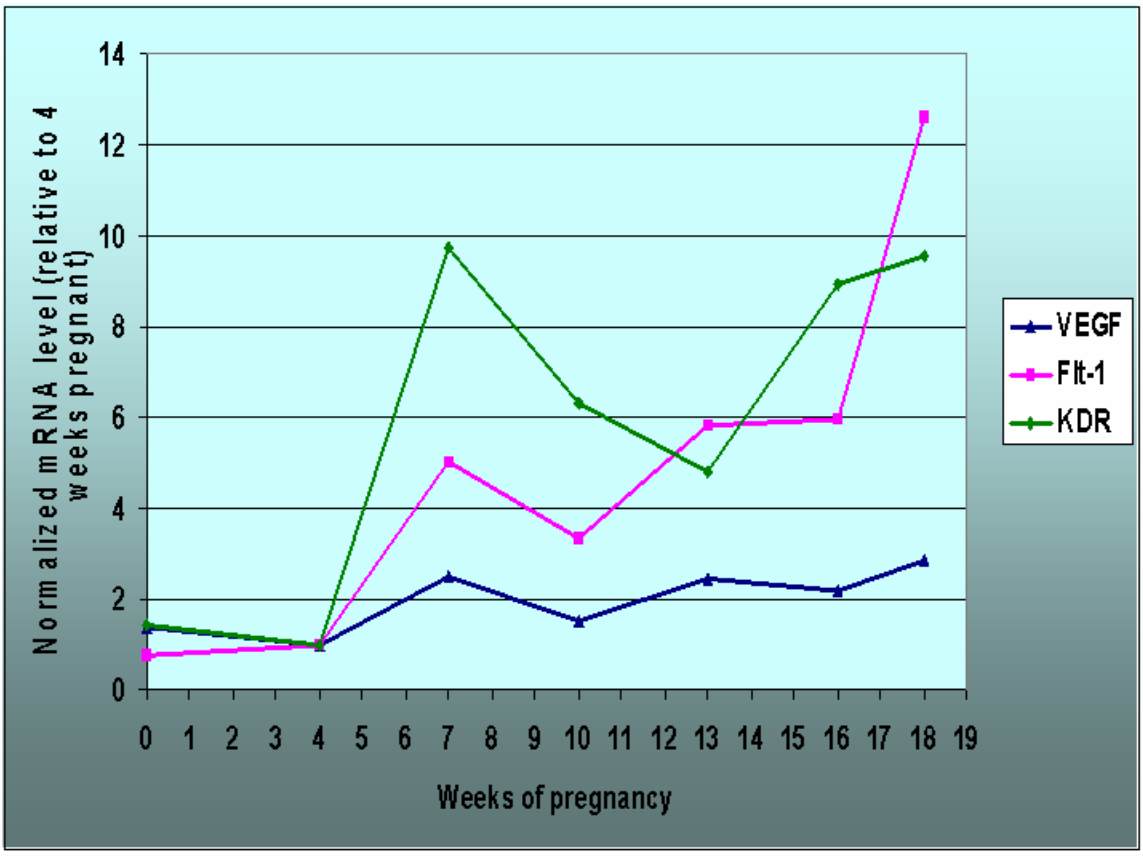

Fig. 74a. Expression of VEGF, Flt-1, and KDR mRNAs in the left ovary of non-pregnant does and at different stages of pregnancy.

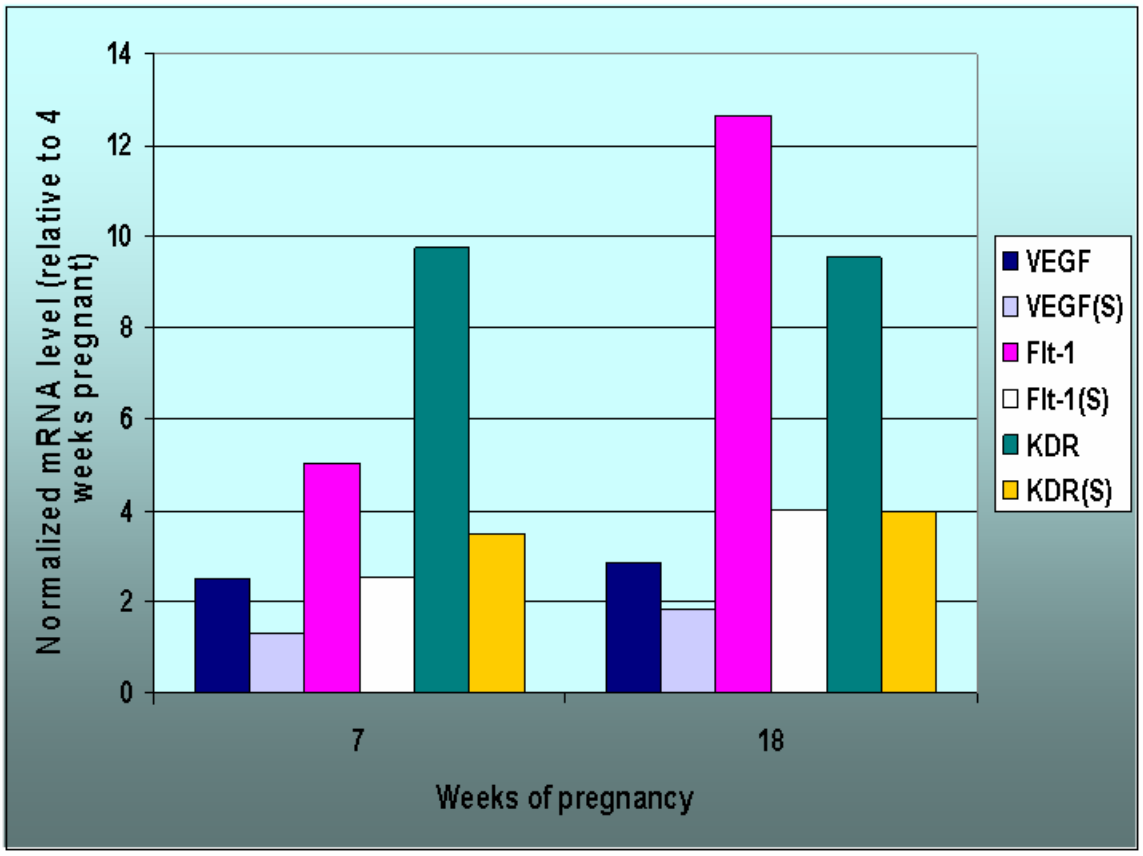

Fig. 74b. Expression of VEGF, Flt-1, and KDR in the left ovary of normal and swainsonine-treated (**S**) pregnant does at 7 and 18 weeks.

Discussion and Conclusions

1. Techniques Employed

Synchronization Protocol

It was imperative to have a large number of does at the same stage of pregnancy to perform our experiments. Commercially-produced timed- pregnant does are extremely costly and difficult to obtain. Furthermore, by using a large estrous-synchronized group it was possible to ensure that all animals received the same conditions of housing and care. We modified an established protocol for estrous synchronization and breeding to obtain the desired number of synchronized pregnant does. Our goal was to achieve a high degree of synchronicity among females, while at the same time achieving a high degree of fecundity.

In general, a synchronization program depends on two basic strategies. The first is the termination of the life of the CL using $PGF_{2\alpha}$, consequently removing its inhibition on gonadotropin secretion, which leads to maturation and ovulation of the existing dominant follicle(s) in those animals that are cycling. The second strategy is the prolongation/simulation of diestrus using progesterone with subsequent maturation and ovulation of the pre-existing follicle(s) upon removal of progesterone effect. Either technique serves to initiate estrus in a group of females in a short period of time resulting in conservation of labor during breeding and parturition (Braun, 1980; Bretzlaff and Madrid, 1985; Morrow, 1986; Amoah and Gelaye, 1989; Smith and Sherman, 1994; Freitas et al., 1997; Kusina et al., 2000; Oliveira et al., 2001).

When using our synchronization protocol, does at days 0-4 of the estrous cycle will not respond to the first dose of prostaglandin: prostaglandin has no effect on those females in estrus and/or in the first few days of diestrus. Does at days 4-17 of diestrus can respond to the first dose of prostaglandin with luteolysis of the CL, and subsequent maturation and ovulation of the pre-existing dominant follicle(s), followed by formation of new CL. By the time of the second prostaglandin injection on day 11, all does should have a CL that is responsive to prostaglandin. Females at days 17-21 are in the stage of natural CL luteolysis and also have the ability to respond to the second injection of prostaglandin. The insertion of ear implants containing norgestomet mimics the presence of a CL with maturation and ovulation of the dominant follicle(s) upon removal of the implant on day 11 (due to removal of the inhibitory effect of progesterone on gonadotropin secretion). Injection of FSH and LH-like hormones (eCG has FSH-like activity; hCG has LH-like activity) on day 10 serves to promote maturation and ovulation of multiple follicles, with a subsequent increase in fecundity. The injection of prostaglandin on day 11 should bring most animals to estrus within 24-72 hours of injection.

This protocol is based on a well-known protocol for estrous synchronization, with minor modifications in the form of addition of a single dose of prostaglandin on the first day of the synchronization scheme to improve the efficacy of the synchronization protocol and subsequent fertility. We also used PG600® instead of either hCG or eCG alone, and exploited the benefits of the male effect. Thus in our protocol, we combined several effective techniques to

obtain high number of pregnant does required to perform our experiments. The value of the first prostaglandin dose is to help synchronize the estrous cycle itself of all animals having a mature CL. This “synchronization before synchronization” concept can be explained as follows. Without the first dose of prostaglandin, animals at days 0-4 would soon have natural CL as would those at 17-21 (after a few days); however, animals at days 4-17 already have a CL, with subsequent application of progesterone, increasing the length of the simulated diestrus. That would cause no harm, but it would have rendered these animals different from the others with respect to their stage of the estrous cycle. The first dose of prostaglandin provides further synchronization of the cycle enhancing the effect of the norgestomet implants.

Introduction of teaser males 15 days before the start of the synchronization program reinforces the “synchronization before synchronization” process. Introduction of intact males at the beginning of the breeding season is well documented to produce a synchronizing effect in and of itself (Morrow, 1986; Smith and Sherman, 1994).

Clearing Technique

Injection of the reproductive tract vasculature with subsequent clearing (rendering transparent) of tissues allowed visualization and studying of the reproductive tract’s vascular system in relation to tissues it supplies. The technique was adopted from Orsini (1962) and Del Campo et al. (1974), with modifications as follows. Blood washout was performed with physiological saline at approximately the normal goat body temperature, as a way to maintain the

normal physiological state of vessels including their diameter to facilitate injection, and to avoid extravasation of the injection medium. The use of an infusion pump instead of hand injection provides better control of intraarterial pressure, is documentable, and is reproducible. Microfil® rather than latex was injected into the vasculature of the reproductive tracts. Microfil® provides complete filling with minimal shrinkage of the vasculature, is easy to prepare, is available in many colors, does not require an acidic environment for curing, and is radio-opaque. Using equal quantity of Microfil and MV diluents resulted in a medium of very low viscosity with ability to cross capillaries. Since capillary crossing was not desirable in this study, we used a mixture of MV and HV diluents to increase viscosity of the final product to avoid crossing of capillaries. We tried the clearing agents (benzol and benzyl benzoate) used by Orsini (1962) and Del Campo et al. (1974), but no satisfactory results were obtained. Methyl salicylate and glycerin were each used in our experiment as clearing agents, and both gave satisfactory results. Alcohol-methyl salicylate clearing produced a stiffer tissue, which, from an aesthetic point, provides a pleasing view for gross observation, but it is difficult to manipulate. Also extended exposure to the strong smell of methyl salicylate was unavoidable (even under a fume hood) during the long study time required to examine such a complex vascular system as that of the reproductive tract. Glycerin clearing produced a more flexible tissue, allowing easier manipulation for a given area. Glycerin has a more pleasant smell than that of methyl salicylate, but from an aesthetic point, does not provide a such pleasing view as that of methyl salicylate.

Radiography

Because radiography was to be used to study the distribution of the reproductive tract vasculature, Microfil® was chosen because of its radio-opacity. However, while radiographs were useful to study vessels' distribution; no more information was obtained from studying them than was available from studying cleared specimens examined with the naked eye. In other words, studying cleared specimens provided enough information to render radiographs unnecessary except perhaps to confirm visual impressions by a second visualization method. Further, due to the inherent disadvantage of radiographs in the form of superimposition of vessels in two dimensional views, determining the definitive supply of certain area by certain branch was difficult.

Microvascular Corrosion Casting/SEM

This method allowed examination of the three-dimensional organization of microvessels including blood capillaries in the uterus and ovary. Complete filling of the reproductive tract vasculature is best achieved by casting *in situ*, before the organs have been excised. Careful control of precasting, casting, and postcasting conditions is critical for obtaining good quality casts (Hodde and Nowell, 1980; Minnich et al., 2001).

Preparation of the animal before casting is imperative to obtain a good quality completely filled vessels system. Precasting conditions include rinsing, as well as the application of vasoactive drugs and anaesthetics. Blood wash-out was performed using heparinized saline, to prevent blood clotting and incomplete exsanguination, to facilitate complete filling of the utero-ovarian vasculature with

identifying endothelial cell impressions on the surface of the cast. The saline was infused at approximately normal body temperature of the goat to prevent vasoconstriction and/or extravasation of casting medium. Vasoconstrictive reactions were also prevented by adding procaine 0.5% to the rinsing solution.

Casting conditions include pressure during rinsing and casting, and the amount of final shrinkage of casting medium. The use of an infusion pump allowed for control of intraarterial pressure, is documentable, and is reproducible. The casting medium was prepared under 4^{o}C to prevent premature polymerization with the result of longer available working time. Batson's No. 17® formula was modified to yield a less viscous (to promote complete filling of microvessels) and more durable (to withstand digestion and electron beam bombardment) medium. However, these advantages were obtained at the expense of more shrinkage. The modified Batson's mixture showed 16.5% shrinkage, which should be considered while obtaining quantitative information from vessels' casts.

Postcasting conditions include thermal burdening during maceration, sputter coating, and SEM inspection. The specimens were kept in warm (40^{o}C) water for 2-3 days to initiate decomposition, which greatly enhanced the maceration process and did not have an adverse effect on the casting medium. The use of Papain and high concentrations of KOH greatly hastened the digestion process with no adverse effect on the casting medium. The modified mixture was stable enough to withstand the high temperature used during maceration with no detectable deterioration. The resulting casts were relatively

large and complicated in architecture, a fact which rendered even coating a cumbersome process. This problem was partially solved by using the tilting and spinning capability of a spacious sputter coater; however, charging problems were inevitable.

Two-dimensional (2D) and three-dimensional (3D) morphometry can be used to obtain quantitative information of vessels' casts. Accuracy of measurements increases with 3D morphometry, but it requires special instruments, which were not available at our institution. We used 2D morphometry to study 3D structures, which was fairly acceptable in areas studied (*i.e.* fetal side of caruncles).

In the case of ovarian casts, no quantitative measurements could be obtained because of absence of areas in the specimens that could be directly compared to each other, as was the case in caruncles. The microvascular system of the ovary was so complicated to the extent that it could not be directly comparable from a quantitative point of view.

VEGF Expression Techniques

Immunohistochemistry revealed the specific location of VEGF protein in uterine and ovarian tissues under normal and affected conditions of angiogenesis, but this type of analysis is at best semi-quantitative. Real-time QPCR was used to measure the amounts of VEGF and its receptors' mRNAs expressed in uterine and ovarian tissues. This technique is more sensitive, specific, and quantitative. In this way, the expression of VEGF mRNA can be

correlated to the distribution of VEGF protein and ultimately to the extent of microvascular development.

Specimens collected were immediately immersed in freshly prepared 4% paraformaldehyde for 4 hours at 4^{o}C to be processed for immunohistochemistry. Paraformaldehyde is a highly polymeric form of formaldehyde possessing all formaldehyde advantages (relatively inexpensive, stable, rapid penetration, causes less shrinkage than any other fixative). Paraformaldehyde was chosen for use because commercial formalin contains 10-14% methanol (a coagulant), which renders it undesirable fixative for immunohistochemical studied.

To ensure specificity of immunostaining for VEGF protein in uterine and ovarian tissues; the following were performed: 1. Slides were incubated with bovine serum albumin and normal horse serum to prevent non-specific binding of the primary antibody to tissue components. 2. Two not one primary antibodies (from two different manufacturers) were used for VEGF immunolocalization. 3. Positive and negative control slides were used.

The QPCR specimens collected were immediately immersed in RNA Later® solution as a way to stabilize RNA, and to assure preservation of the RNA expression pattern. These are prerequisites for accurate gene expression analysis. RNA later® reagent quickly permeates tissues, stabilizing and protecting the RNA expression pattern, and it is far more convenient and safer to handle at room temperature than liquid nitrogen or dry ice.

To ensure accurate quantification of the expression of VEGF and its receptors' mRNAs, the following were performed. 1. A validation experiment

(using serial dilutions of control templates) was done to verify that the amplification efficiencies of targets and reference were equivalent. 2. Probes were chosen to span exon-exon junctions to avoid background signals due to amplification of contaminating genomic DNA in the cDNA preparation. 3. All primers and probes were checked for the absence of self-complementary sequences. 4. Each assay included tested samples, no-template, and non-reverse transcribed RNA controls to verify the cDNA-dependence of signals. 5. All reactions were done in triplicate.

Locoweed Feeding

Commercially available swainsonine is expensive and difficult to obtain in large quantities. Feeding locoweed to does was a rather cumbersome process because of its unpalatablity. Because it was necessary to feed precise amount of swainsonine in a limited time, it was impossible to use starvation to induce the craving appetite for the plant; in addition to this consideration, there was the necessity to keep the does in a good nutritional state during their pregnancies. Thus, locoweed was fed by gavage to ensure the appropriate dose was received by each doe. The required amount was fed twice per day to promote complete digestion and absorption. Serum analysis was performed to obtain as estimate of the amount of swainsonine absorbed.

2. Data Obtained

Synchronization Protocol

The percentage of pregnancies obtained was enough for the purpose intended. All does were in estrus within 72 hours of implant removal and most of

these were in estrus within 24 hours. Thirty eight out of fifty (76%) does were pregnant at 4 weeks. Eighty six fetuses resulted from 38 pregnancies. Thus the protocol described in this work is an efficient and effective route to high rates of conception, high rates of multiple pregnancies.

Cleared Specimens

Uterine vessel nomenclature

Barcroft and Barron (1946) provided a general description of the placental vessels in sheep, which was further developed by Makowski (1968) in sheep and goats; however, due to the limitation of the techniques they used and lack of images showing vascular paths, their description was not fully understandable. In the present study, with complete filling of the maternal vascular system, and the ability to examine vessels in relation to the tissues they supply using tissue clearing technique, full representation of the arterial vessels system was possible (Fig. 14).

Data obtained from cleared specimens

The ovarian artery was tortuous and lay in a close apposition with the uterine branch of the ovarian vein in all does in the present study. The physiological significance of this arrangement in non-pregnant animals (though goats were not studied) was noted by Del Campo and Ginther (1973).The higher effective dose of $PGF_{2\alpha}$ in sheep is due to the presence of mainly a *local* utero-ovarian pathway in sheep *versus* a mainly *systemic* pathway in horses (Ginther, 1974). Goats have similar arrangement to that of sheep, and therefore can be expected to have this *local* utero-ovarian pathway, where substance (such as

$PGF_{2\alpha}$) can pass from the ovarian vein to the ovarian artery and affect structures on the ovary.

The present work newly demonstrated that the architecture of the ovarian artery and vein was maintained throughout pregnancy. It has been demonstrated that the maintenance of luteal function during early pregnancy in ewes (Mapletoft, 1976) and cows (Del campo, 1980) occurs by local vascular transport of a luteotropic substance from the gravid uterus to the ipsilateral ovary. The nature and chemical properties of this substance were not investigated. The transport of luteotropic substance occurs by means of the close apposition of the ovarian artery to the ovarian vein. This physiological supposition is supported by the anatomic architecture of the utero-ovarian vasculature demonstrated in early pregnancy in ewe and cow, and by the anatomy revealed here for goats as well. Maternal recognition of pregnancy occurs around day 13-14 after ovulation in ewe and 15-16 in cows (Senger, 2003). It is achieved by production of certain proteins between days 13 and 21 after ovulation. These include ovine trophoblastic protein-1 (homologous to interferon-α), or bovine trophoblastic protein-1, and pregnancy-specific protein-B (pregnancy-associated glycoproteins (PAGs). Ovine and bovine trophoblastic proteins inhibit oxytocin receptor synthesis by endometrial cells, and promote protein synthesis by endometrial glands. These proteins are not luteotropic. Pregnancy-specific protein-B is produced by binucleate giant cells, and has a luteotropic effect. Maternal recognition by means of production of trophoblastic protein-1 does not require a *local* venoarterial pathway between the uterus and ovary because it is produced

in the uterus and acts on the uterus; however, the other protein (pregnancy-specific protein B) is produced in the uterus but acts on the CL so it does require a pathway to reach the ovary. Study by Bridges et al. (1999) proved that there was no luteal source of pregnancy-specific protein-B in ewes. Pregnancy specific protein can reach the ovary by either a *local* or a *systemic* pathway. We hypothesize that the predominant mechanism in ewes, cows, and does is the local one between the uterus and ovary. We base this hypothesis on the presence of the intimate arterio-venous approximation, and its potential functionality as a *local* venoarterial pathway. More physiological studies are needed to test this hypothesis. Also the molecular weight and possible mechanisms of transfer of PAGs should be considered in future studies. Pregnancy-specific protein-B has a clinical importance. It can be used for pregnancy diagnosis in goats (Humblot et al., 1990).

Ewes are CL dependent till 50 days of pregnancy; thereafter the placenta produces sufficient amounts of progesterone to support pregnancy. Cows are CL dependent till 6-8 months of gestation. Does are CL dependent throughout the entire period of pregnancy (Senger, 2003). Progesterone is produced almost entirely by the CL in goats, and ovarioectomy at any time causes abortion. The presence of this anatomic arrangement of utero-ovarian vessels has only been demonstrated in non-pregnant (Ginther, 1976) and early stage pregnant ewes (Mapletoft, 1976) and cows (Del campo, 1980). Whether this arrangement is present at later stages of pregnancy in ewes or cows has not been studied. This work shows, in the goat, this arrangement was in fact maintained throughout

pregnancy, which fits the fact that the goat is CL dependent throughout pregnancy. Factors produced by the placenta could be transported via this anatomic arrangement to maintain the CL throughout pregnancy. Whether CL maintenance is the only function of this anatomic arrangement cannot be elucidated without further studies on the presence of this anatomic arrangement of the ovarian artery and ovarian vein at later stages of pregnancy in ewes and cows, as well as further work coordinating the physiological and anatomic inter-relationships in all ruminant species.

Special adaptations of the ovarian and/or vaginal arteries were noted in multiple pregnancies: 1. In 66.7% of triplets, the size of the uterine branch of the right ovarian artery was about equal to the that of the continuation of its parent artery. 2. In 16.7% of triplets, the size of the uterine branch of the left ovarian artery was actually larger than that of its parent artery. 3. In half of triplet pregnancies in the right side and 33.3% in the left side, the uterine branch of the ovarian artery gave off a branch that joined a branch of the uterine artery and supplied the uterine horn. 4. The uterine branch of the ovarian artery also gave off an additional branch that supplied the dorsal surface of the area adjacent to the tip of the uterine horn in half of triplets. 5. In one doe with triplet pregnancies at 18 weeks of pregnancy, the left ovarian artery gave rise to an additional branch to the uterus; this branch was larger than the ipsilateral uterine artery. It supplied the entire dorsal surface of the left uterine horn and anastomosed with the uterine branch of the ovarian artery and uterine branch of the vaginal artery. 6. A connecting branch was present between the right uterine artery and the

uterine branch of right vaginal artery in 16.7% of triplets. 7. A connecting branch was present between the left uterine artery and the uterine branch of left vaginal artery in 16.7% of triplets. These adaptations were observed in triplet pregnancies mainly at later stages. This physiological adaptation to multiple pregnancies has not been noted before in the literature. This may be due to lack of anatomical studies on uterine vessels during pregnancy in all animals. These adaptations presumably serve to provide an additional blood supply to the uterus in the case of multiple pregnancies due to the increasing demand of the growing fetuses.

No difference was observed in the origin and distribution of the ovarian, uterine, and vaginal arteries between pregnant and non pregnant does; however, differences in these aspects existed within specimens from pregnant and/or non-does. The ovary is supplied by the ovarian artery. The infundibulum and the area of the uterine tube adjacent to the ovary are supplied by the uterine tube branch of the ovarian artery. The isthmus and area adjacent to the uterus are supplied by the uterine branch of the ovarian artery. The supply of the ampulla is mainly via the uterine tube branch, but in some cases via the uterine branch of the ovarian artery.

The uterus is supplied by branches of the ovarian arteries, uterine arteries, and vaginal arteries. The supply of different parts of the dorsal and ventral surfaces of the uterus is provided in figures 21 and 22. The dorsal and the ventral surfaces of the uterine tip and the adjacent area are supplied by the uterine branches of the ovarian arteries, which anastomose with branches of the uterine

artery. The distribution of the caudal and cranial branches of the uterine artery was consistent in most of the specimens; however, in some specimens the cranial or caudal branch dominated to supply most of the dorsal or ventral surface, respectively, of the ipsilateral uterine horn. The dorsal and ventral surfaces of the area between the middle portion of the uterine horn to the tip were supplied mostly by the branches of the cranial branch of the uterine artery. The supply of the ventral surface of the middle area of the uterine horn was mainly by branches of the caudal branch of the uterine artery. The dorsal surface of the middle portion of the uterine horn was supplied about equally by either the cranial or caudal branch of the uterine artery. The ventral surface of the caudal part of the uterine horn was supplied by the caudal branch of the uterine artery in all specimens studied. The dorsal surface of the caudal part of the uterine horn was supplied by the caudal branch of the uterine artery in most specimens. The dorsal and ventral surfaces of the uterine body were supplied by both the caudal branches of the uterine arteries and uterine branches of the vaginal arteries.

The anastomosis between branches of the right and left uterine arteries introduces the possibility of mixing of substances between the two horns. Substances produced in or introduced into one horn can possibly move to the other horn; *i.e.* substances produced in a gravid horn may move to the non-gravid horn or vice versa.

The uterine branch(es) of the right and/or left vaginal arteries anastomose with branches of one or both caudal branches of the uterine arteries on the ventral surface and/or dorsal surfaces of the uterine body and caudal part of the

uterine horn. The anastomosis was not ipsilateral in all cases; it was with the contralateral artery and/or both arteries (R & L) in some specimens. The size of the right and left vaginal arteries was not equal in some specimens; one or the other dominated to supply both the ventral and dorsal surfaces of the uterine body, while the other supplied just one surface.

Microvascular Casting

Uterus

Qualitative study

A complete description of the caprine caruncular vascular system is provided in this work. As shown morphologically and described in the results section of this study and from the results obtained in the study of Leiser (1987) on the fetal vessels system, we have concluded that goats possess a *multivillous* type placenta, with a combination of concurrent, cross-current, and counter-current components. The direction of blood flow through capillary sinusoids covering the fetal surface of the caruncle and maternal capillaries in the crypts in relation to the capillaries in the fetal villi shows an overall arrangement of a *multivillous* type placenta.

Six layers make up the materno-fetal barrier in epitheliochorial placenta: maternal blood vessels' endothelium, maternal connective tissue, maternal epithelial tissue, fetal epithelial tissue, fetal connective tissue, and fetal blood vessels' endothelium. The efficiency of materno-fetal exchange might be affected in part by the length of interhemal distance of the goat placenta; and it is generally felt that the epitheliochorial placentas are somewhat less efficient at the

transfer than ones with lesser interhemal distance. The idea of considering the epitheliochorial placenta as less efficient may not be accurate because several other factors *i.e.* species-specific degree of permeability of the various layers making up the materno-fetal barrier; the actual thickness of these layers; and fetal and maternal vascular systems arrangement may be very important factors in determining the efficiency of placental transport. The presence of capillary sinusoids on the fetal surface of the caruncle demonstrated here shows that the vascular system arrangement is a critical factor in determining the efficiency of placental transport. Sinusoids may serve to reduce the blood flow resistance and increase efficiency of diffusion (Boyd and Hamilton, 1970). Similarly the presence of maternal crypts may increase the surface area for diffusion. In other words, the presence of capillary sinusoids and crypts may compensate for the negative effect presented by the increased interhemal distance. The present study is the first to demonstrate the presence of capillary sinusoids on the fetal surface of the caprine caruncle. Capillary sinusoids may be functionally devoted to specific transport of certain materials across the materno-fetal barrier, a hypothesis which could be verified only with more thorough studies. It would be useful to investigate the physiological and structural differences between the types of endothelial cells lining sinusoids versus those lining normal capillaries, assuming they exist. This further reinforces the importance of the study of the maternal and fetal vascular systems because it relates directly to the prominent placental function of gas and nutrients exchange.

Some similarities between the human and the ruminant placenta have been noted (Leiser, 1997). The architecture of stem, intermediate, and terminal villi of the fetal vascular trees is similar, which implies that the fetal vascular tree may be a workable model for the human. The presence of capillary sinusoids (noted in this study) adds to this similarity, though the sinusoids exist in the maternal side of the goat placenta and in the fetal side of the human placenta.

Evidence of angiogenesis was observed in all specimens. Intussusceptive angiogenesis contributes largely to placental vascularization and should not be ignored as a possible mechanism of angiogenesis in the reproductive organs. It should be considered as equally possible and important mechanism as sprouting angiogenesis.

Quantitative study

Capillary diameters increased significantly in caruncles from pregnant does compared to non-pregnant ones. Among pregnant does, capillary diameters increased significantly after 4 weeks of gestation. No significant differences were found in capillary diameters among stages of pregnancy at and after 7 weeks, except between 7 and 16 weeks, where a significant increase was observed. It is possible that the 16 week increase represents some sort of structural adaptation to a sudden fetal demand; this might be related to the final development of one or more organ systems. No statistically significant differences were found in capillary density index between non-pregnant and pregnant does and/or among stages of pregnancy.

Ovaries

Observation of the entire ovarian cast allowed study of the branching pattern of the main ovarian vessels and microvasculature. Coiling of the ovarian artery around the uterine tributary of the ovarian vein was discussed earlier in the clearing section of the study. Coiling of the proper ovarian branch of the ovarian artery around the proper ovarian tributary of the ovarian vein was observed by examining microvascular corrosion casts of the caprine ovaries. This coiling may represent a local channel required for product transport and allow the transfer of substances produced in the ovary from the ovarian vein to the ovarian artery (a counter current mechanism). In other words, physiological processes occurring in the ovary can be controlled by not only the uterus, but also by the ovary itself. Exchange of products between the ovarian vein and artery may not be limited to the distal part of the ovarian artery, nor between uterus and ovary.

The spiral configuration of the proper ovarian branch of the ovarian artery may also represent morphological evidence of importance in hemodynamic functions. Such architecture could have a role in regulating blood pressure to various ovarian structures. Generally this configuration serves to minimize arterial blood pressure to a given structure, and reduction of blood flow due to coiling of the artery may also be beneficial to the exchange mechanism. Physiological studies should be performed to further investigate this possibility in ruminants.

Leakage of casting medium observed in advanced stages of antral follicle development is unlikely to be an artifact because it was consistently seen in

follicles of the same stage of development, and no such leakage was observed in adjacent areas. Increased capillary permeability of follicles at that stage of development has also been documented by other researchers (Kardon and Kessel, 1979).

No quantitative information could be obtained from the ovarian casts. The ovarian microvascular system is extremely complex and not quantitatively comparable among specimens.

Immunohistochemistry

Goats are usually referred to as having an epitheliochorial placenta, but this is not entirely true. Because the uterine epithelium is modified by invasion and fusion of binucleate giant cells, its structure is better referred to as "synepitheliochorial" (Wooding, 1992). Prior to detailed study of these structures, the maternal epithelium was thought to be eroded away, leaving the trophoblasts in contact with maternal connective tissue. The term "syndesmochorial" has been used to describe this apparent structure and is still found in some of the older literature describing ruminant placentation, though it is partially correct because the uterine epithelium is eroded at later stages of gestation. The most intense immunoreactivity to VEGF antibody was seen in the fetal epithelium, particularly cytotrophoblasts. A less intense reaction was present in the maternal epithelium, which was eroded at later stages of pregnancy. This staining pattern suggests that it is the fetal tissues, rather than the maternal ones, that are the primary sites for VEGF production. This can be interpreted to mean that the fetus is directing its own survival by producing growth factors that act on both fetal and maternal

tissues. The presence of VEGF protein in the cytotrophoblasts suggests a role in growth and differentiation of these cells.

A prominent feature of the ruminant placenta is the presence of large numbers of binucleate giant cells. These cells arise early as part of the fetal trophoblasts from cells that fail to undergo cytokinesis following nuclear division. They invade and fuse with caruncular epithelial cells to form small syncytia (Wooding, 1992). Binucleate cells secrete placental lactogen and pregnancy-specific protein B. Despite their obvious importance in creating the final form of the caprine placenta and in placental hormone production, binucleate cells did not show any immunostaining to VEGF antibody.

VEGF was localized in the endothelium and smooth muscles of blood vessels. Since it has been reported that cultured smooth muscle cells have no mitogenic effect on endothelial cells (Ferrara, 1992), VEGF is not only important in promoting vascular proliferation and permeability, but also in its survival.

VEGF was localized in both theca and granulosa cells, but the intensity of the reaction was higher in granulosa cells than theca cells, this observation supports the suggestion of Tamanini and De Ambrogi (2004) regarding the site of VEGF production in the follicle that VEGF is produced in the granulosa layer and exerts its effects (thecal vascular bed growth and development) in the theca layer through a paracrine pathway.

VEGF is important during development of the corpus luteum: expression of mRNA encoding VEGF is upregulated during the period of luteal development (Redmer et al., 1996). In our study, VEGF was localized in the corpus luteum at

all stages of gestation we studied, even when there was no growth of the corpus luteum, though in goats it is needed to maintain pregnancy. The implication of this finding is that VEGF is not only important in development of the CL, but also in its maintenance.

Real-time QPCR

In general there was a trend of increased expression of VEGF, Flt-1 and KDR mRNAs with advancing pregnancy in uterine tissues, an observation which correlates well with the increasing levels of angiogenesis that occurs during pregnancy, to meet the increasing requirements of the growing fetus(es). The maximum increase was observed at the 18-week stage (term is 150 days). We observed that regardless of the changes in expression of the target mRNAs in the placentomes, no difference was observed between their expression levels at 13 and 16 weeks of pregnancy; this might indicate that the increase in angiogenesis during pregnancy is not linear and there is a time frame where it does not increase with advanced pregnancy. This observation was also noted in our quantitative study of angiogenesis at the same sequential stages of pregnancy.

No substantial differences were observed in the expression of any of the target mRNAs in ovarian tissues measured at and after 7 weeks. Maximum expression of all three target mRNAs in all tissues was observed at 18 weeks.

There is no development of the corpus luteum during pregnancy; however, VEGF and its receptors' mRNAs were expressed in the ovarian tissues. This observation emphasizes the important role VEGF plays in maintaining the

integrity of the vasculature, not just in its formation. Expression of VEGF and its receptors mRNAs might well be different in the non-CL-dependent pregnancies typical of other species.

We anticipated a difference in the levels of the expression of angiogenic factors between the right and the left ovary based on our observation of the difference in the frequency of the presence of a CL on the right and the left ovary; in most cases the CL is present on the right ovary. However, expression of all target mRNAs increased to a greater degree during pregnancy in the left ovary than the right one, for reasons which are not clear.

Differences in the time-courses of the expression of Flt-1 and KDR mRNAs during pregnancy suggest that each receptor plays a different role in the angiogenic process, or even a different biological function. VEGF may be utilizing either or both of these receptors in different biological contexts. This may be in agreement with the thought that Flt-1 is a 'decoy' receptor, regulate in a negative fashion by preventing VEGF binding to KDR and KDR is the major mediator of the angiogenic enhancing effects of VEGF (Ferrara et al., 2003). In addition, selective Flt-1 ligands such as PlGF (placental growth factor) or VEGF-B (that were not measured in the present study) may be involved (Tjwa et al., 2003). Generally, in placentomes the pattern of VEGF expression was similar to that of Flt-1, not KDR.

Swainsonine

The effects of swainsonine on vascular development were demonstrated in the uterus, a decrease in capillary density index was noted in swainsonine

treated does at 7 weeks of gestation, an effect which could be easily observed by comparing scanning electron micrographs obtained from swainsonine-treated does and those from normal does and was confirmed by digital image analysis (Figs. 43 and 44), as well as in ovaries, focal avascular areas were observed in the corpus luteum of swainsonine-treated does at 7 weeks of pregnancy; these areas correspond to vascular degeneration and diminished angiogenesis. Swainsonine caused dramatic distortion in the uterine and ovarian vasculature in treated does at 18 weeks of gestation.

At the cellular and molecular levels, intensity of the immunoreactivity to VEGF antibody was decreased by treatment with swainsonine at 7 and 18 weeks of gestation. Swainsonine also had an inhibitory effect on the expression of VEGF and its receptors' mRNAs at 18 weeks of pregnancy. Expression of VEGF and its receptors' mRNAs was unaffected by swainsonine at 7 weeks in any of the tissues except the left ovary, where an inhibitory effect was detected. Even though the number of experimental animals used in expression study was low and statistical analysis was not possible, consistent trends were observed over time in tissues recovered from multiple animals. A consistent trend was observed in the effect of swainsonine in the left ovary between week 7 and 18 (Fig. 74b).

This study represents the first quantitative experiment on the effects of swainsonine on vascular development and/or any angiogenic mediator. Demonstration of swainsonine's potential to negatively affect vascular development, and to suppress the expression of genes likely involved in angiogenesis at critical stages of blood vessel proliferation lends credibility to the

suggestion that it or related compounds have potential as anti-cancer drug, given the known dependence of solid tumor growth on angiogenesis (Folkman, 2002). Future quantitative studies utilizing larger populations or different species, higher doses, and/or longer feeding period of swainsonine are required to explore this further, but our findings indicate that swainsonine's possible therapeutic use is well worth more investigation. Results from this study also suggest that the effect of swainsonine on vascular development might be the reason behind its reproductive toxicity.

Overall Discussion

The present study provides a model of vascular pattern and angiogenesis at various levels. At the gross anatomical level, the detailed distribution of vessels supplying the caprine reproductive organs is provided. At the microscopic level, the detailed microvascular architecture of the caruncular and ovarian vascular systems is provided, and quantitative information such as capillary diameter and capillary density index is also included. At the cellular and molecular levels, one of the most important factors promoting angiogenesis (VEGF) was immunolocalized in placentomal and ovarian tissues, and expression of VEGF and its receptors' mRNAs was measured.

At the gross anatomical level, the main vessels supplying the uterus and ovaries (the ovarian, uterine, and vaginal arteries) were followed from their origin to the level of the radial arteries in the uterus and the proper ovarian branch of the ovarian artery in the ovary. Then branches of these arteries (the radial arteries and the proper ovarian branch of the ovarian artery) were studied at the

microscopic level using SEM to the level of the fetal surface of the caruncle in the uterus (where we obtained some measurements) and the distinct vascular spheres corresponding to various stages of follicle and corpus luteum development in the ovary. Thus, at the microscopic level, full description of the three-dimensional organization of the caruncular and ovarian microvascular system, and capillary diameter and capillary density index at the fetal surface of the caruncle are provided.

The data obtained from the study of the cleared specimens at the gross anatomical level emphasize the known importance of understanding the distribution of blood vessels in the female reproductive organs. Coiling of the ovarian artery around the uterine tributary of the ovarian vein provides anatomical interpretation of a physiological process in goats *i.e.* control of the life span of the CL by the uterus via a *local* venoarterial pathway present also in other ruminant species. The architecture of the ovarian artery and vein was maintained throughout pregnancy, which might be a possible route for the transfer of luteotropic substances (such as pregnancy-specific protein-B) from the uterus to the ovary and account for the possible mechanisms of maintenance of CL through out gestation. More physiological investigations are needed to document the implication of this anatomical observation. The gross anatomical work has lead to previously undocumented special adaptations of the ovarian and/or vaginal arteries to multiple pregnancies, adaptation that correlates well with the increasing nutrient demands of the growing fetuses in multiple pregnancies, especially at later stages. The regional supply of different parts of

the dorsal and ventral surfaces of the caprine uterus is provided. This will be helpful to other researchers performing studies on the caprine reproductive organs.

At the microscopic level, this work represents the first study of the uterine vascular system in non-pregnant does or in any non-pregnant farm animal, the first to provide the developmental features of the uterine vascular system during pregnancy in goats, the first to emphasize the role of intussusceptive angiogenesis in the development of uterine vascular system during pregnancy, and the first to provide quantitative information about the uterine vascular system in non-pregnant and pregnant does. The highest level of angiogenesis was observed between non-pregnant and pregnant does and again between 4 and 7 weeks of gestation, which correlates well with fact that most abortions occur at early stages of pregnancy, when the fetal insult is most critical.

At the microscopic level in the ovary, this work represents the first study of the three-dimensional angioarchitecture of the caprine ovary, and the first on corpus luteum microvasculature in any ruminant species. Also this study is the first to provide information about the detailed angioarchitecture of the proximal ramification of the ovarian vessels in any ruminant species and its possible physiological implications.

At the cellular and molecular level, this work represents the first sequential study of the expression and localization of a vitally important angiogenic mediator during pregnancy in goats. VEGF was localized in the caruncular and ovarian tissues of non-pregnant does, and placentomal and ovarian tissues of pregnant

does at all stages of pregnancy. VEGF and its receptors' mRNAs were detected in the caruncular and ovarian tissues of non-pregnant does, and placentomal and ovarian tissues of pregnant does at all stages of pregnancy.

As an application of our model of angiogenesis, we demonstrated the effect of a potential anti-cancer drug (swainsonine) on vascular development. Its effect was demonstrated at the microscopic level both qualitatively and quantitatively. Its effect on an important angiogenic mediator such as VEGF adds to its credibility as a potential anti-cancer drug.

Quite aside from the potential utility of the caprine model as a general one for angiogenesis, the information provided is of importance to improving reproductive technology in goats themselves. The data on placental development supplement and expand on what is already known about the goat, an economically important animal.

Summary

This work utilizes the development of utero-ovarian vasculature during pregnancy in goats as a model of physiological angiogenesis at various levels. The estrous cycle of a group of does was synchronized using a combination of norgestomet ear implants (Synchromate-B®) and prostaglandin (Lutalyse®). Buck goats were introduced on the day of implant removal and kept with the does for four days. Pregnancy check started at 4 weeks then the does were examined and the progress of their pregnancy was monitored by ultrasound every three weeks. After humane euthanization, the reproductive tracts of non-pregnant does, and does at 4, 7, 10, 13, 16, and 18 weeks of gestation were processed differently for each of four experiments.

The first experiment represents a gross anatomical study of the detailed distribution of vessels supplying the caprine reproductive organs using the tissue clearing technique. Arteries of the reproductive tract were injected *in situ* with Microfil®. The tracts were fixed, dehydrated, and rendered transparent to reveal the paths of arteries. No differences were observed in the origin and distribution of the ovarian, uterine and vaginal arteries between pregnant and non-pregnant does; however, differences in these aspects existed within pregnant and/or non-pregnant does. The ovarian artery was tortuous and lay in close apposition to the uterine tributary of the ovarian vein in all does examined. This arrangement was maintained throughout gestation (an observation never mentioned or discussed before this study in any species). In non-pregnant does, this arrangement may serve as a *local* utero-ovarian pathway, where substances (such as $PGF_{2\alpha}$) can

pass from the ovarian vein to ovarian artery and affect structures on the ovary, as in the case of CL luteolysis at the end of non-fertile estrous cycle. During pregnancy, this arterio-venous arrangement may serve to transfer luteotropic substances from the uterus and the ovary, which may assist maternal recognition of pregnancy at early stages; and fit the fact that the goat is CL-dependent throughout pregnancy. The size of the uterine branch of the ovarian artery, mostly at later stages, was equal to or even larger than that of its parent artery and/or the ipsilateral uterine artery in most triplet pregnancies. In some cases of triplets, the vaginal artery contributed a connecting branch to the uterine artery. This physiological adaptation of the ovarian and/or the vaginal arteries, which has never before been noted in the literature, correlates well with the increasing nutrient demands of the growing multiple fetuses, especially at later stages.

The second experiment was a microscopic study of the detailed microvascular architecture of the caruncular and ovarian vascular systems using microvascular corrosion casting and examination in a scanning electron microscope. The vasculature of the uterus and ovaries was injected *in situ* with a mixture of Batson's No.17® and methyl methacrylate, and then processed for observation. In non-pregnant does, vessels entered the base of the caruncle, whose internal convex surface was covered with capillary meshes of regular diameter and form, with no crypts. At 4 weeks of pregnancy, the surface of the caruncle showed a pattern of ridges separated by troughs. At advanced stages, branches of radial arteries ramified over the convex surface of the caruncle. They gave off stem arteries, which penetrated the periphery of the convex surface of

the caruncle from all levels, leading to a mesh of capillaries on the concave surface. On the concave side, capillaries coalesced, forming sinusoids. From these microscopic observations, we concluded that goats possess a *multivillous* type placenta. Also the concept that the epitheliochorial placenta is low in efficiency may not be longer acceptable, because several other factors (*i.e.* vascular system arrangement) may be very important in determining the actual physiological efficiency of placental transport. In the case of the goat placenta, the presence of capillary sinusoids and crypts may compensate for the negative effect presented by the length of the interhemal distance. Evidence of sprouting and intussusceptive angiogenesis was observed. Intussusceptive angiogenesis should be considered as an equally possible and important mechanism as sprouting angiogenesis during placental development. Capillary diameters increased significantly during pregnancy, especially after 4 weeks. The proportion of surface area covered by capillaries in relation to total area measured was 66.8, 68.7, 55.5, 63.5, 70.1, 70.4, 64.5 percent in non-pregnant, 4, 7, 10, 13, 16, and 18 weeks of pregnancy, respectively. In the ovary, coiling of the ovarian branch of the ovarian artery around the ovarian tributary of the ovarian vein was observed. This may represent a local channel required for product transport from the ovarian vein to the ovarian artery and might be morphological evidence of the importance in hemodynamic functions. It may have a role in regulating blood pressure to various ovarian structures. Generally this configuration serves to minimize arterial blood pressure to a given structure,

and reduction of blood flow due to coiling of the artery may also be beneficial to the exchange mechanism.

In the third experiment, uterine and ovarian tissues were collected and immediately immersed in freshly prepared 4% paraformaldehyde for 4 hours at 4^{o}C to be processed for immunohistochemistry. Immunolocalization of VEGF was performed using the avidin-biotin-horseradish peroxidase system. Immunostaining was observed in cytotrophoblasts, maternal epithelial tissues, and vascular endothelium and smooth muscles, but not in binucleate giant cells or connective tissue. No apparent differences were observed in intensity and pattern of VEGF staining associated with advancing gestation. Luteal and follicular cells, and endothelium and smooth muscles of the ovarian vasculature were positively stained. Patterns and intensity of staining of VEGF suggest that the fetal tissues, rather than the maternal tissues, are the primary sites for VEGF production. The fetus is directing its own survival by producing growth factors that act on fetal and maternal tissues. VEGF may have a role in growth and differentiation of cytotrophoblasts, as well as development and maintenance of CL.

In the fourth experiment, uterine and ovarian tissues were collected, and immediately immersed in RNA Later® solution to be processed for real-time quantitative polymerase chain reaction (real-time QPCR). The sequential expression of VEGF and its receptors (fms-like tyrosine kinase, Flt-1 and kinase-insert domain-containing receptor, KDR) was measured. Targets were detected in all studied tissues; however, levels of expression differed according to the

stage of pregnancy. Expression of VEGF and its receptor mRNAs increased with advancing pregnancy, which correlates with the expansion of vasculature during pregnancy. Differences in the time-courses of the expression of Flt-1 and KDR mRNAs during pregnancy suggest that each receptor plays a different role in the angiogenic process.

As an application of our model of angiogenesis, we tested the effect of swainsonine (active compound of locoweed and a potential antic-cancer drug) on the process. Does treated with swainsonine were euthanized at 7 and 18 weeks, after having been given 150 g ground locoweed containing 0.15% swainsonine. Specimens from does treated with swainsonine were prepared as in the case of the normal ones for microvascular casting, immunohistochemistry, and real-time QPCR. No significant differences were found in sinusoidal diameters in treated does at 7 weeks, but a decrease in capillary density index was noted. In the ovary, focal avascular areas were observed in the corpus luteum of swainsonine-treated does at 7 weeks of pregnancy. These areas correspond to vascular degeneration and diminished angiogenesis. Swainsonine caused great distortion in the uterine and ovarian vasculature at 18 weeks. A decrease in intensity of the immunoreactivity to VEGF antibody was observed in tissues from swainsonine-treated does at 7 and 18 weeks. There was no significant effect of swainsonine on the expression VEGF and its receptors' mRNAs in any of the studied tissues (except in the left ovary, where it had an inhibitory effect) at 7 weeks of pregnancy, but it had an inhibitory effect at 18 weeks. This study represents the first quantitative experiment on the effects of swainsonine on angiogenesis

and/or any angiogenic mediator. Demonstration of swainsonine's potential to negatively affect vascular development and suppress the expression of genes likely involved in angiogenesis at critical stages of blood vessel proliferation lends credibility to the suggestion that it or related compounds have potential as anti-cancer drugs.

Quite aside from the potential utility of the caprine model as a general one for angiogenesis, this information is of importance to improving reproductive technology in goats, an economically valuable species in their own right.

References

Al-zi'abi MO, Watson ED, Fraser HM. 2003. Angiogenesis and vascular endothelial growth factor expression in the equine corpus luteum. Reproduction 125:259-270.

Amoah EA, Gelaye S. 1989. Goat breeding using exogenous hormones. Dairy Goat Journal 87:506-510.

AppliedBiosystems. 2001. User bulletin # 2 ABI PRISM 7700 sequence detection system.

Balls L, James LF. 1973. Effect of locoweed (Astragalus spp) on reproductive performance of ewes. Journal of the American Veterinary Medical Association 162:291-292.

Barclay L. 2004. FDA approves Bevacizumab for colorectal cancer: A newsmaker interview with Herbert I. Hurwitz, MD. In: Medscape Medical news.

Barcroft J, Barron DH. 1946. Observation upon the form and relations of the maternal and fetal vessels in the placenta of the sheep. The Anatomical Record 94:569-595.

Barrett S, Blockey MA, Brown JM, Cumming IA, Goding JR, Mole BJ, J.M. O. 1971. Initiation of the estrous cycle in the ewe by infusions of $PGF_{2\alpha}$ to the autotransplanted ovary. Journal of Reproduction and Fertility 24:136.

Berisha B, Schams D, Kosmann M, Amselgruber W, Einspanier R. 2000. Expression and localisation of vascular endothelial factor and basic fibroblast growth factor during the final growth of bovine ovarian follicles. Journal of Endocrinology 167:371-382.

Berisha B, Schams D, Kosmann M, Amselgruber W, Einspanier R. 2000. Expression and tissue concentration of vascular endothelial growth factor, its receptors, and localization in the bovine corpus luteum during estrus cycle and pregnancy. Biology of Reproduction 63:1106-1114.

Bogic LV, Brace RA, Cheung CY. 2001. Developmental expression of vascular endothelial growth factor (VEGF) receptors and VEGF binding in ovine placenta and fetal membranes. Placenta 22:265-275.

Bolt G, Pedersen I, Moller M. 1999. Processing of *N*-linked oligosaccharides on the measles virus glycoproteins: importance for antigenicity and for production of infectious virus particles. Virus Research 61:43-51.

Bowen D, Joseph A, White SL, Bowen CD, Matsumoto K, Olden K. 1993. A preliminary pharmacokinetic evaluation of the antimetastatic immunomodulator swainsonine: clinical and toxic implications. Anticancer Research 13:841-844.

Boyd JD, Hamilton WJ. 1970. The Human Placenta. Cambridge.

Braun WF. 1980. A review of prostaglandin therapeutics in reproduction. Veterinary Medicine, Small Animal Clinician 75:649-656.

Bretzlaff KN, Madrid N. 1985. Synchronization of estrus and fertility in goats with norgestomet ear implant. Theriogenology 24:351-357.

Bridges PJ, Weems YS, Kim LM, Sasser RG, LeaMaster BR, Vincent DL, Weems CW. 1999. Effect of PGF2alpha, indomethacin, tamoxifen, or estradiol-17beta on incidence of abortion, progesterone, and pregnancy-specific protein B (PSPB) secretion in 88- to 90-day pregnant sheep. Prostaglandins and Other Lipid Mediators 58:113-124.

Bunch TD, Panter KE, James LF. 1992. Ultrasound studies of the effect of certain poisonous plants on uterine function and fetal development in livestock. Journal of Animal Science 70:1639-1643.

Burri PH, Hlushchuk R, Djonov V. 2004. Intussusceptive angiogenesis: its emergence, its characteristics, and its significance. Developmental Dynamics 231:474-488.

Cavender JL, Murdoch WJ. 1988. Morphological studies of microcirculatory system of periovulatory ovine follicles. Biology of Reproduction 39:989-997.

Cheung CY, Singh M, Ebaugh MJ, Brace RA. 1995. Vascular endothelial growth factor gene expression in ovine placenta and fetal membranes. American Journal of Obstetric and Gynecology 173:753-759.

Cornil L, Kerbel RS, Dennis JW. 1990. Tumor cell surface B1-4 linked galactose binds to lectin(s) on microvascular endothelial cells and contributes to organ colonization. Journal of Cell Biology 3:773-782.

Daniel PF, Warren CD, James LF. 1984. Swainsonine-induced oligosaccharide excretion in sheep. The Biochemical Journal 221:601-607.

DeGasperi R, Al-Daher S, Daniel PF, Winchester BG, Jeanloz RW, Warren CD. 1991. The substrate specificity of bovine and feline lysosomal alpha-D-mannosidases in relation to alpha-mannosidosis. Journal of Biochemistry 266:16556-16563.

Del Campo CH, Ginther OJ. 1973. Vascular anatomy of the uterus and ovaries and the unilateral luteolytic effect of the uterus: Angioarchitecture in sheep. American Journal of Veterinary Research 34:1377-1385.

Del Campo CH, Steffenhagen WP, Ginther OJ. 1974. Clearing technique for preparation and photography of anatomic specimens of blood vessels of female genitalia. American Journal of Veterinary Research 35:303-310.

Del Campo MR, Mapletoft RJ, Rowe RF, Critser JK, Ginther OJ. 1980. Unilateral utero-ovarian relationship in pregnant cattle and role of uterine vein. Theriogenology 14:185-193.

Dennis J. 1986. Effect of swainsonine and polyinosinic:polycytidylic acid on murine tumor cell growth and metastasis. Cancer Research 46:5131-5136.

Dennis JW, Koch K, Yousefi S, VanderElst I. 1990. Growth inhibition of human melanoma tumor xenografts in athymic nude mice by swainsonine. Cancer Research 50:1867-1872.

Dennis JW, Laferte S. 1985. Recognition of asparagine-linked oligosaccharides on tumor cells by natural killer cells. Cancer Research 45:6034-6040.

Dennis JW, Laferte S. 1989. Oncodevelopmental expression of-GlcNAc β1-6Man a1-6Man β1-6 branching of Asn-linked oligosaccharides in human breast carcinomas. Cancer Research 49:945-950.

Dorling PR, Huxtable CR, Colegate SM. 1980. Inhibition of lysosomal α-mannosidase by swainsonine, an indolizidine alkaloid isolated from Swainsona canescens. The Biochemical Journal 191:649-651.

Elbein AD. 1991. Glycosidase inhibitors: inhibitors of N-linked oligosaccharide processing. FASEB Journal 5:3055-3063.

Ellis GC, James LF, McMullen RW, Panter KE. 1985. Reduced progesterone and altered cotyledonary prostaglandin values induced by locoweed (Astragalus lentiginosus) in sheep. American Journal of Veterinary Research 46:1903-1907.

Fernandes B, Sagman U, Auger M, Demetrio M, Dennis JW. 1991. B1-6 Branched Oligosaccharides as a marker of Tumor Progression in Human Breast and Colon Neoplasia. Cancer Research 51:718-723.

Ferrara N, Gerber H, LeCouter J. 2003. The biology of VEGF and Its receptors. Nature Medicine 9:669-676.

Ferrara N, Houck K, Jakeman L, Leung DW. 1992. Molecular and biological properties of the vascular endothelial growth factor family of proteins. Endocrine Reviews 13:18-32.

Folkman J. 1992. Angiogenesis-retrospect and outlook. In: Steiner R, Weisz PB, Langer R, editors. Angiogenesis. Basel.Bosten.Berlin: Birkhauser Verlag. p 4-13.

Folkman J. 1995. Angiogenesis in cancer, vascular, rheumatoid and other disease. Nature Medicine 1:27-31.

Folkman J. 2002. Role of angiogenesis in tumor growth and metastasis. Seminars in Oncology. 29 (suppl 16):15-18.

Forsman AD, McCormack JT. 1992. Microcorrosion casts of hamster luteal and follicular vasculature throughout the estrous cycle. The Anatomical Record 233:515-520.

Fraser HM, Lunn SF. 2000. Angiogenesis and its control in the female reproductive system. British Medical Bulletin 56:787-797.

Freitas VJF, Baril G, Saumande J. 1997. Estrus synchronization in dairy goats: use of fluorogestone acetate vaginal sponges or norgestomet ear implants. Animal Reproduction Science 46:237-244.

Fujieda S, Noda I, Saito H, Hoshino T, Yagita M. 1994. Swainsonine augments the cytotoxicity of human lymphokine-activated killer cells against autologous thyroid cancer cells. Archives of Otolaryngology--head & neck Surgery 140:389-394.

Gall C. 1996. Goat Breeds of the World: Margraf Verlag.

Garrido C, Saule S, Gospodarowicz D. 1993. Transcriptional regulation of vascular endothelial growth factor gene expression in ovarian bovine granulosa cells. Growth Factors 8:109-117.

Gibson U, Heid C, Williams P. 1996. A novel method for real time quantitative RT-PCR. Genome Research 6:995-1001.

Ginther OJ. 1974. Internal regulation of physiological processes through local venoarterial pathways: a review. Journal of Animal Science 39:550-564.

Ginther OJ. 1976. Comparative anatomy of uteroovarian vasculature. Veterinary Scope 20:1-17.

Goss PE, Baker MA, Carver JP, Dennis JW. 1995. Inhibitors of carbohydrate processing: a new class of anticancer agents. Clinical Cancer Research 1:935-944.

Goss PE, Baptiste J, Fernandes B, Baker M, Dennis JW. 1994. A phase I study of swainsonine in patients with advanced malignancies. Cancer Research 54:1450-1457.

Goss PE, Reid CL, Bailey D, Dennis JW. 1997. Phase IB clinical trial of the oligosaccharide processing inhibitor swainsonine in patients with advanced malignancies. Clinical Cancer Research 3:1077-1086.

Granerus M, Engstrom W. 2000. The effect of glycosylation inhibitors on the proliferation of a wilms tumour cell line. Anticancer Research 20:689-692.

Heid C, Stevens J, Livak K, Williams P. 1996. Real-time quantitative PCR. Genome Research 6:986-994.

Hodde KC, Nowell JA. 1980. SEM of micro-corrosion casts. Scanning Electron Microscopy 2:89-106.

Humblot P, De Montigny G, Jeanguyot N, Tetedoie F, Payen B, Thibier M, Sasset RG. 1990. Pregnancy-specific protein B and progesterone concentrations in French Alpine goats throughout gestation. Journal of Reproduction and Fertility 89:205-212.

Humphries M, Matsumoto K, White S, Molyneux R, Olden K. 1990. An assessment of the effects of swainsonine on survival of mice injected with B16-F10 melanoma cells. Clinical and Experimental Metastasis 8:89-102.

Humphries M, Matsumoto K, White S, Olden K. 1986. Oligosaccharide modification by swainsonine treatment inhibits pulmonary colonization by B16F10 murine melanoma cells. Proceeding of National Academy of Sciences of the United States of America 83:1752-1756.

Humphries M, Olden K. 1989. Asparagine-linked oligosaccharides and tumor metastasis. Pharmacology and Therapeutics 44:85-105.

Humphries MJ, Matsumoto K, White SL, Molyneux RJ, Olden K. 1988. Augmentation of murine natural killer cell activity by swainsonine, a new antimetastatic immunomodulator. Cancer Research 48:1410-1415.

Jacob GS. 1995. Glycosylation inhibitors in biology and medicine. Current Opinion in Structural Biology 5:605-611.

James LF. 1971. Lesions in neonatal lambs resulting from maternal ingestion of locoweed. The Cornell Veterinarian 61:667-670.

James LF. 1972a. Effect of locoweed on fetal development: preliminary study in sheep. American Journal of Veterinary Research 33:835-840.

James LF. 1972b. Syndromes of locoweed poisoning in livestock. Clinical Toxicology 5:567-573.

James LF, Foote W. 1972. Estrogenic properties of locoweed. Canadian Journal of Comparative Medicine 36:360-365.

James LF, Hartley WJ, Nielsen D, Allen S, Panter KE. 1986. Locoweed (Oxytropis sericea) poisoning and congestive heart failure in cattle. Journal of the American Veterinary Medical Association 189:1549-1556.

James LF, Keeler RF, Binns W. 1969. Sequence in the abortive and teratogenic effects of locoweed fed to sheep. American Journal of Veterinary Research 30:377-380.

James LF, Panter KE, Nielsen DB, Molyneux RJ. 1992. The effect of natural toxins on reproduction in livestock. Journal of Animal Science 70:1573-1579.

James LF, Shupe JL, Binns W, Keeler RF. 1967. Abortive and teratogenic effects of locoweed on sheep and cattle. American Journal of Veterinary Research 28:1379-1388.

James LF, Van Kampen KR. 1970. Effect of locoweed intoxication on the genital tract of the ram. American Journal of Veterinary Research 32:1293-1295.

James LF, Van Kampen KR, Hartley WJ. 1970. Comparative pathology of Astragalus (locoweed) and Swainsona poisoning in sheep. Veterinary Pathology 7:116-125.

Jiang JY, Macchiarelli G, Miyabayashi K. 2002. Follicular microvasculature in the porcine ovary. Cell & Tissue Research 310:93-101.

Jiang JY, Macchiarelli G, Tsang BK, Sato E. 2003. Capillary angiogenesis and degeneration in bovine ovarian antral follicles. Reproduction 125:211-223.

Jolly RD, Walkley SU. 1997. Lysosomal storage diseases of animals: an Essay in comparative pathology. Veterinary Pathology 34:527-548.

Kanzaki H, Okamura H, Okuda Y, Takenaka A, Morimoto K, Nishimura T. 1982. Scanning electron microscopic study of rabbit ovarian follicle microvasculature using resin injection-corrosion casts. Journal of Anatomy 134:697-704.

Kardon RH, Kessel RG. 1979. SEM studies on vascular casts of the rat ovary. Scanning Electron Microscopy 3:743-750.

Kaufmann P, Burton G. 1994. Anatomy and genesis of the placenta. In: Knobil E, Neill JD, editors. The Physiology of Reproduction, 2nd ed. New York: Raven Press,Ltd.,New York. p 441-484.

Kawate N, Tsuji M, Tamada H, Inaba T, Sawada T. 2003. Changes of messenger RNAs encoding vascular endothelial growth factor and its receptors during the development and maintenance of caprine corpora lutea. Molecular Reproduction and Development 64:166-171.

Kitai H, Yoshimura Y, Write KH, Santulli R, Wallach EE. 1985. Microvasculature of preovulatory follicles: comparison of in situ and in vitro perfused rabbit ovaries following stimulation of ovulation. American Journal of Obstetric and Gynecology 152:889-895.

Klein JL, Roberts JD, George MD, Kurtzberg J, Breton P, Chermann JC, Olden K. 1999. Swainsonine protects both murine and human haematopoietic systems from chemotherapeutic toxicity. British Journal of Cancer 80:87-95.

Korczak B, Goss P, Fernandes B, Baker M, Dennis JW. 1994. Branching N-linked oligosaccharides in breast cancer. Advances in Experimental Medicine and Biology 353:95-104.

Kornfeld R, Kornfeld S. 1985. Assembly of asparagine-linked oligosaccharides. Annual Review of Biochemistry 54:631-664.

Kosuge T, Tamura T, Nariuchi H, Toyoshima S. 2000. Effect of inhibitors of glycoprotein processing on cytokine secretion and production in Anti CD3-stimulated T cells. Biological & Pharmaceutical Bulletin 23:1-5.

Kusina NT, Tarwirei, Hamudikuwanda H, Agumba G, Mukwena J. 2000. A comparison of the effects of progesterone sponges and ear implants, PGF2alpha, and their combination on efficacy of estrus synchronization and fertility of Mashona goat does. Theriogenology 53:1567-1580.

Leiser R. 1987. Mikrovasckularisation der ziegenplazenta, dargestellt mit rasterelektronisch untersuchten gefassausgussen. Schweiz Archiv Tierheilk 129:59-74.

Leiser R, Kaufmann P. 1994. Placental structure: in a comparative aspect. Experimental and Clinical Endocrinology 102:122-134.

Leiser R, Krebs C, Ebert B, Dantzer V. 1997. Placental vascular corrosion cast studies: a comparison between ruminants and humans. Microscopy Research and Technique 38:76-87.

Lemaire S, Derappe C, Michalski JC, Aubery M, Neel D. 1994. Expression of β1-6 branched *N*-linked oligosaccharides is associated with activation in human T4 and T8 cell populations. The Journal of Biological Chemistry 269:8069-8074.

Livak KJ, Schmittgen TD. 2001. Analysis of relative gene expression data using real-time quantitative PCR and the $2^{-(\text{Delta Delta CT})}$ method. Methods 25:402-408.

Macchiarelli G. 2000. The microvasculature of the ovary: A review by SEM of vascular corrosion casts. Journal of Reproduction and Development 46:207-225.

Macchiarelli G, Nottola SA, Kikuta A, Ohtani O, Murakami T, Motta PM. 1992. The ovary: three-dimensional morphodynamics of the luteo-follicular complex by SEM of vascular corrosion casts and other EM techniques. In: Motta PM, Murakami T, Fujita H, editors. Scanning Electron Microscopy of Vascular Casts: Methods and Applications. Bosten: Kluwer Academic Publishers.

Macchiarelli G, Nottola SA, Picucci K, Tiziana S, Motta PM. 1998. The microvasculature of the corpus luteum in pregnant rabbit. A scanning electron microscopy study of corrosion casts. Italian Journal of Anatomy and Embryology 103 (supp 1):191-202.

Macchiarelli G, Nottola SA, Vizza E, Correr S, Motta PM. 1995. Changes in ovarian microvasculature in hCG stimulated rabbits. A scanning electron microscopic study of corrosion casts. Italian Journal of Anatomy and Embryology 100 (Suppl 1):469-477.

Macchiarelli G, Nottola SA, Vizza E, Kikuta A, Murakami T, Motta PM. 1991. Ovarian microvasculature in normal and hCG stimulated rabbits. A study of vascular corrosion casts with particular regard to the interstitium. Journal of Submicroscopic Cytology 23:391-395.

Makowski EL. 1968. Maternal and fetal vascular nets in placentas of sheep and goats. American Journal of Obstetrics and Gynecology 100:283-288.

Mapletoft RJ, Lapin DR, Ginther OJ. 1976. The ovarian artery as the final component of the local luteotropic pathway between a gravid uterine horn and ovary in ewes. Biology of Reproduction 15:414-421.

Minnich B, Bartel H, Lametschwandtner A. 2001. Quantitative microvascular corrosion casting by 2D and 3D- morphometry. Italian Journal of Anatomy and Embryology 106 (supplement 1):213-220.

Misago M, Tsukada J, Fukuda MN, Eto S. 2000. Suppressive effects of swainsonine and N-butyldeoxynojirimycin on human bone marrow neutrophil maturation. Biochemical and Biophysical Research Communications 269:219-225.

Molyneux RJ, James LF. 1982. Loco intoxication: indolizidine alkaloids of spotted locoweed (Astragalus lentiginosus). Science 216:190-191.

Moremen KW. 2002. Golgi α-mannosidase II deficiency in vertebrate systems: implications for asparagine-linked oligosaccharide processing in mammals. Biochemica et Biophysica Acta 1573:225-235.

Morrow D. 1986. Current Therapy in Theriogenology, 2 ed. Philadelphia: W. B. Saunders Company.

Motta PM, Murakami T, Fujita H. 1992. Scanning Electron Microscopy of Vascular Casts: Methods and Applications. Boston: Kluwer Academic Publishers.

Murakami T, Ikebuchi Y, Ohtsuka A, Kikuta A, Taguchi T, Ohtani O. 1988. The blood vascular wreath of rat ovarian follicle, with special reference to its changes in ovulation and luteinization: a scanning electron microscopic study of corrosion casts. Archives of Histology and Cytology 51:299-313.

Nayak N, Brenner R. 2002. Vascular proliferation and vascular endothelial growth factor expression in the Rhesus Macaque endometrium. The Journal of Clinical Endocrinology and Metabolism 87:1845-1855.

Nelson AC. 1987. Study of rat lung alveoli using corrosion casting and freeze fracture methods coupled with digital image analysis. Scanning Microscopy 1:817-822.

Nopanitaya W, Aghajanian JG, Gray LD. 1979. An improved plastic mixture for corrosion of the gastrointestinal microvascular system. Scanning Electron Microscopy 3:751-756.

Nottola SA, Macchiarelli G, Motta PM. 1997. The angioarchitecture of estrous, pseudopregnant and pregnant rabbit ovary as seen by scanning electron microscopy of vascular casts. Cell & Tissue Research 288:353-363.

Oliveira MAL, Guido SI, Lima PF. 2001. Comparison of different protocols used to induce and synchronize estrus cycle of saanen goats. Small Ruminant Research 40:149-153.

Oredipe OA, Furbert-Harris PM, Laniyan I, Green WR, White SL, Olden K, Parish-gause D, Vaughn T, Griffin WM, Sridhar R. 2003. Enhanced proliferation of functionally competent bone marrow cells in different strains of mice treated with swainsonine. International Immunopharmacology 3:445-455.

Oredipe OA, White SL, Grzegorzewski K, Gause BL, Cha JK, Miles VA, Olden K. 1991. Protective effects of swainsonine on murine survival and bone marrow proliferation during cytotoxic chemotherapy. Journal of National Cancer Institute 83:1149-1156.

Orsini MW. 1962. Technique of preparation, study and photography of benzyl-benzoate cleared material for embryological studies. Journal of Reproduction and Fertility 3:283-287.

Panter K, James L, Stegelmeier B, Ralphs M, Pfister J. 1999. Locoweeds: effect on reproduction in livestock. Journal of Natural Toxins 8:53-62.

Panter KE, Bunch TD, James LF, Sisson DV. 1987. Ultrasonographic imaging to monitor fetal and placental development in ewes fed locoweed (Astragalus lentiginosus). American Journal of Veterinary Research 48:686-690.

Panter KE, James LF, Hartley WJ. 1989. Transient testicular degeneration in rams fed locoweed (Astragalus lentiginosus). Veterinary and Human Toxicology 31:42-46.

Pfister JA, Astorga JB, Panter KE, Molyneux RJ. 1993. Maternal locoweed exposure *in utero* and as a neonate does not disrupt taste aversion learning in lambs. Applied Animal Behaviour Science 36:159-167.

Porwoll S, Fuchs H, Tauber R. 1999. Characterization of a soluble class I alpha-mannosidase in human serum. FEBS Letters 449:175-178.

Ralphs MH, James LF. 1999. Locoweed grazing. Journal of Natural Toxins 8:47-51.

Ralphs MH, Panter KE, James LF. 1990. Feed preferences and habituation of sheep poisoned by locoweed. Journal of Animal Science 68:1354-1362.

Redmer D, Kraft K, Kirsch J, Reynolds L. 1998. Expression and localization of vascular endothelial growth factor (VEGF) in ovine placenta during late pregnancy. Biology of Reproduction 58(supp 1):202.

Redmer DA, Dai Y, Li J, Charnock-Jones DS, Smith SK, Reynolds LP, Moor RM. 1996. Characterization and expression of vascular endothelial growth factor (VEGF) in the ovine corpus luteum. Journal of Reproduction and Fertility 108:157-165.

Reynolds L, Maddock K, Kraft K, Kirsch J, Redmer D. 1998. Expression of vascular endothelial growth factor (VEGF) in ovine uterine and placental tissues of early pregnancy. Molecular Biology of the Cell 9 (supp 1):314a.

Reynolds L, Redmer D. 1998. Expression of the angiogenic factors, basic fibroblast growth factor and vascular endothelial growth factor, in the ovary. Journal of Animal Science 76:1671-1681.

Reynolds LP, Grazul-Bilska AT, Redmer DA. 2000. Angiogenesis in the corpus luteum. Endocrine 12:1-9.

Reynolds LP, Killilea SD, Redmer DA. 1992. Angiogenesis in the female reproductive system. FASEB J 6:886-892.

Risau W. 1997. Mechanisms of angiogenesis. Nature 386:671-674.

Roberts JD, Klein JL, Palmantier R, Dhume ST, George MD, Olden K. 1998. The role of protein glycosylation inhibitors in the prevention of metastasis and therapy of cancer. Cancer Detection and Prevention 22:455-462.

Seftor REB, Seftor EA, Grimes WJ, Liotta LA, Stetler-Stevenson WG, Welch DR, Hendrix MJC. 1991. Human melanoma cell invasion is inhibited in vitro by swainsonine and deoxymannojirimycin with concomitant decrease in collagenase IV expression. Melanoma Research 1:43-54.

Senger PL. 2003. Early embryogenesis and maternal recognition of pregnancy. In: Pathways to pregnancy and parturition, second ed. Washington: Current Conceptions, Inc.

Sexton S, Mitcham A. 1992. The Angora Goat: LANCELOT PRESS. Hantsport, Nova Scotia.

Sharkey AM, Charnock-Jones DS, Boocock CA, Brown KD, Smith SK. 1993. Expression of mRNA for vascular endothelial growth factor in human placenta. Journal of Reproduction and Fertility 99:609-615.

Sharma RP, James LF, Molyneux RJ. 1984. Effect of repeated locoweed feeding on peripheral lymphocytic function and plasma proteins in sheep. American Journal of Veterinary Research 45:2090-2093.

Smith M, Sherman D. 1994. Goat Medicine: Lea & Febiger, A WAVERLY COMPANY.

Stegelmeier BL, James LF, Hall JO, Mattrix MT. 2001. Neurologic disease in range goats associated with Oxytropis Sericea (Locoweed) poisoning and water deprivation. Veterinary and Human Toxicology 43:302-304.

Stegelmeier BL, James LF, Panter KE, Gardner DR, Ralphs MH, Pfister JA. 1998. Tissue swainsonine clearance in sheep chronically poisoned with locoweed (Oxytropis Sericea). Journal of Animal Science 76:1140-1144.

Stegelmeier BL, James LF, Panter KE, Molyneux RJ. 1995a. Tissue and serum swainsonine concentrations in sheep ingesting Astragalus Lentiginosus (locoweed). Veterinary and Human Toxicology 37:336-339.

Stegelmeier BL, James LF, Panter KE, Molyneux RJ. 1995b. Serum swainsonine concentration and alpha-mannosidase activity in cattle and sheep ingesting Oxytropis Sericea and Astragalus lentiginosus (locoweeds). American Journal of Veterinary Research 56:149-154.

Stegelmeier BL, James LF, Panter KE, Ralphs MH, Gardner DR, Molyneux RJ, Pfister JA. 1999. The pathogenesis and toxicokinetics of locoweed (Astragalus and Oxytropis spp.) poisoning in livestock. Journal of Natural Toxins 8:35-45.

Stegelmeier BL, Ralphs MH, Gardner DR, Molyneux RJ, James LF. 1994. Serum α-mannosidase activity and the clinicopathologic alterations of locoweed (Astragalus mollissimus) intoxication in range cattle. Journal of Veterinary Diagnostic Investigations 6:473-479.

Stouffer RL, Martinez-Chequer JC, Molskness TA, Xu F, Hazzard TM. 2001. Regulation and action of angiogenic factors in the primate ovary. Archives of Medical Research 32:567-575.

Stroop C, Weber W, Nimtz M, Gallego G, Kamerling J, Viegenthart J. 2000. Fucosylated hybrid-type N-glycans on the secreted human epidermal growth factor receptor from swainsonine-treated A431 Cells. Archives of Biochemistry and Biophysics 374:42-51.

Sugino N, Kashida S, Karube-Harada A, Takiguchi S, Kato H. 2002. Expression of vascular endothelial growth factor (VEGF) and its receptors in human endometrium throughout the menstrual cycle and in early pregnancy. Reproduction 123:379-387.

Swenson MJ. 1970. Duckes' Physiology of Domestic Animals. Ithaca: Cornell University Press.

Takada S, Shimada T, Nakamura M, Mori H, Kigawa T. 1987. Vascular pattern of the mammalian ovary with special reference to the three-dimensional architecture of the spiral artery. Archivum Histologicum Japonicum 50:407-418.

Tamanini C, De Ambrogi M. 2004. Angiogenesis in developing follicle and corpus luteum. Reproduction in Domestic animals 39:206-216.

Taylor JB, Strickland J, May T, Hawkins DE. 2000. Effect of subacute swainsonine (locoweed; Oxytropis Sericea) consumption on immunocompetence and serum constituents of sheep in a nutrient-restricted state. Veterinary and Human Toxicology 42:199-204.

Taylor JB, Strickland JR. 1998. In vitro effect of swainsonine on bovine and ovine lymphoblastogenesis. Journal of Animal Science 76:2857-2862.

Tjwa M, Luttun A, Autiero M, Carmeliet P. 2003. VEGF and PIGF: two pleiotropic growth factors with distinct roles in development and homeostasis. Cell Tissue Research 314:5-14.

Tulsiani DR, Broquist HP, James LF, Touster O. 1984. The similar effects of swainsonine and locoweed on tissue glycosidases and oligosaccharides of the pig indicate that the alkaloid is the principal toxin responsible for induction of locoism. Archives of Biochemistry and Biophysics 232:76-85.

Tulsiani DR, Broquist HP, James LF, Touster O. 1988. Production of hybrid glycoproteins and accumulation of oligosaccharides in the brain of sheep and pigs administered swainsonine or locoweed. Archives of Biochemistry and Biophysics 264:607-617.

Tulsiani DR, Skudlarek MD, Orgebin-Crist MC. 1990. Swainsonine induces the production of hydrid glycoproteins and accumulation of oligosaccharides in male reproductive tissues of the rat. Biology of reproduction 43:130-138.

Van Kampen KR. 1972. Sequential development of the lesions in locoweed poisoning. Clinical Toxicology 5:575-580.

Van Kampen KR, James LF. 1969. Pathology of locoweed poisoning in sheep. Veterinary Pathology 6:413-423.

Van Kampen KR, James LF. 1971. Ovarian and placental lesion in sheep from ingesting locoweed (Astragalus lentiginosus). Veterinary Pathology 8:193-199.

Wang S, Panter KE, Holynoak GR, Molyneux RJ, Liu G, Evans RC, Bunch TD. 1999. Development and viability of bovine preplacentation embryos treated with swainsonine in vitro. Animal Reproduction Science 56:19-29.

Warren CD, Sadeh S, Daniel PF, Bugge B, James LF, Jeanloz RW. 1983. Induced mannosidosis-excretion of oligosaccharides by locoweed-intoxicated sheep. FEBS Letters 163:99-103.

White SL, Nagai T, Akiyama SK, Reeves EJ, Grzegorzewski K, Olden K. 1991. Swainsonine stimulation of the proliferation and colony forming activity of murine bone marrow. Cancer Communication 3:83-91.

Willett CG, Boucher Y, Tomaso ED, Duda DG, Munn LL, Tong RT, Chung DC, Sahani DV, Kalva SP, Kozin SV, Mino M, Cohen KS, Scadden DT, Hartford AC, Fischman AJ, Clark JW, Ryan DP, A.X. Z, Blaszkowsky LS, Chen HX, Shellito PC, Lauwers GY, Jain RK. 2004. Direct evidence that the VEGF-specific antibody Bevacizumab has antivascular effects in human rectal cancer. Nature Medicine 10:145-147.

Wojczyk BS, Stwora-Wojczk M, Shakin-Eshleman S, Wunner WH, Spitalnik SL. 1998. The role of site-specific N-glycosylation in secretion of soluble forms of rabies virus glycoprotein. Glycobiology 8:121-130.

Wooding FBP. 1992. Current topic: the synepitheliochorial placenta of ruminants: binucleate cell fusions and hormone production. Placenta 13:101-113.

Yamada O, Abe M, Takehana K, Hiraga T, Iwasa K, Hiratsuka T. 1995. Microvascular changes during the development of follicles in bovine ovaries: a study of corrosion casts by scanning electron microscopy. Archives of Histology and Cytology 58:567-574.

Zogakis TG, Libutti SK. 2001. General aspects of anti-angiogenesis and cancer therapy. Expert Opinion on Biological Therapy. 1:253-274.